STUDIES IN CRYSTALLINE AND AMORPHOUS STRUCTURES IN $PbO-V_2O_5-P_2O_5$

STUDIES IN CRYSTALLINE AND AMORPHOUS STRUCTURES IN $PbO-V_2O_5-P_2O_5$

By

BYRON D. JORDAN, B.A.

A Thesis
Submitted to the Faculty of Graduate Studies
in Partial Fulfilment of the Requirements
for the Degree
Doctor of Philosophy

McMaster University
September, 1975

DOCTOR OF PHILOSOPHY (1975)
(Physics)

McMASTER UNIVERSITY
Hamilton, Ontario

TITLE: Studies in Crystalline and Amorphous Structures in $PbO-V_2O_5-P_2O_5$.

AUTHOR: Byron D. Jordan, B.A. (Hiram College).

SUPERVISOR: Professor Crispin Calvo.

NUMBER OF PAGES: ix, 301.

ABSTRACT

The crystal structures of PbV_2O_6 and α-VPO_5, both from within the glass-forming region of PbO-V_2O_5-P_2O_5, have been determined by X-ray methods to help provide models for the local structure of the glass. A temperature dependent displacive disordering of oxygen atoms is found in α-VPO_5. A specimen has been studied which is still ordered at room temperature but appears to be vanadium rich.

X-ray scattering intensities, measured for five compositions of $V_{1+x}P_{1-x}O_5$ glass, are compared with a model for the local structure of the glass based upon structural features from α-VPO_5. Available data on the physical properties of the glass, such as density and electrical conductivity, are discussed in relation to the proposed structural model.

Methodological problems of X-ray scattering from glass, involved with Compton scattering and multiple scattering, are discussed.

ACKNOWLEDGEMENTS

The author wishes to express great thanks to his supervisor Professor C. Calvo for his continued aid, support, and patience with this project. Thanks are also due to Professor I.D. Brown for interesting discussions and to Professor H. Grundy for aid with computer problems. Thanks go to Dr. H.N. Ng for making available his E.P.R. data on α-VPO_5. Appreciation is due to Dr. R.D. Shannon and to my fellow graduate student Dr. P. Frais, Dr. R. Gopal, Dr. F. Hawthorne, and N. Middlemiss for help and interesting discussions. I gratefully acknowledge the National Research Council and McMaster University for financial assistance.

Finally, I am immeasurably grateful to my wife, Kate, for her patience, help, and moral support throughout the course of this work.

Table of Contents

Table of Contents (Continued)

List of Tables

List of Illustrations

List of Illustrations (Continued)

CHAPTER 1

INTRODUCTION

When Fritzsche (1972) reviewed the electrical properties of amorphous semiconductors, one of the categories he used was that of "Semiconducting oxide glasses". Of the glasses listed under that category, half were formed from mixtures of V_2O_5 with other oxides. One of the more studied of the V_2O_5 based glass systems is that formed from V_2O_5 and P_2O_5. Since the work of Denton et al. (1954) and Baynton et al (1957), it has been known that $V_2O_5.P_2O_5$ glasses are semiconductors. Between then and 1965 when Mackenzie reviewed the work to date on amorphous semiconducting oxides several investigations had been made and it had been ascertained that conduction was by electron hopping from vanadium to vanadium. The vanadium was present in both the V^{5+} and V^{4+} oxidation states and the electron hopped from a V^{4+} site to a formerly V^{5+} site. The transfer of the electron was seen to be thermally activated with an activation energy of about .4eV. As the most studied of the semiconducting oxide glasses the vanadium phosphate glasses could be regarded as a prototype of the category or at least the sub-category of vanadium pentoxide based glasses.

Aside from being prototypic, the vanadium phosphate glasses have been found to have some interesting characteristics of their own. Munataka (1960) found in V_2O_5-P_2O_5-BaO glasses that the conductivity reached a maximum for a ratio of V^{4+}/V^{total} of about .2 which is rather problematic because the probability of having both electrons to hop and empty neighboring sites to hop to peaks at a charge carrier to site ratio of one half. Kitiagorodskii et al. (1960) measured the Seebeck coefficient for various values of V^{4+}/V^{total} while holding the phosphate content constant. They found the Seebeck coefficient to vary linearly with V^{4+}/V^{total} but the line does not cross the axis (indicating a change from electron to hole conduction) at 50% V^{4+} as one would expect, but at a considerably lower value. Kennedy and Mackenzie (1967) measured the Seebeck coefficient for a few compositions and found an extrapolation through 50% V^{4+} but a study of many more compositions by Linsley et al. (1970) indicated that the Seebeck coefficient fell on a family of curves, one curve per phosphate content and only those compositions in which the total vanadate content was near to the phosphate content gave curves which extrapolated across the axis at 50% V^{4+}. In this same study Linsley et al.(1970) investigated the conductivity maximum found by Munataka (1960), and they found that the D.C. conductivity, A.C. conductivity, and the thermal activation energy for the conduction process all went through extrema at approximately the same value of

V^{4+}/V^{total} however the value of this ratio yielding the extrema shifted as the phosphate to vanadate ratio was changed. Linsley et al. (1970), Adler (1971), and Sayre and Mansingh (1972) have discussed the behaviour of the conductivity maximum as a function of phosphate content on the assumption that the behaviour is a function of the structural nature of the glass.

If a structural model was needed to explain the changes in the electrical behavior with composition, the structural clues available at the time were problematic. Janakirama-Rao (1966) observed a line in the infrared spectrum of vanadium phosphate glass which was also in V_2O_5 from which he concluded a similar coordination for the vanadium in the glass to that found in V_2O_5 crystals. To explain the decrease in conductivity with increased phosphate content, he proposed that the corrogated sheets from which the structure of V_2O_5 is built are progressively attacked by phosphates and reduced to ribbonsor chains. To explain their nuclear magnetic resonance data, Landsberger and Bray (1970) built upon the argument of Janakirama-Rao and proposed that the phosphate ions come in perpendicular to the V_2O_5 - like sheet and replace a terminal oxygen protruding from the sheet with an oxygen from the phosphate. Both this argument and its antecedent assume quite drastic variation of the local environment of the vanadium, as the content of phosphate in the glass is varied. Density data from several studies which will be shown in a later chapter indicates that the density of the glass varies less in going from one P/V ratio to another than even the mass ratios. The very slight variation in the density is difficult to reconcile with the major restructuring implied by the model of Landsberger and Bray (1970).

The activation energy for conduction is mildly temperature dependent, changing smoothly from about .3eV to .4 eV at room temperature to about .05 eV to .1 eV near liquid nitrogen temperature. Schmid (1968) applied the theory of the small polaron to the conduction in vanadium phosphate glass to explain the temperature dependence of the activation energy. This theory which has had some success in describing conduction in some transition metal oxide crystals (see Austin and Mott, 1969, for review) required some modification for application to the disordered state. Following Schmid's (1968, 1969) application of the small polaron theory to conduction in vanadium phosphate glass, several theoretical and experimental investigations have used vanadium phosphate glasses as a testing ground for ideas regarding small polaron behavior. A number of these studies will be cited in later chapters. One parameter of the small polaron theory that can be extracted from conductivity data is called a polaron radius, and for reasons to be discussed, it could be assumed to be quite sensitive to major structural reordering. Sayre and Mansingh (1972) have found the polaron radius to be constant within experimental error as the phosphate content of the glass ranged from 90% to 50%, contrary to their expectations. This result is difficult to reconcile with the major structural variation inherent in the structural model of Janakirama-Rao (1966) and Landsberger and Bray (1970).

When Adler (1971) reviewed the properties of vanadium phosphate glasses, he lamented the dearth of structural information upon which to build hypotheses with regard to the electrical properties. Up to then, what structural hypotheses were invoked, usually used V_2O_5 as a reference point. Crystalline phases of vanadium phosphate had been reported before then. Brown and Hummel (1965) reported the formation of a crystalline phase in the melt system V_2O_5-P_2O_5 with the stoichiometry VPO_5. An X-ray powder pattern was reported in their paper. A different phase reported by Ladwig (1965), was formed from the dehydration of crystals of $VPO_5.2H_2O$. Ladwig concluded that the hydrates contained layers of $(VPO_5)_\infty$ with the water lightly bound between the sheets. Also in the same year, Kierkegaard and Longo (1965) published the results of a single crystal structural analysis of βVSO_5 (orthorombic phase). The structures of tetragonal phases $MoPO_5$ (Kierkegaard and Westerlund, 1964) and $MoVO_5$ (Eick and Kihlborg, 1966) are isotypic with each other and were related to tetragonal VPO_5 and VSO_5 by Ladwig (1969). Atomic positional parameters for tetragonal α-VSO_5 were refined by Longo and Arnott(1970). The crystal structure of the orthorhombic β-VPO_5 was found to be isostructural with β-VSO_5 and has been given by Gopal and Calvo (1972). A successful conversion from one phase of VPO_5 to another (short of melting and recrystallising) has not been reported. Bordes and Courtine (1972) have reported formation of both forms, but claim that the alpha form cannot be formed from the melt and must be formed by dehydration of the dihydrate as was done by Ladwig (1965). In the course of the present study, α-VPO_5 crystals have been repeatedly grown from the melt, and either powder or single crystal evidence was found that β-VPO_5 crystals were also present in the product. The crystals reported here, which were grown from the melt, had unit cell axes, reproducible from specimen to specimen to within .01 Å but which differed significantly from those reported by Bordes and Cortine (1972).

When the work reported here was begun, the crystal structure of β-VPO_5 (Gopal and Calvo, 1972) was known, and was obviously quite different from the glass structure as proposed by Landsberger and Bray (1970). It was decided to use X-ray diffraction to try to ascertain the average local environment in the glass. The first crystals of α-VPO_5 were grown during preliminary tests of how slowly the melt could be cooled without inducing crystallisation. Once the initial crystals were prepared, attempts were made to grow larger crystals with some success. The crystals were found to have some interesting disorder properties, but proved most useful by providing the most fruitful set of hypotheses for the glass structure.

The vanadium phosphate glasses are but one of several semiconducting glass systems which are formed by the fusion of V_2O_5 with another oxide. On the suspicion that the end member, V_2O_5, may have much in common with the glasses formed by it, Kennedy et al. (1967) investigated some of the properties of crystalline V_2O_5 and amorphous V_2O_5. Unable to produce vitreous V_2O_5 by quenching the melt, they formed the amorphous V_2O_5 by condensation of the vapour in near vacuum. This recurrent theme of similarity between V_2O_5 and its glasses was tested again in the V_2O_5-PbO system. X-ray diffraction of the glass was not done, but a crystalline phase was examined from within the glass forming region of the phase diagram. In phase diagrams prepared by Amadori (1916) and by Shimohira et al. (1967) a deep eutectic (about 500°C) is indicated at the 1/1 V_2O_5 to PbO composition. Rawson (1967) has alluded to the deep eutectic in the PbO-V_2O_5 system as an example of the "liquidus temperature effect" in which a low eutectic is correllated with a glass forming region. In this study PbV_2O_6 crystals were grown several times. The melting temperature of the crystals was found to be about 100°C higher than the reported eutectic and X-ray powder diffraction gave evidence of congruent melting. The crystal structure is given in Chapter 4 and compared briefly with V_2O_5 and the vanadium bronzes.

In Chapter 2 the theory of x-ray scattering from crystalline and amorphous solids is reviewed and computational procedures discussed. Chapter 3 describes the diffractometer used for the study of the glasses and the experimental procedures followed. The major portion of Chapter 3 discusses corrections for Compton scattering and multiple scattering. Chapter 4 describes the crystal structure of PbV_2O_6. The crystal structure of α-VPO_5 and disordering in this crystal are discussed in Chapter 5. In Chapter 6 a model is proposed for the local structure in vanadium phosphate glasses and is tested against the x-ray scattering results. The final chapter is devoted to testing the implications of the glass model against the published physical properties of the glass.

CHAPTER 2

X-Ray Diffraction

2.1 General Features

X-ray diffraction is a scattering experiment in which a beam of X-ray photons are directed at a target and the scattered photon beam intensity is detected at some point in space. Such an experiment is traditionally described by a function of angle and energy known as a differential cross section. The initial beam of X-rays of wavelength λ with angular frequency ω' and polarisation direction $\underline{\varepsilon}_1$ is characterised by a vector $\underline{S}_{in}$ whose magnitude is $2\pi/\lambda$, that defines the direction of propagation. The probability that a photon from this beam will be scattered at the target with energy between ω and $\omega + d\omega$ into a solid angle $d\Omega$ is called the differential cross section and is written as $\frac{d^2\sigma}{d\omega d\Omega}$. The direction of propagation of the scattered beam (from sample to detector) is defined by a vector $\underline{S}_{out}$ of the same magnitude as $\underline{S}_{in}$. The difference vector $\underline{S}_{out} - \underline{S}_{in}$ is denoted as $\underline{S}$ and has a magnitude of $4\pi \sin(\theta)/\lambda$ where 2θ is the angle between $\underline{S}_{in}$ and $\underline{S}_{out}$. The differential cross section of X-ray scattering can be expressed, after Egelstaff (1967), with slight change in notation in terms of the Van Hove (1954) scattering and correlation functions as:

$$\left(\frac{d^2\sigma}{d\Omega d\omega}\right) = \left(\frac{d\sigma}{d\Omega}\right)_{\text{Thomson}} \frac{1}{2\pi} \int d\underline{r}\, dt \left(G_e(\underline{r}, t) - \bar{\rho}_e\right) e^{i(\underline{s}\cdot\underline{r} - \omega t)}$$

where the space and time correlations function $G_e(\underline{r},t)$ is defined in terms of the electron density $\rho(\underline{r})$ as:

$$G_e(\underline{r},t) = \frac{1}{N}\int d\underline{r}' \langle \rho_e(\underline{r}',0) \cdot \rho_e(\underline{r}+\underline{r}', t)\rangle$$

where N is the number of electrons and $\bar{\rho}_e$ is the average electron density. The constant of proportionality expressed explicitly above as $(d\sigma/d\Omega)_{\text{Thomson}}$ is the cross section for X-ray scattering from a singleelectron. Called the Thomson cross section, it can be expressed as (Platzman , 1972).

$$\left(\frac{d\sigma}{d\Omega}\right)_{\text{Thomson}} = \left(\frac{e^2}{mc^2}\right)^2 \left(\underline{\varepsilon}_{in} \cdot \underline{\varepsilon}_{out}\right)^2 .$$

where e is the electronic charge, m the electronic mass, and c is the speed of light. The dot product of the polarisation vectors gives rise to a function of scattering angle which is calculated for a given experimental situation and removed from the scattering data as a polarisation correction. The scattering may be categorised by the energy transfer parameter ω into elastic ($\omega = 0$), inelastic ($\omega \neq 0$), or total scattering (integrated over all ω). The two most relevant inelastic scattering processes for X-rays from electrons are electronic excitations and scattering from atomic vibrations.

The former is ordinarily a photoelectric event in which an electron receives enough energy from the X-ray to expel the electron from its atom with some kinetic energy left over. The scattered X-ray has, in this case, a longer wavelength after scattering. If θ is the half-scattering angle (see above) the spectrum of the scattered X-rays will have in addition to the source spectrum a new line C called Compton modified line with its centre shifted from the parent line in the exciting spectrum by .0485 $\sin^2(\theta)$ Å, to a first approximation. The initial kinetic energy of the electron during the scattering will influence the shape of the shifted line. In the Impulse Approximation (Platzman, 1965 and 1972), the momentum transferred to the electron in the Compton process is called $\underline{K}$. If the electron's mass is m and its initial momentum was $\underline{P}$, the electron's kinetic energy is increased from $P^2/2m$ to $(\underline{P} + \underline{K})^2/2m$, but

$$\frac{(P + K)^2}{2m} = \frac{P^2}{2m} + \frac{K^2}{2m} + \frac{2\ K\ .\ P}{2m} \quad .$$

The shift in the centre of the Compton line is identified with $K^2/2m$ and the $\underline{K}\ .\ \underline{P}\ /m$ term gives rise to the shape of the shifted line. With the momentum transfer, $\underline{K}$, determined by the experimentally set scattering angle, the line shape of the shifted spectrum is determined by a projection of the momentum distribution of the electrons during the scattering. The Compton scattering is, to the present experiment, an undesirable background to be filtered out when possible. The filtration process is found to be imperfect, and some Compton scattering leaks through the monochrometer. This leakage and the relevance of the sample dependent Compton line shape will be discussed below.

The other common form of inelastic scattering comes from the atomic vibrations. The energy transferred to or from the X-ray in the process is minute in comparison to the X-ray energy and is also small in comparison to the natural line width of the exciting spectrum. Experimentally selecting against this inelastic scattering is impractical and, consequently, the "total" scattering is observed with regard to this process. It will be assumed in this discussion that the Compton inelastic scattering, which is incoherent, has been removed experimentally or analytically from this data, and the term "inelastic scattering" will refer to the vibrational scattering.

If the "total" scattering is detected, the corresponding correlation function (Egelstaff,1967; Leadbetter and Wright, 1972a), $G_e(\underline{r}, t)$ becomes $G_e(\underline{r},0)$. The time dependence of the correlation functions will be, consequently, suppressed in following discussions.

An ubiquitous relation in the theory of X-ray scattering is the convolution operation. Let $H(\underline{s})$ and $Q(\underline{s})$ be functions whose Fourier transforms, $h(\underline{r})$, $g(\underline{r})$, respectively, exist. The Convolution theorem (see Amoros and Amoros, 1968) states that the Fourier transform of the product $H(s)\ Q(\underline{s})$ will be the function $m(\underline{r}) = h(\underline{r})*g(\underline{r})$ where the convolution operation (*) is defined by:

$$m(\underline{r}) = h(\underline{r}) * g(\underline{r}) = \int d\underline{r}'\ h(\underline{r}')\ g(\underline{r} - r').$$

The same process works for the reverse Fourier transform from the $\underline{r}$ functions to the $\underline{s}$ functions. It can be seen that effects or aberrations which multiply an intensity function $(\underline{s})$ will enter the corresponding correlation function $(\underline{r})$ as a convolution. It also is important for another property. Under some circumstances a function of a sum of arguments can be expressed as a convolution of functions of those arguments. If, for example, a is a random variable with probability distribution A(a) and b is a random variable, uncorrelated with a, with probability distribution B(b) then the probability distribution C of $c = a + b$, (Margenau and Murphy, 1956) is the convolution of A and B,

$$C(a + b) = A(a) * B(b).$$

This latter property may be exploited in the following manner. Let the position of an electron in space be $\underline{R}$, and let that electron be associated with an atom whose nucleus is at position $\underline{r}'$ in space. The vector $\underline{r} = \underline{R} - \underline{r}'$ will run from the nucleus to the electron. If $\phi(\underline{r}')$ is the density function for the location of the nucleus and $\rho(\underline{r})$ is an electronic density function for the atom, and if these two distributions are considered independent, the electronic density as a function of R can be expressed as a convolution of $\rho(\underline{r})$ and $\phi(\underline{r}')$ and furthermore the Fourier transform of this function will be the simple product of the separate Fourier transforms of $\rho(\underline{r})$ and $\phi(\underline{r}')$.

Although the X-rays scatter from the electronic density, the object of structural investigations with X-rays is usually to ascertain the distribution of atoms. If (Egelstaff, 1967) the electrons associated with an atom are assumed to move with it rigidly and if the internal electronic states are not excited by the X-ray scattering, the differential cross section given above becomes for a monatomic sample,

$$\left(\frac{d^2\sigma}{d\Omega d\omega}\right) = \left(\frac{d\sigma}{d\Omega}\right)_{\text{Thomson}} \frac{1}{2\pi} \left|f(s)\right|^2 \int d\underline{r}\, dt\, e^{i(\underline{s}\cdot\underline{r} - \omega t)} (G(\underline{r},t) - n_o)$$

where $G(\underline{r}, t)$ is a correlation function for the position of the centres of the atoms and n_o is an average atomic number density and $f(s)$ is called the atomic scattering factor and corresponds to the Fourier transform of the electronic density of one atom.

2.2 Scattering from Atoms

For each atomic and several ionic species there are three useful functions tabulated in the literature. These are the form factor, the incoherent intensity, and the anomalous dispersion factors. If $\rho_n(r)$ is the electronic density for electronic state n, the atomic form factor for a spherical atom is

$$f(s) = \int_{\text{atom}} \rho(\underline{r})\, e^{i\underline{s} \cdot \underline{r}}\, d\underline{r} = \underset{\text{electronic states}}{\Sigma_n} \int 4\pi\rho_n(r)\, \frac{\sin(sr)}{sr}\, r^2 dr$$

The functions $\rho_n(r)$ transformed in this way have been computed to various levels of sophistication. Cromer and Waber (1965), for example, used relativistic self-consistent Hartree-Fock-Slater wave functions. Cromer (1969) has also calculated the Compton intensity function from the Waller-Hartree (1929) formula. In this formula, $\langle m|$ is an atomic state, and the matrix element f_{nm} is given below.

$$f_{nm} = \langle n|e^{i\underline{s} \cdot \underline{r}}|m\rangle$$

$$I_{inc} = I_{Thomson} \{Z - \Sigma_n \Sigma_m |f_{nm}|^2\}$$

Z is the atomic number in the above, and the coherent scattering factor is the trace of the f_{nm} matrix. It can be seen that f and I_{inc} each have a maximum value of Z (although for opposite limits of s), and that the coherent intensity, which is proportional to f^2, will have a maximum of Z^2.

When the X-ray beam has an energy slightly in excess of that needed to induce photoelectric emission of an inner electron from one of the target atoms, the absorption will be greatly enhanced. The dispersive response of the medium is related to the absorptive response through an integral transform called a Kramers-Kronig transform. One of the early applications of this transform (Kronig, 1926) was to relate the scattering enhancement to the absorption coefficient. Both effects can be entered into the general formalism by allowing the scattering factor to become complex, such that $f(k)$ becomes $f(k) + \Delta f\ (k,\lambda)$ where the normal $f(k)$ is only a function of the target atom and the Δf terms, real and imaginary parts, are a function also of the wavelength, λ, of the exciting radiation. Rearranging some terms in James (1967) the relationships may be expressed as follows:

$$\Delta f''(\omega_i) = \sum_{\substack{\text{absorption} \\ \text{edges } \kappa}} \frac{mc}{4\pi e^2}\, \omega_i\, \mu_\kappa(\omega_i)$$

$$\Delta f'\ (\omega_i) = \frac{2}{\pi\omega_i} \int_0^\infty \frac{\Delta f''(\omega)\omega^2 d\omega}{\omega_i^2 - \omega^2}$$

The X-ray frequency is denoted as ω_i and μ_κ is the contribution from the κ absorption edge to the absorption coefficient. The absorption coefficient must be known for all frequencies, and either an empirical fit to measured absorption coefficients integrated, or the missing values can be calculated from transition matrix elements between the wave functions which were used for the scattering factor calculations. This procedure was followed by Cromer (1965). An alternative procedure, followed by Cromer and Lieberman (1970), was to treat the entire problem relativistically and to compute the photoelectric absorption cross section theoretically and to numerically transform the results, thus bypassing the semi-empirical procedure.

The effect of $\Delta f'$ is to make the atom scatter as if it had a few more or less electrons. This is not equivalent to a change of ionisation state, because the outer electrons transform to give their contribution to f(s) at low values of s. The $\Delta f'$ increment is reasonably constant for all values of s. When Cr K_α X-rays are scattered from vanadium, the scattering factor for vanadium at a $\sin(\theta)/\lambda$ value of .4. is decreased to two thirds of the uncorrected value.

When the anomalous dispersion is important, the assumption made above that the internal electronic status of the atom are unaffected by the X-ray breaks down. The simple identification of the differential cross section with the Fourier transform of the electronic Van Hove correlation function is less appropriate when anomalous dispersion is significant. Blume (1965), however, has shown that the form of the cross section expression with the atom-atom correlation function remains applicable if the atomic scattering factors are corrected for anomalous dispersion.

2.3 Description of Order

2.3.1 Glass or Liquid

The original $G(\underline{r})$ function needed no subscripts because all the scatterers were electrons. When the scattering centres differ as in a polyatomic glass, one can expand G into a set of functions G_{ij} corresponding to pairs made up of an atom, of type i and one of type j such that:

$$G(\underline{r}) = \Sigma_{ij} G_{ij}(\underline{r})$$

where $G_{ij}(\underline{r})$ can be further separated into two terms, a "self" term and a "distinct" term

$$G_{ij}(\underline{r}) = \delta_{ij} \delta(\underline{r}) + n_{ij}(\underline{r})$$

where the i and j on the self term correspond to the same atom (not just the same type) and the distinct term, $n_{ij}(\underline{r})$, which applies to pairs of different atoms of the same or differing types.

The coherent scattering intensity of the sample relative to the intensity which would be produced by a single electron of the sample will be denoted as I(s). The single electron factor to which I(s) is relative is the Thompson cross section $(\frac{d\sigma}{d\Omega})_{\text{Thompson}} \cdot (d\Omega)_{\text{measured}}$. The intensity I(s) may be further separated into a sum over a set of intensity functions $I_{ij}(\underline{s})$ which correspond to the Fourier transforms of the $G_{ij}(\underline{r})$ function by the following relations.

$$I_{ij}(\underline{s}) = f_i(s)\, f_j(s) \int G_{ij}(\underline{r})\, e^{i\underline{s} \cdot \underline{r}}\, d\underline{r}$$

which, breaking G_{ij} into its self and distinct parts yields

$$I_{ij}(\underline{s}) = f_i(s)\, f_j(s) \int d\underline{r}\, e^{i\underline{s} \cdot \underline{r}} \{\delta_{ij}\delta(\underline{r}) + n_{ij}(\underline{r})\}$$

which reduces to

$$I_{ij}(s) = \delta_{ij}\, f_i^2(s) + f_i\,(s)\, f_j(s) \int n_{ij}(\underline{r})\, e^{i\underline{s} \cdot \underline{r}}\, d\underline{r}$$

and using the average

$$< e^{i\underline{s} \cdot \underline{r}} >_{\text{all angles}} = \frac{\sin(sr)}{sr}$$

the intensity becomes

$$I(s) = \Sigma_i\, f_i^2\,(s) + \Sigma_{i \neq j} 4\pi \int r^2 dr\, n_{ij}(r)\, \frac{\sin(sr)}{sr}\, f_i(s) f_j(s)$$

In the above notation $\underline{r}$ or $\underline{s}$ without a vector sign refers to the vector's magnitude. The function $n_{ij}(\underline{r})$ is a pair distribution function for atoms of types i and j, and the sums are taken over all atoms. If a "unit of composition" (Warren, 1969) is taken to include a convenient set of atoms with the appropriate stoichiometry, for example, one vanadium, one phosphorus and five oxygens for VPO_5 glass, and if N is the number of such units in the sample, some simplification can occur in the above integral. The integral's first problem is convergence, and to ameliorate this, an average atomic number density N/V (sample volume) can be added and subtracted from the density $n_{ij}(r)$. The resulting intensity becomes:

$$\frac{I(s)}{N} = \Sigma_{uc} \{ f_i^2(s) + 4\pi f_i(s) f_j(s) \int r^2 dr \frac{\sin(sr)}{sr} (n_{ij}(r) - n_o)$$

$$+ 4\pi \, \Sigma_{uc} f_i(s) \, f_j \frac{(s) n_o}{s} \underbrace{\int r dr \sin(sr)}_{\substack{\text{integral over} \\ \text{sample volume}}}$$

Information is extracted from the X-ray intensities by either Fourier transforming the intensities to give pair functions or by calculating the intensities from a model structure and making a comparison in the intensity domain. A model structure could also be used to fit the pair function. In practice both domains are useful. Before the X-ray intensity can be Fourier transformed to yield a pair function, it must be scaled to electronic units and purged of all intensity that does not represent single coherent scattering events. Since,

$$I(s)_{eu} = \beta I_{obs}(s) - L(s)I_{inc.}(s) - I_{air}(s) - I_{mult}(s) - I_{s.a.}(s) .$$

The number β scales the intensity to electronic units and $I_{inc}(s)$ is the sum over the unit composition of the atomic I_{inc} relative to the Thomson cross section. The incoherent term is multiplied by a leakage function for the monochrometer which describes the angularly dependent efficiency of the monochrometer for removing Compton scattered X-rays. Multiple scattering (X-ray scattered more than once within the target) and small-angle scattering and air scattering must be removed, if they are significant. It is assumed that any real background (γ-rays) and absorption and polarisation corrections have been treated as preliminary corrections. All the corrections in the above equation will be collected into a single function B(s). The normalisation constant β is determined either by reference to an external intensity standard (Wagner, 1972), or as in the case of the present study, by the requirement that the scaled intensity minus the B(s) function should oscillate evenly about the independent scattering term $\Sigma f_i^2(s)$. Alternatively, the scaled intensity could be said to oscillate about $\Sigma f_i^2(s) + B(s)$. Details of the various corrections, functions, and procedures are given in a later section under the topic of data treatment. The function i(s), defined below, is the function to be Fourier from which the total pair distribution function may be extracted, and is given by:

$$i(s) = \beta I_{obs}(s) - B(s) - \Sigma_{uc}\ f_i^2(s).$$

The function I(s) has been normalised to the Thomson cross section such that I(s) represents the scattering of the sample relative to the scattering of a single electron. In this system of units, called electronic units, $f^2(0)$ is Z^2 in electron^2 and $n_{ij}(r)$ is in units of atoms squared times their respective electron content squared to give electron^2 units also.

Up to this point it has been assumed that the indicated Fourier integrals are really Fourier integrals, which they would be, were it possible to continue the volume integral to infinity. This defect may be formally corrected by introducing a function $T(\underline{r})$ which is one inside the irradiated volume of the sample and equal to zero outside this volume. Keeping in mind that the scattered intensity is proportional to the square amplitude of the Fourier transform of the scatterer density, or equivalently, the Fourier transform of that density's self convolution, one can see that the function $T(\underline{r})$ will enter the intensity function as its transform square or will enter the atomic density function as its convolution square, $v(\underline{r})$(Wagner, 1972). Unless the sample is a suspension of very fine particles, it can be assumed that the volume of the sample is many orders of magnitude greater than the molecular ordering which governs the function $n_{ij}(r) - n_o$. For the transform of that function it can normally be taken for granted that $n_{ij}(r) - n_o$ will be zero long before $v(r)$ is significant. For the integral of n_o this is not true, and this integral is proportional to the transform of $v(r)$. If the sample is of microscopic dimension, the reciprocal nature of the Fourier transform dictates that its transform be confined to very low values of s. In a normal experiment the scattering from this term of the cross section will be engulfed by the source beam and inaccessible to measurement. Any minute portion of this small-angle scattering which may extend into the domain of measurement is assumed to have been calculated and substracted from the observed intensities. Warren (1969) has given an expression for this correction for the type of scattering geometry used in the present experiment. The term in the intensity function that arises from the delta function in $G_{ij}(r)$ is called the independent scattering and is a sum of $f_i^2(k)$ terms. In practical units and at reasonably accessible angles, Warren's small-angle term reduces to

$$\frac{I_{eu}^{\text{small angle}}}{I_{eu}^{\text{indep.}}} \simeq \frac{\text{density(atoms/cc)}\,D(\text{cm})\,\lambda^4(\mathring{A})\,\mu(\text{cm}^{-1})\times 1.1\times 10^{-9}}{\alpha\ (\text{degrees})\qquad \sin^4(\theta)}$$

where D is the X-ray tube to sample distance, α is the angular divergence of the beam, λ is the wavelength, and μ is the linear absorption coefficient. In this experiment, any measurement, taken at angles for which this correction exceeded one half percent, was considered qualitative only and excluded from all calculations.

The function i(s) could simply be Fourier transformed to give an electronic density correlation function (Leadbetter and Wright, 1972a), $\tilde{D}_e(r)$, given by

$$\tilde{D}_e(r) = \frac{2}{\pi} \int_0^\infty si(s) \sin(sr) dk$$

or could be expressed in terms of the electronic density ρ_e by

$$\tilde{D}_e(r) = 4\pi r \{\rho_e(r) * \rho_e(r) - \bar{\rho}_e\} .$$

The electronic correlation function is relatively featureless with very broad peaks because the electronic clouds around each atom are convoluted with the interatomic peaks. The function is further broadened by the termination effect. The ideal expression above must be altered to take into consideration the physical fact that an X-ray cannot change its direction of flight by more than 180 degrees. There is a maximum s less than or equal to $4\pi/\lambda$. If $\Xi(s)$ is defined to be one for all s less than or equal to s_{max} and to be zero for all s greater than s_{max}, the alteration may be expressed as follows.

$$D_e(r) = \frac{2}{\pi} \cdot \int_0^{s_{max}} s i(s) \sin(sr) ds = \frac{2}{\pi} \int_0^{\infty} \Xi(s) s i(s) \sin(sr) ds$$

The transform of $\Xi(s)$ is now convoluted with $\tilde{D}_e(r)$ to give $D_e(r)$, which is experimentally accessible. The atomic pair correlation function can be extracted from $D_e(r)$ by deconvolution through the convolution theorem.

If the target were a monatomic material, dividing $i(s)$ by $f^2(s)$ would deconvolute the electronic cloud from the atomic pair correlation function. The termination effect (the transform of $\Xi(s)$) would remain. For a polyatomic target material, a partial deconvolution can be effected by the use of a sharpening function $f_e^2(s)$ which is the square of the average scattering factor, normalised to be one at $s = 0$, by

$$f_e^2(s) = \{\Sigma_{uc} f_i\}^2 / \{\Sigma_{uc} Z_i\}^2 .$$

That which is still left of the electronic cloud after the partial deconvolution with $f_e^2(s)$ joins the termination effect in the production of a resolution function $P_{ij}(r)$ which must be convoluted with any model peak before comparison may be made with the transform of the experimental intensity. The atomic pair distribution, weighted by the product of the numbers of electrons, can be expressed after Leadbetter and

Wright (1972a) as the following:

$$D(r) = \Sigma_{ij} d_{ij}(r) = \Sigma_{ij} \tilde{d}_{ij}(r) * P_{ij}(r)$$

where

$$P_{ij}(r) = \frac{1}{\pi} \int_0^\infty \Xi(s)\, f_i(s) f_j(s) \frac{M(s)\cos(sr)ds}{f_e^2(s)}$$

A function M(s) has been included in the definition of $P_{ij}(r)$. This represents a weighting function which is often included to counter the effect of the termination effect which has been greatly enhanced by the sharpening function. D(r) represents the following transform of the intensity:

$$D(r) = \frac{2}{\pi} \int_0^\infty \Xi(s) \frac{si(s)M(s)\sin(sr)ds}{f_e^2(s)}$$

where the common forms of M(s) are

$$M(s) = 1$$

or $M(s) = e^{-\alpha s^2}$ (with α chosen such that $M(s_{max})$ is about .1)

or $M(s) = \sin(\pi s/s_{max})/(\pi s/s_{max})$.

All three forms of weighting function have been used in this study. The third function in the list is due to Lorch (1969) and has been found by Leadbetter and Wright (1972a) to be more efficient in combating the distortions caused by termination than the Gaussian weighting function. The general idea is to include in the $P_{ij}(r)$ resolution function any aberration that may be in the transform of the reduced intensity.

The D(r) function, the transform of the reduced intensity, has been expressed above as a sum over $d_{ij}(r)$ functions, each of which was a convolution of the resolution function $P_{ij}(r)$ with an ideal pair correlation function $\tilde{d}_{ij}(r)$. An equivalent description of the structure can be found in the pair distribution function of Warren (1969). In Warren's formalism, a sum is explicitly taken over a set of distances r_ν with due regard to the convoluting effect of $P_{ij}(r)$. With each distance, could be associated a function $\delta(r - r_\nu)$ and the distribution of r_ν values could be entered into the formalism with a convolution. In the formalism of Leadbetter and Wright (1972a), the function to be fitted would be D(r) which oscillates about zero and represents a deviation from the average densities. Expressing this explicitly,

$$D(r) = \Sigma_{ij}\ d_{ij}(r) = \Sigma_{ij}\ r(4\pi n_{ij}(r) - 4\pi n_j^o) * P_{ij}(r).$$

The term containing the average atomic density may be isolated as $D_o(r)$, where

$$D_o(r) = 4\pi r\{\Sigma_{uc} Z_i\}^2 n^o$$

and

$$n^o = \Sigma_j n_j^o .$$

The function which Leadbetter and Wright (1972c) call the total correlation function, $D(r) + D_o(r)$, oscillates about a ramp function $D_o(r)$ the slope of which is proportional to the average electron density. When the total correlation function is multiplied by $\pi/2$ it is the same as that used by Mozzi and Warren (1969) and discussed by Warren (1969), and called by them the pair function distribution curve. As noted by Leadbetter and Apling (1974) there are some advantages to the use of the total correlation function when fitting a model, and this is the function which will be plotted in the present report. The equivalence between the $d_{ij}(r)$ based description of a structure to Warren's pair function description has been demonstrated by Renninger <u>et al.</u> (1974). The total correlation function, with Warren's $\pi/2$ convention, will be called $W(r)$, where

$$W(r) = \Sigma_{uc} \Sigma_\nu \frac{\pi}{2} C_{ij\nu} P_{ij}(r - r_\nu)/r_\nu = \frac{\pi}{2} (D(r) + D_o(r)).$$

The function $r(D(r) + D_o)$ follows the quadratic function $4\pi r^2 \{\Sigma_{uc} Z_i\}^2 n_o$ and is called the radial distribution function. A peak in the radial distribution function due to a single r_{ij} distance will not be symmetric, as it is in the W(r) function, because of the skewing effect of multiplication by r.

Distortions inherent in the glassy state may make the description of a given interatomic pair $d_{ij}(r_\nu)$ by $\delta(r - r_\nu)$ inadequate, and a distribution of r_ν values must be introduced. This was done, for example, by Leadbetter and Apling (1974) by generating a set of r_ν defined by a Gaussian distribution centred on an $\overline{r_\nu}$,and summing over the set. An alternative procedure, used in this study, uses the Convolution Theorem to produce the same result directly. Let $t_\nu(x)$ be a Gaussian distribution with width parametrised by σ_ν and normalised to unit area. If atoms of types i and j are $r_\nu \pm \sigma_\nu$, Angstroms apart, including vibrations and distortions in σ_ν, and if there are $C_{ij\nu}$ such vectors (for example the four P-O distances in a PO_4 tetrahedron), $\tilde{d}_{ij}(r)$ may be expanded in the following form, where a d'_{ij} is the total correlation equivalent of $d_{ij}(r)$,

$$\tilde{d}_{ij}(r) = \Sigma_\nu \, \delta(r - r_\nu) * t_\nu(r) \, C_{ij\nu} \, .$$

The Gaussian function t_ν of arbitrary distance argument x is defined by:

$$t_\nu(x) = \frac{e^{-x^2/2\sigma_\nu}}{\sqrt{2\pi\sigma^2}}$$

and its Fourier transform is:

$$T_{\nu}(k) = e^{-s^2\sigma_{\nu}^2/2} .$$

A modified peak function, broadened by convolution with the Gaussian function $t_{\nu}(x)$ can be generated from the relation:

$$P_{ij}^{\nu}(x) = P_{ij}(x) * t_{\nu}(x) = \frac{1}{\pi} \int_0^{\infty} ds \, \Xi \, \frac{(s)M(s)T}{f_e^2(s)} \nu(s) f_i(s) f_j(s) \cos(sx)$$

where the convolution theorem has been applied. The functions $d'_{ij}(r)$ may now be expressed in terms of a sum of P_{ij}^{ν} functions by:

$$d'_{ij}(r) = \tilde{d}'_{ij}(r) * P_{ij}(r) = \Sigma_{\nu} C_{ij\nu} P_{ij}^{\nu}(r - r_{\nu}) .$$

In practice this procedure is very easy to implement because all the functions in the integral over s, except cos (sx), are very slowly varying functions of s. The $P_{ij}(x)$ function in general has a peak at x = 0 which is on the order of half an Ångstrom in extent with small oscillations continuing outward from there. If x is confined to be less than 1.25 Å it was found that a nine point Gaussian quadrature algorithm sampled the integrand adequately. Gaussian quadrature involves a weighted sum of integrand values, taken at s_n positions which are dictated by the roots of an n^{th} order Legendre polynomial (Kopal, 1955). Once s_{max} is given, the integrand can be evaluated at nine chosen values of s and stored, except for $T_\nu(s)$ and cos (xs) which must be calculated for each call of the subroutine.

A great deal of computing could be saved if the K-approximation of Warren, Krutter and Morningstar (1936) were applicable. If the scattering factors of all the atoms in the target material are similar, as they would be for a mixture of near neighbours on the periodic table, then constants K_i and K_j might be found to satisfy the following relation:

$$K_i \; K_j \;\simeq\; \frac{f_i(s)\; f_j(s)}{f_e^2(s)}$$

On the following page is a graph of the above function of s for the peaks in $V_{1+x}P_{1-x}O_5$ glass for the five compositions examined in this study. Because $f_e^2(s)$ is an average over the unit composition, it changes with stoichometry. It can be seen from the graphs that the K-approximation is inapplicable for this study. The illustration following that shows $P_{ij}^{\nu}(r - r_\nu)$ where r_ν is one Angstrom and σ_ν is one tenth of an Angstrom. The vanadium-vanadium peak is also plotted for four vanadium ionisation states to illustrate the relative insensitivity of P_{ij} to that factor.

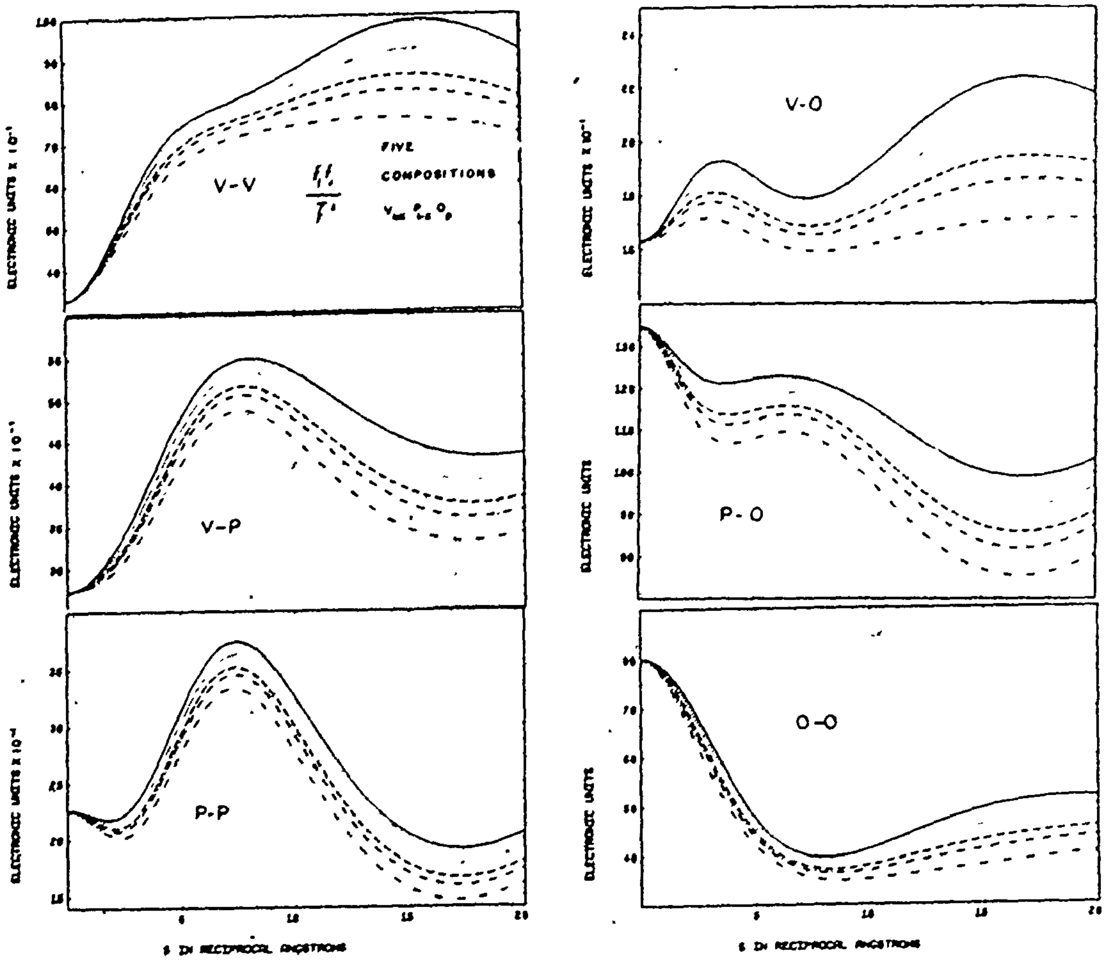

Illustration 2.1. The functions $f_i(s)\, f_j(s)/ \bar{f}^2(s)$ are plotted for the five compositions of vanadium phosphate glass investigated in the present experiment. The compositional dependence comes from the average scattering factor in the denominator.

Illustration 2.2 (a)

The peak functions P^{ν}_{ij} (r − 1.0 Å) are plotted with σ_{ν} = .1 Å for each type of atom pair in VPO_5.

Illustration 2.2 (b)

The vanadium-vanadium P^{ν}_{vv}(r − 1.0 Å) peak functions for four vanadium ionisation states.

The curves correspond to:

———	V^{0+}
.....	V^{2+}
- - -	V^{3+}
-.-.-	V^{5+}

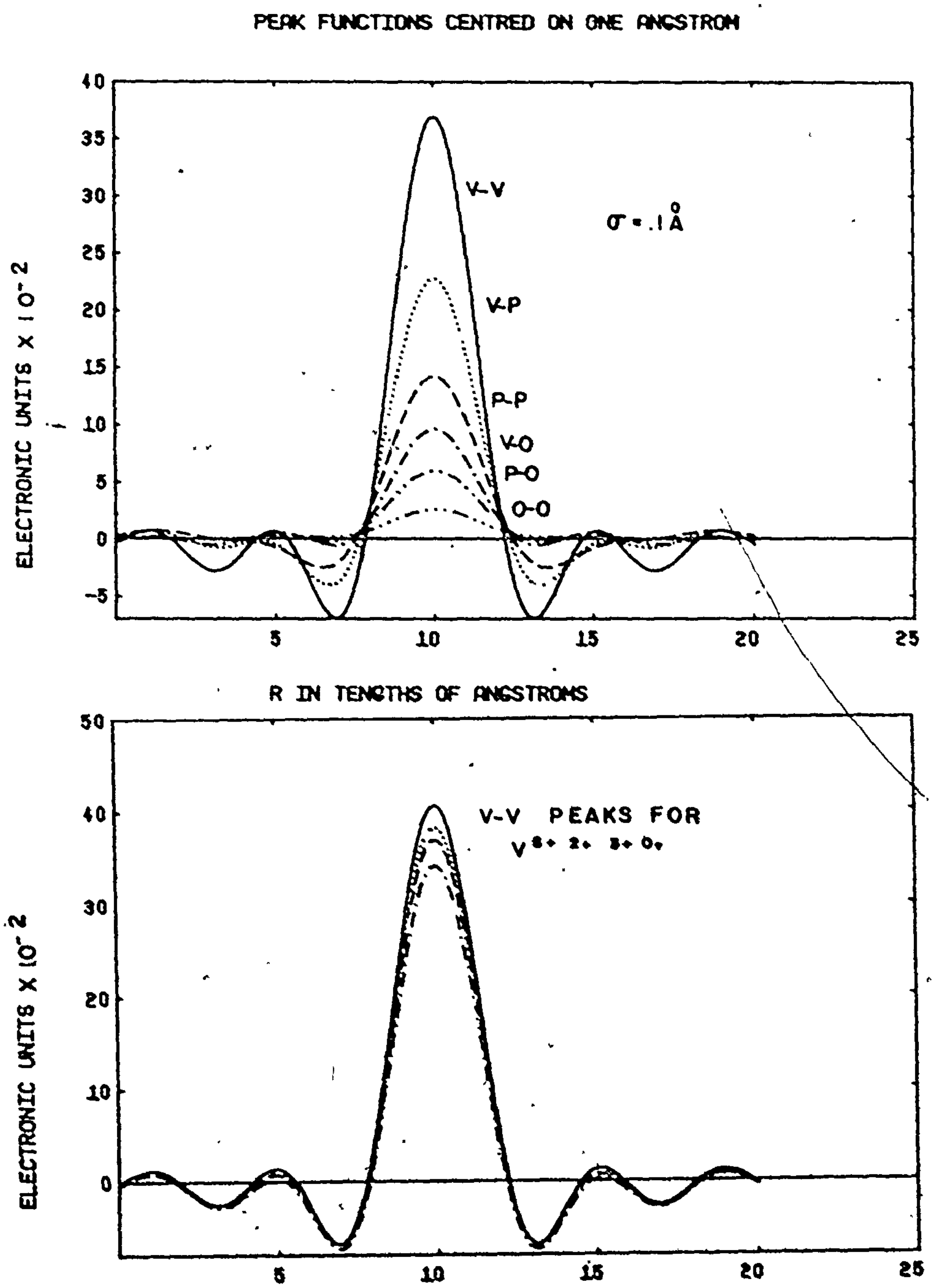
PEAK FUNCTIONS CENTRED ON ONE ANGSTROM
ELECTRONIC UNITS X 10^-2
40
35
30
25
20
15
10
5
0
-5
V-V
V-P
P-P
V-O
P-O
O-O
σ = .1 Å
5
10
15
20
25
R IN TENGTHS OF ANGSTROMS
ELECTRONIC UNITS X 10^-2
50
40
30
20
10
0
V-V PEAKS FOR
V 5+ 2+ 3+ 0+
5
10
15
20
25

2.4. X-ray Scattering from Crystals

In the beginning of this chapter, the differential scattering of X-rays from a collection of electrons was expressed in terms of an electron density Van Hove correlation function $G_e(\underline{r}, t)$. The time dependence was later suppressed and $G_e(\underline{r})$ was expressed in terms of the electron density $\rho(\underline{r})$ as:

$$G_e(\underline{r}) = \frac{1}{N} \int d\underline{r}' < \rho_e(\underline{r}') \rho_e(\underline{r} + \underline{r}')>.$$

This is almost the self convolution of $\rho_e(\underline{r})$. It is the convolution of $\rho_e(\underline{r})$ with $\rho_e(-\underline{r})$ or:

$$G_e(\underline{r}) = < \rho_e(\underline{r}) * \rho_e(-\underline{r})>.$$

If $\rho_{\underline{s}}$ is the Fourier transform of $\rho_e(\underline{r})$,

$$\rho_{\underline{s}} = \int d\underline{r}\, e^{i \underline{s} \cdot \underline{r}} \rho_e(\underline{r})$$

then the Fourier transform of $G_e(\underline{r}) = < \rho_e(\underline{r}) * \rho_e(-\underline{r})>$ is $\rho_{\underline{s}}\, \rho_{-\underline{s}}$ or $\rho_{\underline{s}}\, \rho^*_{\underline{s}}$ where the asterisk as a superscript implies complex conjugation. The scattered intensity will then be proportional to $\underline{\rho}*\underline{\rho}$.

In a perfect crystallite the electron density averaged over a time long compared to vibrational periods, is assumed to be periodic in all three dimensions. It is assumed that there can be chosen three noncoplanar vectors $\underline{a}_1$ $\underline{a}_2$ and $\underline{a}_3$ such that:

$$\rho(\underline{r}) = \rho\,(\underline{r} + m\underline{a}_1 + n\underline{a}_2 + p\underline{a}_3)$$

where m, n, and p are any integers . A parallelopiped of volume $V_c = \underline{a}_1 * (\underline{a}_2 \times \underline{a}_3)$ is repeated throughout the crystal and is called the unit cell. The Fourier transform of the electron density in the crystal is now:

$$\rho_{\underline{S}} = \int_{\text{crystal}} d\underline{r}\; e^{i\,\underline{S}\,\cdot\,\underline{r}}\, \rho(\underline{r})$$

which becomes

$$\rho_{\underline{S}} = \Sigma_{m,n,p} \int_{\text{unit cell}} \rho(\underline{r})\; e^{\,i\underline{S}\,\cdot\,(\underline{r} + m\underline{a}_1 + n\underline{a}_2 + p\underline{a}_3)} d\underline{r}$$

$$\rho_{\underline{S}} = \Sigma_{m,n,p} \int_{\text{unit cell}} d\underline{r}\; \rho(\underline{r})\; e^{i\underline{S}\,\cdot\,\underline{r}}\; e^{i\underline{S}\,\cdot(m\underline{a}_1 + m\underline{a}_2 + p\underline{a}_3)}$$

and, because the second exponential is independent of $\underline{r}$ becomes:

$$\rho_{\underline{S}} = \int_{\text{unit cell}} d\underline{r}\; \rho(\underline{r})\; e^{i\underline{S}\,\cdot\,\underline{r}}\; \{\sum_m \sum_n \sum_p e^{i\underline{S}\,\cdot\,(m\underline{a}_1 + m\underline{a}_2 + m a_3}\,\}$$

Let the vectors $\underline{b}_1$, $\underline{b}_2$, and $\underline{b}_3$ be defined $\underline{b}_i \cdot \underline{a}_j = 1$ if $i = j$ or is zero if $i \neq j$, and let the vector H(h, k, l) be defined as:

$$\underline{H}\,(h, k, l) = h\underline{b}_1 + k\underline{b}_2 + l\underline{b}_3.$$

If $\underline{s} = 2\pi\ \underline{H}\,(h, k, l)$ for some integers h, k, and l, the sum in the bracket, above becomes:

$$\Sigma_m\, \Sigma_n\, \Sigma_p\, e^{2\pi\, i(h\underline{b}_1 + k\underline{b}_2 + l\underline{b}_3)\,\cdot\,(m\underline{a}_1 + n\underline{a}_2 + p\underline{a}_3)}$$

which enumerates the cells in the crystal. If $\underline{s} \neq 2\pi\ \underline{H}(h, k, l)$ then the sum is zero. The scattering intensity is seen to cluster into a discrete set of angles defined by the vectors $\underline{H}$ (h, k, l) which are called points of the "reciprocal lattice".

The above relations imply an intensity distribution in which discrete spots of infinitesmal width contain all the intensity. If the crystal is finite, the sums over m, n, and p cannot range to infinity, and the sum gives rise to a narrow but finite spot width (see Warren, 1969). Also, the crystals one finds in the laboratory are composed of domains. The planes of these domains are not perfectly parallel to those of other domains. The angular range over which this mis-match extends is called the "mosaic spread". It is desirable that all domains in a crystal have an equal opportunity to contribute to the measured intensity of each spot. Toward this end, the intensity of a spot is measured as the measured scattering angle is moved through the ideal value. The intensity is integrated over the angular extent of the spot either mechanically or analytically. The result is called the integrated intensity. If the experimental situation is such that some spots are passed through the diffracting condition more quickly than others, a systematic error results. This systematic error is corrected for by a geometrical function specific to the experimental apparatus called the Lorentz correction. As in the case of scattering from glasses, the X-ray polarisation must also be corrected for.

The integrated intensity of a spot, corrected for Lorentz and polarisation effects will be called $I_{h,\,k,\,l}$. It was seen above that:

$$\rho_{\underline{s}} = \phi' \int_{\text{unit cell}} d\underline{r}\ \rho(\underline{r})\ e^{i\underline{s}\cdot\underline{r}}\ \delta(\underline{s} - 2\pi\ \underline{H}(h,\,k,\,l))$$

where ϕ' is a constant of proportionality which includes the number of cells in the crystal. It was also noted that the intensity is proportional to $\rho_{\underline{s}}\ \rho^*_{\underline{s}}$, and consequently

$$I_{h,\,k,\,l} = \phi\ F_{(h,\,k,\,l)}\ F^*_{(h,\,k,\,l)}$$

where ϕ is another proportionality constant and F, called the structure factor, is

$$F(h,\,k,\,l) = \int_{\text{unit cell}} d\underline{r}\ \rho(\underline{r})\ e^{2\pi i\ \underline{H}(h,\,k,\,l)\cdot\underline{r}}\ .$$

Let the following approximation be made for the electron density in the unit cell,

$$\rho(\underline{r}) = \Sigma_j \, \xi_j * t_j * \delta(\underline{r} - \underline{r}_j)$$

where j runs over the set of atomic positions $\underline{r}$ and ξ_j is the electron density of atom j and t_j is a normalised Gaussian function introduced earlier in this chapter. The asterisks indicate convolution. The density ξ_j need not be spherical. By the convolution theorem the Fourier transform of $\rho(\underline{r})$ will be a product of the Fourier transforms of its components. The structure factor becomes:

$$F\,(h,\, k,\, l) = \Sigma_j \, f_j\,(\underline{H})\, T_j(\underline{H})\, e^{2\pi i\, \underline{H} \cdot \underline{r}_j}$$

where f_j is the atomic scattering factor and T_j is the transform of t_j. If the spherical atom approximation is made, f_j is only a function of the magnitude of $\underline{H}$. The function T_j called the temperature factor is often anisotropic (see Stout and Jensen, 1968) and can be defined as:

$$T_j = e^{-\, \Pi^{+} \beta \Pi}$$

where Π = (h, k, l) and β is a 3 x 3 matrix. A matrix U may be defined such that:

$$\beta_{mn} = 2\pi^2 \underline{b}_m \cdot \underline{b}_n U_{mn}$$

where the reciprocal cell basis vectors $\underline{b}_m$ have been defined above. The U matrix can be interpreted as $U_{mn} = < u_m u_n >$ where u_m is a displacement of the atom in the m^{th} direction The square root of U_{11}, for example, represents a mean amplitude of vibration for that atom in the x direction. The matrix U corresponds to an ellipsoid of vibration, and U will only be diagonal if the principal axes of the ellipsoid lie along the x, y,and z directions of the unit cell.

It has been assumed above that, averaged over time, all unit cells are identical. Some crystals, however, are partially disordered in one manner or another. Krivoglaz (1969) has discussed in detail the influence of various forms of disorder in the diffraction pattern. Only a brief outline will be noted here. If the disorder is a distortion which modulates the translational period a broadening of the diffraction spot can result. A small concentration of one atomic species substituting on a lattice can manifest itself as:

(1) a change in the average unit cell

(2) an increase in the apparent temperature factor U_{mn} due to minor fluctuations in position from one cell to the next.

(3) an average observed structure factor, which is calculated from a weighted average of the atomic scattering factors.

and (4) average interatomic spacings.

A diffuse background relatatedto short range correlations among defects is sometimes observable.

2.5 Structure Determination and Refinement

The Fourier transform of the scattered intensities gives the electronic density correlation function but does not give the electronic density. The electronic density at fractional coordinates (x, y, z) in the unit cell can be expressed as (Buerger, 1960)

$$\rho(x, y, z) = \frac{1}{V_{cell}} \Sigma_h \Sigma_k \Sigma_l F(h, h, l)\ e^{-2\pi i(hx + ky + lz)}.$$

The numbers F(h, k, l) are complex and have both a magnitude and a phase. A function called the Patterson function (Buerger, 1960) is calculable directly from the observed integrated intensities. This function A(x, y, z) given by:

$$A(x, y, z) = \frac{1}{V^2_{cell}} \Sigma_h \Sigma_k \Sigma_l |F(h, k, l)|^2\ e^{2\pi i(hx + ky + px)}$$

is proportional to the Van Hove function $G_e(\underline{r})$ introduced earlier. It is sometimes possible to derive trial positional coordinates for the heavier atoms in a structure from an analysis of the Patterson function. If this can be done, the phases from the calculated structure factors from these atomic co-ordinates can be used as trial phases for the observed structure factors. The greater the percentage of the electron density of the cell that is known, the more reliable will be the phases. The trial phases can then be used to calculate an electron density function, from which more atoms may be found. In the discussion of scattering from amorphous solids, mention was made of the spurious ripples in the Fourier transform of the intensity due to the termination of the data at some maximum scattering angle. A function which alleviates much of the termination problem is the difference synthesis $\Delta\rho(x, y, z)$ defined (Stout and Jensen, 1969) by:

$$\Delta\rho(x, y, z) = \frac{1}{V_c} \Sigma_n \Sigma_k \Sigma_l (|F_o| - |F_c|)e^{i\alpha_c} e^{-2\pi i(hx + ky + lz)}$$

where V_c is the volume of the cell and F_o is the observed F (h, k, l) and F_c is the calculated F(h, k, l) and α_c is the phase of F_c.

Although some refinement of the crystal structure can be done with a difference synthesis, least-squares refinement of the structural parameters is now more common. If p_i is a structural parameter (a position coordinate temperature factor for example), F_{or} is the r^{th} observed structure factor and F_{cr} is the r^{th} calculated structure factor and w_r is a weight applied to the r^{th} observation, then the vector $\underline{v}$ (equal in dimension to the number of parameters being refined) can be defined (Stout and Jensen, 1969) as:

$$v_i = \sum_{r\,(\text{observations})} w_r(F_{or} - F_{cr}) \frac{\partial|F_{cr}|}{\partial p_i}$$

The matrix $\underline{A}$ can be defined as:

$$A_{ij} = \Sigma_r \; w_r \frac{\partial|F_{cr}|}{\partial p_i} \frac{\partial|F_{cr}|}{\partial p_j}$$

and the vector $\underline{x}$ of shifts in parameters $x_i = p_i^{new} - p_i^{old}$ can be found by solving the matrix equation $A\underline{x} = \underline{v}$.

2.6 Corrections for Physical Effects

A crystal fully bathed in the X-ray beam will have the intensity of its (h, k, ℓ) reflection attenuated by a factor, A, given by:

$$A = \frac{1}{V} \int_{crystal} e^{-\mu(T_{in} + T_{out})} dv$$

where T_{in} and T_{out} are the lengths of the paths of the incident and scattered rays inside the crystal for a scattering taking place in volume element dv. The volume of the crystal is denoted as V and μ is the linear absorption coefficient. The absorption correction entails the calculation of an approximation to this integral for each reflection's angular setting and the division of the intensity I(h,k,ℓ) by A.

This absorption is anisotropic only to the extent determined by the crystal shape. If, however, the scattering process itself significantly contributes to the attenuation of the X-ray beam, an apparent increase in absorption will be observed in the intensity of some of the stronger reflections. If a regime of crystalline perfection is called a domain, and if the domains are misaligned relative to each other by a small angular distribution called the mosaic spread, that part of the attenuation due to interference effects between multiply scattered beams inside a single perfect domain is called primary extinction. If the primary beam incident upon a domain inside to a crystal has been attenuated by extinction in a previously travelled domain, the effect is called secondary extinction. Under the assumption that spherical domains are misaligned within a small mosaic spread, Zachariasen (1963, 1967) derived a correction formula for the effects of extinction. Larson (1967) discussed ways of including a parameter for secondary extinction in the least-squares refinement of a structural model. The form of correction used in the present experiments is one of Larson's

(1967). The corrected calculated structure factor, $F_c^{corr.}$ is given by:

$$F_c^{corr.} = F_c(1 + g\ \beta\ F_c^2)^{-\frac{1}{2}}$$

where g is a refined parameter and β is a function calculated from the scattering angles.

Several papers recently (for example, Coppens and Hamilton, 1970; Thornly and Nelmes, 1974; and Becker and Coppens, 1975) have extended the treatment of secondary extinction by considering an anisotropic domain shape and an anisotropic mosaic spread. It was suspected that α-VPO_5 should exhibit anisotropic secondary extinction. To guage the severity of the anisotropy, the g parameter defined above was refined for two restricted subsets of the intensity data. The first set corresponded to (h, k, 0) and (h, k, 1) reflections and the second set included only (h, 0, ℓ) and (h, 1, ℓ) reflections. These subsets correspond to the zeroth and first layers for the X-ray beam nearly normal to or nearly parallel to the plate of the crystal. It was found that the g value refined for the two subsets were within expected error of each other and of the g value for the total reflection set. It was judged from this that the degree of anisotropy in the secondary extinction for α-VPO_5 did not warrant further treatment.

CHAPTER 3

APPARATUS

All of the X-ray scattering data on the glass samples in this study was recorded on a diffractometer which was designed for the study of scattering from liquids. The diffractometer was built at McMaster to the specifications of D. Crump who based its design on that of an instrument at Oak Ridge National Laboratory. In this kind of machine, known as a theta-theta diffractometer, the sample remains stationary while the detector and X-ray source move about a common horizontal axis. A Bragg-Brentano para-focussing system is used, in which a divergent beam of X-rays from the line focus of the tube is passed through a beta filter, then directed with a divergence slit and soller slit assembly onto the top surface of the sample. The scattered radiation passes through a scatter slit, which limits the solid angle "seen" by the detector, then through a second set of soller slits to a receiving slit. Beyond the receiving slit the beam diverges onto a curved crystal monochromator of LiF and diffracts from it onto the crystal of a scintillation counter. The focussing system is symmetric about the axis of rotation with the divergence slit and scatter slit being equidistant from this axis and the receiving slit being the same distance from this axis as the focal point of the X-ray tube. The opening in the receiving slit should match the projected width of the focal point on the X-ray tube.

The scattering system consists of three units; the source, the sample chamber, and the detection assembly. The source, which includes an X-ray tube and housing with a wheel containing various filters manufactured by Phillips Electronics and soller slit and divergence slit assembly, is mounted on a shelf and arm of three quarter inch thick aluminum. The detection assembly consists of an AMR monochromator unit, with the scintillation counter and slit housings mounted onto the monochromator base which in turn is secured to another shelf and arm unit also of three quarter inch thick aluminum. The two aluminum arms are each connected to a nine inch rotary table and counterbalanced by weights hanging from steel cables wrapped around the table and riding in a groove. The two rotary tables have been carefully aligned about a common horizontal axis. Running through the centres of the two tables along the common axis is a closely fitting steel rod which has its centre scribed on one end. This rod marks the axis for alignment of the slit system. The drive wheel for each table is fitted with a gear which is driven by a common worm gear. The worm gears, of opposite pitch are connected to a common shaft, which in turn is driven through a set of bevel gears by a Slo-Syn synchronous motor. This motor, through the shaft with the two worm gears, drives the two tables to turn in opposite directions at a rate of .6 degrees per minute. The gears connecting the tables to the worm gear shaft can be disconnected from the table drive with the removal of a set pin, thereby allowing the detector or source angle to be set independently by turning a crank. The crank on the detector table can be removed and replaced by a notched aluminium plate which acts as a cam to activate a micro-switch for use in step scanning. The detection electronics, operating in either a set time or a set count mode generates a five second pulse to the synchronous motor when a count is completed. In this five seconds the cam will be moved far enough so that the micro-switch will be activated and the motor, which is connected to its power supply through either the micro-switch or the goniometer control, will continue to turn until the next notch on the cam is reached. Cams have been made for two, three, four, six, eight, or ten steps per degree. The vernier on the table drive allows the angular setting to be read to the nearest quarter minute, and the step scanning system advances the angle to within this precision.

The X-ray tube housing was designed to accommodate a Philips X-ray tube, with a take-off angle of four degrees. The focal spot to rotation axis distance was chosen to be the same as that of the Phillips PW1380 horizontal powder diffractometer so that slits from that machine could be used on the theta-theta diffractometer. A standard Phillips beta filter assembly is fitted on the housing. Cooling water for the tube is supplied through a closed circuit controlled temperature and pressure plumbing system used in common with the other X-ray generators in the building. The power for the tubes comes from a GE XRD-6 power supply operating in its constant potential full-wave rectification mode.

The GE 75KVP generator and power supply should be stable under the operating conditions of these experiments, according to the manufacturers specifications, to better than .1 percent in voltage and .05 percent in current. At no point was the generator run at more than one quarter of its maximum operating power. Nevertheless, the counting strategy for the experiment was so chosen that diurnal drifts in the electronics of the source or detection system of one half percent or more, if they should appear, would merely shift the background slightly and not appear as spurious signal. Two X-ray tubes were used in this experiment. The first, a molybdenum target tube, is a Phillips PW2105/00 broad focus high intensity type which was run at 50 KV potential and 22 mA tube current. This corresponds to approximately two thirds its recommended maximum operating power. The other tube is a fine focus high intensity chromium target tube, also from Phillips. It was run at only 30 KV and 20 mA, which corresponds to half mximum power.

The detection chain begins with a focusing LiF crystal monochromator from A.M.R. Industries, model 7-202H. The X-rays are focussed onto the crystal of a scintilation counter powered by a Phillips PW4025 stabilised high voltage power supply. The pulses from the counter are shaped with a PW1365 and passed into a PW4280 amplifier which operates as a single channel analyser to discriminate against spurious electronic noise on the one end and against higher harmonic reflections from the monochromator on the other end. The pulses passed by the analyser go into a PW4237 counter-timer. The counter-timer runs a chart recorder through a PW1362 ratemeter for preliminary runs, or for quantitative data in the step-scanning mode it dumps the time and count onto a paper tape printer through a PW4255 printer control and signals a step advance through the PW1364 step scanner. Data was taken in either constant time or constant count mode depending on the conditions and scattering rate for that scan, always ensuring that at least half percent statistics were justified.

In the normal unfiltered spectrum of a Molybdenum X-ray tube, running at 50 KV potential, the desired Mo K_α peak will be riding part of the way up the back of the bremstrahlung band. A zirconium beta filter will suppress the Mo K_β line and most of the bremstrahlung with energy above the Mo K_β peak, but will not suppress the bremstrahlung tail below the Mo K_β peak. A crystal bremstrahlung selects out

FIGURE 3.1

SLIT OPTICS

The sample plane is indicated by the base line. The divergence slit, S_1, limits the beam from the X-ray tube to an angle $2\beta_1$. The receiving slit, S_3, approximates the focal area of the X-ray tube. A scatter slit, S_2, limits the angular range "seen" by S_3 to $2\beta_2$. After passing through S_3, the X-rays diverge onto the curved monochromator crystal, M, and diffract onto the face of the detector D.

SLIT OPTICS

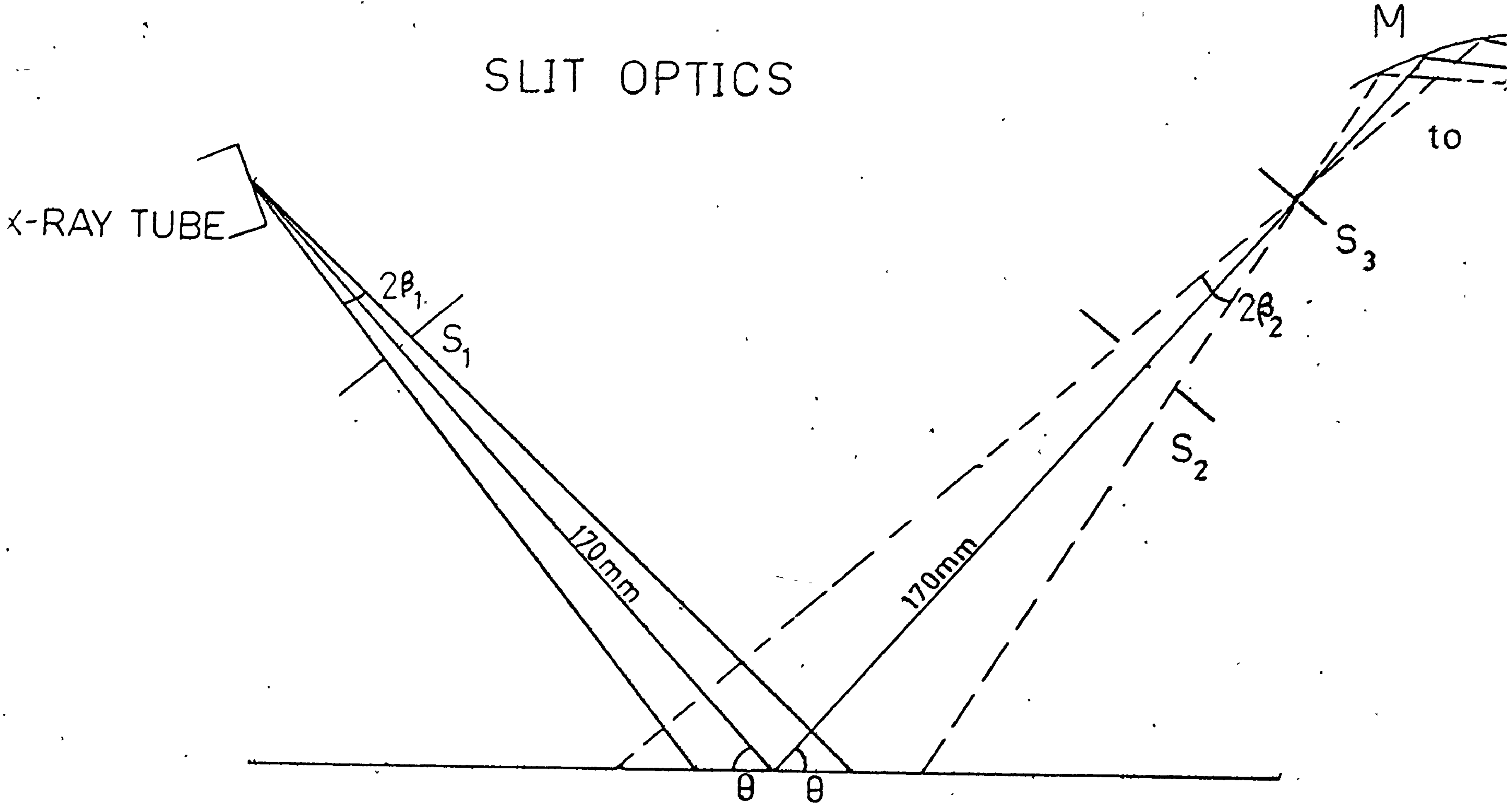

only a narrow pass band around the desired wavelength and, hence, would eliminate the problem of the bremstrahlung tail. The spectrum of a chromium X-ray tube running at 30 KV potential has its K-alpha doublet well removed from the bremstrahlung band. In this circumstance, the desired part of the spectrum should be well isolated with only a vanadium beta filter and a single channel analyser to discriminate against high energy bremstrahlung which may escape the vanadium filter. The monochromator was used for the data taken with the molybdenum tube, and the analyser was set to accept approximately ninety percent of the radiation passed by the monochromator. The monochromator crystal was removed when data were taken with the chromium tube and the analyser set to accept approximately fifty percent of the radiation passed by the beta filter.

3.1 Alignment

When a properly aligned diffractometer is set to zero in the angle, a horizontal line will pass in turn through the focal line of the X-ray tube, the centre of the divergence slit, the axis of rotation, the centre of the scatter slit, and the centre of the receiving slit. To allow for alignment, several degrees of freedom were built into the diffractometer. The scatter slit and receiving slit assemblies ride on and are secured to a track on the base of the monochromator unit. This unit is secured to a plate which in turn is bolted to the arm of the diffractometer. Slight tilting and vertical translational freedom is possible in the positioning of this plate against the arm. Screws in plates temporarily c-clamped to the arm allowed the plate position to be manipulated. The sample chamber rides on a plate which travels vertically along a beveled track, drawn by a screw. When the sample chamber is removed and its plate translated up to its maximum, the scribe marks on the rod marking the axis of the diffractometer are visible. The centre was found in the cross-hairs of a cathetometer telescope pointing parallel to the axis of the diffractometer. An aluminium cylindrical plug with a shelf cut into it along its axis was inserted in the mount for the sample chamber and lowered until its centre was found in the cross-hairs. The slits were replaced with plates in which were cut windows one side of which coincided with the centre of the plate. The shelf on the plug and the monochrometer unit were levelled with a shop level and manipulated until a plate acting as a straight edge was level and flush with each slit and the axis plate. Fine adjustment of the whole unit was later done using rocking curves of the main beam (well attenuated with filters) and one sixth degree divergence and scatter slits. Once the detection slits are aligned with the centre of rotation, the divergence slit may be opened and the theta angle of the X-ray tube advanced until a maximum intensity is seen through the scatter and receiving slits.

A knife edge attachment may then be secured to the shelf on the centre plug and further rocking curves taken until one is assured that the beam passes through the axis and all slits. At this point a small divergence slit may be inserted and adjusted vertically until it too straddles the beam. A problem was encountered at this point. Because it is desirable in general, and in this experiment necessary, to be able to align the detector slits once and to only realign the easy side when tubes are changed, it is therefore required that it be possible to zero the two sides independently. This was only possible to within the range in which one can simultaneously mesh the driving gears of the two tables onto the worm gears on the common drive shaft. To remedy the situation, the drive shaft was severed between the worm gears and a joint consisting of a male and a female plug each with a flange, was inserted. When the pair are joined, the flanges are flush against one another, and one flange has a circle of sixteen holes, while the other has fifteen holes, equally spaced. This causes a vernier effect as the two segments of shaft are rotated to each other, and one need only place a set pin through the pair of holes that most closely align to rejoin the shaft.

3.2 The Sample Chamber

The sample chamber used throughout this experiment is a Materials Research Corporation vacuum furnace attachment.

The unit consists of a water cooled vacuum chamber with beryllium windows which allow scans from zero to over seventy degrees in theta, although the diffractometer will not go beyond sixty nine degrees. The chamber has capability for use from $77^{\circ}K$ to over $1600^{\circ}C$ but its only use in this experiment was to orient the sample and eliminate air scatter from the data taken with chromium X-rays. For that part of the experiment no vacuum guage was used and only a fore pump used for evacuation, but an observed increase of over thirty percent in the X-ray count rate on evacuation indicated that, for the purpose of X-ray scattering, most of the air was gone. The transmission factor of air for chromium X-rays is quoted by the International Tables of X-ray Crystallography as 68% for a path of ten centimeters. The volume of air "seen" by both the X-ray tube and detector is a function of angle, therefore, air scattering when significant, must either be eliminated or corrected analytically. The former option was chosen.

The sample chamber is mounted against the travelling sample chamber plate with a plug and is held in position against rotation around the diffractometer axis by two set screws. The plate holding the chamber translates vertically with the turning of a screw, thereby providing a second degree of freedom. The third degree of freedom is a tilt around a horizontal axis perpendicular to the axis of the diffractometer. This tilt is provided by the sample table inside the sample chamber. In this experiment the glass slabs were secured to the sample table with plasticene and a level placed on the top surface. The chamber was rotated and the tilt adjusted until the surface was level in both directions. The theta angle was then advanced to approximately twelve degrees and a matching scatter slit and divergence slit pair were inserted. The sample height was then adjusted to maximize the intensity. The following illustrations show how this works. In diagram A, the divergent beam and area "seen" by the detector are indicated at a theta of 20 degrees. If a very weakly absorbing sample is raised from point 1 to point 3 the maximum intensity will be reached at point 2, where the most sample is seen by both elements. For such samples, it has been suggested that one slit be chosen larger than the other, thereby giving an intensity versus height graph like C . In case C the centre could be found as half the way from 2 to 2'. The situation changes for an absorbing sample. If a ray penetrates to a depth d from the surface and comes out at an angle theta it will be attenuated by a factor exp (+2 $\mu d \csc(\theta)$), where μ is the linear absorbtion coefficient. For the glasses in this experiment a ray (MoK_α) penetrating to a depth of .1mm will be attenuated by approximately exp(+2). It can be seen that in this case only a very thin layer of the surface effectively takes part in the scattering. In this case the surface area "seen" by both sides determines the intensity

Figure 3.2

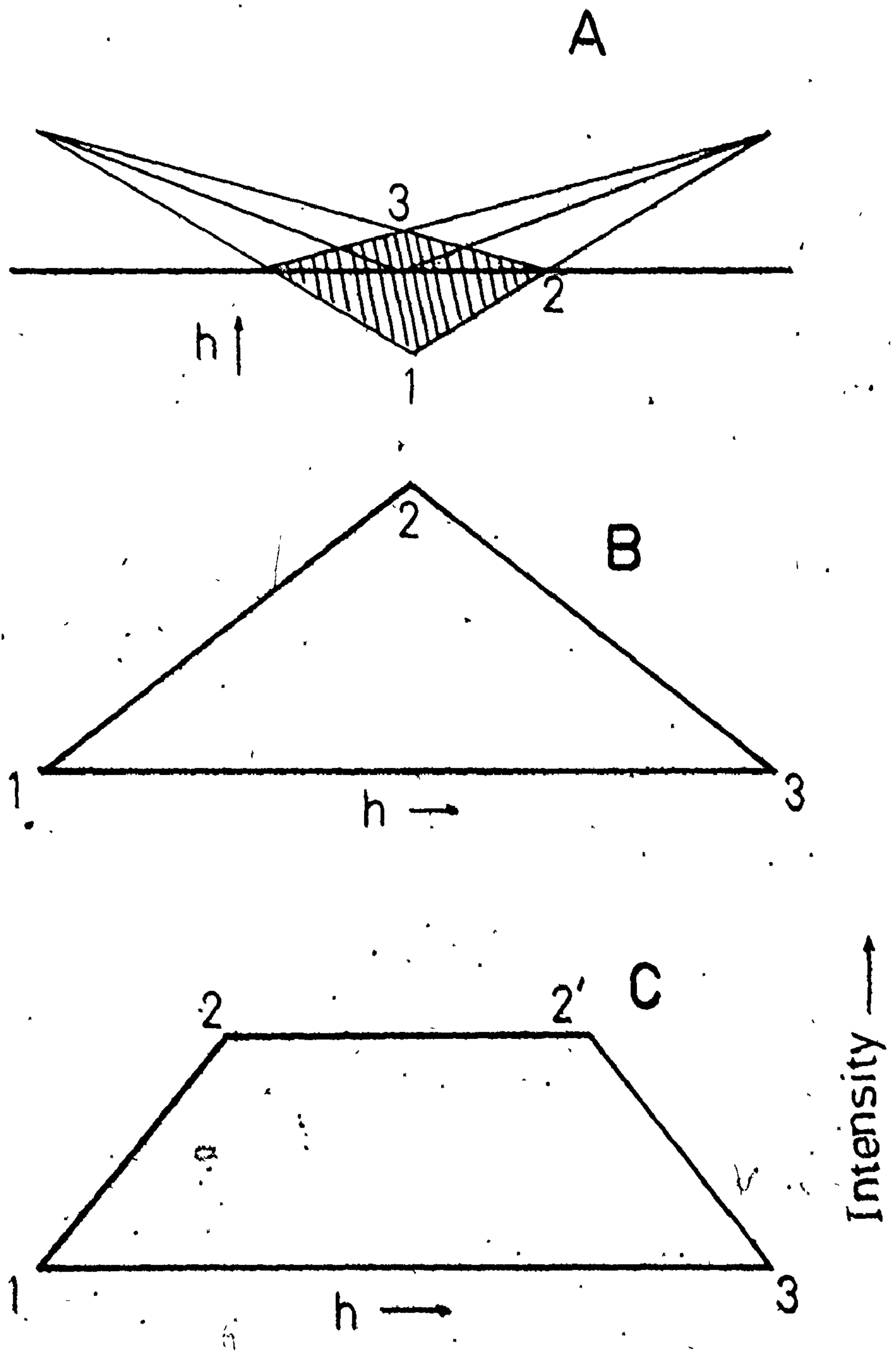

and graph B is observed. It has been predicted that the intensity should be often quite sensitive to the orientation and positioning of the sample. To test the reliability of the total method, a sample was leveled and positioned, the intensity scatter measured, then removed from the chamber. It was then reinserted into the chamber, relevelled, and its height reset. The intensity was reproduced to within one percent.

One can more closely assess the approximations used in this technique of positioning the sample holder, by referring to the next two illustrations. The illustration entitled "Geometrical Parameters" shows the diverging beam on the left and the diverging line of sight on the right. The case illustrated is the overviewing one in which more sample is "seen" than is illuminated. As the sample rises into view no intensity is detected until the height reaches H_1 after which the intensity rises linearly until H_2 is reached. The intensity forms a plateau from H_2 to H_3 at which point it ramps down to zero again at point H_4. If one considers the four lines which bound the divergent paths as functions of the parameters on the diagram, one can easily calculate the intensity as a function of sample height, which is proportional to the length of a horizontal line segment connecting the appropriate beam boundaries. Six cases are illustrated on the following page. The slit openings are given in degrees and theta is noted on each. The ordinate on each is the length

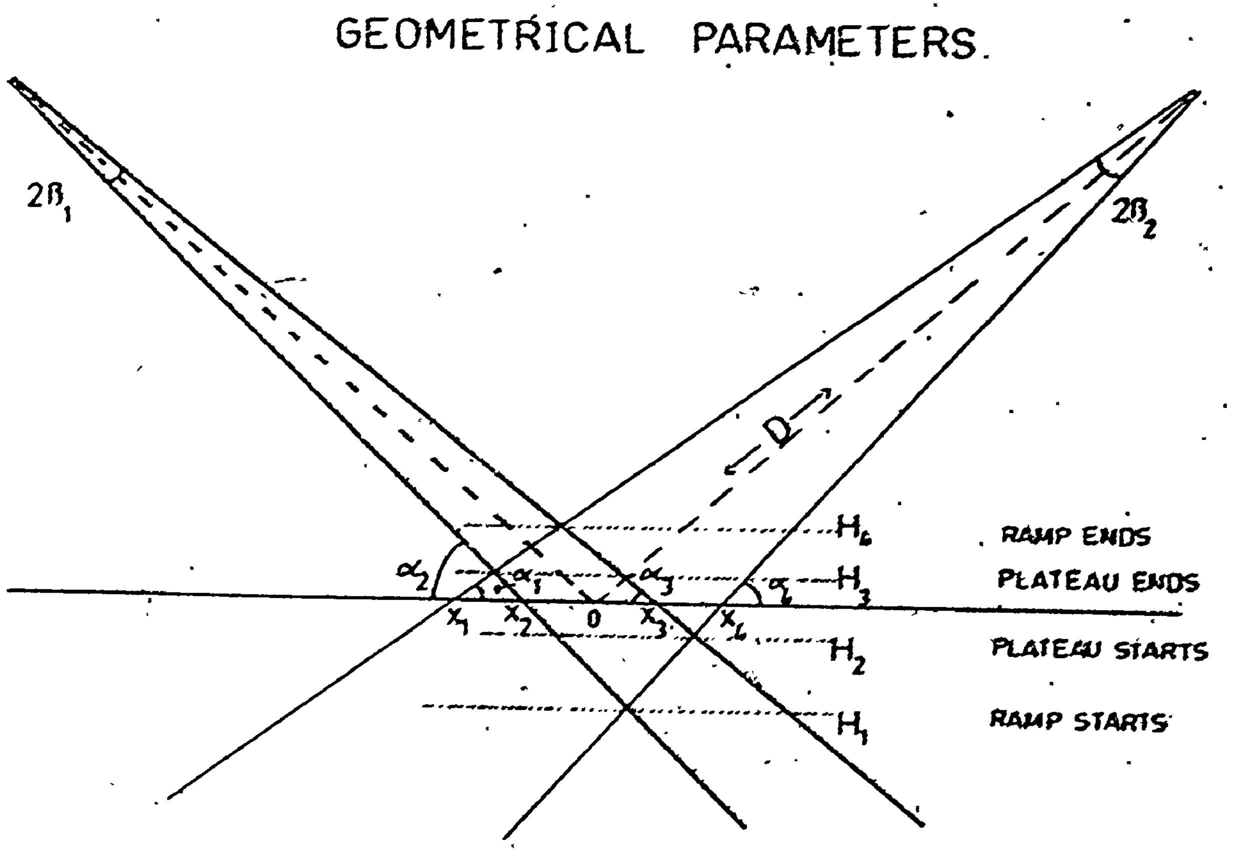

FIGURE 3.3 The details of the scattering geometry for the case in which the scatter slit ($2\beta_2$) and the divergence slit ($2\beta_1$) are not necessarily equal.

FIGURE 3.4

A schematic of the scattering intensity versus sample height curves was given by Figure 3.2. The details of the scattering geometry for the case in which the area "seen" by the detector exceeds the area illuminated by the X-ray beam were given in Figure 3.3. Calculated examples with sample height in millimetres are given here. To guage the sensitivity of the procedure used here to position the sample upon the alignment of the diffractometer, each graph contains five curves corresponding to equal increments of misalignment of the main beam from zero to one half degree. In some of the graphs the five curves superimpose too closely to be resolved.

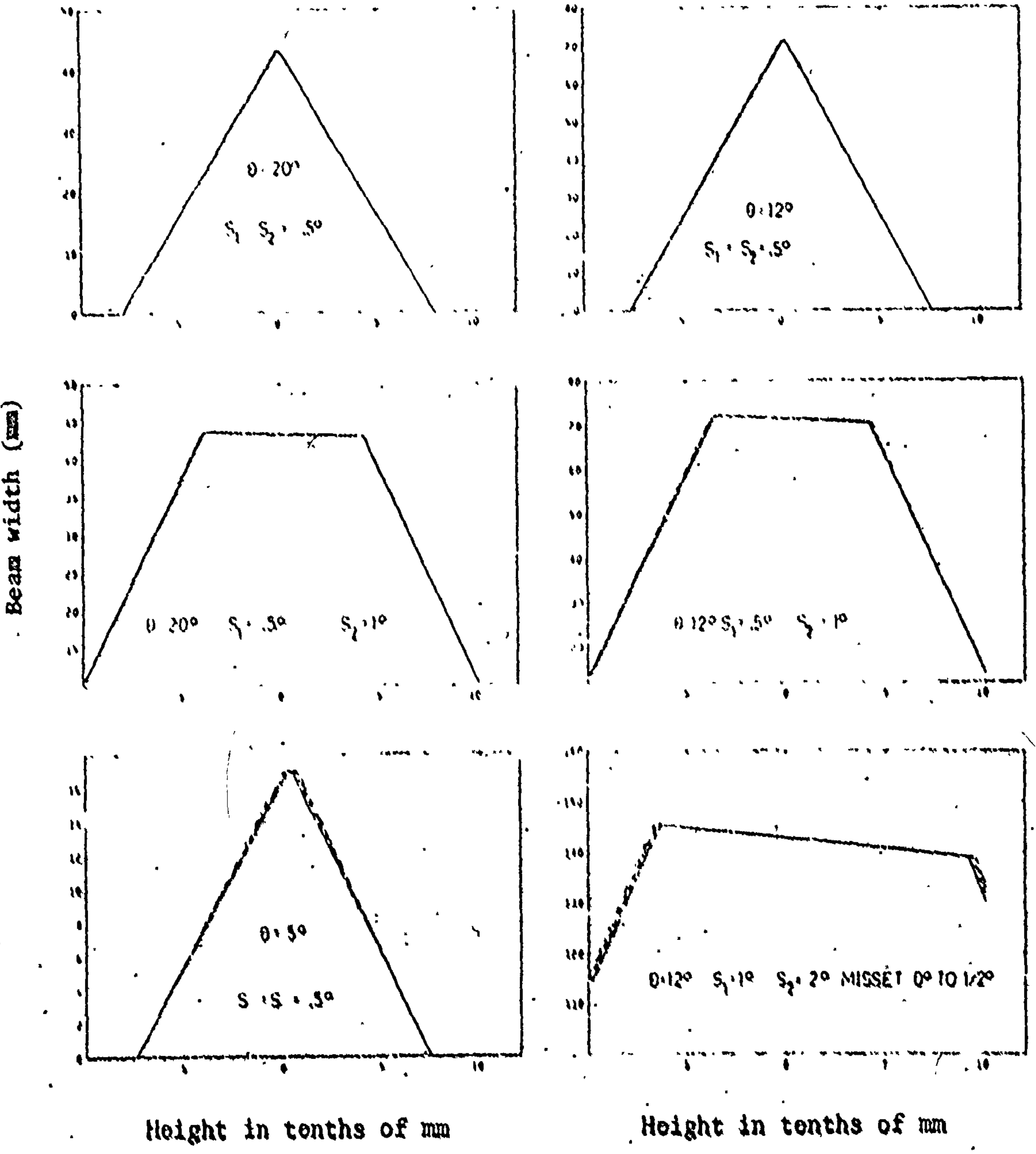
Beam width (mm)
θ = 20°
S1 = S2 = .5°
θ = 12°
S1 = S2 = .5°
θ = 20° S1 = .5° S2 = 1°
θ = 12° S1 = .5° S2 = 1°
θ = 5°
S = S = .5°
θ = 12° S1 = 1° S2 = 2° MISSET 0° TO 1/2°
5
0
5
10
Height in tenths of mm
Height in tenths of mm

of the above mentioned line segment in millimetres and the abscissa is the sample height in tenths of millimetres. Each graph contains five curves to show the degree of change introduced if one of the beam paths is missaligned from zero degrees to an extreme of one half degree. Examination of the graphs shows a total travel of approximately one millimeter and a sensitivity in most cases allowing the centre to be estimated to within one or two tenths of a millimeter. The effect of misalignment is seen to be inconsequential.

This technique was suggested in a review by Furukawa (Furukawa,1960) and criticised by Wagner (Wagner, 1965). Wagner found that the position and height of maxima in the intensity from liquid metals varied with sample height h, and that the maximum did not correspond to the axial position. His argument is based on the absorption factor A, where

$$A = (1 + \tan \epsilon \cot(\theta))/ 2\mu \quad .$$

In this expression theta is the usual half scattering angle and epsilon is the angle made with the horizontal to the plane tangent to the meniscus at the point the centre of the beam intersects the sample surface. Elaborating on his argument, if the height is displaced by h the beam will shift $h\cot(\theta)$ off centre. If the radius of curvature of the meniscus is R_m, $\tan(\epsilon)$ is approximately $h\cot(\theta)/R_m$. A, and hence the intensity is now proportional to

$(1 + (h/R_m)\cot^2(\theta))$, which is a rather strong function of angle. It should be noted, however, that the functional dependence on h is really on h/R_m and for a flat specimen epsilon, and hence A, is not a function of h. In such a case one would expect the above procedure would find the correct sample position. To say that in the absence of a meniscus the correct vertical position will be found does not imply a freedom from the cotangent aberration due to tilt of the sample. A test of the level used to position the sample indicated that a tilt of fifteen minutes caused much more deviation than was accepted in the positioning of the samples, but a ten minute error was possible.

8.3 Data Treatment

Once the intensity has been recorded over several overlapping segments of scattering angle it must be processed through three stages of reduction to yield structural information. The first stage applies polarisation and absorption corrections on each segment. The second stage scales the segments into one curve and prepares the data for the third stage which subjects it to an affine transformation which isolates that part of the measured intensity due to single coherent scattering events and compensates for the angular variation in scattering power which distinguishes X-ray data from neutron data.

The first programme in the reduction series reads the complex atomic or ionic scattering curves, the stoichiometry, absorption coefficient, and slit sizes and angular variables for each data set and punches for each intensity measured a card containing s, theta, the slits sizes, the corrected intensity in counts per minute, the statistical variance, the average squared scattering factor, the average scattering factor squared, and the incoherent cross section. These cards act as the "raw" data for subsequent processing. The polarisation is given by the following function (Wagner, 1972) where $c = 1$ in the absence of any monochromator and $c = \cos^2(2\alpha)$ with an ideally mosaic monochromator after the sample, with the monochromator crystal parallel to the sample. Alpha is the Bragg angle of the crystal in the monochromator. The polarisation term P is

$$P(2\theta) = \tfrac{1}{2}(1 + c\cos^2(2\theta)) .$$

The absorption correction used is the one published by Milberg (1958) which allows for the case in which the sample is overviewed. For an effectively infinite sample thickness and equal viewing and illuminating slits, this function reduces to the one derived and experimentally verified by Levy, Agron, and Denford (1959). Referring again to the illustration "Geometrical Parameters" in Fig. 3.3, one can see the regions of the sample for which the various cases of the Milberg correction apply. In case one the bottom of the sample does not reach as far as H_2. Case two applies when the bottom is between point H_2 and H_1, and case three applies when the sample is effectively infinite, i.e. beyond H_1. Which case is applicable depends on the slits and also on the scattering angle. The approximation is made that the incident beam has cross section A at the sample and no divergence upon penetrating the sample. The demarkation of the viewed area is also approximated by two parallel lines A+2a apart. This is once again a "beam" crossection. If the width of the beam perpendicular to the scattering plane is Z, the following functions may be computed. If I_o is the incident intensity, the corrected intensity I may be computed from K, d, g, and r, where

$$K = I_o AZ/2\mu$$

$$d = 2\mu A \csc(2\theta)$$

$$r = 2\mu A \csc(2\theta)$$

and

$$g(t) = 1 - \exp(-2\mu t \csc(\theta))$$

and

Case 1 $0 \leq t \leq \frac{1}{2}a \sec(\theta)$

$$I = Kg(t)$$

Case 2 $\frac{1}{2}a \sec(\theta) \leq t \leq \frac{1}{2}(A + a) \sec(\theta)$

$$I = K(g(t) + (\frac{2t\cos(\theta)}{A} - \frac{a}{A} + \frac{1}{d})\exp(-2\ t\csc(\theta)) - \frac{\exp}{d}(-r))$$

Case 3 $\frac{1}{2}(A + a)\sec(\theta) \leq t$

$$I = K(1-(1-\exp(-d)\exp(-r)/d)$$

In the above μ is the linear absorption coefficient and t is the sample thickness. The absorption coefficient of the [illegible] phosphate glasses for Mo K_α is 30 cm^{-1} or larger, and absorption as a function of angle is quite flat. These corrections, although minor, were applied.

The data set as punched by the first programme is suitable not only for input to the radial distribution function series of programmes, but is also available to programmes which apply non-linear least squares minimization algorithms to test for aberrations in the data caused by air scatter or by sample tilt of the form suggested by Wagner (1965). The significance of the air scatter contribution can be assessed by a simple approximation. At low angle where air scatter is most important its ratio to the sample scatter will be in the ratio of square electrons per structural unit of air to that of the sample times the ratio of the number of accessable scattering units. In reference again to the illustration "Geometrical Parameters" (Figure 3.3) the air above the sample accessible to scatter is approximately the triangular prism defined by $X_1X_3H_4$. The sample available for scattering is in a volume $(\mu)^{-1}$ deep and with the same area of surface as the lower bound of the air volume unit. The common surface, which is a function of scattering angle, cancels out and the ratio of volumes becomes ½ $H_4(\mu)$. Given the ratio of densities and molecular weights, the air scatter contribution for vanadium phosphate glasses is found to be in the order of ½ percent. Were it not removed experimentally, air scatter would have given a significant angularly dependent aberration to the data taken with chromium Kα X-rays because μ is an order of magnitude greater in that case and, as noted above, the ratio of air scatter to sample scatter is proportional to the linear absorption coefficient.

The second programme in the series merely uses the overlap between the various segments of data and internally normalizes them into a single function of s. The variance for each intensity point is always scaled along with the intensity at every stage of computation in this study. All subsequent computation such as normalization, Fourier transformation, model generation and fitting, reliability tests, etc., is done by a subroutine library communicating by labeled Common. The data produced by the second programme are read by this system.

When properly normalized, the intensity will oscillate about sum of the independent scattering function (the average of the square of the atomic scattering functions) and the background. The true background from cosmic rays and other sources in this experiment is seldom greater than one part in three hundred of the apparent background, but the term background function, or B(s), will be used to include all scattering not due to single coherent scattering events. If not already removed, background and air scatter could be included in this function, but its greatest components are the Compton scattering and the doubly scattered X-rays. Some authors would isolate the Laue monotonic scattering term ($\langle f^2\rangle - \langle f\rangle^2$)

from the independent scattering term, in which case, the intensity would be said to oscillate about the square of the average scattering function plus B(s). If one goes to low enough angle Warren (1969) has shown that another, small-angle, contribution must be subtracted. More will be said about the background contributions, term by term, below. For now it can be assumed that a smooth curve, can be generated from the sum of several contributions all of which can be put on the same scale with the independent scattering function. The intensity should oscillate evenly about this curve after it has been scaled with a scale constant K. Several algorithms have been suggested for the calculation of this constant and some studies have used more than one algorithm to check self consistency, (Black and Cundall, 1965).

In the first method the average intensity above some high value of s is divided by the average of $\bar{f}^2$+ B(s). It is assumed that only small ripples of the oscillatory contribution are still present. This method has the disadvantage that the incoherent contribution which may be present must be well known.

The second method, known as the integral method, and attributed to Norman and Krogh Moe, involves an integral of the experimental and theoretical scattering functions (Norman, 1957). The justification for this technique lies in the form of the radial distribution function, D(r), where,

$$D(r) = 4\pi\ r(\rho(r) - \rho_0) = (2/\pi) \int_0^\infty si(s)\sin(sr)ds$$

As r goes to zero $\rho(r)$ is zero and the left side becomes $-4\pi\rho_0 r$ and the right side is simplified by approximating sin (sr) by sr. The r may be eliminated from both sides and the i(s) broken into its components. The s^2 remaining in the integrand unduly accentuates the high s contributions, and Warren (1969), has suggested a Gaussian damping factor, $\exp(-4(s/s_{max})^2)$, be applied to the integrand. The following is the resultant equation for the normalization constant K, where TSF (theoretical scattering function) signifies the independent scattering plus the background function and M(s) signifies the above Gaussian convergence factor divided by the square of the average scattering function per electron ($M(0) = 1$).

$$K \int s^2 I_{exp} M(s)ds = \int s^2 M(s)TSF\ ds - 2\pi\ \rho_u(\Sigma_{uc} Z)^2$$

In the above, ρ_u stands for the number density of units of composition and Z is the number of electrons on each atom and the sum is taken over the unit of composition. The integral method of normalization has the advantage that it is much less sensitive to the incoherent high angle contribution and emphasizes the middle range in s, where both the TSF and I_{exp} are most free from aberration deriving from incomplete correction. If the first two methods of normalization agree well, then the high angle contributions have probably been computed properly. If the match is poor, the high angle part of i(s) will give large ripples to the RDF at low r. The disadvantage to this method is the need to calculate the TSF, with its several contributions, to reasonable accuracy when not all parameters are well enough known.

A third method relies again on the radial distribution function, D(r). As mentioned above, D(r) ($= 4\pi r(\rho(r) - \rho_0)$) at low enough r is linear with a slope of $- 4\pi\rho_0$. If any function can be drawn through I_{exp} so that it equals $\langle I_{exp}\rangle$ for a local range of s to isolate the oscillatory part, the magnitude of the resulting i(s) need only be adjusted to make the low r slope of RDF fit the experimentally known density. Alternatively, the normalisation can be done by one of the methods above and the density measured from the resulting slope. Konnert and Karle (1973) have used an empirical TSF, and Kaplow (1965) discusses the adjustment of the density as a parameter in a reduction scheme. Cargill has argued (1971) that the density that most closely fits the D(r) function at small r may not be the true bulk density if medium range fluctuations or clusters (20-50 Å) exist in the glass and data is not taken to low enough angle to detect the small-angle scattering from these fluctuations. This must be regarded as a caveat for those wishing to follow the procedure of Konnert and Karle.

Each of the above procedures were used in this study. To avoid the problems in the empirical background approach that Cargill warned about, data was taken down to very low angle on each specimen with chromium X-rays. With slits as small as one sixth degree and a wavelength of 2.29 Å it was possible to go to an s value of .1 to .2 with each sample before the area of illumination exceeded the sample surface. Below that angle a correction proportional to csc(θ) would be required to compensate for X-rays failing to illuminate the sample. In most cases data were recorded to within one third of a degree of zero in theta. The object of the search was not to collect quantitative data, for aberrations of a serious nature could plague a reflection small-angle experiment, but rather the scan sought a strong exponential rise in the intensity that would signal the presence of significant medium range density fluctuations. Bishop and Shevchick (1974) recently published the results of a careful transmission small-angle experiment on chalcogenide glasses in which they found significance in the absence of small angle scattering.

In implementing the empirical background procedure a variation of the algorithm of Konnert and Karle (1973) was used. Overlapping segments of s were chosen, and for each segment a function $B(s)_\nu = \exp(-(\alpha + \beta s + \gamma s^2))$ is calculated by fitting a least squares quadratic function to the natural logarithm of the intensity. The resulting B(s) is a sum over ν of $B(s)_\nu$ $W(s)_\nu$ here the weighting function is shown below.

Weighting Function

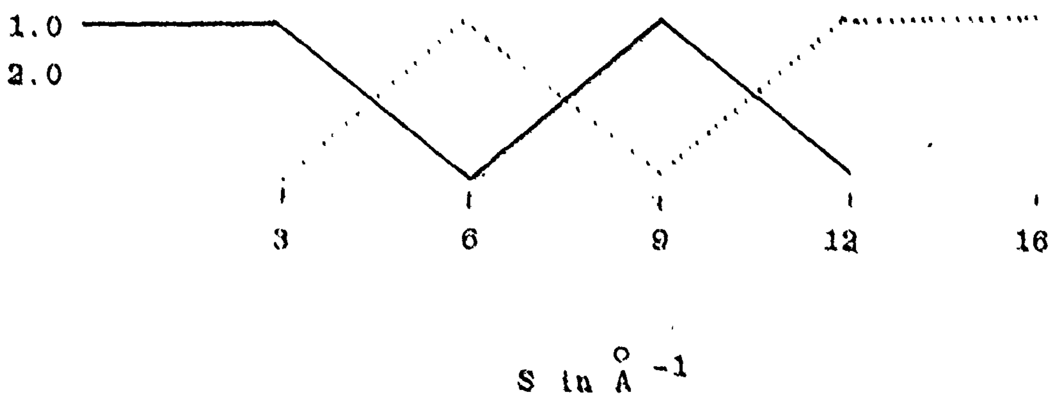

The data in the region below the first peak in the intensity were not included in the fit, because they tended to pull B(s) down unphysically at low s.

A calculation of the Compton contribution is need for the implementation of the other normalization procedures. The Compton contribution is a product of three functions, the atomic Compton intensities $\Sigma_{uc} I_{inc}(s)$, the Breit-Dirac function for a counter $(\lambda/\lambda')^2$, and the monochromator leakage function L (s). The atomic intensities are tabulated (Cromer, 1969) or fitted to a parametric expression (Hajdu, 1972).

The tabulated or computed Compton term rises from zero at low s through an inflection in the medium range near eight reciprocal Angstroms and asymptotically approaches Z, the number of electrons in the atom, at high s. Since the coherent cross section scales as Z^2, one would expect the relative importance of the Compton term to decrease at high Z. For vanadium, for example, the incoherent contribution at high s is about twice the coherent, whereas with lead the coherent is about three times as strong as the incoherent. The experimenter working with medium or light scatterers faces the prospect of counting X-rays at high angle to the best statistical variance his system stability warrants, only to find after subtracting off most of the signal as incoherent background, that the errors on the signal of interest are disappointingly large. One way to avoid this problem is to experimentally remove the Compton scattering before detection. Warren and Marvel (1965) proposed a scheme based on flourescence in a molybdenum foil excited by rhodium K_α X-rays which have been scattered by the sample. The match in wavelengths of Rh & Mo is such that very little of the Compton scattering is able to excite the flourescence and remains undetected. Warren and Mozzi (1970) describe a procedure using the survival rate after transmission through a molybdenum foil, to measure that portion of the Compton which survives filtration by the flourescence technique. Strong and Kaplow (1966), however, have compared the flourescence scheme with a scheme which uses bent and ground LiF crystal monochromators in both the source and receiving beams, and found the count rate to be six times greater with the monochromator. The counting rate for the flourescence scheme was of the same order of magnitude as the background.

Aside from the Warren and Marvel scheme, several alternatives are left for the experimentalist to choose from. One alternative is to use a beta filter only (Konnert, 1973) accepting all the Compton scattering, or to use solid state detection (Dwiggins, 1971) with a light energy resolution or a wide pass-band balanced filter (Ruppersberg, 1972). The balanced filter (Young, 1962) has some advantage in resolution over the bare beta filter. The other main alternatives are to use crystal monochromators in either the source or detection beam. A crystal monochromator in the detection beam filters out part, but not all, of the Compton scattering. Until the flourescence is made more efficient or until solid state detectors become available with resolution equivalent to it, the choice will be mainly between accepting part or all of the Compton scattering. As mentioned above, the disadvantage in accepting all the Compton scattering is that the error arising from the counting statistics on the net signal is large. One cannot increase the counting time indefinitely without reaching the point at which the stability of the counting system becomes the limiting factor. Assuming one is already near this limit with a monochromator it is simple to calculate the factor by which the intensity must be enhanced in going to another method, for example balanced filters, to get the same precision. If R is the ratio of coherent scattering to total scattering, the enhancement must be greater than R^{-2}. For vanadium, one order of magnitude increase would suffice, but for phosphorus, an intensity increase of about forty would be needed. For the present experiment, a zirconium-yttrium balanced filter was fabricated, but the increase in intensity over the crystal monochromator was not appreciable enough to warrant its use.

The disadvantage to using any method which only partially eliminates the Compton scattering is that an efficiency function must be found which measures how much of the Compton scattering, at a given angle, will survive filtration by the monochromator. The crystal monochromator itself, has been faulted for several aberrations by Black and Cundall (1965), and its finite width acts as a fourth slit in the optical system. Strong and Kaplow (1966) note some of the same shortcomings but further note that appropriate cautions and proper absorption correction eliminates the problem. Experiences in this study tend to corroborate Strong's conclusion.

3.4 The Monochromator Leakage Function

Once the decision is made to use a partial filtration technique, the efficiency function of the monochromator must be found. The monochromator (or balanced filter, or solid state detector) may be seen as a band-pass filter which passes only radiation between a pair of wavelengths λ_1 and λ_2. The region from λ_1 to λ_2 is called the pass-band and $\lambda_2 - \lambda_1$

the band width. A convenient unit for wavelength shifts and band widths is the X unit (X.U.) which is, to a close approximation, one thousandth of an Angstrom. I will present an attempt at parametrization of the efficiency function in order to guage how sensitive the net intensity is to the values of the parameters.

Consider a K_α X-ray scattering from an electron in the glass sample through a scattering angle 2θ. If the electron were initially at rest, the scattering would be inelastic, and would impart momentum to the electron. The energy shift for the X-ray, increases its wavelength by an amount $\frac{2h}{mc}\sin^2(\theta)$ where h is Plank's constant, m the electron mass, and c the speed of light. In X units the shift is $48.52 \sin^2(\theta)$. The division of scattered X-rays between elastic and inelastic is determined by a recoil factor called the Breit-Dirac factor and is equal to the cube of the ratio of the initial wavelength to the shifted wavelength. The square instead of the cube is used when a counter is used for detection (Compton, 1951). The electron was not initially at rest, and its momentum distribution provides a line shape to the shifted X-rays in much the same way as it does to the angular distribution of gamma-rays in two gamma position decay. As the position of the centre of this distribution is shifted as a function of angle, the line broadens. If one takes the trend noted by Compton and Allison (1951) and expresses it in terms of angle, the line width is seen to be proportional to sin (θ) whereas the centre was proportional to the square of the sine. Ruland (1964) has claimed that for tightly bound electrons and moderately weak X-rays the width is proportional to $s^2/(a^2 + s^2)$ and both the former and Ruland's functional form will be tested below. The maximum line width is a function of the sample from which the X-rays are being scattered and is used below as an adjustable parameter, of the order of ten to twenty X units. If one assumes a line shape and is given the centre and width as a function of angle, and if one places a boundary at some wavelength representing the top of the monochromator pass band, one may integrate the lineshape up to the boundary to find what proportion of the Compton X-rays lies within the pass-band. In the model below a Gaussian lineshape, normalized to the Breit-Dirac factor is shifted from each member of the K_α doublet, weighted by the intensity ratio in the doublet, and is integrated to the edge of the pass-band. The integral of a Gaussian can be expressed in terms of the error-function. This treatment differs from Ruland's (1964) in a few respects. It treats the components of the alpha doublet separately as in the paper by Warren and Mozzi (1970) and it uses a step function for a pass-band. Ruland used a Lorentzian for both the pass-band and the Compton profile.

One other term is included in the monochromator efficiency calculations. The bottom of the pass-band cuts off all X-rays which reach the monochromator with a too high an energy wavelength. However, if X-rays of higher energy have been allowed to fall on the sample, some of them may be Compton scattered into the pass-band. Cargill noticed this (Cargill, 1970), but estimated in his case that no more than four percent of the total observed intensity at high angle was due to this "downscatter". Working within Ruland's formalism, Shevchik (1973) considered how the downscatter would effect the monochromator efficiency. In Shevchik's model the K-alpha doublet is approximated by a peak of height E_0 and width $\Delta\lambda$, and the Bremstrallung is approximated by a block E_s high and going from the minimum bremstrahlung wavelength to the K-alpha doublet. The downscatter will rise as a function of s as the leading edge moves across the pass-band until as much intensity is leaving the top of the band as enters the bottom. This is illustrated on the diagram, taken essentially from Shevchik's paper. Taking the limit of his arctangent, he finds that the downscatter contribution will be approximately constant at high s, and will be equal to the number CD = $(E_s b/E_0 \Delta\lambda)$ which he estimates from a published spectrum to be about ten percent for a pass band (b) of 20 X.U. Comparing this with the appropriate curve from Ruland's paper one finds only about five percent of the Compton intensities originates from the K-alpha doublet. This effectively [illegible] the

Figure 3.5

Terms in Shevchik's expression for the downscatter.

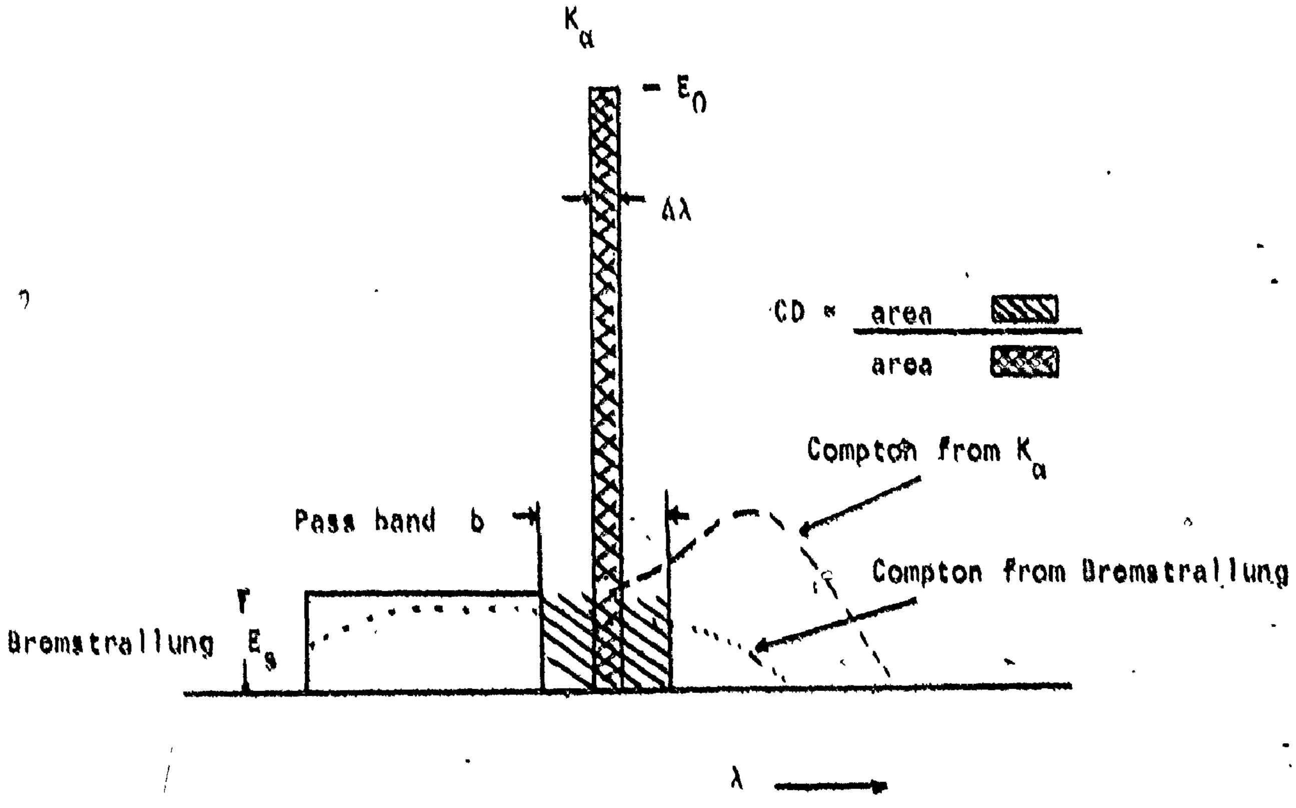

function and admits to the counter about fifteen percent of the Compton cross section.

3.5 Experimental Determinations

Two procedures have been given in the literature for measuring the leakage function. Lawrence *et al.* (1972) measured an intensity curve with a beta filter in the source beam and assumed this to contain the full Compton contribution. They then measured the intensity curve with the monochromator in place and normalised the curves together at small angles where the Compton contribution is absent. The leakage function was extracted from the difference in the two curves. At an s of about 14 Å^{-1} their leakage function is about 14% which compares with a 15% leakage value predicted for a monochromator with a .020 Å pass band. Cargill (1970) measured the pass-band on his bent LiF monochromator to be .016 ± .002 Å. According to Ruland's curves (1964), Lawrence's pass-band would have to have been on the order of .040 Å to have yielded a leakage function that high if there were no downscatter

Levy et al.(1966) and Esval (1968) have used a procedure which assumes that at high enough angle all the leakage will be due to only downscattered photons. At high enough angle, they assume that all the downscattered photons come from beyond the beta filter absorption line. Their procedure involves placing a beta filter before and then after the sample and comparing the intensities measured for the two cases. At best, this procedure only fixes the value of the leakage function at very high angle. The assumption that the leakage function at high enough angle is due just to the downscatter is supported by the results of Strong and Kaplow (1966) who measured the Compton contribution surviving their bent LiF monochromator and found the Compton intensity to vanish beyond an s of twelve reciprocal Angstroms. Their source beam was also crystal monochromated, thereby eliminating downscatter. The assumption that all the relevant downscatter at high angle originated beyond the beta filter line, is more difficult to justify because the Compton line has considerable width at high angle. X-rays which originally had wavelengths between the beta filter line and the K_α doublet will give rise to a Compton line, the centre of which may be beyond the pass-band at high angles, but the tail of which may have significant contribution to the downscatter within the pass-band. To ignore these X-rays, would cause one to underestimate the leakage function.

3.6 The Downscatter Algorithm

The following algorithm was used to generate the downscatter function used in this study. After Shevchik (1973), the intensity of the bremstrahlung is taken to be a constant function of λ below the lower edge of the pass-band. Even allowing for the breadth of the shifted line, it is not likely that an X-ray originating more than .06 Å below the pass-band, can be shifted into it. The relevant portion of the bremstrahlung is that short strip between the K_β and the K_α lines. The percent change with λ in the bremstrahlung intensity in that short strip is not large.

In the computer programme, a range of 60 X.U. is taken below the pass band, and for each wavelength in this range a Gaussian peak is shifted and broadened in the same way as it was done for the alpha doublet. The probability of spilling into the pass-band is evaluated from the integral of the gaussian. This probability being essentially a smooth, easily evaluated, function of wavelength, it can be integrated to a reasonable degree of accuracy with a six point Gaussian quadrature algorithm. Along with the contribution from the alpha doublet, this integral is evaluated at each scattering angle of interest. The ratio of downscatter to normal Compton intensity is a function of the X-ray spectrum, and is treated herein as a free parameter.

In figures 3.6-3.10, the ratio of bremstrahlung to characteristic radiation is held constant and is estimated, after Shevchik, from the spectra in the International Tables for Crystallography. The first two sets have identical parameters but the first has the width of the Compton profile varying as a function of angle according to Ruland's expression, and the second set has it set proportional to s. The only significant difference can be seen in the leading edge of the downscatter curve. Essentially Ruland's function delays the onset of monochromator action until slightly higher angles, but once the s gets into a region in which the Compton cross section is going to have even a minor contribution, the two methods of calculation give essentially identical results.

One of the reasons for doing these calculations was to güage the degree and manner in which the leakage depends on its various parameters. Consistent with the assumption of Shevchik (1973), the maximum height of the downscatter function at high s is found to be roughly proportional to the band width. Through the downscatter, the Compton intensity's influence upon the normalisation constant for the total intensity is largely determined by the size of the band width. The slope of the leakage function is influenced by the width of the Compton profile, but of all the parameters this is perhaps the least consequential, and a rough estimate of its value should suffice. The position of the inflection point in the leakage function is largely determined by the distance in wavelength between the K_α lines and the top of the

Figure 3.6

Leakage function components

(a) The downscatter alone.

The width of the pass band, B, is set at 16 X U. The maximum width of the shifted line is varied from 12 to 18 X U at five equal intervals, and a curve is plotted for each value.

(b) The Q(s) function without downscatter.

(c) The total leakage function.

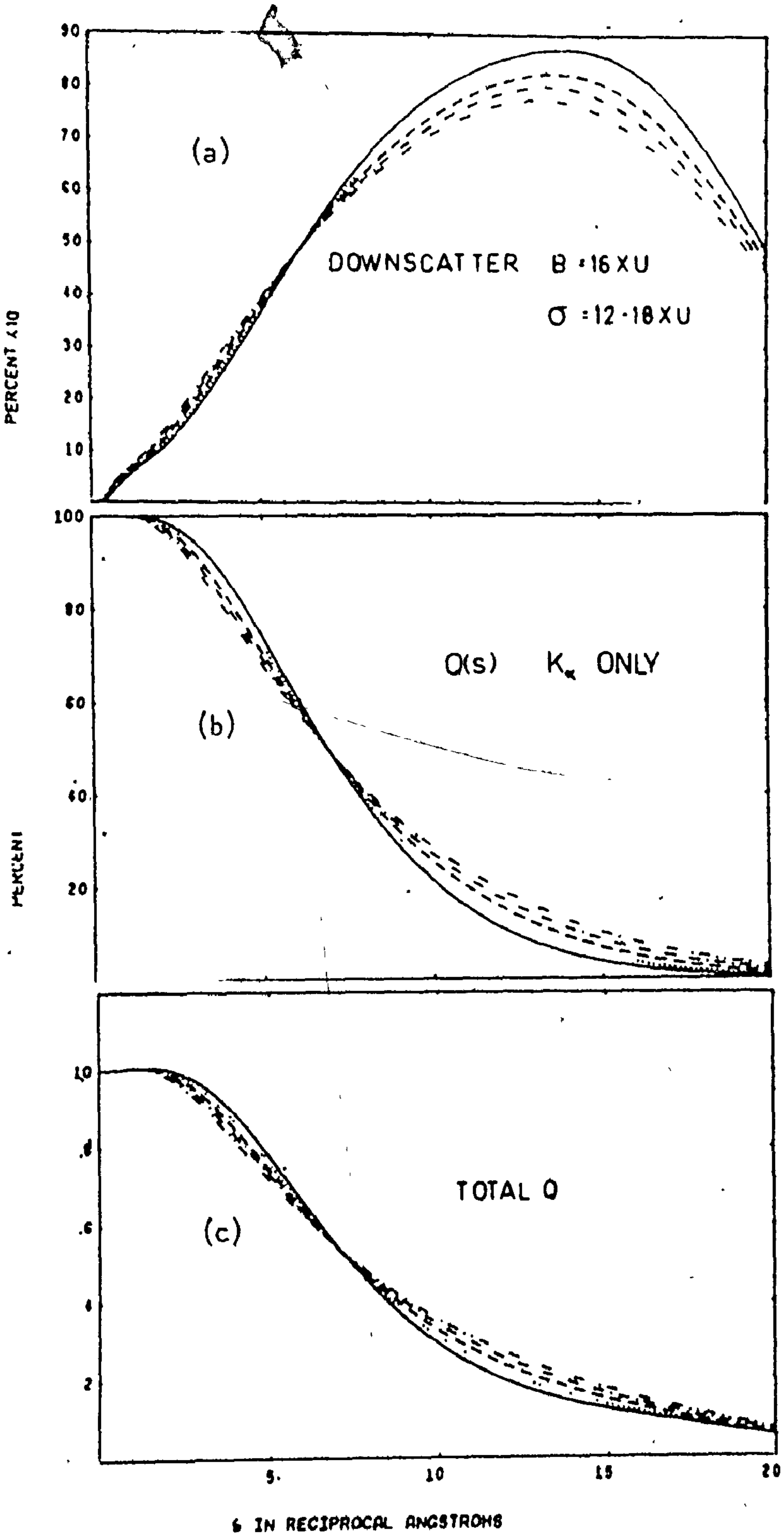
90
80
70
60
50
40
30
20
10
PERCENT X10
(a)
DOWNSCATTER B = 16 XU
σ = 12 - 18 XU
100
80
60
40
20
PERCENT
(b)
Q(s) K$_\alpha$ ONLY
1.0
.8
.6
.4
.2
(c)
TOTAL Q
5
10
15
20
s IN RECIPROCAL ANGSTROMS

Figure 3.7

Leakage function components

(The same as Figure 3.7 except the maximum σ is lower and σ varies with s according to Ruland's function)

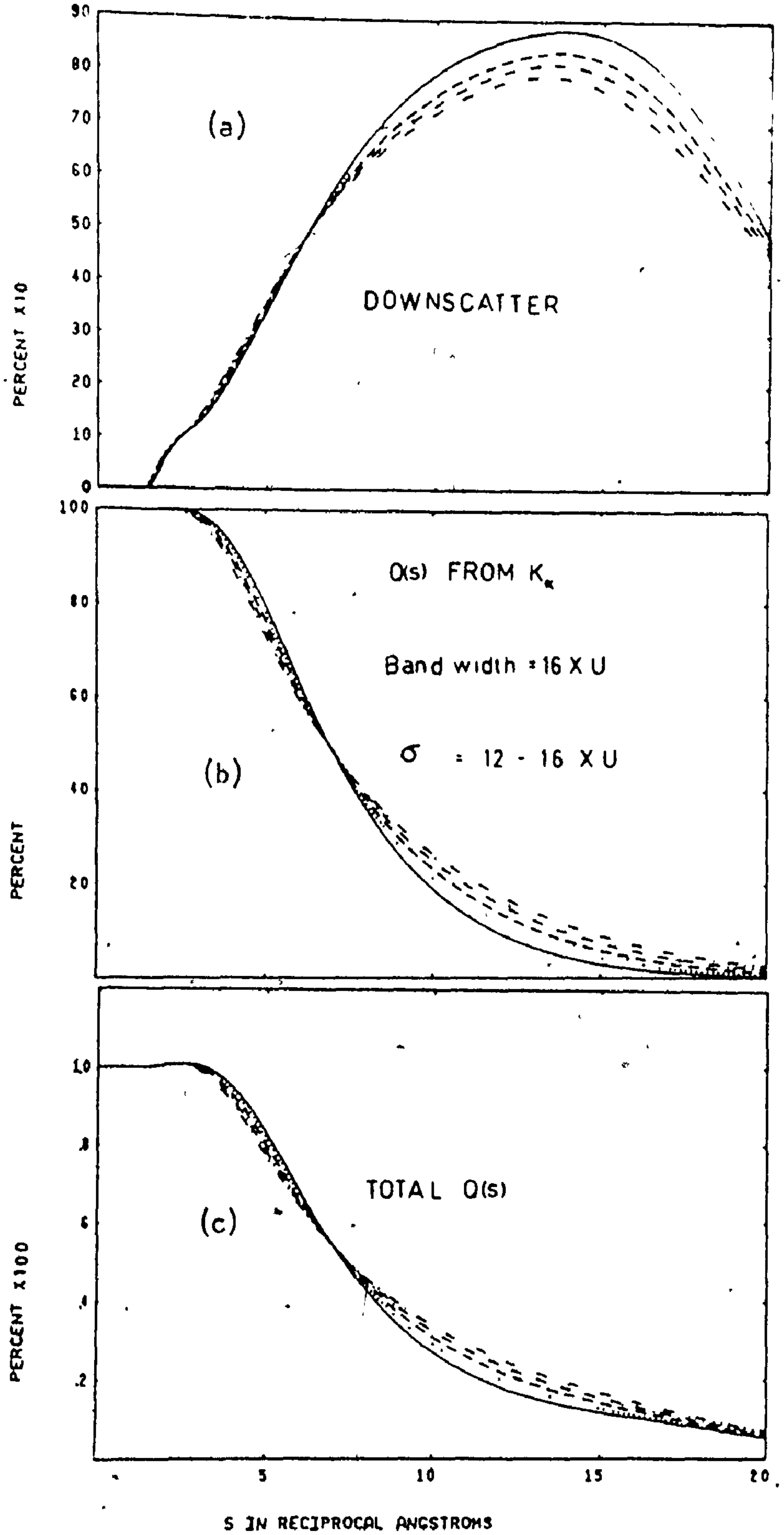
(a)
DOWNSCATTER
PERCENT X10
0
10
20
30
40
50
60
70
80
90
(b)
Q(s) FROM K_α
Band width = 16 X U
σ = 12 - 16 X U
PERCENT
20
40
60
80
100
(c)
TOTAL Q(s)
PERCENT X100
.2
.4
.6
.8
1.0
5
10
15
20
S IN RECIPROCAL ANGSTROMS

Figure 3.8

The influence on the Compton intensity
of the position of the centre of the pass band
relative to the K_α line.
Two series are shown; one with σ of 15 XU, and one
with σ of 10 XU. The band width is 16 XU for all graphs.

(a) The total Q function.
This is the coefficient of the Compton intensity
in the total scattering function.

(b) The Compton contribution.
This is the Compton intensity for VPO_5 glass
in electronic units.

(c) The ratio of the Compton contribution to
the total background function (including the
independent scattering intensity).

Each graph has five functions. The pass band has been shifted from zero to six XU in the direction of shorter wavelength.

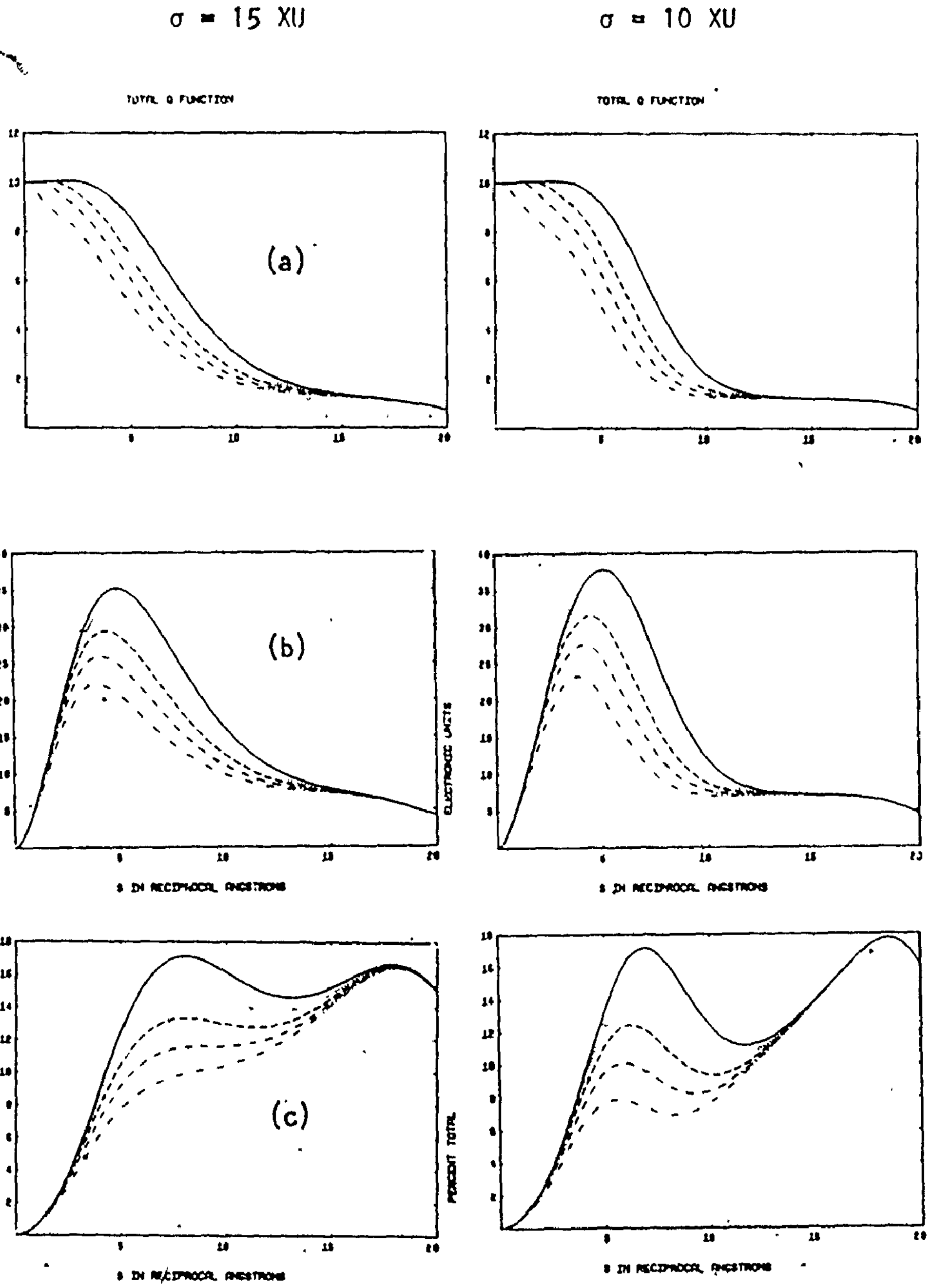
σ = 15 XU
σ = 10 XU
TOTAL Q FUNCTION
TOTAL Q FUNCTION
(a)
(b)
(c)
ELECTRONIC UNITS
PERCENT TOTAL
S IN RECIPROCAL ANGSTROMS
S IN RECIPROCAL ANGSTROMS
S IN RECIPROCAL ANGSTROMS
S IN RECIPROCAL ANGSTROMS
5
10
15
20

Figure 3.9

The influence of pass band shift on the

Compton intensity

$\sigma = 20$ XU

Band width = 14 XU

The centre of the pass band is shifted 1-5 XU toward

shorter wavelength.

(a) The total Q(s) function

Notice that this function exceeds 1.0 for a short span of s. This is bacause the downscatter is regarded as extra intensity when the Compton intensity is scaled with the coherent scattering.

(b) The Compton contribution to the total scattering for VPO_5 glass (in electronic units).

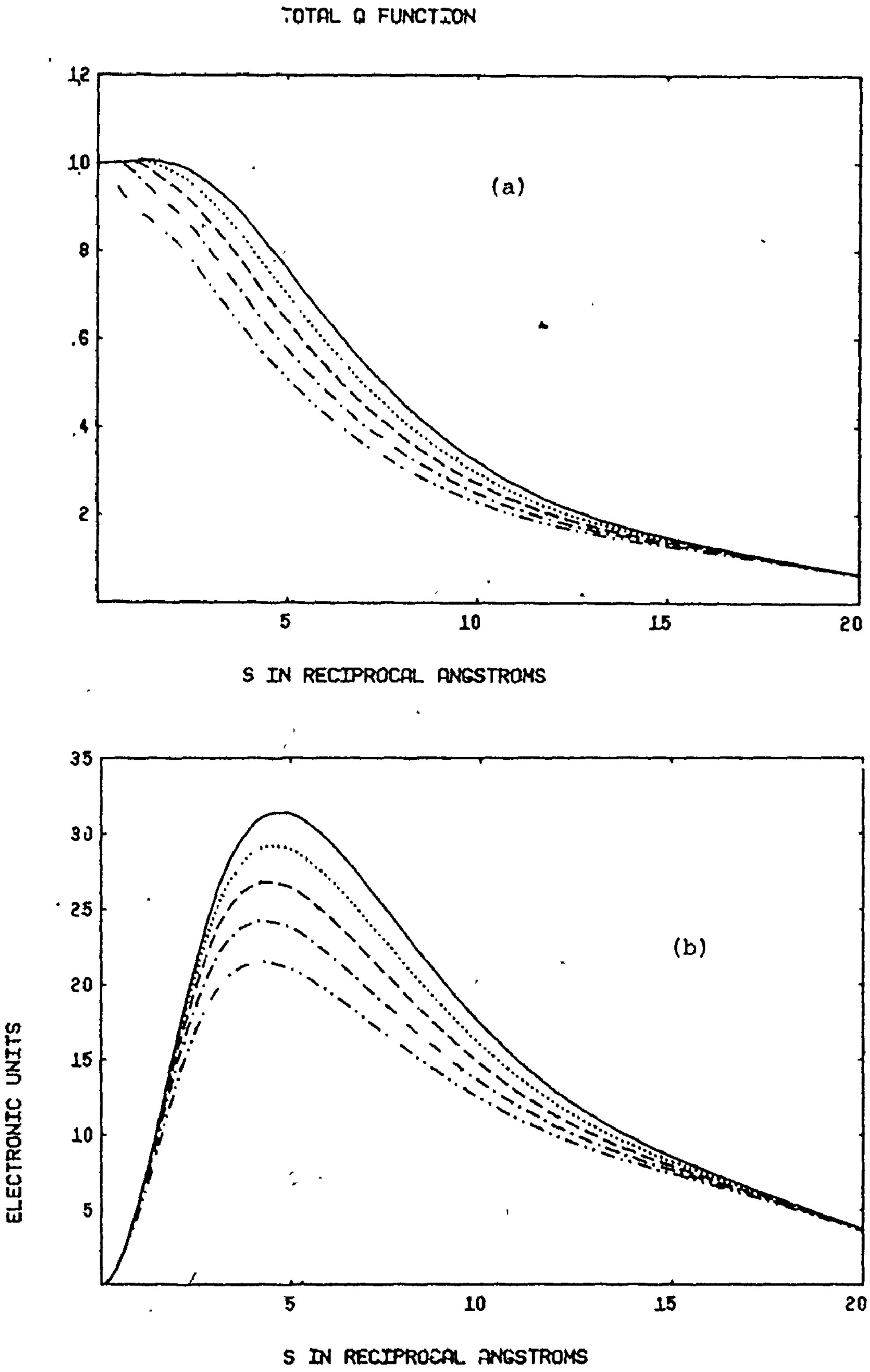

TOTAL Q FUNCTION

Figure 3.10

The calculated Q(s) function with measured points

Band width = 16 XU

The top of the pass band is fixed at 713 XU.

σ varies from 16 XU to 24 XU with increments of 2XU.

(a) Total Q(s) function expressed as a percent transmission with points from Lawrence _et al_. (1972)

(b) The ratio of the Compton scattering for VPO_5 glass to the total scattering expressed as a percent.

TOTAL Q FUNCTION

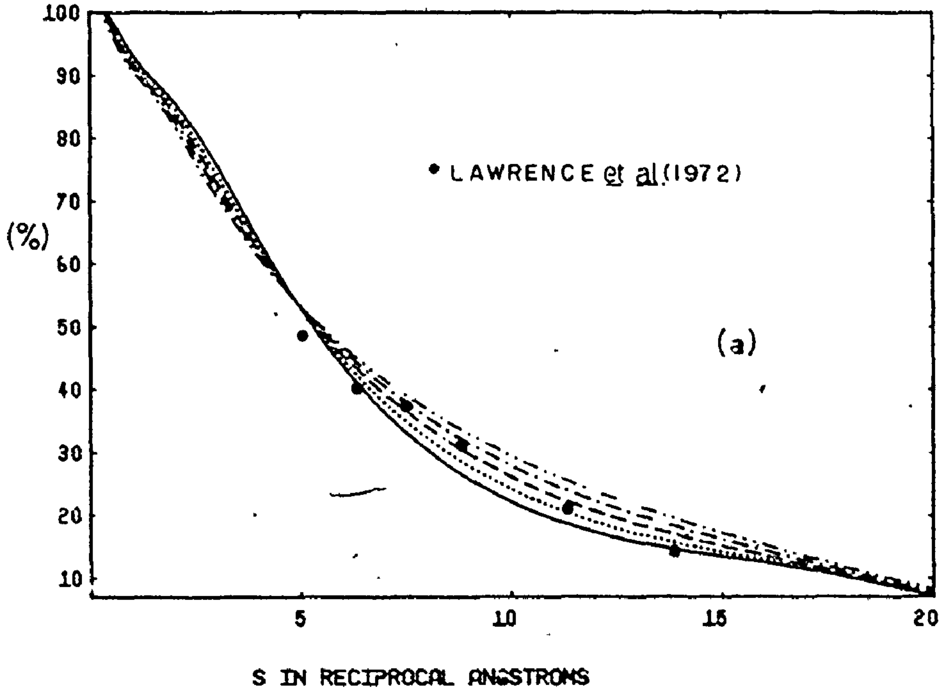

COMPONENT FOR VPO5 GLASS

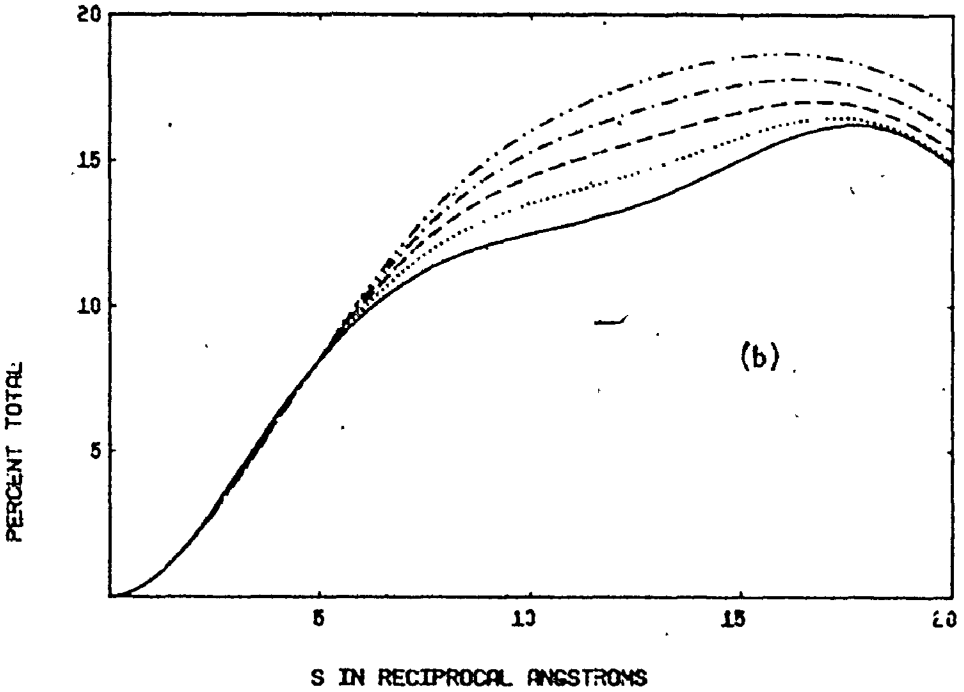

pass-band. If the monochromator is perfectly tuned, the K_α lines will be in the centre of the pass-band. In such a case, the inflection point on the leakage function will be determined by the band width. Should the bandwidth be on the order of 16 X.U. as measured by Cargill (1970), the K_α doublet could be as much as 5 X.U. off centre without great loss of intensity. This last factor is not very influential on the high s portion of the leakage function, but it does have a strong influence on the Compton contribution in the middle range of s.

The bandwidth can be measured once and henceforth be considered a constant of the instrument. The white radiation to K_α radiation ratio can be estimated from measured spectra, and for a given set of operating conditions, could also be considered a constant of the instrument. If one could assume that the K_α doublet is always centred in the passband, then measured leakage functions such as that given by Lawrence et al. (1972), would be much more useful. They give a leakage value of .653 for an s value of 3.77 $\mathring{A}^{-1}$ which is rather interesting, considering that two thirds of the Compton scattering originates from the K_{α_1} line, and that at that scattering angle this two thirds will still be mid-way between the components of K_α doublet. This implies that their monochromator was so tuned that the top of their pass-band sat so close to the $K_{\alpha 2}$ line that nearly all the Compton originating in that line was lost. A leakage function calculated with a bandwidth of .016 Å, α_{max} of .017 Å, and shifted such that the top of the pass-band is at .713 Å falls close to their measured values. A graph showing this is in Figure 3.10.

3.7 Multiple Scattering

It is assumed in the interpretation of the measured scattering intensities that all the X-rays considered have scattered only once while in the sample. If it can be taken for granted that the secondary scattering is either too small to be significant or so slowly varying that an empirical background correction contains it, then no further concern is necessary. Algorithms have been developed to calculate the secondary scattering, and it has been estimated that a correction as high as ten percent (Warren, 1969) in silica glass is needed. This shows that it is not necessarily small enough to ignore in an a priori background correction. It was found in the course of the present study that oscillations of significant magnitude and frequency may appear in the secondary scattering at high angle. The empirical background correction procedure will not adequately handle this component.

Strong and Kaplow (1967) devised a very flexible Monte-Carlo algorithm for the calculation of secondary scattering. At about the same time Warren and Mozzi (1966) developed a closed form equation for secondary scattering from a flat, effectively infinitely thick sample, in the reflection mode. It is Warren's algorithm which will be used here. Dwiggins and Park (1971) extended Warren's method to the case of reflection or transmission from thin slabs of weakly absorbing material. For the case in which the linear absorption constant times the thickness is much greater than one, the influence of the finite of the sample thickness dwindles, and Warren's infinite sample equations become adequate.

The variables in Warren's approximation are defined in the diagram on the following page which was copied from figure one of Warren and Mozzi (1966). The X-rays enter from the left and intersect the sample surface with an angle theta. The original beam lies in the XZ plane and the XY plane is parallel to the sample surface. The X-ray is first scattered in volume element dV_1 and travels a distance r before scattering again in element dV_2. It then leaves the surface of the sample with again the angle theta. Polarisation effects due to a crystal monochrometer are ignored, but the polarisation caused by each reflection in the sample is included in the function PF, where

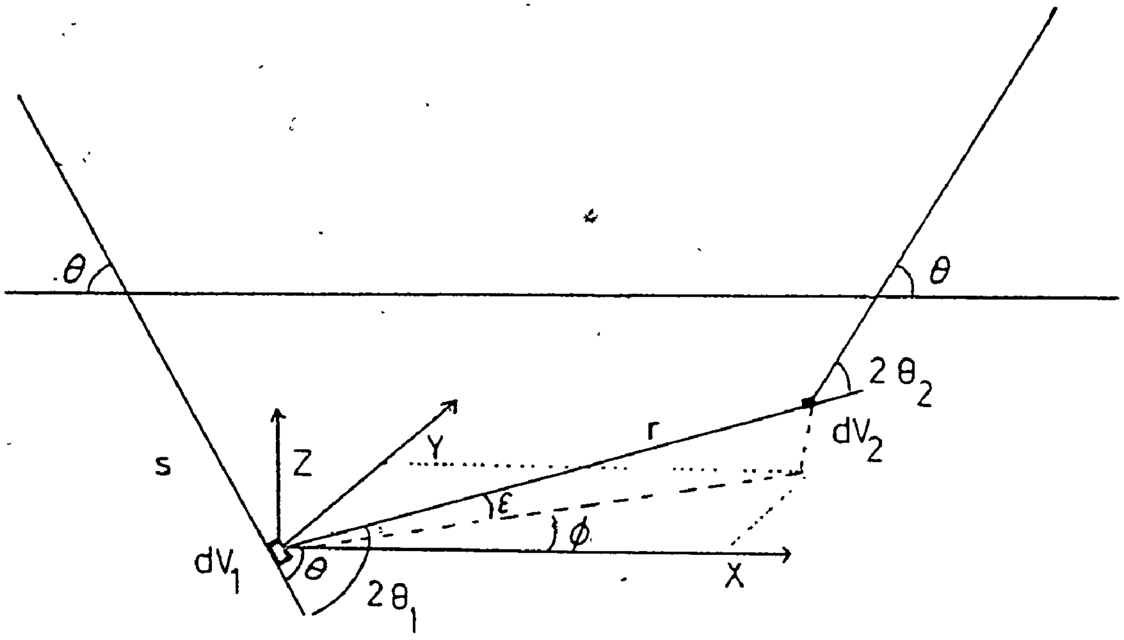

Figure 3.11. Angles in the double scattering event.

$$PF = \tfrac{1}{2}(p_1^2 + p_2^2 + (p_1 p_2 - \cos(2\theta)^2)$$

where

$$p_1 = \cos(2\theta_1) = \cos(\theta)\cos(\phi)\cos(\varepsilon) - \sin(\theta)\sin(\varepsilon)$$

and $p_2 = \cos(2\theta_2) = \cos(\theta)\cos(\phi)\cos(\varepsilon) + \sin(\theta)\sin(\varepsilon)$

The initial penetration distance s and the distance between scattering events r are integrated over to give an absorbtion term of the following form;

$$\sin(\theta)/(2\mu^2)\ (\sin(\theta) + |\sin(\varepsilon)|)\quad .$$

The intensity of scattered X-rays is expressed in terms of $J(2\theta)$ which is in electronic units, and is approximated in Warren and Mozzi (1966) by $\Sigma\ f_i^2$ (+the incoherent intensity where applicable). First order scattering has only one J function, but the second order scattering has a $J(2\theta_1)$ in volume dV_1 and $J(2\theta_2)$ in volume element dV_2, and the probability of a combined scattering event is proportional to the product of the two J's. The probability of a scattering event is also proportional to the probability of the X-ray encountering a scattering centre. The density of scattering units is denoted as n. Because one eventually wants to subtract the secondary scattering intensity I(2) from the primary I(1), and because they have several variables in common which may be eliminated by using the expression for I(1) into that for I(2). The scattering cross section for an electron remains as does the density of scattering units andthe linear absorption coefficient. The ratio of the latter two is simplified as

$$\frac{n}{\mu} = N/\Sigma\ A_i\mu_i$$

This latter is a simplification in the sense that the mass density of the sample has been factored out. The N is Avagadro's number and the A_i and μ_i are the atomic weights (atomic units) and mass linear absorption coefficient. The sum is taken over the atoms in the stoichiometric unit. It may appear that this term destroys the invariance of the expression to choice of the structural unit, but the invariance is restored in the sum over f^2 to which J is normalised. The expression at this stage is

$$\frac{I(2)}{I(1)} \doteq \sigma_e \frac{2\sin(\theta)}{(1+\cos^2(2\theta))} \frac{n}{\mu J(2\theta)} \int_{-\pi}^{\pi}{}_{\phi} \int_{-\pi/2}^{\pi/2}{}_{(\epsilon)} \frac{PFJ(p_1)J(p_2)\cos(\epsilon)d\epsilon d\phi}{\sin(\theta) + |\sin(\epsilon)|}$$

The symmetry of the integrand allows its reduction. If the X-rays scatter to the left or right, as viewed from above the sample, of the I(1) scattering path in their travels between dV_1 and dV_2 before being scattered at dV_2 back into the I(1) path, we have a negative or positive ϕ. Because of the symmetry of the scattering, only positive ϕ need appear in the integral and a factor of two compensates for the negative ϕ. Taking ε to $-\varepsilon$ interchanges p_1 and p_2 but the product $J(p_1)$ $J(p_2)$ is invariant. The range of ε can be reduced to positive values alone. Taking ϕ to $\pi - \phi$, takes p to $-p$ which corresponds to adding 45° to the scattering angle θ to which J corresponds. The integrals of ϕ from 0 to $\pi/2$ and from $\pi/2$ to π can be computed simultaneously by replacing $J(p_1)\ J(p_2)$ by $J(p_1)\ J(p_2) + J(-p_1)\ J(-p_2)$. Lastly, it can be seen that ε appears only as $\sin(\varepsilon)$. A change of variable of $x = \sin(\varepsilon)$ saves computing the sine and cosine of epsilon. If one now defines a current $J'(2\theta)$ as

$$\frac{J'(2\theta)}{J\ (2\theta)} = \frac{I(2)}{I(1)}$$

which is now the secondary scattering in the same units as the primary scattering, the expression for J' is

$$J'(2\theta) = \sigma_e \frac{8N}{\Sigma A_i \mu_i} \frac{\sin(\theta)}{(1+\cos^2(2\theta))} \int_0^{\pi/2}\int_0^1 \frac{PF(J(p_1)J(p_2)+J(-p_1)J(-p_2))}{\sin(\theta) + x}\, dx\, d\phi$$

In Warren and Mozzi's paper (1966) in which the above is all derived, it is assumed that J may be approximated by the sum of f^2 with or without the Compton component. J is parametrised, and the integral is evaluated and tabulated for various values of the parameters. In the present study, J was either taken as a cubic spline interpolation of the normalised measured intensity, extrapolated above and below the measured domain in s by the TSF function, or J was taken to be the TSF function itself. Gaussian quadrature was used for the integration, which was performed for each θ at which data were taken. When the TSF was extended to include the Compton scattering with the downscatter function described above, computation became rather costly, and great savings were realised by using spline interpolation for the TSF also. With this approximation, the J' can be calculated for a whole data set, with either or both definitions of J, in less than one minute of computer time. Reliance on tabulated values should not be necessary.

On the following page is a graph of J' for the vanadium phosphate glass with fifty percent vanadate composition. A few features of the curve warrant notice. The secondary scattering is scaled by the linear absorption coefficient. Warren computed (Warren, 1969) that secondary scattering should be a nine percent (maximum) effect in silica glass. On the basis of absorption coefficient scaling the VPO_5 glass should have a three percent effect, which is approximately what is found. Warren's (1969) curve, in percent secondary scattering, peaks as theta goes through 45^o, and this same behavior appears on the present curve of J' as a change of slope near an s of 12 $\overset{o}{A}^{-1}$. The most important feature of the curve is the oscillatory component above 10 $\overset{o}{A}^{-1}$ in the curve computed from I(s) but not in the one computed from TSF. The amplitude of the oscillation is

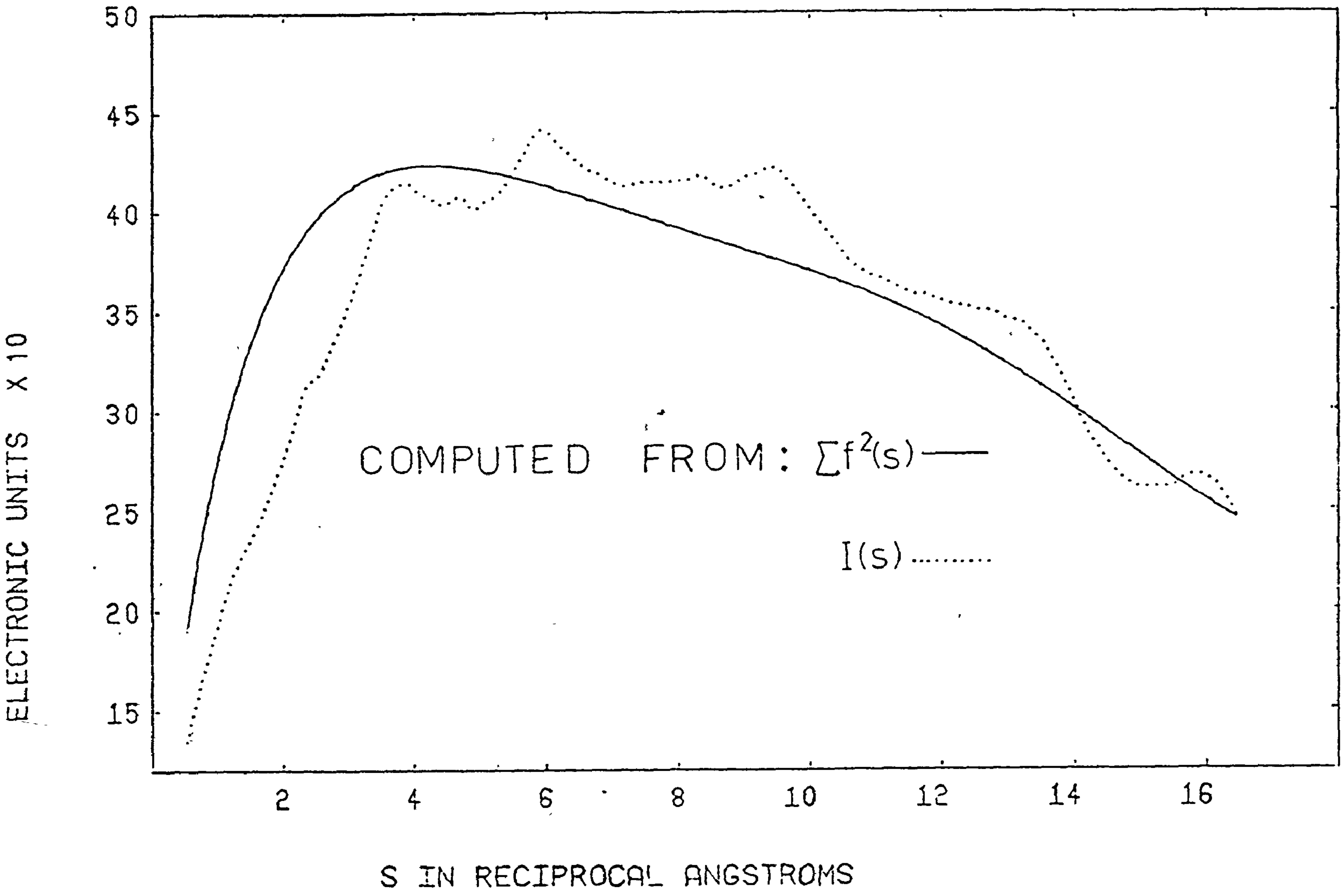

Figure 3.12 Warren secondary scattering intensity for VPO_5 glass.

——— Calculated from Σf_1^2

- - - - - Calculated from I(s)

on the order of half an electronic unit. Although I(s) is on the order of seventy units, its oscillatory portion i(s) has an amplitude of only two electronic units. This constitutes approximately a thirty percent systematic correction to i(s) which could not be removed by an empirical background correction such as that of Konnert and Karle (1973), because one of the constraints built into such a system requires the empirical background to be monotonic over regions of the order of the period of oscillation of the signal, i(s). In this case the spurious signal has a wavelength on the same order as that of i(s). Were oscillations of the same relative magnitude to occur in silica glass, they would constitute nearly a one hundred percent correction to i(s), and there is no guarantee that the spurious signal would interfere constructively with the true signal. This estimate is based on the scaling of the secondary scattering with the linear absorption coefficient. It should be kept in mind that i(s) is only a few percent of I(s) for most glasses of interest, and that I(s) is the function used to calculate J', the secondary scattering intensity. A large correction to i(s) from this effect will still not significantly change J', so there is no advantage to using corrected I(s) to calculate J' again. In their Monte-Carlo calculations, Strong and Kaplow (1967) used both the independent scattering and the scattering computed from two pseudo-liquids. The J' from one pseudo-liquid qualitatively follows that of the independent scattering, but the J' from the other pseudo-liquid has structure. Only four sample points were computed in the region of interest.

One other question with regard to this problem is worthy of note. The above treatment follows that of Warren and Mozzi and ignores the effects of crystal monochromators Malet et al. (1973) treat the problem of double scattering more generally, and includes the effects of a monochromator in the source beam. For the special case of an infinite slab, their results reduce to the ones quoted above except for the polarisation factor which appears outside the integral in both treatments. In the treatment of data in this study the term $1+\cos^2(2\theta)$ in the above is replaced by $(1+\cos^2(2\alpha)\cos^2(2\theta))$ to bring it into correspondence with Malet's result. The polarisation correction corresponding to a monochromator before the sample differs from that corresponding to the monochromator after the sample by a multiplicative constant. The function used here differs from Malet's by that constant.

The above has listed all the ingredients in the data treatment used in this study. The specific treatment sequence used is the following. The intensity, corrected for absorption and polarisation is merged into a single curve from its segments. It is then normalised using the Krogh Moe (1956) algorithm to a theoretical background function which includes the Compton scattering times a filter function incorporating the downscatter contribution. Once normalised, the intensity is used to calculate the secondary scattering which is then added to the background function and a new normalisation constant found. This normalisation is fine-tuned with a least-squares minimisation algorithm to minimise the ripples at small r in the radial distribution function. Attempts to refine the bulk density, were discontinued when it was found that the ripples due to the termination effect made the apparent density but not the normalisation constant, a function of the size of the domain in r space expected to be structure free. At this point the intensity and background were plotted and a radial distribution curve calculated. The secondary scattering is then subtracted from the intensity and an empirical background calculated. The empirical background gives a slightly improved fit to the intensity at high angle, and the above procedure of first including the secondary scattering in the background and then subtracting it from the intensity ensures its proper contribution to the normalisation but also removes the systematic spurious contribution to the signal before the empirical background is fitted. In their treatment of the empirical background function, Konnert and Karle (1973) use a minimisation routine operating on the small r ripples to fit the background function. An alternative approach is to treat the ripples as the transform of a correction function to the empirical background, and to calculate the correction by Fourier transforming the ripple to scattering space. That this has an equivalent effect to Karle's minimisation procedure was acknowledged by him in the question period following a paper delivered to the American Crystallographic Association (Karle, 1974). In the present study a single back-transformation correction following the formation of the empirical background function was found to give a very clean region below the first peak. In general the a priori background function gave a reasonably clean region at low r to its radial distribution function, and the empirical corrections served only as a fine tuning of the background function.

The reasoning behind the back-transform correction mentioned above may warrant further discussion. Aside from the ripples in the secondary scattering cross section, which at this point will be considered a correction to the intensity rather than a component of the background function, the background function may be considered to be the sum of the independent scattering function (Σf^2) and the Compton component. Both of the latter terms are Fourier transforms of atomic wave functions, and consequently, should not exhibit oscillations in scattering space which would correspond to lengths in real space that extend well beyond the radius of an atom. Any electrons which cannot be considered to be localised on the parent atom will be considered for the purposes of this study to be part of the radial distribution function, and consequently their scattering is ascribed to the signal as opposed to the background. It can be seen from the above that a rather clear demarcation can be found between the intra-atomic and the inter-atomic regimes and that spurious detail in the low r region can be identified with the intra-atomic scattering i.e. the background function. If the real background function is called $\Omega(s)$ and it is approximated by Ω_o and if its transform leads to non-physical signal in r-space which would be absent in the transform of Ω, then this spurious signal may be identified with the transform of $\Omega_o - \Omega$.

Several workers have investigated the generic causes of the ripples at low distance in the pair function or radial distribution function. Leadbetter and Wright (1972c) and Kaplow et al.(1965) perturbed their intensity functions and measured the effect on the ripple magnitude. The most outstanding cause of the ripples is improper normalisation, and the choice of normalisation constant may be fine tuned (as it was in the present study) by minimising the amplitude of the ripples. The ripple amplitude is only one parameter, but Rahman (1965) has generated an infinity of parameters to be minimised by the further requirement that the pair function be not only zero but flat in the low distance region. Flatness implies that all Fourier coefficients of D(r) in that region vanish. Rahman Fourier transforms that part of the radial distribution function to an arbitrary μ-space and compares the result with the transform of the ideal function for each value of μ. He finds that neutron scattering data fits his function better than X-ray data and suggests that his equations be used to find the normalisation constant and to test the quality of the data. As investigated by (Leadbetter and Wright, 1972c and Kaplow et al., 1965) the atomic scattering factors may be slightly in error, or the Compton contribution may be inadequately treated (Levy, et al.,1965), or the multiple scattering may be a problem. All these factors have been shown to have a form which will give rise to the low distance ripples. They are also factors from which (except multiple scattering) neutron scattering does not suffer. It should be no surprise that Rahman found better agreement with neutron data.

The final stage of analysis, once the radial distribution is available, is to fit a model to it. Original attempts to use least-squares refinement on the model, for which programmes had been written, were abandoned when it became obvious that the number of variables had become prohibitive. Aside from computer space limitations, a basic problem in any such least-squares refinement is to find parameters which are not correlated. Once the α-VPO_5 perturbed crystal model had been shown to have reasonable success in predicting the positions and strengths of the most prominant features, various warps and perturbations were considered and whole classes of peaks were shifted or broadened to correspond to that perturbation. The semi-empirical bond-strength criteria of Brown and Shannon (1973) were used as a quantitative guide in estimating the more likely form of relaxation for the perturbed crystal to take. A pair distribution function was then calculated for the perturbed structure and compared with the experimental pair distribution function. This procedure allowed the systematic consideration of adjustments to the model, while avoiding some of the problems that variable correlation would cause in a least-squares strategy.

The calculation of the radial distribution function or the pair distribution function involves the evaluation of an integral of the form ∫y(s)sin(rs)ds where the kernel of the transform, sin(rs), may for some rs combinations be a rapidly varying function of s. There is particular cause for concern when the kernel is changing sign after sampling only a few data points of y(s). A partial solution of the problem is to interpolate the relatively slowly varying function y(s) onto a finer grid of s values and to use a quadrature algorithm which is sensitive to rapid changes in the quadratures. Another solution is to use a quadrature algorithm which is specifically designed to ameliorate the problem for integrals with a sinosoidal kernel. In 1928 L.N.G. Filon presented just such an algorithm (Filon, 1928) for the evaluation of ∫y(s)sin(rs)ds when y is tabulated for evenly spaced intervals of s. A separate sum is taken over even and odd indexed data and a weighted combination of these sums is formed where the weighting factors are functions of the arguments. The algorithm is discussed in a text by Kopal (1955), and a specific form for the x-ray problem is given in a review by Wagner (1972). However, Wagner's form has some typographical errors. The form as used in this study is given below.

$$z(r) = \int_a^b y(s)\sin(rs)ds$$

$$\Delta \equiv b - a$$

$$p \equiv \Delta r$$

$$\psi \equiv \cos(p)$$

$$\phi \equiv \sin(p)$$

$$\alpha \equiv \psi\phi/p^2 + 1/p - 2\phi^2/p^3$$

$$\beta \equiv (1 + \psi^2 - 2\psi\phi/p)(2/p^2)$$

$$\gamma \equiv 4(\phi/p - \psi)/p^2$$

$$Ev = \sum_{i=2,4,...}^{198} \sin(rs_i)y(s_i)$$

$$Od = \sum_{i=1,3...}^{199} \sin(rs_i)y(s_i) - \tfrac{1}{2}\sin(rs_{199})y(s_{199})$$

$$\Gamma \equiv y(s_1)\cos(rs_1) - y(s_{199})\cos(rs_{199})$$

$$z(r) = \Delta(\alpha\Gamma + \beta Od + \gamma Ev)$$

This algorithm reduces to Simpson's quadrature when the integrand is smoothly varying with respect to the tabulation interval. The specific numbers 198 and 199 are given above for clarity but a 400 interval subroutine was used alternatively with the 200 interval routine when needed.

The last step in the analysis was to calculate a curve in scattering space which could be compared directly with the data. The model intensity is calculated by the equation below where C_{ij} is the multiplicity of a Gaussian peak of width u_{ij} and centred on the interatomic distance r_{ij} in the pair distribution function.

$$i(s)_{mod} = \Sigma_{\substack{pairs\\ij}} C_{ij}\, f_i f_j \frac{\sin(sr_{ij})}{sr_{ij}} e^{-\frac{1}{2}u_{ij}s^2} \quad W(r_{ij},Rmod)$$

If peaks are only supplied to the model for $r_{ij} < Rmod$ there will be large fluctuations in $i(s)_{mod}$ at smaller s values corresponding to a termination effect very similar to that seen at small r in the transform of the reduced intensity because i(s) is not given beyond some finite value s_{max}. One way around this problem is supplied by the quasi-crystalline model, in which one sees the local order as described by the finite model as a crystallite imbedded in a mass of constant density equal to the average density of the crystallite. One then calculates the scattering by the uniform matrix surrounding the crystallite and includes that in the model intensity as a correction. The $W(r_{ij}, Rmod)$ in the equation above is a weighting function which merges the matrix term with the model term. It is given by Leadbetter and Wright as below along with their function for the matrix continuum scattering (Leadbetter, 1972a).

$$\xi \equiv r_{ij}/Rmod$$

$$W(\xi) \equiv (\xi - 1)^2(\xi + 2)/2 \qquad \xi<1$$

$$W(\xi) = 0 \qquad \xi>1$$

$$i_o(s) = .75\,\pi\,Rmod^3\,\Sigma_i\Sigma_j\, f_i f_j \rho_j^o\, \{(\frac{1}{y^4} - \frac{1}{y^6})\cos(2y) - \frac{2\sin}{y^5}(2y) + \frac{1}{y^4} + \frac{1}{y^6}\}$$

$$y = sRmod/2$$

This function for $i_o(s)$ corresponds to a spherical crystallite and would not be expected to work well for a highly anisotropic model such as the one proposed in this study, however it does work reasonably well in this case.

CHAPTER 4

CRYSTAL STRUCTURE OF PbV_2O_6

4.1 Preparation and Preliminary Investigation

The initial investigation of cell dimensions and space group was performed on specimens provided by Dr. R.D. Shannon, but several subsequent attempts were made to grow larger or more equidimensional crystals. The following procedure was followed in those preparations. Stoichiometric amounts of PbO (Fisher Scientific) and V_2O_5 (Fisher Scientific) were melted together and the temperature reduced slowly through the melting point. The melting point was determined by differential thermal analysis to be 600 ± 5°C. Most of the crystals grew as very thin yellow-brown needles, often clustered into a sheath of nearly parallel needles. Some crystals had very dark, nearly opaque, colouration. The crystals were often glued together by a black vitreous matrix. Density measurements were not made because the intimacy with which the crystals were mixed with the matrix militated against the isolation of enough purely crystalline sample. No chemical analysis was performed. X-ray photographs had indications of orthorhombic symmetry with extinctions for h odd in hk0 and k+ℓ odd in 0kℓ. Two possible space groups which fit this symmetry are $Pn2_1a$ and Pnma. Attempts were made to refine the structure in each space group.

The first crystal upon which diffractometer data was taken was a needle .02 X .02 X .4mm. This was mounted onto a Syntex P$\bar{1}$ diffractometer with a graphite crystal monochromated MoKα X-ray source. The angles for fifteen reflections with 2θ values between twenty and twenty-five degrees were refined to give the cell dimensions. The cell constants found, with standard error in parentheses, are a = 9.771(10), b = 3.684(4), and c = 12.713(13) Å. With a formula weight of 405.07 grams per mole, an assumed four formula units per cell and a cell volume of 457.6 $Å^3$, this gives a calculated density of 5.89 g/cm^3.

The intensities were measured using a 2θ scan with variable scan rate depending upon the maximum counting rate in the intensity profile. The scanning rate in degrees 2θ per minute varies from 2^o/min to 24^o /min. The diffractometer then measures the background on both sides of the spot so that an interpolated background correction can be made. Reflections whose calculated standard deviation exceeded one third of the intensity were tagged as "unobserved" and those reflections whose integrated intensity, after correction for background, was indicated as negative were deleted. Within a sphere of 2θ less than fifty degrees, 759 unique reflections were measured. Using the programmes in the X-ray 71 Programme series, the intensities were corrected for polarization, the Lorentz effect, and absorption.

The absorption correction applied to this crystal approximated the crystal shape as a cylinder. The needle axis corresponded to the short axis (b) of the cell. In a cylindrical crystal absorption correction, the data set is divided into subsets according to the angle that the scattering plane makes with the needle axis. In this case each subset was defined by the index k. An effective absorption coefficient is calculated for that subset by the relationship (Buerger,1960)

$$R\mu_{effective} = \mu R/\cos(\nu)$$

where R is the radius of the cylinder, μ is the linear absorption coefficient, and ν is the angle between the X-ray beam and the cylinder axis. For any given subset the transmission factor varies slowly with scattering angle, but the degree of this variation is quite similar between subsets except for a multiplicative constant. The greatest effect of a cylindrical absorption correction is to apply a relative scale constant to each subset. It follows that the greatest manifestation of systematic error due to inadequate absorption correction will be to scale one subset relative to the others.

A Patterson function was calculated from the intensities and solved for the positions of the lead and vanadium atoms. The space group assumed at this point was Pnma.

A difference synthesis readily yielded the positions of the oxygen atoms, and least squares refinement was begun. The scattering curves for O^{2-} and Pb^{3+} and the dispersion corrections were taken from the International Tables for X-ray crystallography (1963), and the scattering curve for V^{5+} was taken from Cromer and Waber (1965). When the refinement had progressed to the point at which the thermal and positional parameters were shifting only slightly relative to their errors, the data was separated into subsets as had been done in the absorption correction and different scale constants were refined for each subset. Enough systematic variation in the higher k index sets was found to warrant further attention.

A new crystal was grown, which was more equidimensional, and use was made of a microscope attachment which had since become available, to measure the dimensions more closely. The dimensions were found to be .016 x .016 x .04mm. Reflections from eight quadrants were measured, corrected for absorption and then averaged. In this way the effectiveness of the absorption correction could be monitored by comparing the intensities for symmetry equivalent reflections. Only 649 unique reflections remained after the averaging. The absorption corrections were calculated with the programme Absorb written by R.F. Stewart . A 4 x 4 x 8 integration grid was used and found adequate to make symmetry equivalent reflections equivalent. / The intensities from the first data set were scaled and averaged with the second set. There was not total overlap between the segments of reciprocal space sampled by the two data sets, so the composite data set contained 816 unique reflections. With the new data set, refinement was continued. Anisotropic temperature factors were refined on the metal atoms only. With so much of the scattering power of the unit cell dominated by the metal atoms, as in this structure, the thermal parameters of the weaker scatterers are not as well defined. Only isotropic temperature factors were refined for the oxygens.

In the final few cycles of refinement, a weighting function was used. When a weighting function is used, the quantity minimized by the least-squares algorithm is the weighted residual, R_w, which is defined as:

$$R_w = \sum_{i=1}^{N} w_i(|F_o| - |F_c|)^2/\Sigma\, w_i|F_o|^2$$

where F_o and F_c represent the observed and calculated structure factors respectively, and the index i runs through all N reflections. The difference between the moduli of the observed and calculated structure factors is often denoted as Δ. The weighted residual is to be distinguished from the often quoted conventional "R" factor, or reliability index. That index is defined as

$$R = \Sigma|\Delta_i|/\Sigma|F_o|_i$$

where once again the index i runs over the data set. One criterion for choosing a weighting function is to require that the function being minimized, R_w, not be dominated by the small or large structure factors. The weighting scheme used in this study was developed by the following procedure. The histogram of Δ^2 was plotted for intervals of $|F_o|$ and a function w expressed as a polynomial in $|F_o|$ to make a histogram of $w\Delta^2$ reasonably flat, and such that

$$\Sigma_\nu \, w_\nu \, \Delta_\nu^2 \, /(N - M)$$

equals one, where ν labels the histogram intervals, N is the number of reflections, and M is the number of refined variables. This method (Cruickshank, 1961) assumes the Δ's are due to random measurement errors in F_o, not to model errors.

An isotropic parameter was refined to correct for the effects of secondary extinction (Larson, 1967). The weighting function used in the final refinement was $w = 1/(19 - 1.28F_o + .0077F_0^2)$. The refinement was terminated when the parameter shifts were all less than one tenth of their standard deviations. The weighted residual at that point was .058 and the conventional "R" factor was .052.

No acceptable refinement could be achieved in space group $Pna2_1$.

The final atomic coordinates are give in Table 4.1 and the interatomic distances and angles in Table 4.2. The observed and calculated structure factors are given in Table 4.3.

4.2 Description of the Structure

The space group Pmna provides mirror planes perpendicular to the b axis and separated by half the b spacing. All of the atoms are on these mirror planes. The vanadium environment could be described as a distorted octahedron. The vanadium is shifted toward one of the oxygens to form a short bond 1.615(15) Å for V(2) and 1.650(14) Å for V(1). Trans to the shorter bond is the longest bond 2.737(14) Å for V(1) and 2.566(14) Å for V(2). These bonds lie in a mirror plane. Of the four equatorial oxygens, two lie in the same plane as the vanadium, and two are in the adjacent mirror planes. The equatorial V-O bond lengths vary from 1.660(14) Å to 2.062(15) Å. The VO_6 groups share edges, the shared oxygens in each case being one equatorial oxygen and the apical oxygen with the long bond to its vanadium. This is so arranged that the long bond of one vanadium is an equatorial bond of its neighbour in the plane and is also an equatorial bond of a vanadium in the planes above and below it. If the pair of vanadate octahedra in the same mirror plane are idealized as forming a dominoe, the double chain of octahedra running up the b axis could be visualized as a stack of dominoes with the alternate dominoes in the stack displaced toward a corner such that even layers are above each other and odd layers above each other (Fig. 4.1). Two V-O bands on each vanadium point out of the stack. One of these corresponds to the shortest apical oxygen and the other to

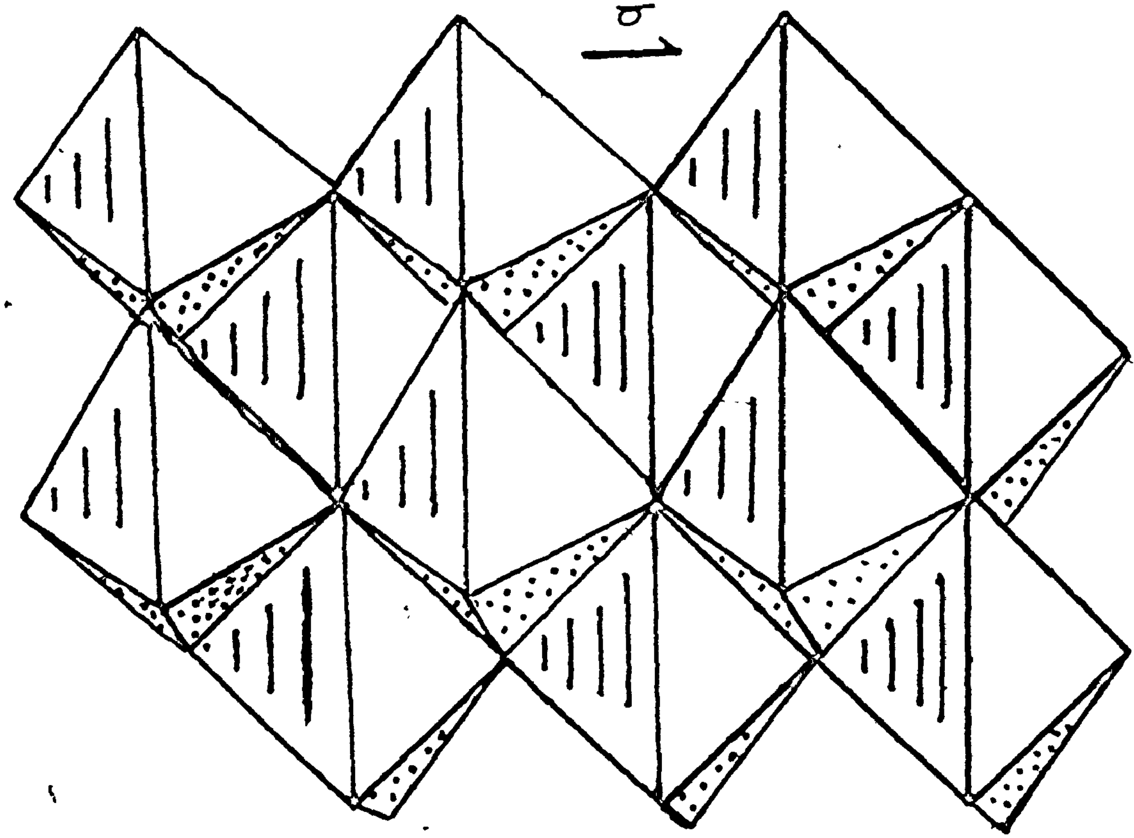

Figure 4.1 The Chain of VO_6 pairs in $Pb\ V_2\ O_6$.

Table 4.1 Atomic Parameters for PbV_2O_6 with Estimated Standard Deviations in Parentheses

atom	x	y	z	U_{11}+	U_{22}	U_{33}	U_{23}
Pb	0.12832(8)	¼	0.11552(6)	0.0183(4)	0.0206(4)	0.0127(3)	0.0009(3)
V(1)	0.0048(3)	¼	0.6240(2)	0.0070(11)	0.0158(11)	0.0119(12)	-0.0002(10)
V(2)	0.2399(3)	¼	0.4101(2)	0.0077(16)	0.0200(16)	0.008(1)	0.0017(10)
O(1)	0.3072(14)	¼	0.9328(11)	0.012(3)			
O(2)	0.0323(14)	¼	0.4098(10)	0.009(2)			
O(3)	0.2809(15)	¼	0.2870(11)	0.014(3)			
O(4)	0.3925(16)	¼	0.4767(12)	0.016(3)			
O(5)	0.9883(14)	¼	0.7522(10)	0.011(3)			
O(6)	0.1729(14)	¼	0.6053(11)	0.012(3)			

Symmetry transformations

a = x,y,z
b = -x, 1/2+y, -z
c = 1/2+x,y,1/2-z
d = 1/2-x,1/2+y,1/2+z
e = -x,-y,-z
f = 1/2-x,-y,1/2+z

+Thermal factor equals $\exp{-2\pi^2[b_1{}^2h^2U_{11} + \ldots + 2b_1b_2hkU_{12} + \ldots]}$ and the b_i's are reciprocal lattice vectors.

Table 4.2 Bond Lengths and Angles in PbV_2O_6 with standard errors in parenthesis

bond	distance (Å)		angle	(degrees)	angle	(degree)
Pb-0(3)	2.641(14)		0(3)a-Pb-0(4)c	151.4(5)	0(4)c-Pb-0(4)d	67.5(4)
-0(4)c	2.586(15)		-0(4)d	127.9(3)	-0(5)b	86.5(4)
-0(4)d	2.559(10)	(2x)	-0(5)b	72.8(4)	-0(6)d	128.6(3)
-0(5)b	2.703(10)	(2x)	-0(6)d	68.3(4)	-0(1)a	100.0(4)
-0(6)d	2.680(10)	(2x)	-0(1)a	108.7(4)	0(4)d-Pb-0(5)b	84.7(3)
-0(1)a	2.907(14)		0(5)b-Pb-0(6)d	80.8(3)	-0(6)d	61.9(4)
			-0(1)a	136.8(2)	-0(1)a	59.8(4)
			-0(4)d	152.7(5)	-0(4)d	92.1(3)
			-0(5)b	85.9(3)	-0(6)d	121.2(4)
			-0(6)d	141.1(4)	0(1)a-Pb-0(4)d	59.8(4)
			0(6)d-Pb-0(1)a	61.7(3)	-0(6)d	61.7(3)
			-0(6)d	86.9(3)		
V(1)-0(2)a	2.737(14)		0(2)a-V(1)-0(5)a	176.6(6)	0(5)a-V(1)-0(6)a	107.3(7)
-0(5)a	1.650(14)		-0(6)a	76.1(6)	-0(1)c	101.5(7)
-0(6)a	1.660(14)		-0(1)c	75.1(5)	-0(2)b	101.0(4)
-0(1)c	2.062(15)		-0(2)b	78.2(4)	0(6)a-V(1)-0(1)c	151.2(6)
-0(2)b	1.926(4)	(2x)	0(1)c-V(1)-0(2)b	75.3	-0(2)b	98.9(4)
					0(2)b-V(1)-0(2)e	146.3(7)
V(2)-0(3)a	1.615(15)		0(3)a-V(2)-0(4)a	105.2(7)	0(4)a-V(2)-0(1)d	97.7(5)
-0(4)a	1.714(15)		-0(1)d	101.8(4)	-0(2)a	150.5(7)
-0(1)d	1.920(4)	(2x)	-0(2)a	104.2(7)	-0(6)a	75.2(6)
-0(2)a	2.029(14)		-0(6)a	179.6(6)	0(1)d-V(2)-0(2)a	76.2(4)
-0(6)a	2.566(14)		0(2)a-V(2)-0(6)a	75.3(5)	-0(6)a	78.1(4)
					0(1)d-V(2)-0(1)f	146.9(7)

Table 4.2 Observed and calculated structure factors for PbV_2O_6

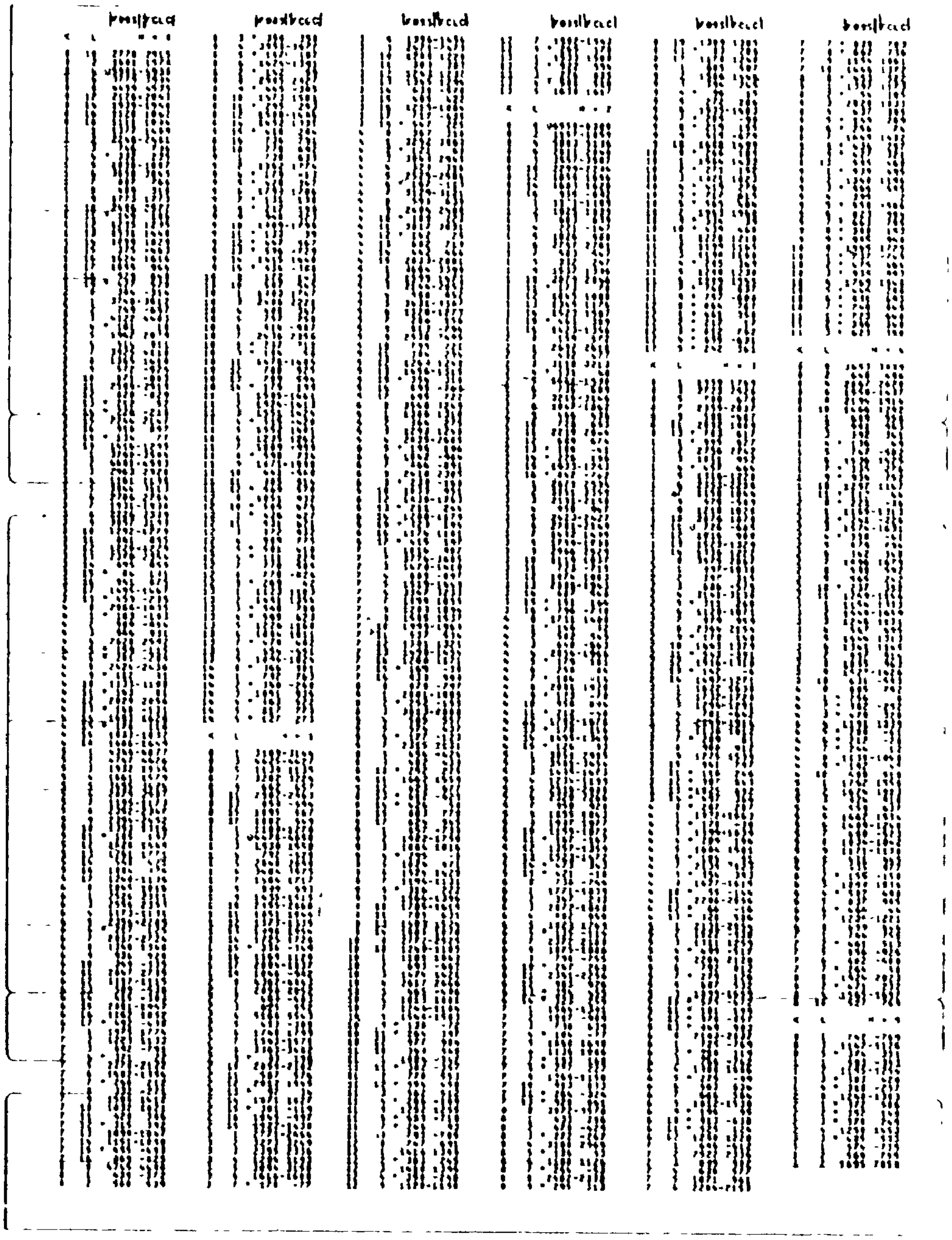

the shortest equatorial oxygen. Both of these oxygens are bonded to a lead, but the strongest Pb-O bond corresponds to the equatorial oxygen of the vanadium. The stacks of vanadate dominoes are bonded to other stacks only by the lead atoms; no oxygens are shared between stacks. Each lead co-ordinates to three stacks, forming nine Pb-O bonds ranging in length from 2.563(10) Å to 2.904(14) Å. The lead is co-ordinated to three oxygens in its own plane and three from each of the planes above and below. The components are so arranged that the vanadate octahedra of one double chain (stack of dominoes) is related by a glide plane to those of another double chain.

4.3 Discussion

Although the structural form of the lead meta-vanadate is new, it shares common features of other related structures. Several meta-vanadates are known to have the brannerite structure (Ruh and Wadsley, 1966). These metavenadates are of the form MV_2O_6 where M is Cd, Zn, Ca, Cu, and Mg (Augenault and Rimsky, 1968; Bouloux and Galy, 1969; Bouloux _et al_., 1972; Ng and Calvo, 1972; Calvo and Manolescu, 1973; Gopal and Calvo, 1974). If one visualizes the dominoes in PbV_2O_6 to share outside corners with those of another stack, one could see how such a meshing of stacks would form sheets. This is how the vanadate octahedra in brannerite are joined. The apex oxygen of the

PbV_2O_6 and the equatorial terminal oxygen would each bridge to another VO_6 unit in the brannerite structure. With the vanadate octahedra forming sheets in brannerite, the other metal atoms are situated between sheets.

One neighbor of PbV_2O_6 on the phase diagramme is PbV_2O_7, the structure of which is known (Shannon and Calvo, 1973). In this structure, the vanadium is found in separate V_2O_7 bridged tetrahedra. The structure of PbP_2O_6 contains infinite chains of PO_4 ions bridged together (Jost, 1964), but the phosphate tetrahedra are paired in such a way as to look like a condensation of P_2O_7 ions into an infinite chain. The lead meta-vanadate did not follow this pattern from the pyrovanadate.

Another phase diagramme neighbour of lead meta-vanadate is beta lead vanadium bronze, $Pb_xV_2O_5-\beta$, (Darriet et al., 1969; Galy et al., 1970; Goodenough, 1970). This structure is more closely related to the PbV_2O_6 than was brannerite. This structure has the same double chain of vanadate octahedra (stack of dominoes) as the PbV_2O_6 but the terminal equatorial oxygen (the one which had been most closely bound to the lead) of the outermost octahedra in the double chain of PbV_2O_6 is shared between two double chains in the vanadium bronze. These shared corners bridge the double chains into sheets as in brannerite but the chains are less intimately meshed, and the apex terminal oxygens (the very shortest V-O bonds in PbV_2O_6) remain terminal oxygens in the bronze. A new structural feature is found in the beta bronze which was absent in the lead meta-vanadate. This is a ribbon of edge sharing VO_5 square prisms. If the dominoes are now placed side by side with half of their long edges in common, a serrated ribbon can be formed. This is an idealization of the ribbons in the beta vanadium bronze. The ribbons run parallel to the double chains and the corners sticking out of the opposite sides of the ribbon (the serrations) join the ribbons to the double chains of different sheets. This cross links one sheet to another but leaves large channels bounded on two sides by ribbons and two sides by sheets. The lead atoms are found in the channels.

Without bridging into sheets but cross-linked by ribbons, the double chain found in PbV_2O_6 is also found in V_4O_9 (Wilhelmi and Waltersson,1971) and V_3O_7 (Waltersson et al., (1974). The double chains in PbV_2O_6 are only bound to each other through the lead. The cross-linking of the ribbons in the bronze along with condensation into sheets provides a network which does not require the lead to hold it together. Similar cross-linking networks hold together V_3O_7 and V_4O_9 without the assistance of a lead or similar ion. The structure of PbV_2O_6 is so dependent upon the lead, that one would not expect order to remain if the stoichiometry were altered much by deleting lead. The onset of new cross-linking elements such as a ribbon might lead to a random structure intermediate between the lead meta-vanadate and the lead beta vanadium bronze.

A paper on the crystal structure of PbV_2O_6 by B. Jordan and C. Calvo has been published in the Canadian Journal of Chemistry (1974).

FIGURE 4.2

A projection of the structure of PbV_2O_6 down the b axis. Shaded bonds and atoms lie in the plane $y = \frac{3}{4}$ and open bonds and atoms lie in the plane $y = \frac{1}{4}$. The smallest circles are vanadium atoms and the large circles are oxygens. The intermediate sized circles are lead atoms. It can be seen that only the lead atoms connect one chain of vanadate octahedra pairs to another.

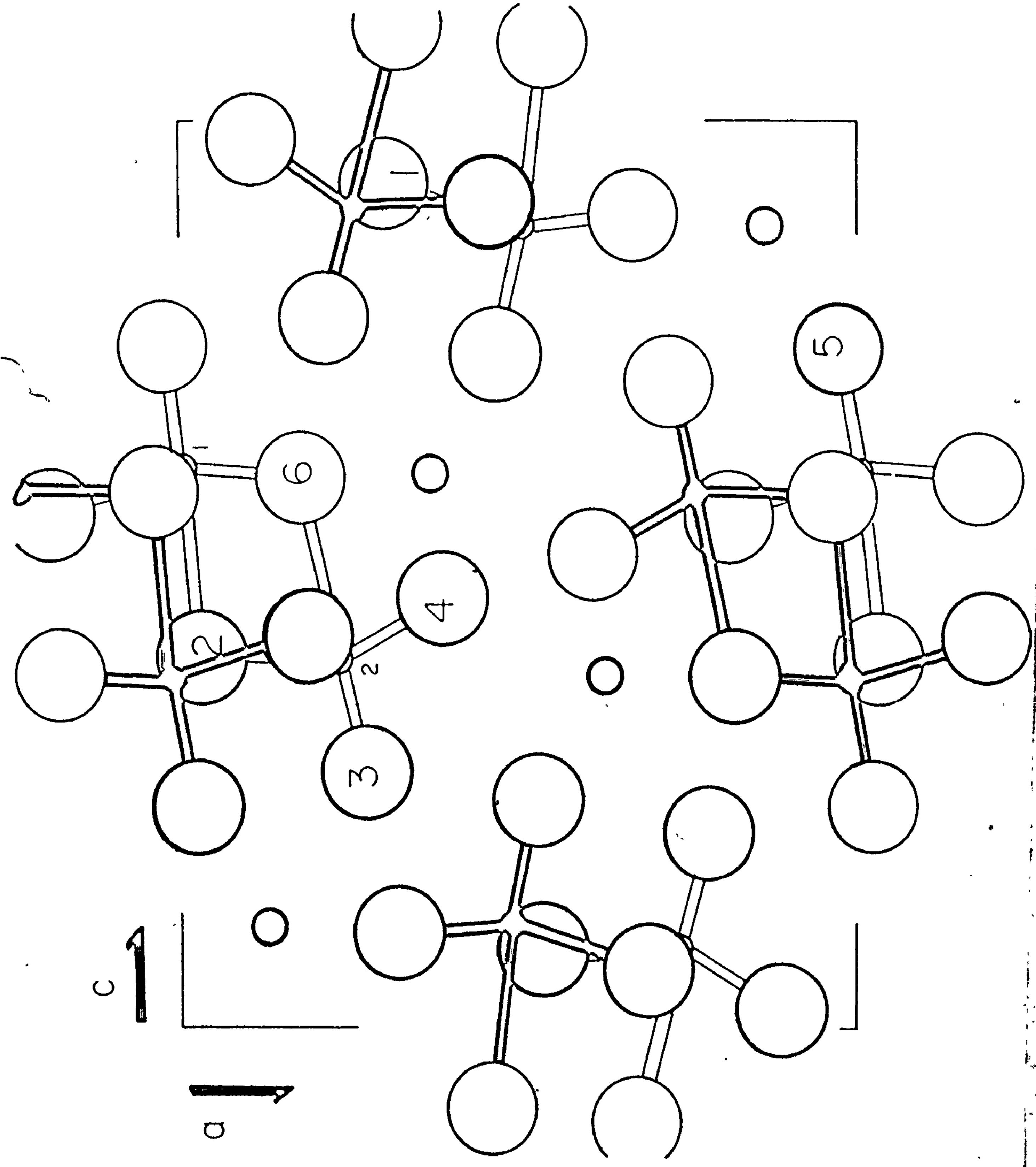

FIGURE 4.2

CHAPTER 5

CRYSTAL STRUCTURE AND DISORDER IN α-VPO_5

5.1 Preparation and Initial Investigation

In the course of preparing samples of VPO_5 glass, it was decided to test how slowly the melt could be cooled without inducing crystallization. Following the procedure for the preparation of β-VPO_5 outlined by Gopal (1972), stoichimetric proportions of (Fisher Scientific) V_2O_5 and fresh P_2O_5 (Fisher Scientific) were mixed and heated to 800°C and the melt allowed to cool with the thermal relaxation of a small furnace (about 2 - 3hr.). Thin mica-like plates of yellow crystal formed on the surface of the charge, with a black glass filling the rest of the crucible. These crystals appeared different from those of the beta phase that Gopal had prepared, and X-ray precession photographs readily exhibited tetragonal symmetry with extinctions for h+k odd in hk0. The cell dimensions were close enough to those of tetragonal $VMoO_5$ (Eick and Kihlborg, 1966) to suggest that the new crystals were isotypic with that structure. An attempt was then made to grow better specimens for intensity measurements. This time the V_2O_5 and P_2O_5 were weighed in stopped bottles which were filled in a dry box in stoichimetric proportion, mixed well, and transferred in a platinum crucible to a preheated furnace (200°C). This was to avoid as much as possible the hydration of the P_2O_5. The temperature was increased and the melt allowed to equilibrate overnight at 850°C. The melt was then cooled at between ten and fifteen degrees per hour through 700°C, at which point the furnace was turned off and allowed to cool to room temperature. The crystals this time were not confined to the surface of the charge, but were distributed throughout the crucible, suspended in a partially vitreous matrix. Repeating the procedure with an even slower cooling rate (2-5°C/hr.) produced an even larger proportion of the charge crystallized and larger crystals. Crystals with considerable mosaic spread could be cleaved and sliced into specimens suitable for X-ray diffraction with a smaller mosaic spread. The larger specimens, before cutting, grew up to 3 mm square and .2 to .3 mm thick. Even for the optimal crystals the reflections on precession photographs were about three times longer in the $\underline{c}^*$ direction than in the $\underline{a}^*$ or $\underline{b}^*$ direction. One specimen was heated with a steady stream of hot air while mounted on a precession camera. It was hoped to be able to measure the thermal expansion by taking several exposures, with the film shifted, on the same film. The spot shape made measurements difficult, however it could be seen that the $\underline{c}$ axis expanded about an order of magnitude more than the $\underline{a}$ and $\underline{b}$ axes. The expansion coefficient for $\underline{c}$ appeared to be about $5 \pm 3 \times 10^{-5}\ {}^{\circ}C^{-1}$ When the temperature exceeded 500°C the spot shape extended greatly indicating a considerable increase in disorder.

A platelet with dimensions 1.5 x 1.5 x .1 mm was mounted on the Syntex P$\bar{1}$ diffractometer and cell dimensions were found from a least squares refinement of 2θ values from 11 reflections. The cell constants were found to be a = b = 6.014(7) Å and c = 4.434(2) Å. The crystal was tetragonal, so the angles were 90 degrees. The extinctions were consistent with the space group P4/n. With two formula units per cell, (formula weight of 161.91 grams per mole), and a cell volume of 160.37 $Å^3$, the density was calculated to be 3.353 g/cm^3. As with the lead meta-vanadate difficulties in getting a large enough collection of isolated crystals prevented the experimental determination of density. Had the density been slightly less, a flotation technique using bromoform could have been used as it was for some of the glasses in this study.

With the Syntex P$\bar{1}$ diffractometer, all those reflections in one hemisphere defined by $2\theta < 60^o$ were measured with a θ-2θ scan. The scanning rate varied with the peak height of the intensity profile, taking on values between two and twenty-four degrees per minute. The diffractometer receded 1^o on both sides of the spot to measure the backgrounds. The background under the peak was interpolated from these values and the integrated intensity corrected. Those reflections which yielded negative intensities after correction for background were deleted, and those whose standard error exceeded one third of the intensity were tagged as unobserved. Lorentz and polarization corrections were made with the programmes in the X-ray 71 programme package, and correction for absorption was made with the programme Absorb written by R.F. Stewart, and using a linear absorption coefficient of 32.6 cm^{-1}. After the absorption correction was applied the symmetry equivalent reflections were averaged. After averaging, 248 unique reflections remained.

5.2 Refinement

The atomic positions from $VMoO_5$ (Eick and Kihlborg, 1966) were used as initial parameters, with the phosphorus substituting for the Mo. The scattering curves and dispersion corrections for P and O were taken from the International Tables of X-ray Crystallography (1963), and the scattering curve for V^{5+} was taken from Cromer and Waber (1965). The refinement was done with the full-matrix least-squares programme written by J.S. Stephens. The weighting function used was $w = 1/(2.5 + .01F_o^2)$ where F_o stands for the observed structure factor. The reason for using this kind of weighting scheme was noted in the previous chapter. When the positional and isotropic temperature factors had converged, the temperature factors were allowed to become anisotropic. The U_{33} component, corresponding to vibration in the soft z direction was large. This could be from positional disorder or large vibrations in a soft direction. On 0(2) alone, the oxygen in the general position, the temperature parameter U_{11} was found to be quite large. This parameter indicated a shearing motion of the lattice with the PO_4 tetrahedra and VO_6 octahedra librating together. The amplitude (root-mean-square) of the travel of 0(2) was indicated to be about .5 Å. The "motion" indicated by this thermal parameter straddled the position x = ¼, so a model was tested in which 0(2) was statistically divided between two positions on either side of x = ¼ with variable occupancy. The weighted residual R_w immediately dropped from .12 to .10 when the occupancy was refined. In the final refinement the occupancy was found .67 ± .02 indicating one third of the oxygens were in the minority position. The final weighted residual R_w was .089. Nine reflections of the 248 unique reflections were so anomalous that they were not included in the final refinement. The final difference map contained a residual at the vanadium site of approximately three percent of a vanadium. Peaks of about one percent of a V atom and of equal height to each other are found in the difference map at(¼. ¼, .653) and(¼, ¼, .405). The parent crystal from which the X-ray specimen was cut, was given to Dr. H.N. Ng for an EPR experiment. Ng (1972) found the signal strength to be consistent with a V^{4+}/V^{total} concentration of less than one percent. In the glass model below, will be introduced a grouping called a V_2O_9 unit. This is invoked to account for the accommodation of the glass structure for a moderate amount of V^{4+} which is formed when oxygen is evolved. If that mechanism were applied in the crystal in the same manner as it is applied in the glass, and if a 1% V^{4+} concentration is present a peak of the right magnitude and in the right position to account for the residual noted above. It does not, however, predict the second matching residual.

Twinning, with the twins related by a mirror plane which passes through the P positions, and with the minor twin occupying about one percent of the crystal volume, is another possible source of the ghost peaks on the $(\frac{1}{4},\frac{1}{4},z)$ line in the difference map. The peak positions predicted by such twinning, however, are in only fair agreement with those observed.

5.3 Description of the Structure

The basic structural units are a PO_4 tetrahedron and a tetragonally distorted VO_6 octahedron. The phosphorous sits at a special position which has $\bar{4}$ (S_4) symmetry and the PO_4

Table 5.1

Atomic and Thermal Parameters for αVPO_5 with standard errors in parentheses.

	x	y	z	$U_{11}(\mathring{A}^2)$*	$U_{22}(\mathring{A}^2)$	$U_{33}(\mathring{A}^2)$	$U_{12}(\mathring{A}^2)$	$U_{13}(\mathring{A}^2)$	$U_{23}(\mathring{A}^2)$
V	1/4	1/4	0.2139(5)	0.0019(14)	U_{11}	0.0165(11)	-	-	-
P	1/4	3/4	1/2	0.0030(18)	U_{11}	0.0189(16)	-	-	-
O(1)	1/4	1/4	0.858(2)	0.011(5)	U_{11}	0.018(4)	-	-	-
O(2)	0.1965(13)	0.9522(12)	0.2987(17)	0.012(3)	0.009(3)	0.0227(3)	-0.001(3)	-0.002(3)	0.002(3)
O(3)†	1/2-x	y	z	U_{11}	U_{11}	U_{33}	$-U_{12}$	$-U_{13}$	U_{22}

* Calculated from $B_{ij} = 2\pi^2 b_i b_j U_{ij}$ where $T = \exp[-(B_{11}h^2 + 2B_{12}hk + \cdots)]$ is the thermal factor in the structure factor expression.

† Derived from parameters of O(2) with a site occupancy of 0.33(2).

Table 5.2

Bond Lengths and Angles in αVPO_5 with standard errors in parentheses

bond	distance	angle	(degrees)	angle	(degrees)
V-0(1)	1.580(11)	0(1)-V-0(2)	101.6(2)	0(2)-V-0(2)b	87.7(3)
-0(2)	1.858(7)	-0(1)	180.0	-0(2)c	156.7(4)
-0(1)a	2.853(11)				
P-0(2)	1.541(8) (4X)	0(2) - P - 0(2) c	109.1(4)		
		- 0(2) d	109.7(4)		

Transformations

a = x, y, 1-z; b = y, 1/2-x, z; c = 1/2-x, 1/2-y, z; d = 1/2+x, -y, -z

FIGURE 5.1

Illustration of the network of PO_4 tetrahedra and VO_6 distorted octahedra forming a sheet in α-VPO_5. The outline of a unit cell (with origin at $\bar{4}$) is denoted by the dark square. The vanadyl oxygens (O(1)) are not shown. The sheet is seen in projection down the c axis.

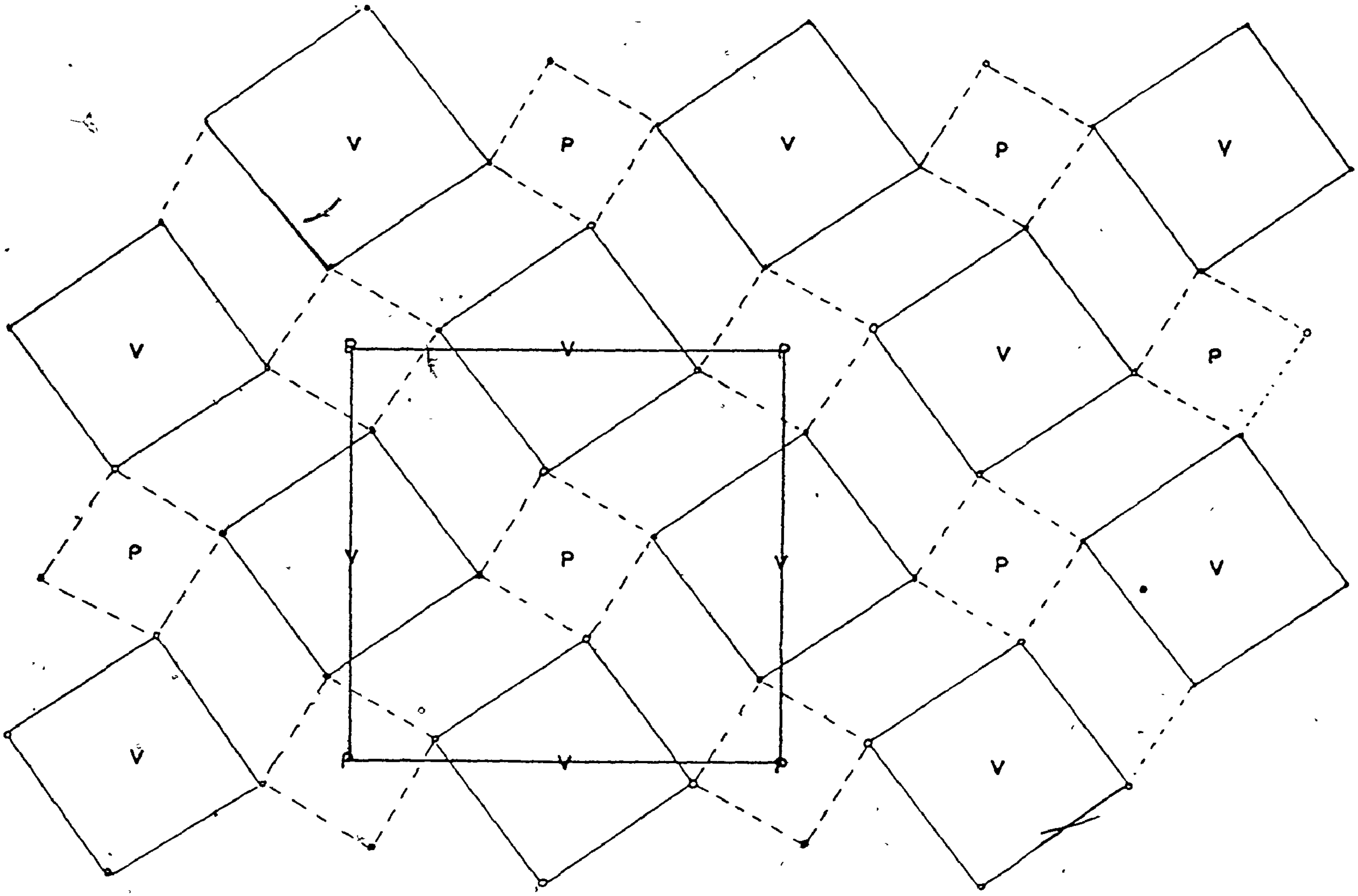
V
P
V
P
V
V
V
V
P
P
P
P
V
V
V
V

Figure 5.2

Sheet of α-VPO_5 in projection down the c-axis emphasizing the PO_4 tetrahedra. The P lie on the n-glide plane. Oxygen O(1) is not shown. Oxygens above the glide plane are shown as circles and those below the glide plane by dashed circles. Vanadium atoms above the glide plane are shaded and those below the plane are unshaded circles.

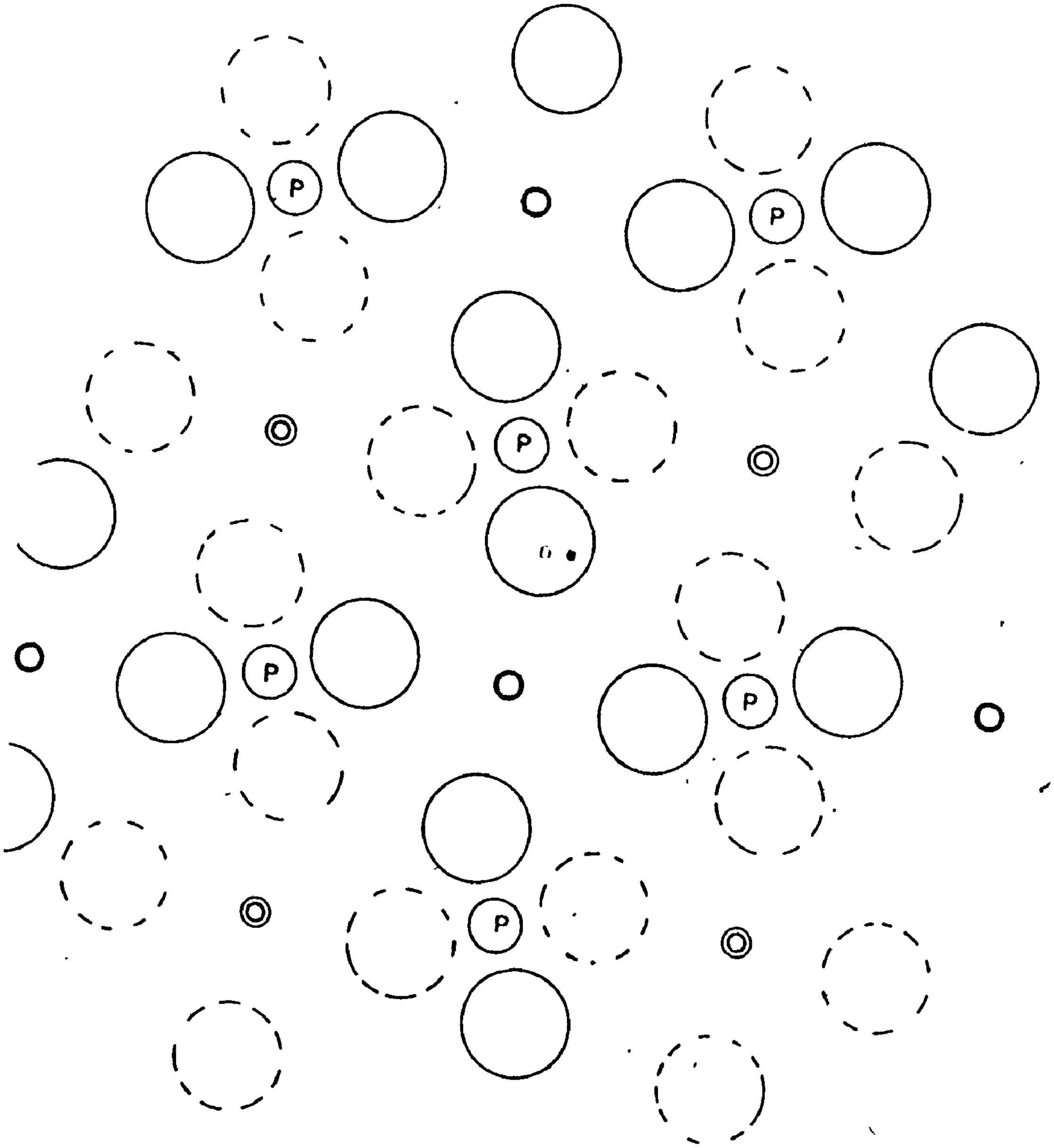
P
P
P
P
P
P

FIGURE 5.3

A projection of the unit cell (origin at $\bar{1}$) of α-VPO_5 down the $\underline{c}$ - axis. The small circles denote P atoms and the double circles denote the vanadium and vanadyl oxygen. Oxygen-oxygen distances are shown. The minority oxygen positions in the disorder description are indicated by the dashed lines.

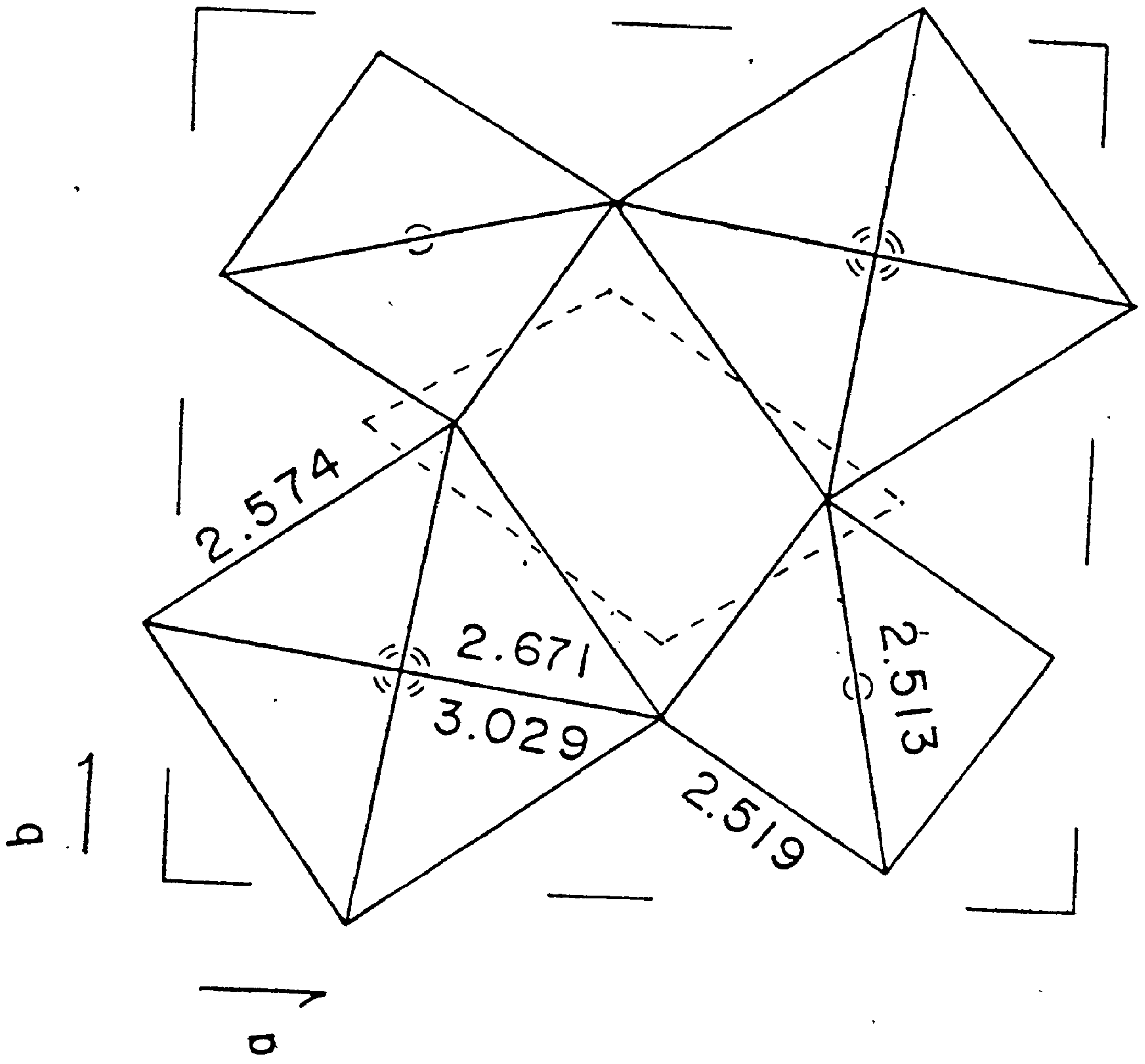
2.574
2.671
3.029
2.513
2.519
b
a

L= 0

H	K		|FOBS|	|FCLC|
0	2		59	61
0	6	U	52	33
0	8		27	18
1	1		11	8
1	3		46	36
1	5		12	6
1	7		16	15
2	2		32	32
2	4		41	40
2	6		39	37
2	8		23	25
3	1	U	30	24
3	3		25	26
3	5		5	4
3	7		6	6
4	2		49	48
4	4		36	37
4	6		36	32
5	1	U	8	1
5	3		7	7
5	5		9	9
6	2		38	36
6	4		27	25
7	1		14	13
7	3		9	9
8	2		27	27

L= 1

H	K		|FOBS|	|FCLC|
0	1		39	37
0	6		6	5
0	7		5	5
0	0		21	23
0	5		7	7
0	7		14	14
0	4		7	8
0	3		47	41
0	8		3	2
1	1		39	42
1	5		22	22
1	6		22	19
1	8		9	10
1	7		13	13
1	7		23	23
1	4		27	25
1	7	U	16	6
2	2	*	1	1
2	4		6	5
2	5		9	9
2	3		21	21
2	8		5	4
2	7		17	18
2	6		7	6
3	1	U	15	3
3	3		19	21
3	2		22	22
3	4		18	16
3	6		17	13
3	1		27	26
3	7		14	15
3	5		20	20
4	6		6	9
4	1		19	19
4	4		6	6
4	3		25	24
4	2		9	7
4	5		14	14
4	7		10	12
5	3		19	19
5	1		25	23
5	2		11	12
5	6		14	15
5	4		11	11
5	5		13	15
6	4		5	3
6	5		12	12
6	3		11	12
6	2		6	6
6	1		16	16
7	2		20	20
7	1		13	14
7	3		13	14
7	4		10	11
8	2		5	4
8	1		7	9

L= 2

H	K		|FOBS|	|FCLC|
0	8	*	3	1
0	5		9	9
0	0		35	40
0	3		5	4
0	2		8	9
0	6		4	4
0	4		10	11
0	1		3	4
0	7		3	3
1	1		33	34
1	2		28	27
1	2		12	10
1	6		4	1
1	3		43	45
1	4		3	1
1	5		26	25
2	3		3	3
2	2		5	5
2	1		15	14
2	4		8	4
2	5		7	7
2	6		7	7
3	1		39	39
3	2		2	3
3	7		19	20
3	5		21	22
3	3		37	38
3	6		4	4
3	4		7	5
4	6		9	6
4	1		5	4
4	2		11	9
4	5		4	4
4	4		4	5
4	3	U	5	1
5	5	*	1	1
5	1		22	21
5	2		5	6
5	4		5	5
5	5		22	23
5	3		23	25
6	1		6	4
6	3		4	5
6	5		4	3
6	2		6	7
6	4	U	7	1
7	2	*	1	0
7	3		22	22
7	1		27	26

L= 3

H	K		|FOBS|	|FCLC|
0	5		9	9
0	0		12	14
0	2		29	30
0	7		12	11
0	1		22	23
0	4		21	22
0	3		23	24
0	6		20	21
1	2		12	13
1	5		5	4
1	4		15	16
1	1		7	9
1	6		13	14
1	7	*	3	2
1	3	U	6	2
2	3		16	16
2	5		9	9
2	7		12	12
2	2		35	37
2	1		11	10
2	4		24	25
2	6		16	17
3	3	*	2	1
3	5		5	5
3	6		10	11
3	4		13	13
3	2		16	17
3	1	U	6	2
4	6		16	16
4	4		19	20
4	5		11	11
4	1		14	15
4	2		21	21
4	3		16	16
5	5	*	2	[illegible]
5	4		9	9
5	1		8	8
5	3		4	3
5	2		10	11
6	4		19	19
6	3		10	10
6	1		13	12
6	2		16	17
7	1	*	2	1
7	2		14	14

L= 4

H	K		|FOBS|	|FCLC|
0	2		16	16
0	4		15	15
0	0		21	21
0	1		7	7
0	5		13	13
0	6		13	12
0	3		3	3
1	3	*	2	1
1	6		6	5
1	2		15	15
1	1		6	4
1	4		7	7
1	5		4	3
2	4		13	13
2	2		12	13
2	6		12	12
2	3		8	9
2	5		11	12
2	1		16	18
3	1	*	2	2
3	3	*	2	0
3	2		8	8
3	5		4	2
3	4		10	9
4	4		13	13
4	1		9	9
4	5		8	8
4	3		7	5
4	2		14	14
5	3		3	2
5	4		9	9
5	1		4	4
5	2		10	10
6	1		8	8
6	2		13	12

L= 5

H	K		|FOBS|	|FCLC|
0	4	*	2	8
0	1		8	7
0	0		8	6
0	3		7	7
0	2		3	2
0	5		6	6
1	4		6	6
1	1		19	19
1	2		7	6
1	3		13	12
2	4		4	3
2	2		7	7
2	1		7	6
2	3		6	6
3	4		6	6
3	1		14	15
3	3		12	12
3	2		7	6
4	1		6	6
4	3		6	6
4	2	U	4	1

L= 6

H	K		|FOBS|	|FCLC|
0	0		6	5
0	1		9	7
0	2		4	3
1	2		13	11
1	1		7	6
2	1		14	12

Table 5.3 Observed and calculated structure factors for 2 VPO_5. Those reflections with (*) were "unobserved" and those denoted by U were not included in the refinement.

TABLE 5.4

Structure Factors for Some Sensitive Reflections With and Without the Minority O2 Contribution

H	K	L	F observed	F calculated With disorder	Without
3	5	0	5.44	5.25	2.43
5	3	0	7.59	8.33	10.97
3	7	0	7.00	6.78	3.92
7	3	0	10.22	9.86	12.55
2	4	0	44.23	42.12	34.35
4	2	0	52.10	50.38	57.41
4	6	0	38.73	33.83	39.70
6	4	0	28.67	27.14	20.96
3	5	0	5.44	5.25	2.43
5	3	0	7.59	8.33	10.97
1	4	1	24.85	24.28	28.69
4	1	1	20.68	19.91	16.18
3	4	1	20.06	16.27	9.30
4	3	1	27.17	24.26	31.61
2	5	1	9.57	9.48	6.98
5	2	1	12.66	12.55	15.58
1	2	2	12.96	11.31	6.65
2	1	2	15.98	15.87	19.40

H	K	L	F observed	F_c disordered	F_c ordered
1	3	2	46.57	46.44	51.76
3	1	2	42.00	40.37	34.81
3	4	3	14.68	13.81	10.63
4	3	3	17.59	17.11	19.85

is an undistorted tetrahedron with a P-O bond length of 1.541 (8) Å. The vanadium and O(1) atoms lie on the fourfold axis. The four equatorial V-O(2) bonds are equivalent by symmetry and are found to be 1.858(7) Å long. The vanadium is shifted above the plane of its equatorial oxygens and towards one O(1) with which it forms a very short bond of 1.580(11)Å, which will be called a vanadyl bond. Trans to the vanadyl bond is a long V-O(1) bond of length 2.853(11) Å . The VO_6 octahedra form chains running up the fourfold axis (z direction). Another chain of vanadate octahedra with its vanadyl bond pointing antiparallel to those of the first chain is related by the n-glide operation to the first chain. Each vanadium shares bridging oxygens O(2) with four phosphates. Each phosphate shares oxygens with four vanadiums, each from a different chain. The arrangement involves only corner sharing. If one starts with one VO_6 and one PO_4 and repeatedly applies the n-glide operation a corrugated sheet will be generated. An alternative to viewing the structure in terms of infinite chains of vanadate octahedra cross-linked by PO_4 ions, is to view it as built up from sheets loosely bound together by only the long 2.853(11) Å V-O(1) bonds.

5.4 Temperature Variation

In one experiment a crystal, contained in a cryotip cooling device, was mounted on the Syntex P$\bar{1}$ diffractometer. The crystal was enclosed in a berylium shroud which was evacuated.

After finding an orientation matrix at room temperature the crystal was taken to -190 ± 5°C and a new cell found The new cell was found to be a = 6.010(10) Å and c = 4.367(8)Å. This gives a thermal expansion coefficient of 7.2(8) x 10^{-5}/C°. The thermal expansion of the a axis is an order of magnitude less and is not resolved within experimental error. V_2O_5 and α-VPO_5 are both layer structures with the layers held together by a long V-O bond trans to a vanadyl bond. It would not be surprising if the energetics of separating the layers were quite similar in the two structures. Kennedy et al.(1967) have measured the thermal expansion of crystalline V_2O_5 and found the values of 2.0 x 10^{-6} along a, 8.0 x 10^{-6} along c, and 5.54 x 10^{-5} along b. It is the expansion along the b axis in V_2O_5 which corresponds to the separation of layers.

The nitrogen gas which cools the Cryotip through the Joule-Thompson effect, is expended rather rapidly when the Cryotip is operating at -190°C. After finding a new unit cell it was only possible to measure the intensities of a few reflections. Several n-glide extinction violations were found in which the intensity was several times its standard deviation (Table 5.7). Attempts to observe with films any n-glide violations or indications of a doubling of an axis were not successful. A rotation photograph was taken on one specimen at nearly -190°C with no new reflections observed. Precession photographs have been taken at temperatures near -150°C with no new spots observed. In these experiments, nitrogen gas, cooled in a liquid nitrogen heat exchanger, was passed over the crystal. A thermocouple near the crystal recorded the temperature.

In another experiment, integrated and non-integrated zero and first layer precession photographs were taken of a crystal held at a series of temperatures between -150°C and +200°C. By blowing a steady stream of either cold nitrogen gas or hot air over the crystal a temperature stable to ±3°C over a day's duration was usually attainable. The object of this experiment was to observe some sections of reciprocal space which had been calculated to be particularly sensitive to the O(2) disorder parameter. A table listing several sensitive reflections is given (5.4) along with a map(5.8) indicating the intensity distribution expected for an ordered arrangement, and one corresponding to full disorder. Photographs of the hkl net are shown in figure 5.4 which are representative of a series which demonstrate a definite progression from quite well ordered at -130°C to nearly total disordering (population of each O(2) alternative site = ½) at +100°C. A diffuse background can be seen in some of the higher temperature photographs. This may be spurious, or it may be disorder diffuse scattering (Krivoglatz, 1969).

It was deemed desirable to repeat this experiment on the diffractometer. Because the crystals appeared to be generally close to the disordered form at room temperature, cooling was seen as a more fruitful experiment. Due to the loss of one specimen at a very inconvenient time, it was decided to mount a specimen from a newly prepared batch and proceed with the experiment. The new batch of crystals had come from an attempt to use the Czochralski crystal growing technique and had come from a section of the charge which was rather late to crystallize. The first crystals to have formed had been β-VPO_5 and an unidentified body centred form. The α-VPO_5 crystals formed toward the outer rim of solidified portion exhibited a much better X-ray spot shape when photographed than had previous specimens. One of these crystals in the form of a small plate was mounted on the Cryotip for cooling. The c axis of this specimen was significantly larger than that of previous specimens. Several crystals of α-VPO_5 had been mounted on the Syntex $P\bar{1}$ at one time or another and it was found that a specimen-to-specimen reproducibility of cell constants was consistent with the standard errors produced by the least-squares with maximum deviations on the order of .007 to .01 Å. The cell measured for the new crystal was a = 6.011(4) and c = 4.452(4) Å. It was also soon apparent that the new specimen was almost completely ordered at room temperature. It was used in the experiment anyway to see how it changed with temperature. Before cooling, a data set was taken on the new crystal.

Attempts to refine the room temperature data set on the new "ordered" specimen lead to a minimum R factor of .12 to .15 with the temperature factors going small or negative. After some effort, an idea which had proven rather fruitful in the analysis of the vanadium phosphate glasses was tried. It was hypothesised that the crystal was off stoichiometry with tetrahedral vanadium substituting for the phosphate. A partial vanadium was placed at the phosphate site and the population factors of the phosphorus and vanadium were varied. With a stoichiometry set as $V_{1.08 \pm .01}P_{.92 \pm .01}O_5$ the data set refined with reasonable temperature factors to an R factor of .076 and a weighted residual of .090. This is comparable with the result of the "stoichiometric" crystal. Small data sets were taken at temperatures as low as -100°C, and another larger data set was taken at room temperature after the cooling. Tables 5.5 and 5.6 pertain to the initial room temperature data. Positional parameters of the stoichiometric and nonstoichiometric crystals generally match within standard error. The value of U_{33} is about fifty percent higher for all atoms in the non-stoichiometric crystal and the U_{11} and U_{22} in this crystal for the metal atoms is comparable to an oxygen temperature factor. This is true both before and after cooling, but at -100°C the temperature factors are about half the room temperature values. The temperature factors reflect more random displacement of the pentavalent ions in the non-stoichiometric crystal. The assumption is

TABLE 5.5

H	K	L	F(OBS)		F(CALC)
0	5	1	7.77		6.45
1	5	1	21.98		19.42
2	5	1	5.96		5.09
3	5	1	20.55		19.77
4	5	1	16.94		17.39
0	6	1	6.45		5.58
1	6	1	27.07		24.44
2	6	1	7.14		7.00
3	6	1	13.53		13.57
0	7	1	14.77		13.15
0	0	1	21.90		24.24
0	1	2	4.76		4.07
1	1	2	36.87		36.40
2	1	2	19.96		17.92
3	1	2	32.11		33.02
4	1	2	5.41		5.41
5	1	2	15.20		15.64
6	1	2	6.15		5.67
0	2	2	9.76		9.04
1	2	2	5.57		4.98
2	2	2	5.41		5.47
3	2	2	.69	*	1.69
4	2	2	12.79		13.69
5	2	2	3.47		3.90
6	2	2	5.75		6.03
0	3	2	6.72		5.35
1	3	2	53.97		52.35
2	3	2	2.90		3.12
3	3	2	34.36		37.43
4	3	2	2.82		3.63
5	3	2	21.82		23.97
0	4	2	10.00		10.29
1	4	2	.69	*	.83
2	4	2	2.28		2.16
3	4	2	7.48		8.06
4	4	2	4.25		4.89
5	4	2	6.00		6.91
0	5	2	8.39		8.44
1	5	2	29.23		26.97
2	5	2	8.05		8.24
3	5	2	17.10		18.13
4	5	2	2.24		1.23
0	6	2	3.53	*	3.67
1	6	2	1.98		1.91
2	6	2	6.52		6.71
0	0	2	41.40		42.81
0	1	3	22.14		24.30
1	1	3	7.65		8.66
2	1	3	7.84		7.52
3	1	3	5.33		4.86
4	1	3	12.77		12.35
5	1	3	10.03		9.10
0	2	3	29.94		28.73
1	2	3	15.52		16.33
2	2	3	33.65		33.98
3	2	3	15.22		16.56
4	2	3	14.51		15.10
5	2	3	10.00		10.99
0	3	3	24.34		23.39
1	3	3	7.30		7.42
2	3	3	14.01		15.30
3	3	3	2.30		2.60
4	3	3	15.93		18.69
5	3	3	1.45	*	1.24
0	4	3	21.30		19.80
1	4	3	16.57		17.35
2	4	3	24.42		26.43
3	4	3	7.27		9.02
4	4	3	15.31		17.32
0	5	3	8.95		8.60
1	5	3	.82	*	1.23
2	5	3	6.67		1.15
3	5	3	5.37		5.55
0	0	3	13.41		14.48
0	1	4	7.09		5.57
1	1	4	5.24		5.04
2	1	4	18.17		18.18
3	1	4	3.25		3.63
4	1	4	10.06		9.07
0	2	4	14.94		14.51
1	2	4	9.96		9.85
2	2	4	10.43		11.15
3	2	4	6.29		6.38
4	2	4	13.38		13.88
0	3	4	2.55		1.93
1	3	4	.85	*	.29
2	3	4	6.69		7.53
3	3	4	1.74	*	.76
0	4	4	15.30		13.83
1	4	4	4.16		4.10
2	4	4	9.22		10.18
0	0	4	22.46		29.01
0	1	5	8.30		7.34
1	1	5	19.79		15.47
2	1	5	6.78		6.11
0	2	5	1.82	*	1.05
1	2	5	6.77		6.47
0	0	5	7.11		6.83

H	K	L	F(OBS)		F(CALC)
2	0	0	73.33		76.07
4	0	0	58.30		55.44
6	0	0	34.37		31.76
1	1	0	11.49		11.10
3	1	0	13.38		13.39
5	1	0	6.45		6.79
7	1	0	12.26		10.21
0	2	0	80.62		76.07
2	2	0	32.19		35.90
4	2	0	54.54		57.73
6	2	0	34.41		33.87
1	3	0	49.00		49.88
3	3	0	24.71		25.57
5	3	0	8.50		8.61
0	4	0	65.25		55.44
2	4	0	30.07		30.63
4	4	0	34.62		35.38
1	5	0	12.88		10.86
3	5	0	1.08	*	.84
5	5	0	7.59		8.11
0	6	0	38.90		31.76
2	6	0	36.38		35.12
1	7	0	17.59		15.41
0	1	1	44.02		43.53
1	1	1	43.20		46.87
2	1	1	13.22		11.34
3	1	1	31.21		30.03
4	1	1	14.57		14.63
5	1	1	28.11		24.16
6	1	1	10.01		9.12
0	2	1	6.01		6.61
1	2	1	19.16		19.63
3	2	1	23.43		24.99
4	2	1	10.05		10.37
5	2	1	14.25		14.02
6	2	1	6.70		6.50
0	3	1	52.69		44.30
1	3	1	21.55		20.69
2	3	1	20.30		21.58
3	3	1	18.97		20.18
4	3	1	25.65		31.24
5	3	1	16.98		17.32
6	3	1	9.20		10.05
0	4	1	9.67		8.32
1	4	1	30.14		28.06
2	4	1	2.86		3.00
3	4	1	6.68		7.35
4	4	1	6.23		6.31
5	4	1	5.32		5.75

OBSERVED AND CALCULATED STRUCTURE FACTORS FOR $V_{1.08}P_{.92}O_5$

* $I(H,K,L) < 3\sigma(I(H,K,L))$

TABLE 5.6

Atomic and Thermal Parameters for α-$V_{1.08}P_{.92}O_5$ with standard errors in parentheses.

	x	y	z	$U_{11}(\mathring{A}^2)$	$U_{22}(\mathring{A}^2)$	$U_{33}(\mathring{A}^2)$	$U_{12}(\mathring{A}^2)$	$U_{13}(\mathring{A}^2)$	$U_{23}(\mathring{A}^2)$
V	¼	¼	.2165(5)	.010(3)		.028(2)			
P(V)	¼	$\frac{3}{4}$	½	.014(3)		.029(2)			
O(1)	¼	¼	.862(2)	.027(8)		.017(4)			
O(2)	.1965(7)	.9498(7)	.297(1)	.013(3)	.010(2)	.031(3)	-.000(2)	.002(2)	-.000(2)

Weight $w^{-1} = .9 + .20F + .005\ F^2$

$R = .076$

$R_w = .090$

147 reflections included.

TABLE 5.7

Reflections violating n-glide extinction rule ((H,K,0) reflections with H + K even should be absent) deleted from data set of $V_{1.08}P_{.92}O_5$ after cooling to below -100 °C (still on Cryotip goniometer with Be cap). For all reflections L=0.

H	K	$F_{observed}$ (σ)	H	K	$F_{observed}$(σ)
6	1	7.2 (3)	1	6	6.9 (3)
1	8	2.2 (8)			
4	7	3.3 (6)			
2	7	2.2 (7)			
4	5	3.8 (4)	5	4	3.9 (6)
2	5	4.4 (4)			
0	5	3.6 (7)	5	0	4.1 (6)
3	2	8.2 (3)	2	3	10.6 (2)
0	3	2.3 (8)			
4	3	3.9 (5)			

made that the presence of tetrahedral vanadium could inhibit the librational motion connected with the disordering found in the stoichiometric crystals by essentially raising the transition temperature. The amount of expansion of the c axis found is commensurate with the expansion predicted for an eight percent substitution of VO_4 for PO_4 in the glass model. Also, from the minor amount of change found in the vanadium phosphorus peak in the X-ray pair distribution function of the glass it was assumed in the glass model that the glass equivalent of the crystalline a and b axes change very little with substitution. One would expect that the effective P-O bond length would visibly lengthen, but the uncorrected P-O bonds are identical within error between the two crystals. The higher temperature factors on the pentavalent ions in the non-stoichiometric crystal lengthen the thermally corrected (Megaw, 1973) bond lengths to a value more in line with expectation.

5.5 Discussion

The oxygen position O(2) in α-VPO_5 has been described in terms of an orientational disordering of the polyhedra of the structure. This effect changes with temperature to give nearly total disordering slightly above room temperature. In the isostructural compounds $VMoO_5$ (Eick and Kihlborg, 1966), $NbPO_5$ (Longo and Kierkegaard, 1966), $TaPO_5$ (Longo *et al.*, 1971), $MoPO_5$ (Kierkegaard and Westerlund, 1964), and VSO_5 (Longo and

Arnott, 1970) anisotropic temperature factors were not refined in all cases but one, and one cannot ascertain whether the disorder feature seen here is present in any of the related structures. In the one other case in which anisotropic temperature factors have been refined, $MoPO_5$ (Kierkegaard and Longo, 1970), there appears to be no indication of the O(2) disordering. Most of the temperature factors of that structure are close to their counterparts in α-VPO_5 except the U_{33} of O(2) which is two thirds to half the corresponding value in α-VPO_5. In $VMoO_5$ Eick and Kihlborg (1966) find crystals off stoichiometry in both directions, with the V or Mo substituting on the site of the minority element. It is also interesting to note that the observed change in cell constants was not isotropic. When the larger tetrahedron substituted for the smaller one, the percentage c axis expansion was four times that of the a axis. Whatever the difference between the assumed stoichiometric and assumed non-stoichiometric α-VPO_5 crystals, that difference is physical and not an accident of analysis. This is because intensity distribution in reciprocal space is visibly different for an "ordered" and a "disordered" α-VPO_5 crystal, and the assumed non-stoichiometric crystal is "ordered" at room temperature. A further test was made of the intensities. The population parameter for tetrahedral vanadium was set midway between the stoichiometric value and the 8% substitution found optimal for the non-stoichiometric crystal. Identical parameters were put into the model and both data sets refined.

The assumed non-stoichiometric crystal refined back to 8%, and the assumed stoichiometric crystal refined back to stoichiometry.

A paper on the crystal structure of α-VPO_5 has been published by B. Jordan and C. Calvo in the Canadian Journal of Chemistry (1973).

Table 5.8

Approximate $F^2_{calc.}$ for the ordered and disordered cases for one area of reciprocal space. The numbers show an intensity distribution indicative of the degree of disorder.

(h 1 1)		(h 3 1)			
		361	56	225	(5 k 1)
		1024	36	169	(4 k 1)
900	-	441	72	484	(3 k 1)
		449			
		400			

Approximate Intensity Distribution for 100 % Majority O(2) Position Occupancy

---

		400	170	220
		440	36	320
620	-	440	440	400
		480		
		620		

Approximate Intensity Distribution for 50 % Occupancy in O(2) and in O(2)' Positions

Figure 5.4

First layer precession photographs of an α-VPO_5 crystal above and below room temperature.

(a) The crystal was cooled by a stream of cooled nitrogen gas. During exposure to X-rays the temperature varied from 139°K to 150°K. Some ice formation tended to block X-rays going toward the lower left quadrant of the film. Because of this Laue group equivalence is destroyed but the local relative distribution of intensities in a given corner of the film should be insensitive to the ice absorption problem. Note the loss of reflections (h, 4, ℓ) above (h, 4, 1).

(b) The same crystal as in (a) but heated to 158 ± 2°C by a stream of hot air. Note the changes from (a) and particularly the move toward a mirror symmetry across the diagonals of the film (h, h, 1). There are local fluctuations in the dark cloud which surrounds the centre of the film which may be disorder diffuse scattering. Many photographs, simple and integrated, first and zero layer were taken as a function of temperature from 110°K to over 600°K were taken and those shown are representative of the observed trends.

(a)

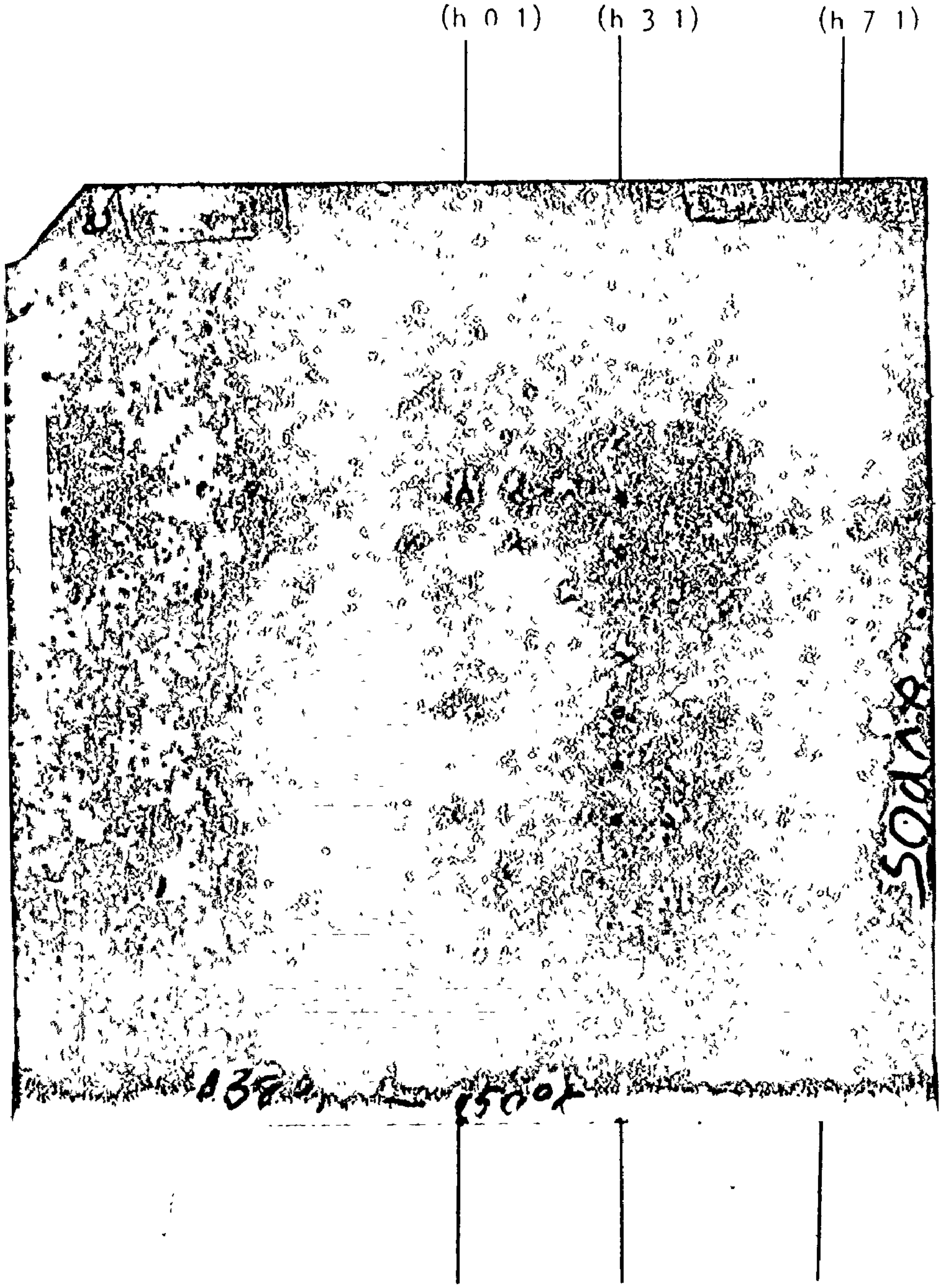

(b)

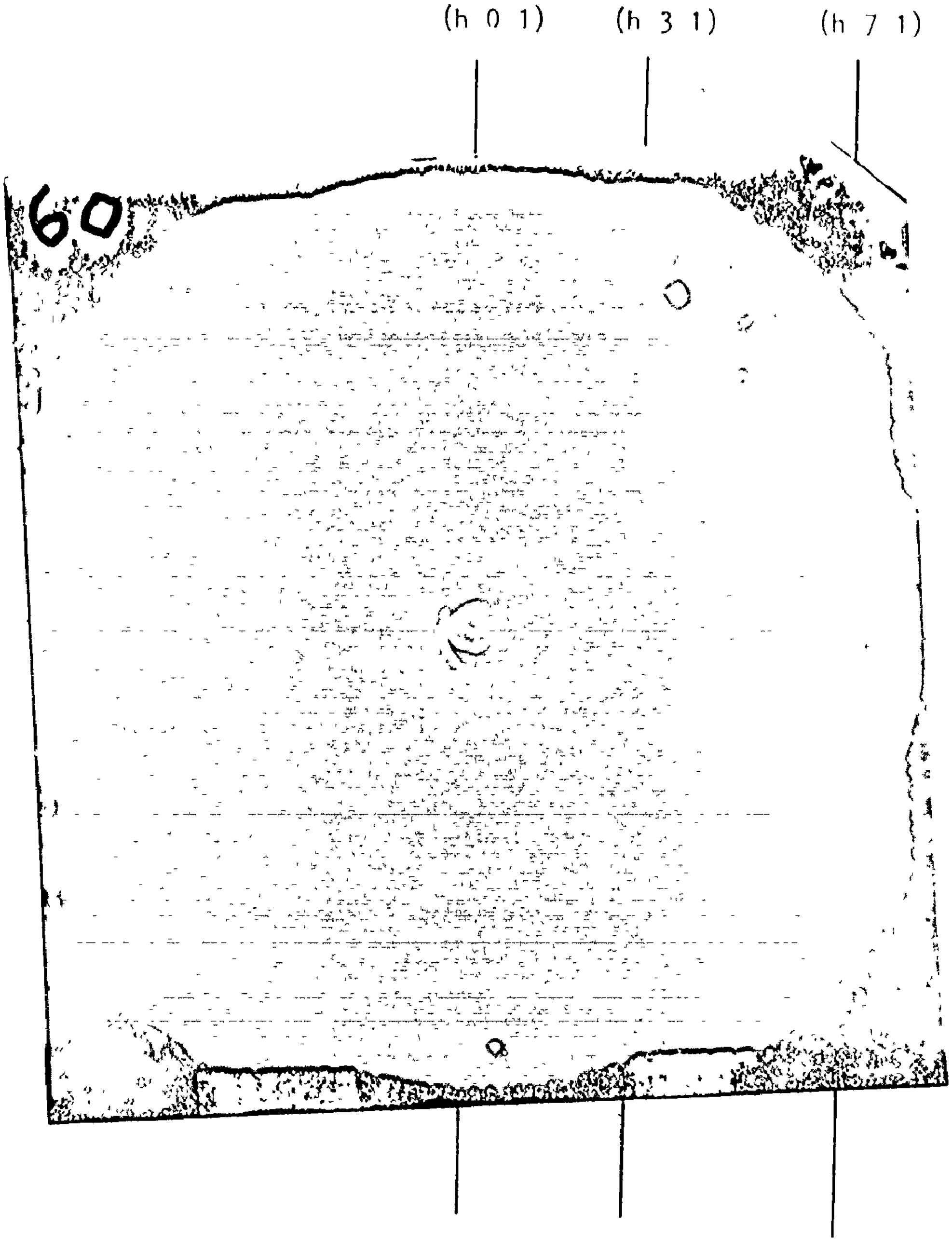

CHAPTER 6

THE MODEL

6.1 General

A model is proposed, which is based on the α-VPO_5 crystal structure. A high density of slip dislocations, in what would be the easiest shear direction yields the necessary free volume to match the measured density. Stoichiometry is changed by replacing PO_4 groups with VO_4 groups, and by allowing the VO_6 units to rotate about the fourfold axis to adjust for the larger tetrahedral ion to oxygen distance. When it is found that reasonable agreement with experiment was achieved without making any allowance for the oxygen released in the reduction of the vanadium, a new grouping V_2O_9 is proposed to accommodate the oxygen loss and yet not be inconsistent with the X-ray data.

This model does not intend to imply that the glass is merely a collection of small crystallites. The most ordered feature of the model is the sheet, which is originally taken from the α-VPO_5 crystal structure. Even two dimensional periodicity, however, is assumed to be greatly perturbed by distortions made locally to accommodate VO_4 substitution and V^{4+}. This distortion would make the sheet more consistent with a two dimensional paracrystalline (Hoseman and Bagchi, 1962), rather than crystalline, translational ordering. It is hypothesised that the extent of the sheet is great enough that features on the edge of a sheet are not necessary to explain the X-ray results, or merely that features internal to the sheet adequately outnumber those on the boundary of a sheet or in connective regions between sheets.

6.2 The Sheet

The basic structural feature of the model is an α-VPO_5-like sheet, composed of VO_6 units PO_4 units In α-VPO_5 (which has space group P4/n), the n-glide operation, combined with the fourfold axis, operating repeatedly on a single VO_6-PO_4 pair, generate a corrugated sheet. The units of the sheet are all connected by V-O-P bridging oxygen bonds. The phosphorus sits on the n-glide plane at a site of $\bar{4}$ symmetry, and its z value is invariant. Two oxygens of each PO_4 unit lie above the plane and two below, each bridging to a vanadium. The vanadium and one oxygen sit on the four-fold axis, and vanadium forms one short (1.58 Å) bond and one long (2.8 Å) bond with this oxygen. This short bond will be referred to as the vanadyl bond, and for descriptive purposes will be said to point in the direction of a vector from the vanadium to the oxygen. If the sheet were viewed down the "a" or "b" axis, the vanadyl oxygens protruding from the sheet would appear as rows of oxygens, with the rows running parallel to the line of sight. Those octahedra with their vanadyl bonds pointing in the same direction are related by "a" or "b" translations.

Adjacent rows are generated by the n-glide operation yielding alternately anti-parallel rows of vanadyl oxygen atoms.

6.3 The Slip

If the vanadyl oxygens are viewed as protrusions from the average surface of a sheet, then trans to these oxygens is a recess into which the vanadyl oxygen from the layer below fits. The sheets are very weakly bound, and should easily be separated. The weakness of the binding is demonstrated by the ease of shearing or deforming a crystal and by the disordering behaviour discussed in Chapter 5. A liquid by definition yields to any shearing stress and a glass quenched from a fluid melt could be suspected of maintaining some of the features which had allowed the melt to flow. Because of the relative weakness of the intersheet bonding the likeliest candidate to relieve a shearing stress is a slipping of sheets relative to each other. Two slip directions are releyant. A slip along the diagonal of half a cell brings the apices of the vanadyl protrusions into coincidence. Such a slip has been proposed by Perlstein (1970) to explain the electrical properties of V_2O_5. In his model the slip is accompanied by the loss of some of the vanadyl oxygen and the formation of direct bonds between the

FIGURE 6.1

A cross sectional view of four layers. The central two are aligned as in crystalline α-VPO_5. The interface between the top two and between the bottom two sheets illustrate the two cross sectional manifestations of the proposed slip operation. The O-O repulsion distance between the upper pair of oxygens on a PO_4 unit and a vanadyl oxygen pointing toward the PO_4 is expected to be or exceed 2.8 Å. The vanadium atoms in the second layer from the bottom are at least 7 Å removed from the nearest vanadium atom in the layer below.

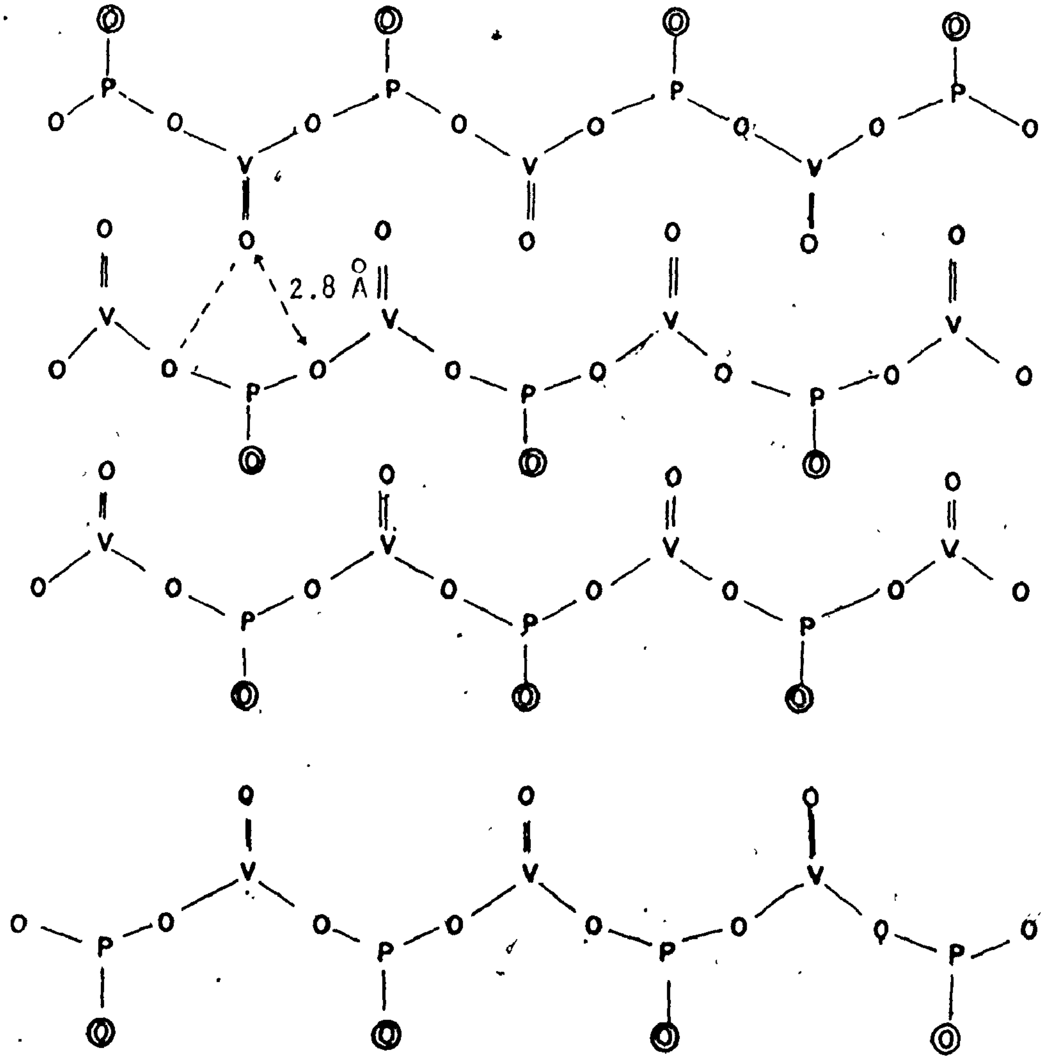

DOUBLE LAYER WITH SLIP

vanadium atoms brought into juxtaposition. If the slip is to take place without the loss of any features of the sheets, the sheets must be separated from each other by four Angstroms to allow the vanadyl oxygens to slip past each other without approaching closer than a normal oxygen-oxygen distance. The other slip direction is half a lattice spacing along a and b. This translation would still leave the same rows of protrusions aligned, but the translation would be parallel to the rows of protrusions. This slip brings half of the phosphate groups into line with the four-fold axis of VO_6 group. The vanadyl bond from above points directly at a phosphorus atom. Oxygen-oxygen repulsion between the vanadyl oxygen and the upper oxygens of the nearest phosphate group is directed at an angle from the axis. The net layer separation necessary to bring about such a slip is only 1.5 to 1.8 Angstroms, giving a 34% to 40% expansion per layer per slip. If all layer interfaces were antiphased in this fashion, a new crystalline order would be imposed. If alignment or antiphasing (slipping) were equally probable, each sheet would on the average be aligned with one other sheet above or below. This is the situation that appears most consistent with the X-ray data and the measured density. If the free volume associated with an antiphasing occurs on the average only every second interface, the expansion imposed on the "crystal" is only 17% to 19% in agreement with the measured densities. The bilayer arrangement is incorporated into the analysis of the X ray data in two ways. In the calculation of the pair distribution function, pairs of atoms within a sheet are given a weight of one and pairs of atoms from different sheets are given the weight one half.

One of the arguments frequently put forward to dispute quasi-crystalline descriptions of glasses is that the void distribution due to the interfacing of quasi-crystallites should give rise to small-angle scattering. This aspect is discussed by Bishop and Shevchik (1974), Shevchik and Paul (1974), and Bagchi (1972). If the interfaces are an intimate part of the short-range order, as they are in the present case, the influence of the interfaces will appear in the usual high angle scattering regime, with perhaps extra peaks due to the void-void distribution function. It will be seen that just such a peak appears with the appropriate position and width as an observable shoulder on the lower side of the first maximum in the X-ray intensity curves.

6.4 Substitution

$VOMoO_4$ is isostructural with α-$VOPO_4$ and Eick and Kihlborg (1966) have found a variation in cell constants in crystals made off stoichiometry which they interpret as a substitution of the excess metal onto the site of the minority metal constituent. The sizes of the MoO_4 and VO_4 units are much more closely matched than are PO_4 to VO_4.

Reported in another chapter is evidence which suggests that a crystal prepared in connection with the present study may be as much as four percent off stoichiometry ($V_{1.08}P_{.92}O_5$). The deviation from stoichiometry is believed to be achieved in this crystal by substituting tetrahedral VO_4 units for PO_4 units. It is not known how much substitution can be effected in crystalline α-VPO_5 without the loss of crystalline order. It has been reported by Brown and Hummel (1965) that β-VPO_5 is not stable beyond ten percent substitution of V for P.

According to Vegard's law, (Klug and Alexander, 1974), the lattice constants of a solid solution should interpolate linearly between those of the end members. Neglecting second order terms, this implies a linear interpolation for the density of the crystalline solid. The measured density of the glasses would be consistent with a solid solution model, although for lack of a vanadium end member $VOVO_4$(V_2O_5 is structurally too different for comparison), a quantitative interpretation ofthe slope is difficult. On the basis of all this, the hypothesis is made that at least over the region studied, change in stoichiometry is effected by simple substitution of VO_4 units for PO_4. It could be expected that the longer V-O bond in comparison to P-O should introduce some structural alteration. A rotation of the VO_4 group in the xy plane in the direction which increases the bend in the P(V) - O - V bond, would allow for much of the increased tetrahedral size.

The substitution is implemented in the calculation of the pair distribution function in the following manner. Using distances taken from the α-VPO_5 crystal structure, the stoichiometric VPO_5 pair distribution function is calculated with a composition weighted scattering factor at the tetrahedral site. The justification for the first step is that the second and third neighbour P-O and P-V pairs will be little effected by the substitution. Adjustment in the first neighbour environments is accomplished by substracting initial electron density and inserting new density elsewhere. An appropriate proportion of the 1.54 Å P-O peak is deleted and a tetrahedral V-O peak inserted at 1.714 Å. An appropriate proportion of the O-O peak at 2.5 Å from the PO_4 group is moved to 2.8 Å for the larger VO_4 group. The V-P pair at 3.26 Å is shifted only slightly to a value between 3.28 Å and 3.33 Å with increasing vanadium content. All shifting is done by subtracting density at the P-X distances and inserting density at the V-X characteristic distances. With regard to the vanadium to phosphorous separation, it should be noted that some of the distortion introduced by the larger tetrahedral unit will be in the separation in the z direction of the tetrahedral and octahedral units.

To the extent that rotations in the xy plane can accommodate the effect of the larger ion, the vanadium-phosphorus separation can remain constant.

The manner in which the z component of the separation between the octahedral vanadium site and the tetrahedral site adjusts to the presence of vanadium on the tetrahedral site may vary with VO_4 concentration. When each VO_6 has only one VO_4 neighbour, the VO_6 may rotate slightly about V, causing the vanadyl bond to deviate from the normal to the sheet. When the VO_4 outnumber the PO_4 about a given VO_6, a rigid group translation of the VO_6 in the z direction may result.

6.5 Sensitivity to Various Features

Because the phosphorus lies on the glide plane, peaks to which it contributes are quite prominent. A vector drawn from P to another atom in the same sheet, for example above the glide plane, will be matched by a vector to an atom below the glide plane at the same separation. Vanadium, will have peaks in different positions for its pairs above and below the glide plane, and one of these members will often involve crossing into another sheet. Most vectors of consequence, less than five Angstroms, will have much less of a z component than x or y. Because of this, distortions along z or involving the sheet to sheet separation are much less consequential in the pair function. Rotations of the octahedra and tetrahedra in the xy plane leave the P and V sites invariant and in general move the oxygens nearly tangentially to most of the V-O and P-O vectors.

6.6 Reduced Vanadium

With increasing phosphate content, the percentage of total vanadium which is reduced increases. The local environment of V^{4+} is detectably different from that of V^{5+}. The ionic radius of V^{4+} is at least .05 Å larger than that of V^{5+} (Shannon and Prewitt, 1969). Two configurations appear in the literature which give equivalent valence bond strength sums as defined in Brown and Shannon (1973). The first of these appears in β-$VOSO_4$ (Kierkegaard and Longo, 1965) and $VOSO_4 \cdot 5H_2O$ (Ballhausen et al. 1968) in which the bond length of the vanadyl complex is relatively unaltered from that in octahedral V^{5+} complexes, such as α-VPO_5, but the equatorial oxygens are pushed out to about 2.03 Å and the long bond trans to the vanadyl is shortened to about 2.3 Å. In α-$VOSO_4$ (Longo and Arnott 1970) and to an even greater extent in $VOMoO_4$ (Eick and Kihlborg, 1966), both of which are isostructural with α-VPO_5, the vanadyl bond is longer than in the VPO_5 structure (1.63 Å in $VOSO_4$ and 1.677 Å in $VOMoO_4$) and the bond trans to it is longer than in the cases noted above but still shorter than in α-VPO_5. These bonds for the sulphate and molybdate are 2.47 Å and 2.59 Å respectively. The equatorial oxygen bonds are 1.97 Å in the molybdate but remain at 2.04 Å in the sulphate.

The pair distribution function is sensitive enough to the position of the equatorial V^{4+} - 0 bond length to indicate a preference for the 1.97 Å position over the 2.04 Å position. Concommitant with this choice, the vanadyl bond is assumed in the model for the glass to be lengthened to approximately the value found in the molybdate.

As with the treatment of the tetrahedral vanadium, the correction curve for the reduced vanadium was calculated by subtracting a fraction of the appropriate V^{5+} peak and introducing a fractional peak at the V^{4+} positions. The relevant new positions are 1.677 Å for the vanadyl bond and 1.97 Å for the equatorial, bridging, V-0 distance. The long bond trans to the vanadyl is also taken from its VPO_5 position and transferred to 2.588 Å to maintain consistency with the $VOMoO_4$ vanadium environment.

6.7 The V_2O_9 Group

This element of the model was chosen more for what it does not do than for what it does. When it was found that a reasonable fit to the pair distribution function could be obtained with no considerations given to the effect of the lost oxygen, it was apparent that whatever new complex resulted from the loss of the oxygen, it causes only minor perturbations to the basic structure. If the vanadium is reduced by loss of oxygen, and every two V^{4+} ions correspond to one lost oxygen, and if forty or more percent reduction of vanadium is to be expected in some compositions, and if the chemical rearrangement caused by the lost oxygen is major, then there ought to be evidence for it in the X-ray curves.

The proposed configuration to accommodate the loss of oxygen is the following. In a bilayer, an outside vanadyl oxygen is removed and the vanadium bonded to it is reflected through the plane of its bridging oxygens to form a single bond with the vanadyl equatorial oxygens from the level below The resulting complex can be seen as two tetragonal prisms, $V^{4+}0_5$ units, sharing a bridging oxygen at the apex. Relative to its layer, the lower vanadium need not move at all. The shift of the upper vanadium is in the z direction and the only pair function peak to be significantly shifted will be the V-P peak for the upper vanadium alone. This adjustment takes a fraction of the 3.26 Å V-P peak, equal to one half the concentration of V^{4+} relative to the number of six coordinated V sites, and moves it to 3.06 Å. As the vanadium content increases, this adjustment diminishes greatly because of the decrease in the concentration of V^{4+}. The other feature of the pair distribution function which is changed is the V-V peak between sheets. The formation of such a complex would give rise to a peak near 3.9 Å which would involve both vanadiums in the pair. A drawing of the V_20_9 complex is on the following page. The equatorial V-0 distances are assumed unchanged(1.97 Å).

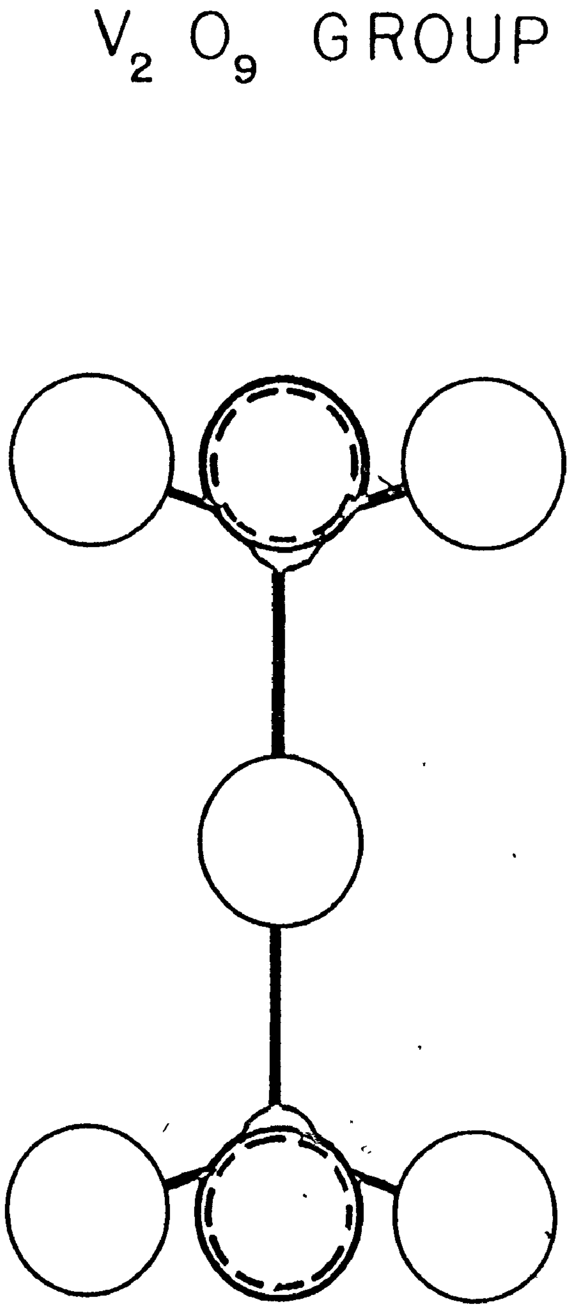

Figure 6.2 The proposed V_2O_9 group. The large circles are oxygen atoms and the small filled circles, partially eclipsed by the oxygens above the page, are vanadium atoms. The dashed circle indicates the oxygen below the plane of the page.

The greatest drawback of the hypothesized V_2O_9 complex is the dearth of evidence for its existence anywhere else. Were it a stable environment for vanadium, one would think that it should have appeared in the structure of some crystals studied to date. It does appear without comment in a diagram in Perlstein's (1970) paper on the conductivity in V_2O_5 in which he proposes slip dislocations with resultant bonding changes. The V_2O_9 unit could be viewed as a pyrovanadate V_2O_7 ion with an extra terminal oxygen on each end. In $Mg_2V_2O_7$ (Gopal and Calvo, 1974) an extra terminal oxygen can be found 2.44 Å from the one vanadium and 2.87 Å from the other. The extra oxygen on the pyrovanadate group in TeV_2O_9 is so close that the pyrovanadate groups form chains (Darriet and Galy, 1973). Each vanadium in the latter structure is five coordinate with the V-O bond lengths ranging from 1.64 Å to 2.08 Å.

The fit of the pair distribution function is slightly improved, particularly from the proposed 3.9 Å V-V peak, by the inclusion of the V_2O_9 unit in the model, however slight adjustment of the widths of the neighboring peaks can yield nearly as good a fit in the absence of this feature from the model. The X-ray evidence is consequently ambivalent with regard to this feature. Any alternative explanation of the effect of the lost oxygen would be highly constrained by the need to maintain the basic α-VPO_5 pair distribution function. A graph indicating the fit to the $V_1P_1O_5$ glass pair function, with and without the V_2O_9 feature is on the following page.

In the calculation fo the pair distribution function, the equatorial V-O bonds were treated as if they were on a normal VPO_5 vanadium site. They were set to the value found in α-VPO_5 or that found in $VMoO_5$ according to the concentration of V^{4+} per octahedral site. Although two electrons are liberated on the formation of a V_2O_9 group, it is not assumed that these electrons must remain there. In the absence of evidence to the contrary, it is assumed that the electrons will be distributed evenly among the octahedral (including V_2O_9) sites. Because both the V^{4+} and V_2O_9 populations scale identically, their separate influences on the equatorial V - O bond length would be very difficult to extract from a pair distribution function. It was assumed in the model pair distribution function calculation that the equatorial V-O bond lengths expanded and contracted with the arrival and departure of the hopping electron in the same way on the V_2O_9 sites as it would on a vanadyl site. It remains open to speculation whether the parameters found to be consistent with the experimental curve represent an average response between the two types of V^{4+} environment or whether the responses are indeed similar. It is a deliberate part of the model that all tetrahedrally coordinated V are pentavalent.

Figure 6.3 shows the experimental pair function for VPO_5 glass with the calculated pair function with and without the V_2O_9 hypothesis. The parameters r_{ij}, C_{ij}, and σ_{ij} are tabulated in table 6.1 for the unperturbed VPO_5 glass model. Changes to these parameters which are made to account for V^{4+} or tetrahedral vanadium have been described above. Figure 6.4 displays the low angle Cr K_α X-ray data on four compositions of the glass. The experimental relative intensity, corrected for absorption and polarisation is tabulated for five compositions of glass in tables 6.2 to 6.6. Figures 6.5 to 6.9 contain the measured intensity, the radial distribution function and g(r) for each composition of the glass. Figures 6.5 to 6.9 also contain graphs comparing the observed and calculated reduced intensities and total pair functions. All glasses were prepared by melting Fisher V_2O_5 and P_2O_5 in a vitreosil casserole in air. The glasses were quenched to room temperature from 900°C. A piece of each glass was then briefly melted in a vitreosil mold and quenched again from 900°C.

FIGURE 6.3

The pair function for VPO_5 glass with and without the V_2O_9 hypothesis.

(a) This graph includes the V_2O_9 unit in the calculated pair function. It also illustrates how the model function is controlled.

Key.

——	Experimental curve
....	Bare model function when $x \neq 0$ this function is the $x = 0$ model with averaged scattering functions.
- . -.	The perturbation which subtracts old peak intensity and inserts new. This curve perturbs for V^{4+} changes.
-----	This curve perturbs for VO_4 when present and also includes the c-axis translation generated compound peak located at about 4.4 Å.
-..-..	The total model function to compare with the experimental curve.

(b) The same as (a) but with the V-P peak at 3.26 Å broadened and the V_2O_9 contribution deleted.

PAIR FUNCTION AND MODEL

FOR $V_1P_1O_5$ GLASS

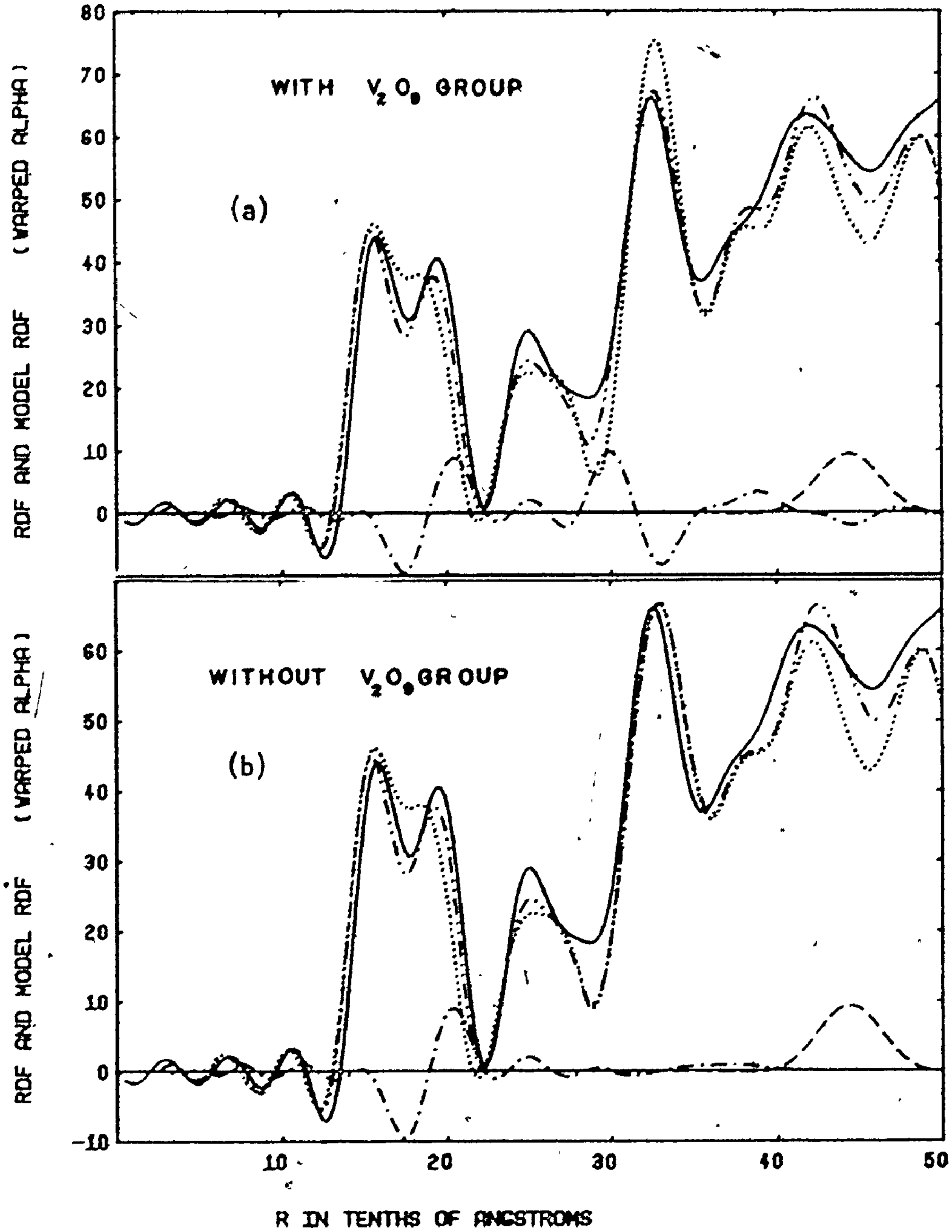

TABLE 6.1

INTERATOMIC DISTANCES

	P - O				O - O				V - O				P - P		
#	r_{ij}	C_{ij}	σ_{ij}	#	r_{ij}	C_{ij}	σ_{ij}	#	r_{ij}	C_{ij}	σ_{ij}	#	r_{ij}	C_{ij}	σ_{ij}
1	1.54	8	.085	9	2.67	8	.11	2	1.58	2	.03	6	4.25	4	.15
16	4.93	12	.18	10	3.59	4	.22	3	1.856	8	.09	46	6.14	4	.3
17	3.41	4	.25	11	4.8	6	.15	4	2.856	1	.21	48	6.01	4	.2
22	3.39	12	.13	12	2.51	12	.11	18	5.12	4	.16				
23	3.89	12	.13	13	3.6	4	.12	19	4.43	4	.15				
24	3.72	6	.12	14	2.6	8	.11	20	4.12	8	.25		P - V		
31	4.90	12	.15	26	3.08	4	.11	21	3.65	8	.19	5	3.26	8	.11
34	4.13	8	.25	27	4.91	4	.16	25	4.26	4	.25	15	4.37	4	.24
				28	4.63	8	.15	32	4.18	4	.24	43	6.46	4	.35
				29	5.12	8	.16	33	3.72	4	.18	45	6.85	16	.37
				30	4.72	8	.15	42	5.90	16	.2				
				35	2.99	4	.15	44	4.21	8	.15				
				36	4.17	8	.15						V - V		
				37	4.96	8	.15					7	4.66	2	.15
				38	4.09	4	.15					8	4.94	4	.15
				39	4.61	16	.15					47	6.01	4	.2
				40	3.03	4	.2								
				41	2.98	4	.14								

FIGURE 6.4

Intensities of Cr. K_α X-rays reflected from four compositions of $V_{1+x} P_{1-x} O_5$ glass at low scattering angles. When the scattering angle falls below some θ_o value, determined by the size of the sample and the slit width, the sample ceases to intercept all of the incident beam. At this point the scattered intensity should diminish but parasitic scattering in the background should increase as the main beam is approached. An approximate estimate of θ_o is indicated on all graphs except (c) by an arrow. All of graph (c) falls below θ_o. The reader is referred to Shevchik and Paul (1974) for graphs of glass samples with and without small-angle scattering for comparison. Apling (1973) has interpreted scattering data on As_2S_3 glass as implying a layered structure. Bishop and Shevchik (1974) have examined the small-angle scattering from As_2S_3 glass and have found no evidence of an exponential rise in the 3Å to 50 Å size regime. They interpret this lack of small angle scattering as supportive of the layered structure model for As_2S_3 glass.

$V_{1+x} P_{1-x} O_5$ glass.

(a) $x = .6$
(b) $x = .33$
(c) $x = .2$
(d) $x = 0$

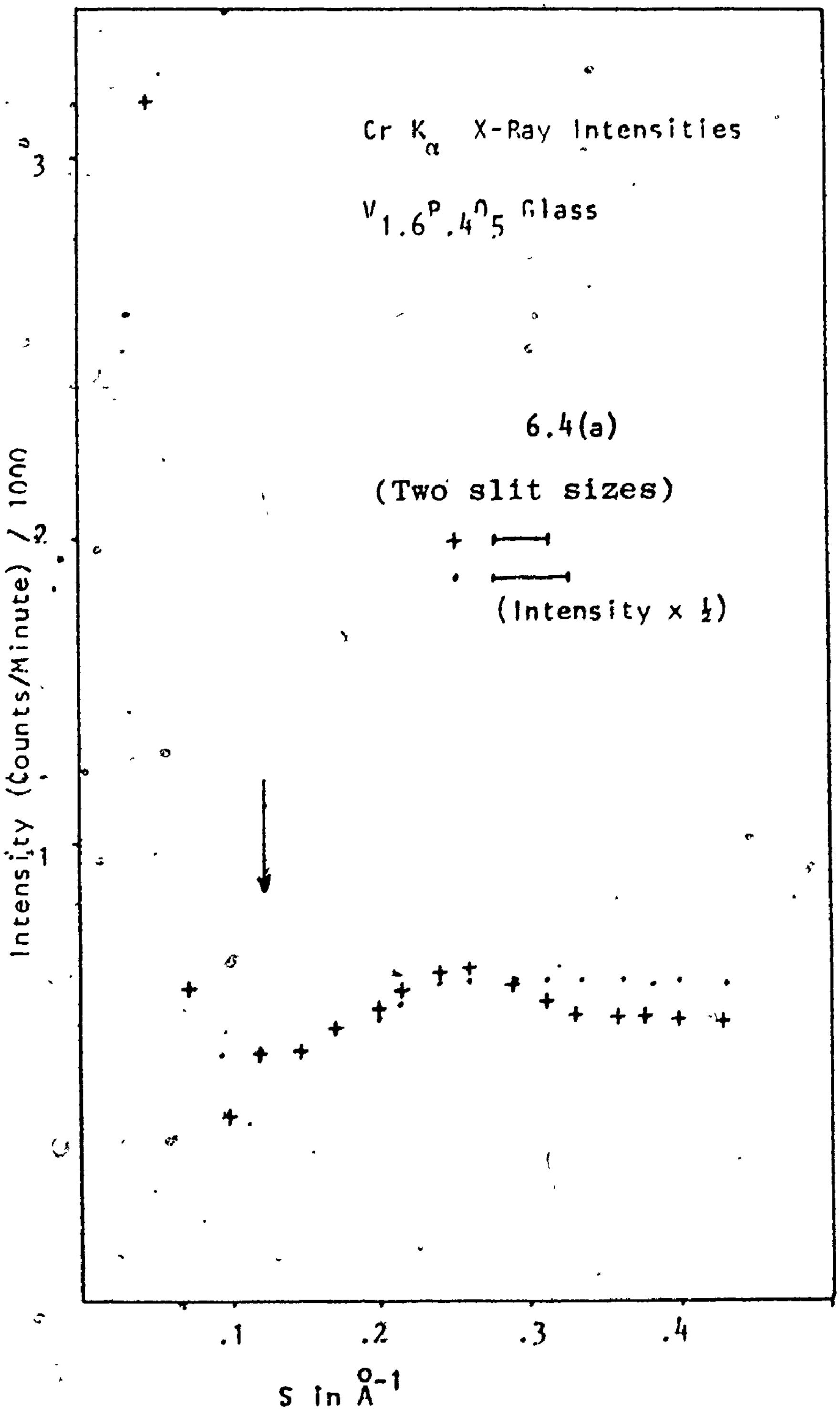
Cr Kα X-Ray Intensities
V1.6P.4O5 Glass
6.4(a)
(Two slit sizes)
+
•
(Intensity x ½)
Intensity (Counts/Minute) / 1000
3
2
1
.1
.2
.3
.4
S in Å-1

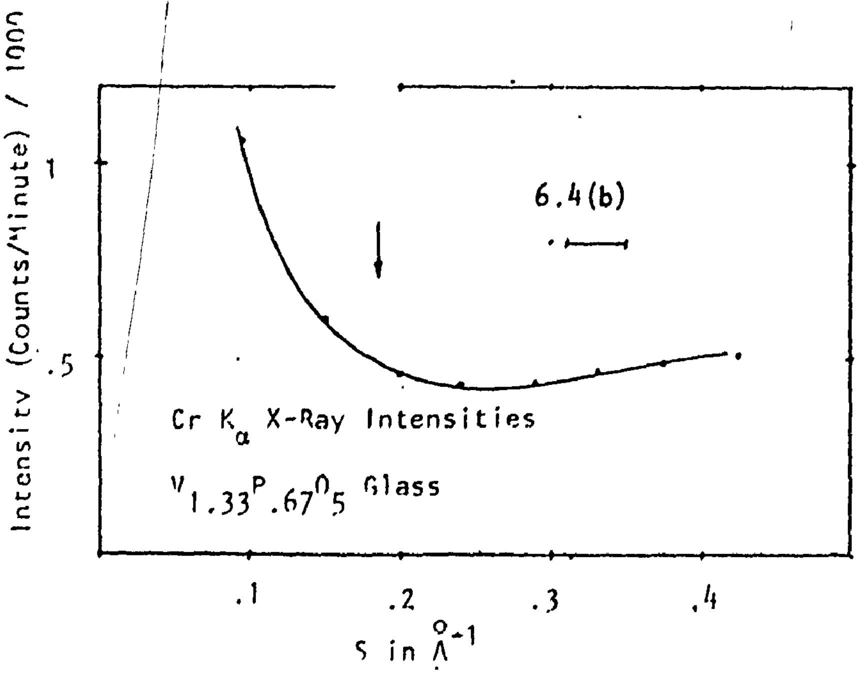
Intensity (Counts/Minute) / 1000
1
.5
6.4(b)
Cr K_α X-Ray Intensities
$V_{1.33}P_{.67}O_5$ Glass
.1
.2
.3
.4
S in $\mathring{A}^{-1}$

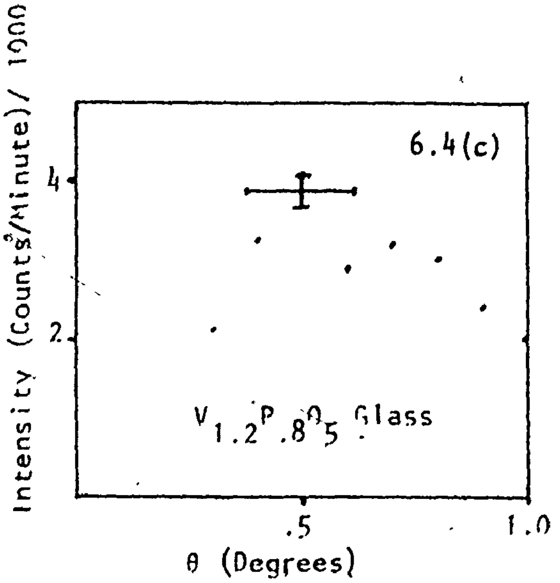
Intensity (Counts/Minute)/ 1000
4
2
6.4(c)
$V_{1.2}P_{.8}O_5$ Glass
.5
1.0
θ (Degrees)

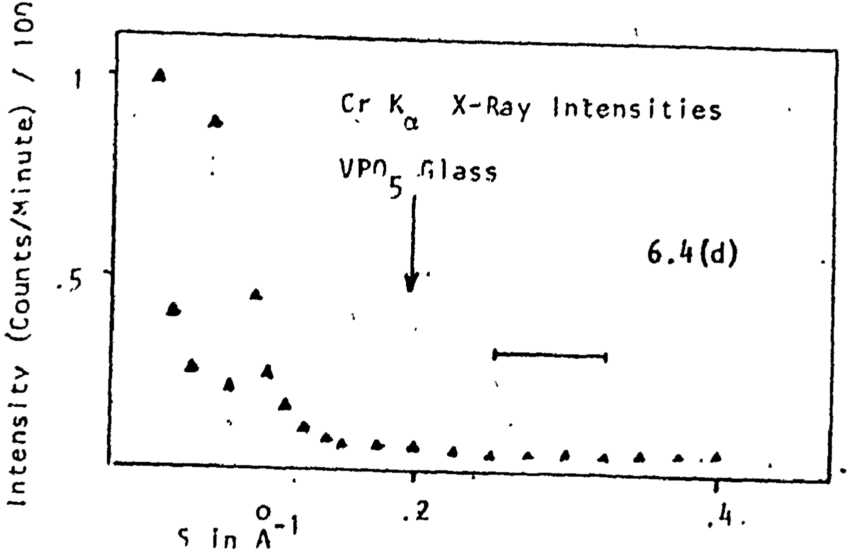
Intensity (Counts/Minute) / 1000
1
.5
Cr K_α X-Ray Intensities
VPO_5 Glass
6.4(d)
.2
.4
S in $\mathring{A}^{-1}$

S x 100	I(S)	S x 100	I(S)	S x 100	I(S)
92	1943 (10)	100	1989 (10)	107	2042 (10)
115	2310 (11)	123	2734 (12)	131	3170 (13)
138	3796 (14)	146	4518 (15)	154	5205 (16)
161	5765 (17)	169	6047 (18)	177	6111 (18)
184	5907 (17)	192	5579 (17)	200	5101 (16)
207	4654 (15)	215	4145 (15)	223	3654 (14)
230	3208 (13)	238	2922 (12)	246	2623 (12)
253	2367 (11)	261	2131 (10)	269	1985 (10)
276	1963 (10)	284	1914 (10)	291	1930 (10)
299	1976 (10)	307	2041 (10)	314	2099 (10)
322	2153 (11)	329	2239 (11)	337	2289 (11)
344	2349 (11)	352	2377 (11)	360	2422 (11)
367	2475 (11)	375	2501 (11)	382	2533 (12)
390	2567 (12)	397	2641 (12)	405	2656 (12)
412	2682 (12)	420	2565 (12)	427	2501 (12)
435	2436 (11)	442	2347 (11)	450	2206 (11)
457	2160 (11)	465	2074 (11)	472	2032 (11)
479	1932 (10)	487	1868 (10)	494	1828 (10)
502	1718 (10)	509	1644 (10)	516	1571 (9)
524	1529 (9)	531	1498 (9)	539	1435 (9)
546	1412 (9)	553	1369 (9)	561	1385 (9)
568	1364 (9)	575	1355 (9)	582	1325 (9)
590	1327 (9)	597	1318 (9)	604	1298 (9)
612	1248 (8)	619	1219 (8)	626	1205 (8)
633	1152 (8)	641	1143 (8)	649	1066 (8)
655	1071 (8)	662	1058 (8)	669	1034 (8)
676	1005 (8)	683	1018 (8)	690	969 (8)
697	972 (8)	705	988 (8)	712	979 (8)
719	1017 (8)	726	1001 (8)	747	1001 (5)
761	936 (4)	775	938 (4)	788	956 (4)
802	910 (4)	816	887 (4)	830	878 (4)
843	841 (4)	857	851 (4)	870	813 (4)
884	716 (3)	897	736 (3)	910	776 (3)
923	767 (3)	937	778 (3)	950	765 (3)
963	744 (3)	975	746 (3)	988	735 (3)
1001	726 (3)	1014	728 (3)	1026	712 (3)
1037	707 (3)	1051	703 (3)	1064	688 (3)
1076	663 (3)	1088	634 (3)	1100	679 (3)
1112	675 (3)	1124	653 (3)	1136	668 (3)
1148	667 (3)	1160	654 (3)	1171	655 (3)
1183	665 (3)	1195	642 (3)	1205	639 (3)
1217	629 (3)	1228	628 (3)	1239	620 (3)
1250	614 (3)	1261	608 (3)	1271	603 (3)
1282	618 (3)	1293	684 (3)	1303	583 (2)
1314	597 (2)	1324	576 (2)	1334	587 (2)
1344	591 (2)	1354	583 (2)	1364	585 (2)
1374	581 (2)	1383	582 (2)	1393	576 (2)
1402	573 (2)	1412	573 (2)	1421	573 (2)
1430	578 (2)	1439	568 (2)	1448	567 (2)
1457	565 (2)	1465	562 (2)	1474	568 (2)
1482	559 (2)	1491	561 (2)	1499	562 (2)
1507	555 (2)	1515	560 (2)	1523	557 (2)
1531	556 (2)	1538	554 (2)	1546	551 (2)
1553	553 (2)	1561	551 (2)	1568	552 (2)
1575	546 (2)	1582	549 (2)	1589	546 (2)
1595	546 (2)	1602	544 (2)	1608	540 (2)
1615	543 (2)	1621	547 (2)	1627	544 (2)
1633	545 (2)	1639	549 (2)	1645	545 (2)

RELATIVE INTENSITY - CORRECTED FOR ABSORPTION AND POLARISATION

Table 6.2 $V_{1.6}P_{.4}O_5$ glass

			I(')		I(S)
[illegible]	3467 (96)	[illegible]	3811 (90)	[illegible]	4557 (84)
115	5037 (71)	123	4815 (70)	131	4665 (69)
138	10936 (99)	146	11775 (111)	154	17136 (124)
161	15616 (133)	169	21847 (137)	177	21745 (138)
184	20546 (136)	192	19554 (132)	200	18157 (128)
207	16549 (122)	215	15215 (117)	223	14748 (111)
230	12515 (105)	238	11277 (101)	246	10424 (97)
253	9587 (92)	261	9047 (90)	269	8690 (85)
276	7595 (83)	284	7209 (81)	291	7128 (80)
299	7361 (81)	307	7539 (83)	314	7445 (84)
322	8078 (85)	329	8753 (87)	337	8158 (87)
344	8547 (88)	352	8509 (84)	360	8585 (89)
367	8748 (90)	375	8945 (91)	382	8984 (91)
390	8530 (92)	397	9541 (94)	405	9453 (95)
412	9495 (94)	420	9516 (94)	427	9510 (94)
435	9181 (93)	442	8915 (91)	450	8726 (90)
457	8460 (87)	465	7983 (86)	472	7490 (84)
479	7353 (83)	487	7240 (83)	494	6949 (81)
502	6780 (26)	509	6488 (26)	516	6282 (25)
524	5994 (25)	531	5751 (25)	538	5516 (24)
546	5376 (24)	553	5226 (24)	561	5158 (23)
568	5139 (23)	575	5036 (23)	582	5058 (23)
590	5018 (23)	597	5002 (23)	604	4977 (23)
612	4896 (23)	619	4833 (23)	626	4841 (23)
633	4739 (23)	640	4538 (23)	648	4467 (22)
655	4447 (22)	662	4260 (22)	669	4162 (22)
676	4081 (22)	683	3973 (21)	690	3881 (21)
697	3815 (21)	705	3763 (11)	719	3736 (11)
733	3759 (11)	747	3881 (11)	761	3841 (12)
775	3857 (12)	788	3823 (12)	802	3756 (12)
816	3670 (12)	830	3567 (11)	843	3466 (11)
857	3353 (11)	870	3246 (11)	884	3162 (11)
897	3069 (11)	910	3089 (11)	923	2982 (11)
937	2960 (11)	950	2918 (11)	963	2870 (11)
977	2842 (11)	988	2806 (11)	1001	2767 (11)
1016	2741 (11)	1026	2720 (11)	1037	2646 (11)
1055	2614 (11)	1066	2556 (11)	1076	2461 (10)
1088	2432 (10)	1100	2421 (10)	1112	2394 (10)
1124	2389 (10)	1136	2232 (10)	1148	2259 (10)
1160	2245 (10)	1171	2237 (10)	1183	2156 (10)
1194	2107 (10)	1205	2150 (10)	1217	2143 (10)
1228	2116 (10)	1239	2072 (10)	1250	2092 (10)
1261	2066 (10)	1271	2036 (10)	1282	2081 (10)
1293	1988 (10)	1303	1971 (9)	1314	1937 (9)
1324	1933 (9)	1334	1930 (9)	1344	1908 (9)
1356	1891 (9)	1364	1876 (9)	1374	1861 (9)
1383	1829 (9)	1393	1838 (9)	1402	1801 (9)
1412	1774 (9)	1421	1703 (9)	1430	1745 (9)
1439	1710 (8)	1448	1705 (8)	1457	1701 (8)
1465	1664 (8)	1474	1625 (8)	1482	1619 (8)
1491	1604 (8)	1499	1590 (8)	1507	1596 (8)
1515	1569 (8)	1523	1566 (8)	1531	1553 (8)
1538	1545 (7)	1546	1519 (7)	1553	1508 (7)
1561	1493 (7)	1568	1484 (7)	1575	1473 (7)
1582	1465 (7)	1589	1465 (7)	1595	1465 (7)
1602	1459 (7)	1608	1446 (7)	1615	1431 (7)
1621	1423 (7)	1627	1412 (7)	1633	1422 (7)
1639	1412 (7)	1645	1415 (6)		

RELATIVE INTENSITIES - SCALED AND CORRECTED FOR ABSORPTION AND POLARISATION

$Y_{1.33}P_{.67}O_5$ GLASS

Table 6.3

S x 100	I(S)	S x 100	I(S)	S x 100	I(S)
38	497 (8)	46	886 (9)	53	847 (11)
61	1279 (13)	69	1482 (14)	77	1617 (16)
84	2021 (17)	92	2309 (16)	100	2026 (19)
107	2713 (20)	115	3108 (21)	123	3542 (22)
131	4837 (24)	138	4582 (25)	146	4045 (26)
154	6345 (30)	161	6962 (31)	169	7042 (32)
177	7011 (31)	184	6572 (30)	192	6145 (29)
200	5713 (28)	207	5202 (27)	215	4613 (26)
223	4347 (25)	230	4882 (24)	238	3635 (22)
246	3361 (22)	253	3106 (21)	261	2921 (20)
269	2640 (19)	276	2488 (16)	291	2246 (8)
307	2415 (8)	322	2608 (9)	337	2728 (9)
352	2705 (9)	367	2716 (9)	382	2854 (9)
397	2948 (9)	412	3011 (9)	427	3016 (9)
442	2911 (9)	457	2721 (9)	472	2559 (9)
487	2405 (8)	502	2266 (8)	516	2154 (8)
531	2008 (8)	546	1852 (8)	561	1768 (7)
575	1676 (7)	590	1666 (7)	604	1642 (7)
619	1614 (7)	633	1578 (7)	648	1517 (7)
662	1498 (7)	676	1377 (7)	690	1318 (7)
705	1266 (6)	719	1247 (6)	733	1244 (6)
747	1216 (6)	761	1239 (7)	775	1245 (7)
788	1298 (7)	802	1248 (7)	816	1218 (7)
830	1197 (7)	843	1161 (7)	857	1126 (6)
870	1093 (6)	884	1061 (6)	897	1038 (6)
910	1016 (6)	923	998 (6)	937	963 (6)
950	959 (6)	963	990 (6)	975	944 (6)
988	931 (6)	1001	930 (6)	1014	913 (6)
1026	870 (6)	1039	861 (6)	1051	854 (6)
1064	843 (6)	1076	814 (6)	1088	757 (6)
1100	724 (6)	1112	725 (6)	1124	717 (6)
1136	711 (6)	1148	702 (6)	1160	703 (6)
1171	669 (6)	1183	681 (6)	1194	679 (6)
1205	693 (6)	1217	664 (6)	1228	668 (6)
1239	660 (6)	1250	644 (6)	1261	641 (6)
1271	641 (6)	1282	632 (5)	1293	624 (5)
1303	628 (5)	1314	617 (5)	1324	611 (5)
1334	597 (5)	1344	583 (5)	1354	588 (5)
1364	563 (5)	1374	533 (5)	1383	583 (5)
1393	569 (5)	1402	551 (5)	1412	553 (5)
1421	552 (5)	1430	549 (5)	1439	532 (5)
1448	532 (5)	1457	535 (5)	1465	521 (5)
1474	510 (5)	1482	518 (5)	1491	505 (4)
1499	490 (4)	1507	502 (4)	1515	497 (4)
1523	493 (4)	1531	495 (4)	1538	488 (4)
1546	491 (4)	1553	486 (4)	1561	484 (4)
1568	486 (4)	1575	481 (4)	1582	483 (4)
1589	479 (4)	1595	470 (4)	1602	479 (4)
1608	485 (4)	1615	481 (4)	1621	483 (4)
1627	467 (4)	1633	476 (4)	1639	459 (4)
1645	468 (4)				

RELATIVE INTENSITIES - SCALED AND CORRECTED FOR ABSORPTION AND POLARISATION

$V_{1.2}P_{.8}O_5$ CLASS

Table 6.4

S × 100	I(S)	S × 100	I(S)	S × 100	I(S)
54	1742 (21)	61	2254 (23)	69	2221 (23)
77	2348 (24)	84	2644 (24)	92	2933 (26)
100	3300 (26)	107	3150 (27)	115	3547 (29)
123	3649 (30)	131	4464 (33)	138	5163 (35)
146	5964 (38)	154	6617 (40)	161	7206 (41)
169	7148 (41)	177	6975 (41)	184	6629 (40)
192	6233 (38)	200	5946 (37)	207	5515 (36)
215	5000 (34)	223	4538 (33)	230	4236 (32)
238	3415 (30)	246	3037 (13)	253	3360 (13)
261	3271 (12)	268	3028 (12)	276	2790 (11)
284	2602 (11)	291	2696 (11)	299	2665 (11)
307	2747 (11)	314	2842 (12)	322	2963 (12)
329	3016 (12)	337	3051 (12)	344	3139 (12)
352	3190 (12)	360	3185 (12)	367	3167 (12)
375	3219 (12)	382	3209 (13)	390	3320 (13)
397	3364 (14)	405	3422 (13)	412	3463 (13)
420	3463 (13)	427	3400 (13)	435	3363 (13)
442	3251 (13)	450	3162 (13)	457	3060 (12)
465	2912 (12)	472	2827 (12)	479	2727 (12)
487	2698 (6)	502	2545 (9)	516	2376 (9)
531	2288 (5)	546	2054 (7)	561	1933 (5)
575	1872 (5)	590	1875 (5)	604	1636 (5)
619	1614 (5)	633	1774 (5)	648	1702 (5)
662	1604 (4)	676	1560 (4)	690	1630 (4)
705	1377 (4)	719	1351 (4)	733	1549 (4)
747	1352 (4)	761	1309 (4)	775	1379 (4)
788	1350 (4)	802	1336 (4)	816	1260 (4)
830	1206 (4)	843	1226 (4)	857	1195 (4)
870	1146 (4)	884	1115 (4)	897	1062 (4)
910	1069 (4)	923	1066 (4)	937	1031 (4)
950	1016 (4)	963	1013 (4)	975	992 (4)
990	948 (4)	1001	976 (4)	1014	969 (4)
1026	945 (4)	1038	926 (4)	1051	915 (4)
1064	888 (4)	1076	862 (4)	1088	840 (4)
1100	823 (4)	1112	800 (4)	1124	792 (4)
1136	768 (4)	1148	778 (4)	1160	763 (4)
1171	752 (4)	1183	755 (4)	1194	743 (4)
1205	732 (4)	1217	731 (4)	1228	723 (4)
1239	716 (4)	1250	706 (4)	1261	702 (4)
1271	690 (3)	1282	663 (3)	1293	679 (3)
1303	667 (3)	1314	663 (3)	1324	663 (3)
1334	655 (3)	1344	653 (3)	1354	642 (3)
1364	637 (3)	1374	630 (3)	1383	625 (3)
1393	620 (3)	1402	615 (3)	1412	606 (3)
1421	598 (3)	1430	609 (3)	1439	584 (3)
1448	576 (3)	1457	577 (3)	1465	567 (3)
1474	568 (3)	1482	559 (3)	1491	552 (3)
1499	550 (3)	1507	543 (3)	1515	543 (3)
1523	535 (3)	1531	537 (3)	1538	534 (3)
1546	529 (3)	1553	530 (3)	1561	523 (3)
1568	524 (3)	1575	523 (3)	1582	520 (3)
1589	515 (2)	1595	514 (2)	1602	515 (2)
1608	509 (2)	1615	512 (2)	1621	507 (2)
1627	513 (2)	1633	505 (2)	1639	500 (2)

RELATIVE INTENSITIES - CORRECTED FOR ABSORPTION AND POLARISATION

VPO_5 GLASS

Table 6.5

S x 100	I(S)	S x 100	I(S)	S x 100	I(S)
261	3428 (28)	268	3343 (28)	276	3359 (28)
284	3466 (29)	291	3506 (29)	299	3835 (30)
307	4062 (31)	314	4300 (32)	322	4570 (33)
329	4779 (34)	337	4888 (34)	344	4940 (35)
352	5102 (35)	359	5165 (35)	367	5174 (36)
375	5299 (36)	382	5503 (36)	390	5410 (36)
397	5527 (37)	405	5784 (38)	412	5603 (37)
420	5040 (37)	427	5028 (37)	435	5478 (37)
442	5302 (36)	450	5107 (36)	457	4926 (35)
465	4269 (35)	472	4513 (34)	479	4407 (34)
487	4310 (33)	494	4151 (32)	502	3694 (32)
509	3930 (32)	516	3710 (31)	524	3543 (30)
531	3469 (30)	539	3355 (30)	546	3204 (29)
553	3209 (29)	561	3142 (15)	575	3050 (14)
598	2992 (14)	614	2914 (14)	631	2943 (14)
653	2082 (14)	668	2082 (14)	682	2070 (14)
676	2538 (14)	698	2417 (13)	705	2310 (13)
719	2233 (13)	733	2200 (13)	747	2197 (13)
761	2281 (13)	779	2221 (13)	786	2242 (13)
802	2198 (13)	810	2102 (13)	838	2150 (13)
843	2835 (13)	857	1903 (13)	878	1924 (13)
884	1806 (13)	897	1823 (13)	918	1797 (13)
923	1722 (12)	937	1694 (12)	958	1721 (12)
963	1607 (12)	975	1671 (12)	988	1638 (12)
1001	1567 (12)	1016	1569 (12)	1026	1572 (12)
1039	1517 (12)	1051	1527 (12)	1064	1487 (12)
1070	1479 (12)	1080	1499 (12)	1100	1428 (12)
1112	1365 (12)	1124	1362 (12)	1136	1320 (12)
1140	1299 (11)	1162	1322 (12)	1171	1279 (11)
1183	1268 (11)	1194	1259 (11)	1205	1247 (11)
1217	1227 (11)	1228	1214 (11)	1239	1237 (11)
1250	1193 (11)	1261	1171 (11)	1271	1170 (11)
1282	1160 (11)	1293	1139 (11)	1303	1129 (11)
1314	1112 (11)	1324	1091 (11)	1334	1060 (10)
1344	1078 (10)	1354	1078 (10)	1364	1026 (10)
1374	1047 (10)	1383	1025 (10)	1393	1024 (10)
1402	1013 (10)	1412	1007 (10)	1421	980 (10)
1430	974 (10)	1439	967 (10)	1448	963 (9)
1457	950 (9)	1465	942 (9)	1474	933 (9)
1482	920 (9)	1491	913 (9)	1499	879 (9)
1507	880 (9)	1515	839 (9)	1523	880 (9)
1531	895 (9)	1538	804 (8)	1546	856 (8)
1553	872 (8)	1561	801 (8)	1568	862 (8)
1575	805 (8)	1582	840 (8)	1589	847 (8)
1595	849 (8)	1602	851 (8)	1608	862 (8)
1615	826 (8)	1621	827 (8)	1627	823 (8)
1633	832 (8)	1639	824 (7)	1645	828 (7)
1650	814 (7)	1656	826 (7)		

RELATIVE INTENSITIES - SCALED AND CORRECTED FOR ABSORPTION AND POLARISATION

$V_{.8}P_{1.2}O_5$ GLASS

Table 6.6

Figure 6.5

Functions for $V_1P_1O_5$ glass

(a) The measured intensity I(s) in electronic units (Intensity Scale divided by 100).

(b) The radial distribution function $r\,(D(r) + D_o(r))$ and $r\,D(r)$, before back transform of $r < 1\ \mathring{A}$ region.

(c) The same as (b) but after the ripples in the $r < 1\ \mathring{A}$ region have been filtered by back transform. Graph (b) is only included with this composition to illustrate the degree of ripple which was removed.

(d) The correlation function $g(r) = (D(r) + D_o(r))/D_o(r)$.

(e) The calculated and experimental W(r) which is $\frac{\pi}{2}\,(D(r) + D_o(r))$ in electronic units.

(f) The calculated and experimental si(s) and si(s) M(s) where:

$$M(s) = \langle f(o)\rangle^2 / \langle f(s)\rangle^2 .$$

The dotted function is the unperturbed model function (no adjustment for V^{4+}).

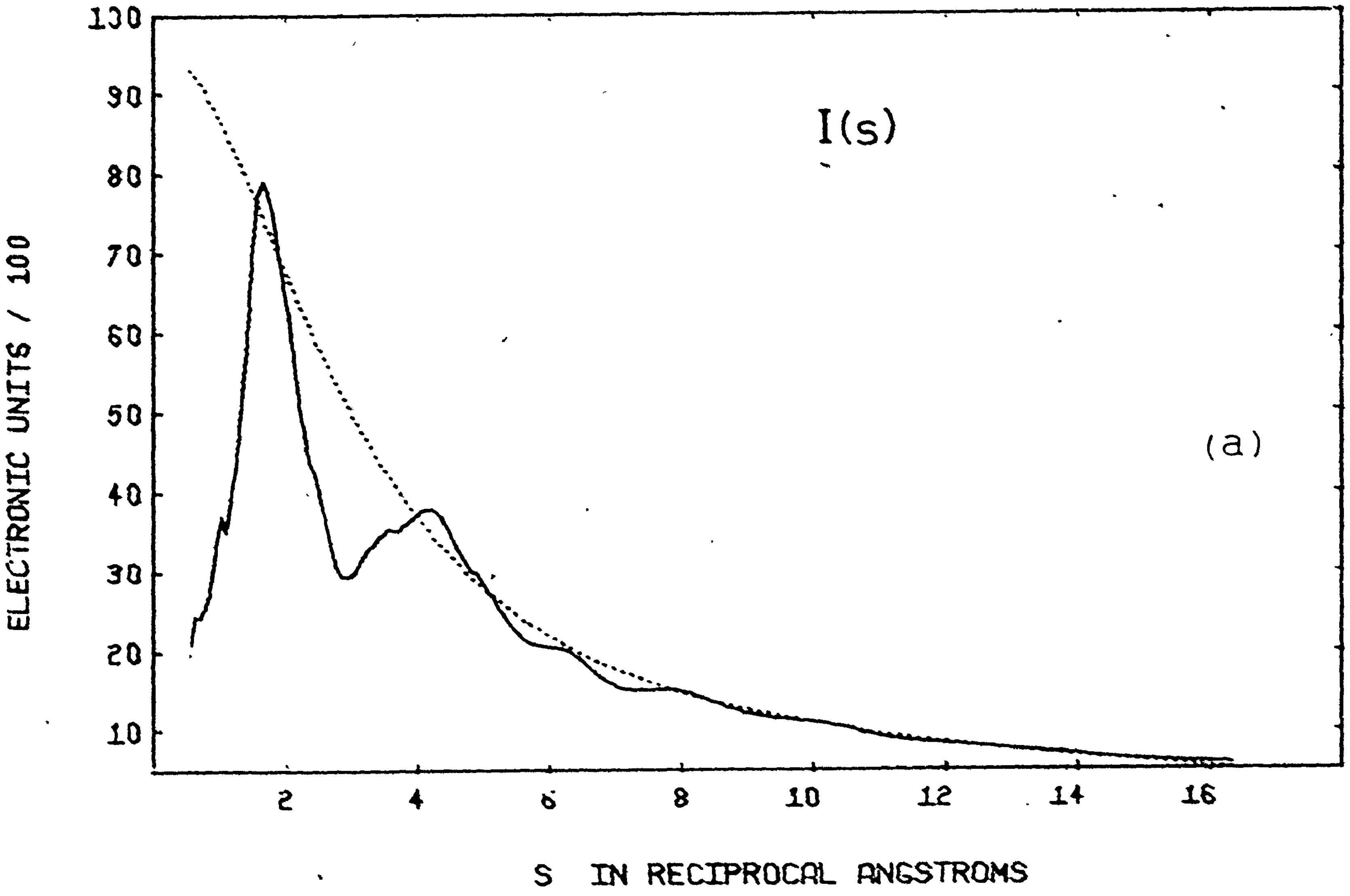
I(s)
(a)
ELECTRONIC UNITS / 100
130
90
80
70
60
50
40
30
20
10
2
4
6
8
10
12
14
16
S IN RECIPROCAL ANGSTROMS

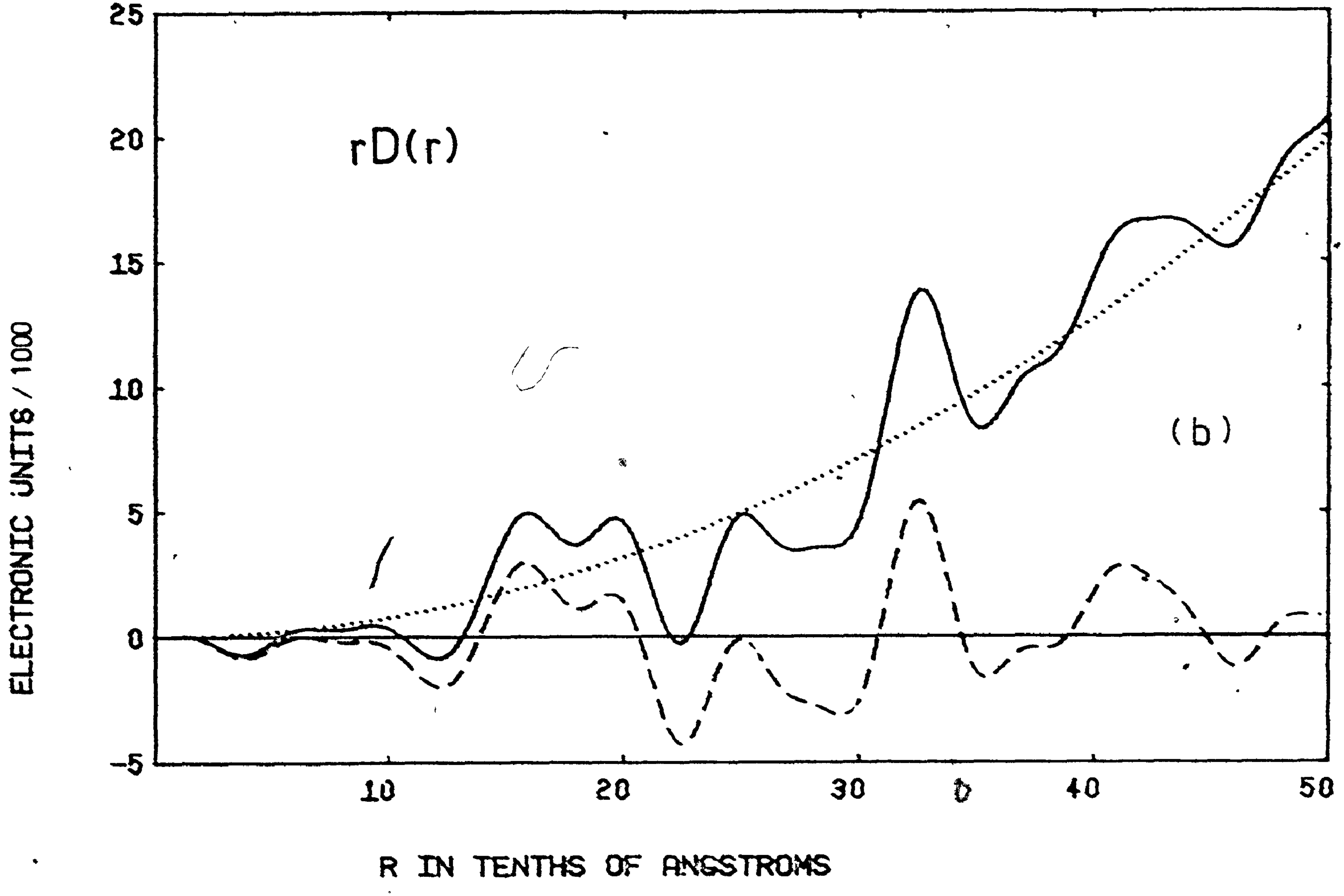
rD(r)
(b)
ELECTRONIC UNITS / 1000
25
20
15
10
5
0
-5
10
20
30
40
50
R IN TENTHS OF ANGSTROMS

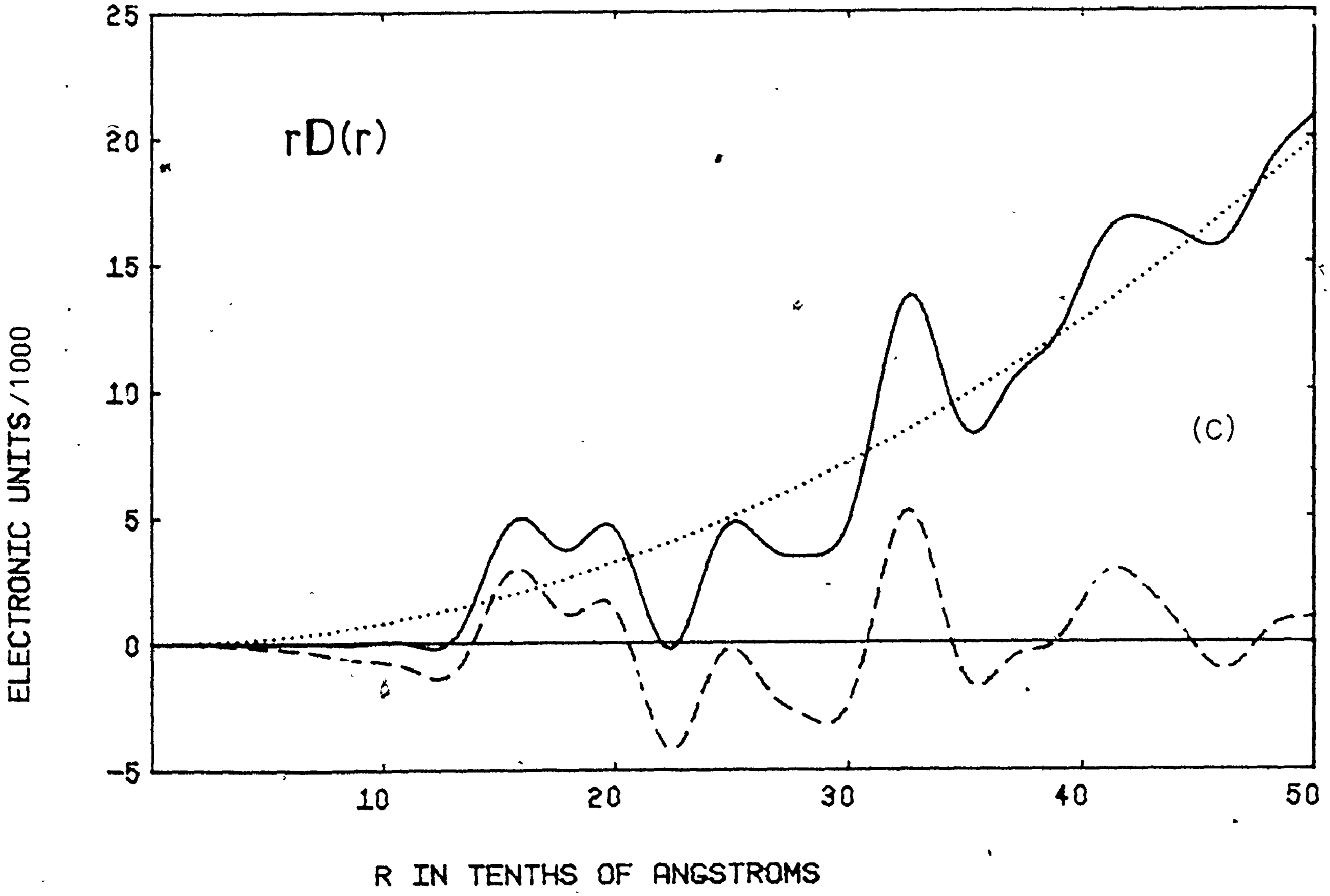
rD(r)
(C)
ELECTRONIC UNITS/1000
25
20
15
10
5
0
−5
10
20
30
40
50
R IN TENTHS OF ANGSTROMS

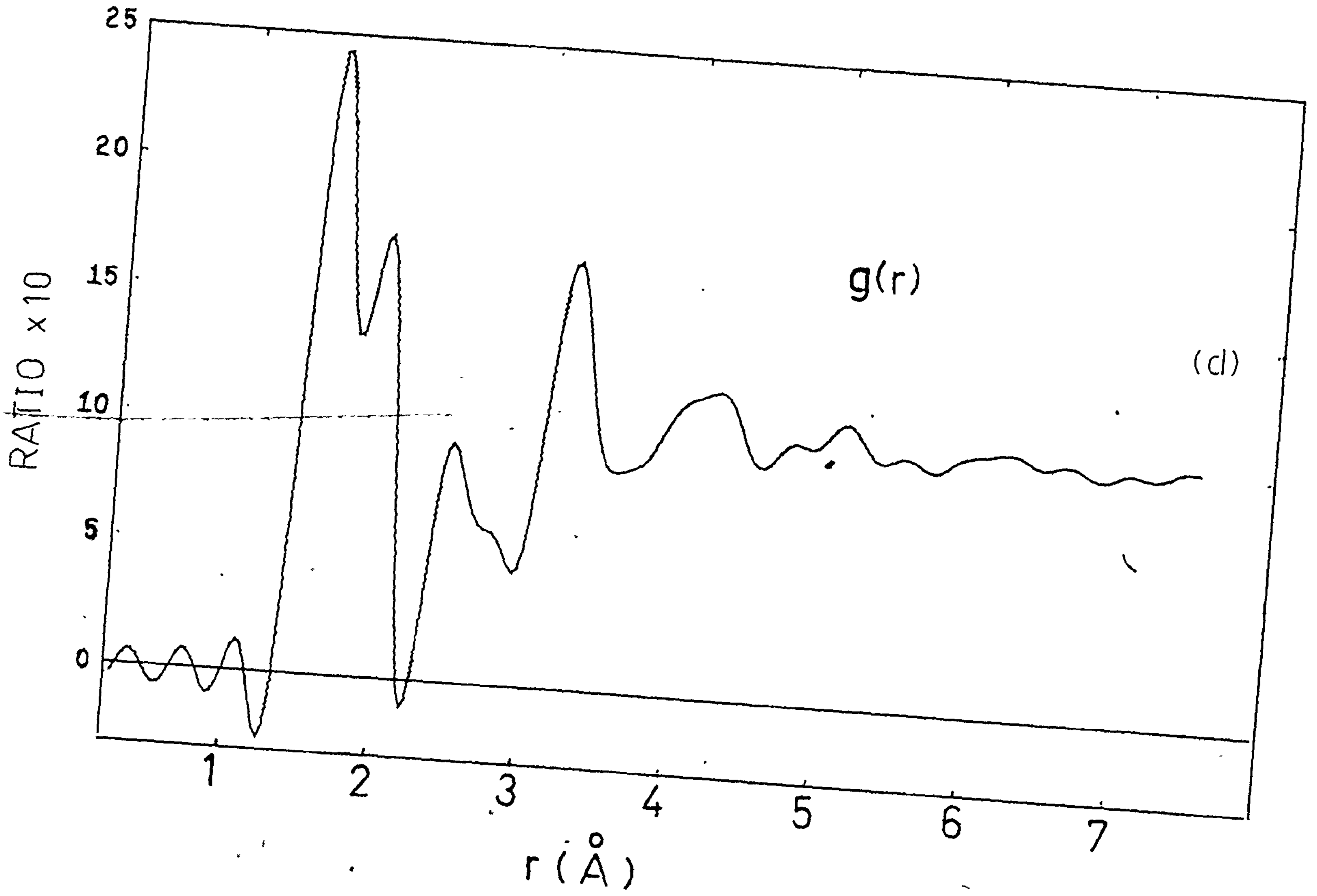
25
20
15
10
5
0
RATIO ×10
g(r)
(d)
1
2
3
4
5
6
7
r (Å)

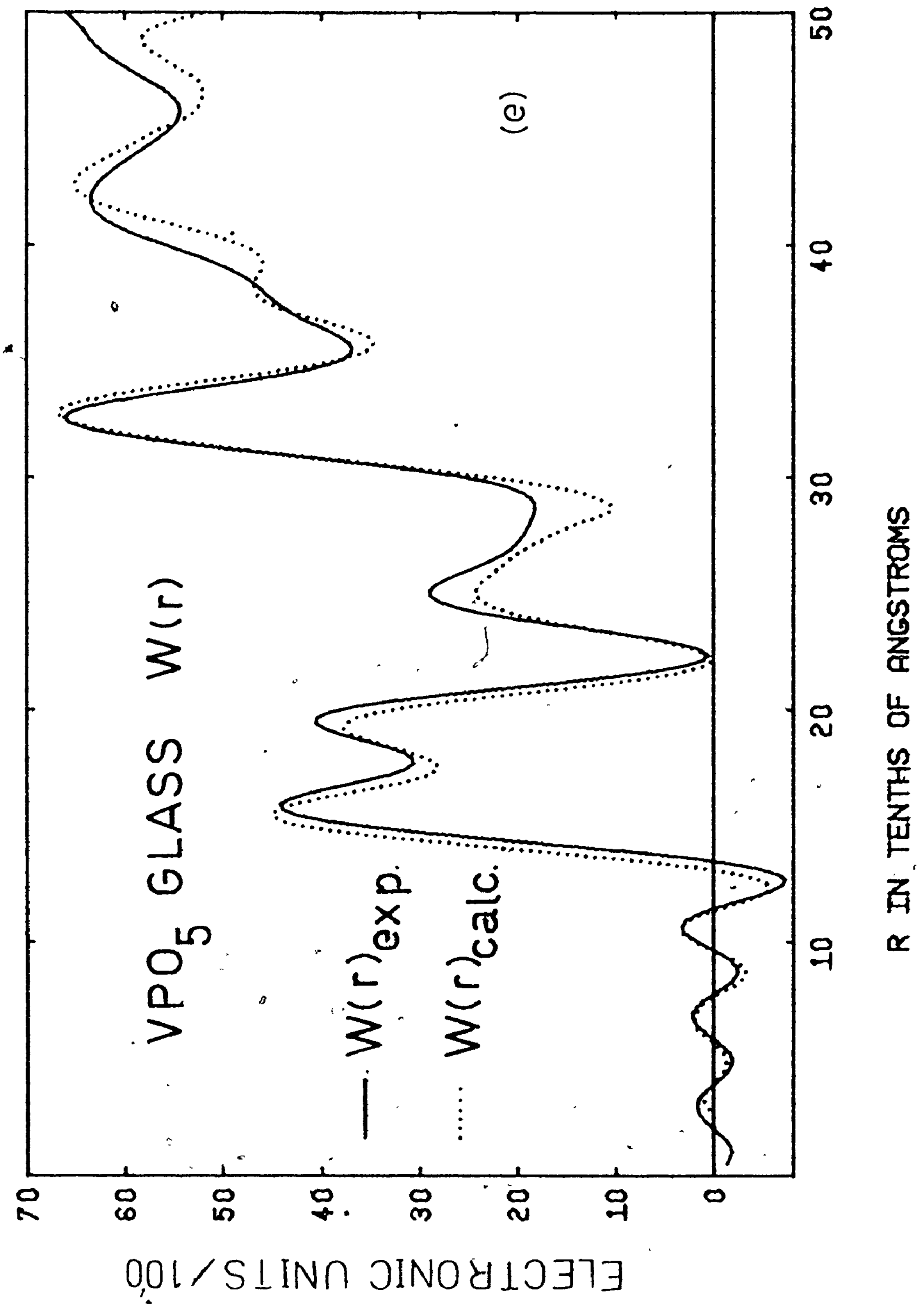
VPO5 GLASS W(r)
— W(r)exp.
····· W(r)calc.
(e)
ELECTRONIC UNITS/100
0
10
20
30
40
50
60
70
R IN TENTHS OF ANGSTROMS
10
20
30
40
50

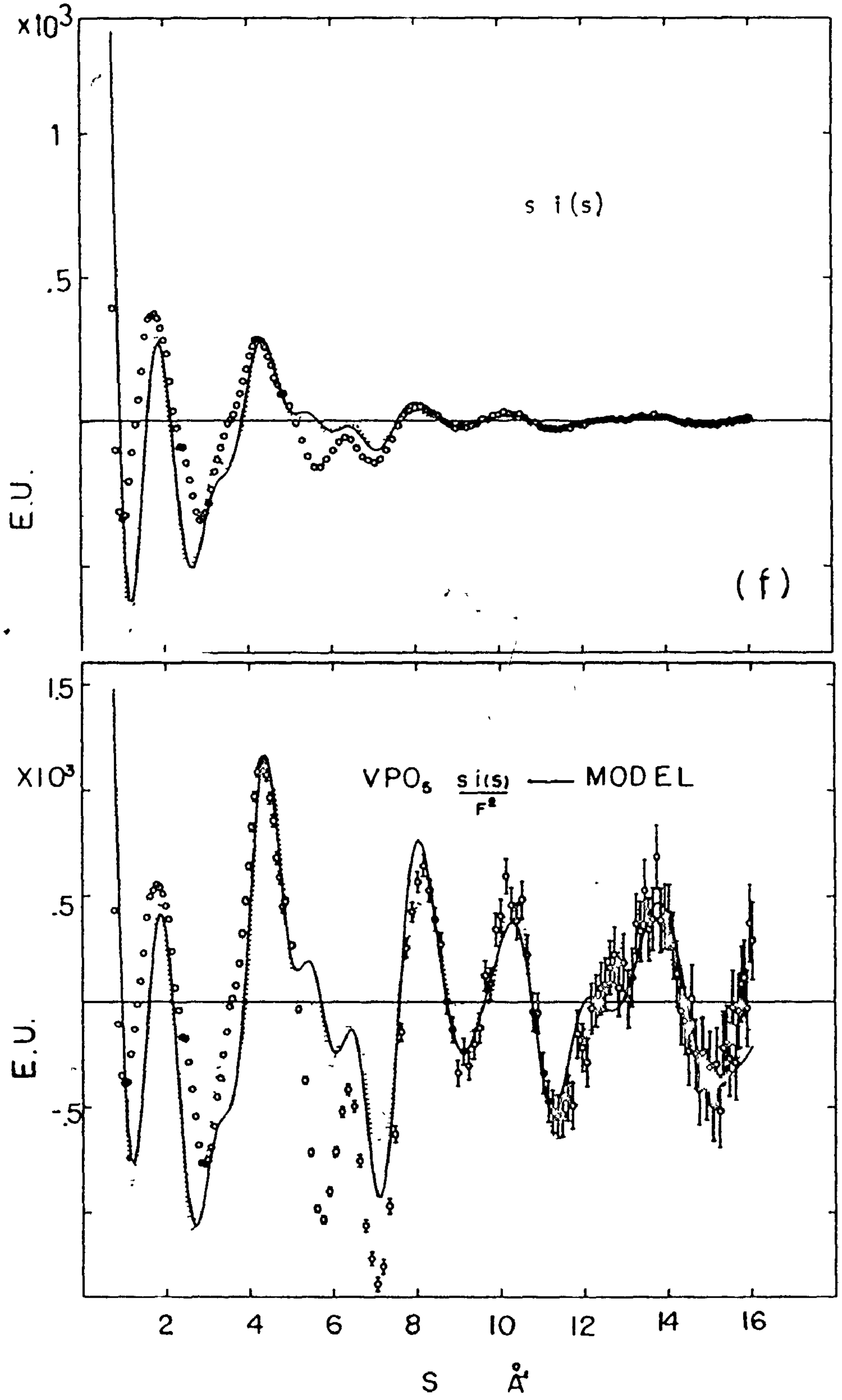
x10^3
1
.5
s i(s)
E.U.
(f)
1.5
X10^3
VPO5 s i(s)/F² —— MODEL
.5
E.U.
-.5
2
4
6
8
10
12
14
16
S Å⁻¹

Figure 6.6

Functions for $V_{1.2}P_{.8}O_5$ Glass

(a) The measured intensity I(s) in electronic units.

(b) The radial distribution function $r(D(r) + D_o(r))$ and $r\ D(r)$.

(c) The correlation function $g(r) = (D(R) + D_o(r))/D_o(r)$.

(d) The calculated and experimental W(r) which is $\frac{\pi}{2}(D(r) + D_o(r))$ in electronic units.

(e) The calculated and experimental s i(s) curves and s i(s) M(s) where $M(s) = \langle f(o)\rangle^2/\langle f(s)\rangle^2$, The dotted function is the unperturbed model function with average (V,P) scattering factors.

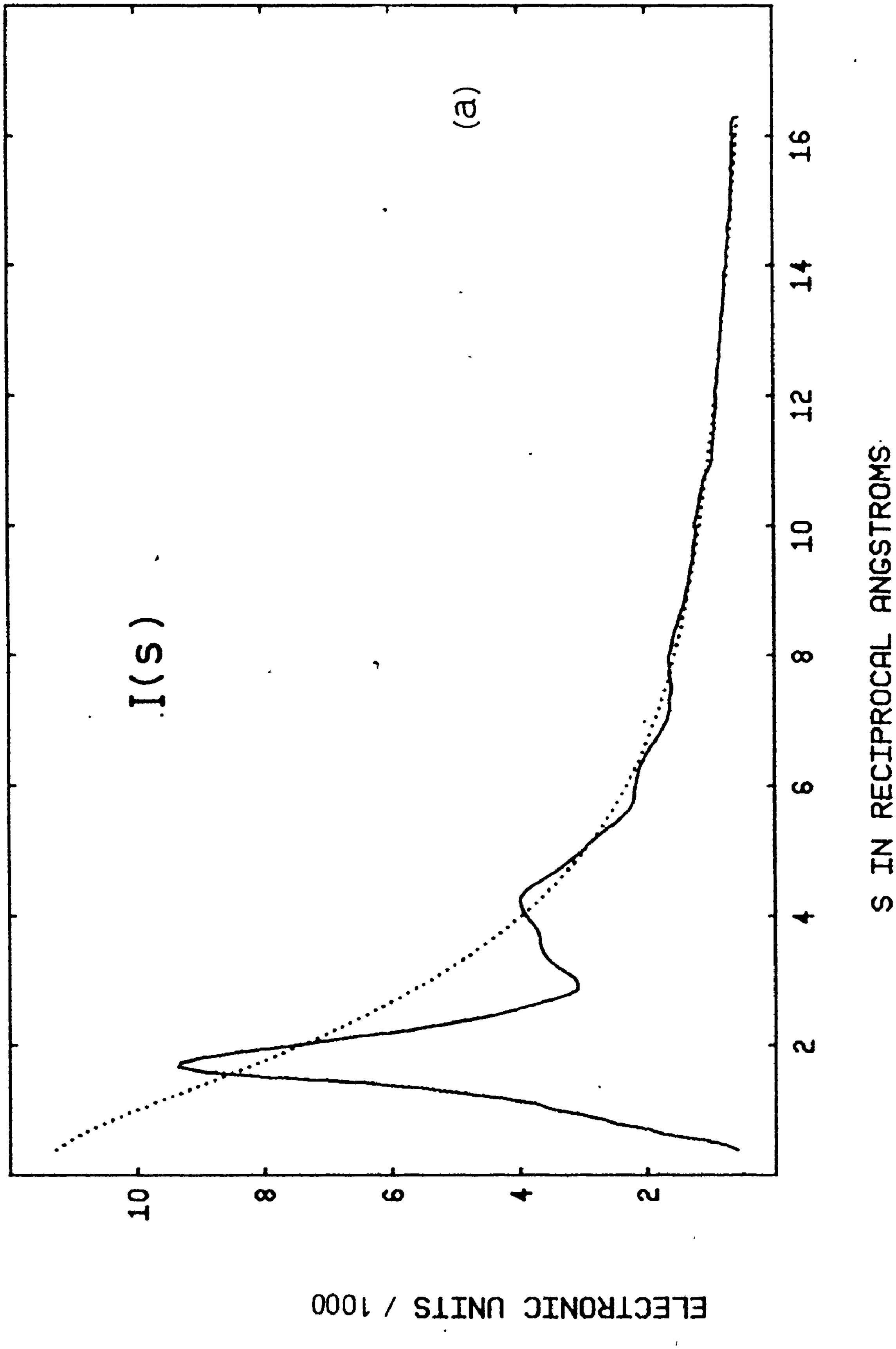
(a)
I(S)
ELECTRONIC UNITS / 1000
2
4
6
8
10
S IN RECIPROCAL ANGSTROMS
2
4
6
8
10
12
14
16

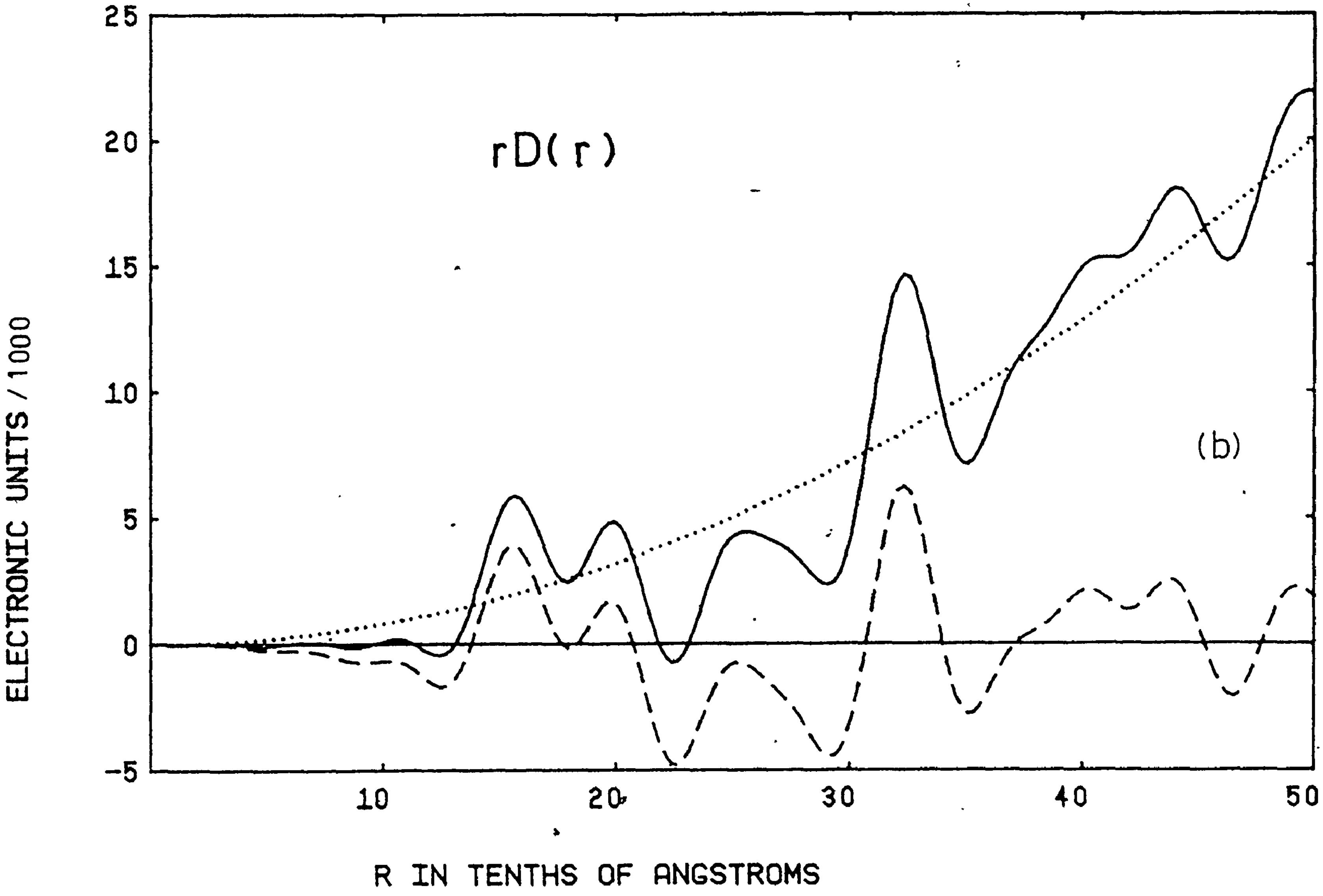
rD(r)
(b)
ELECTRONIC UNITS / 1000
R IN TENTHS OF ANGSTROMS
25
20
15
10
5
0
−5
10
20
30
40
50

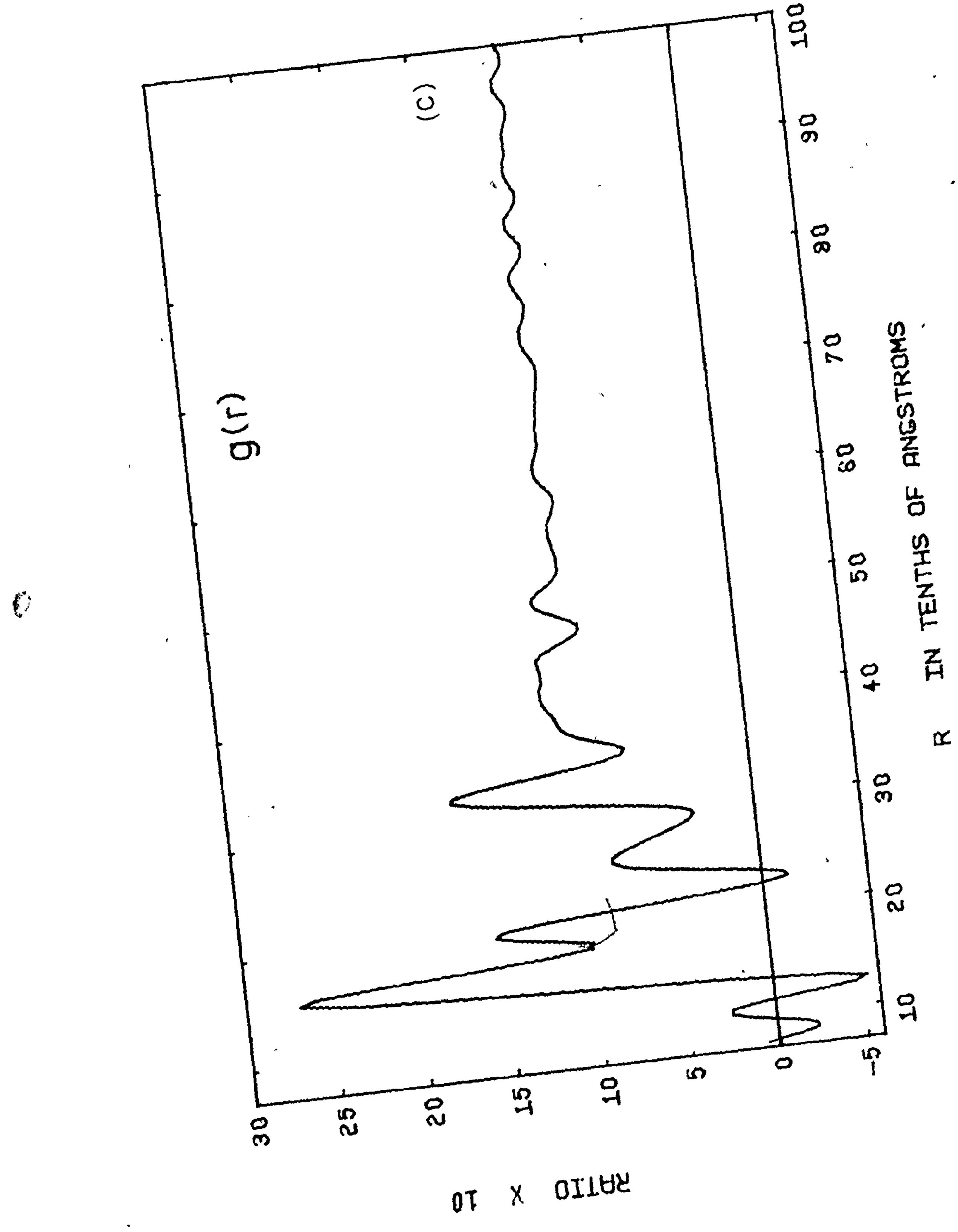
g(r)
(C)
RATIO X 10
30
25
20
15
10
5
0
-5
R IN TENTHS OF ANGSTROMS
10
20
30
40
50
60
70
80
90
100

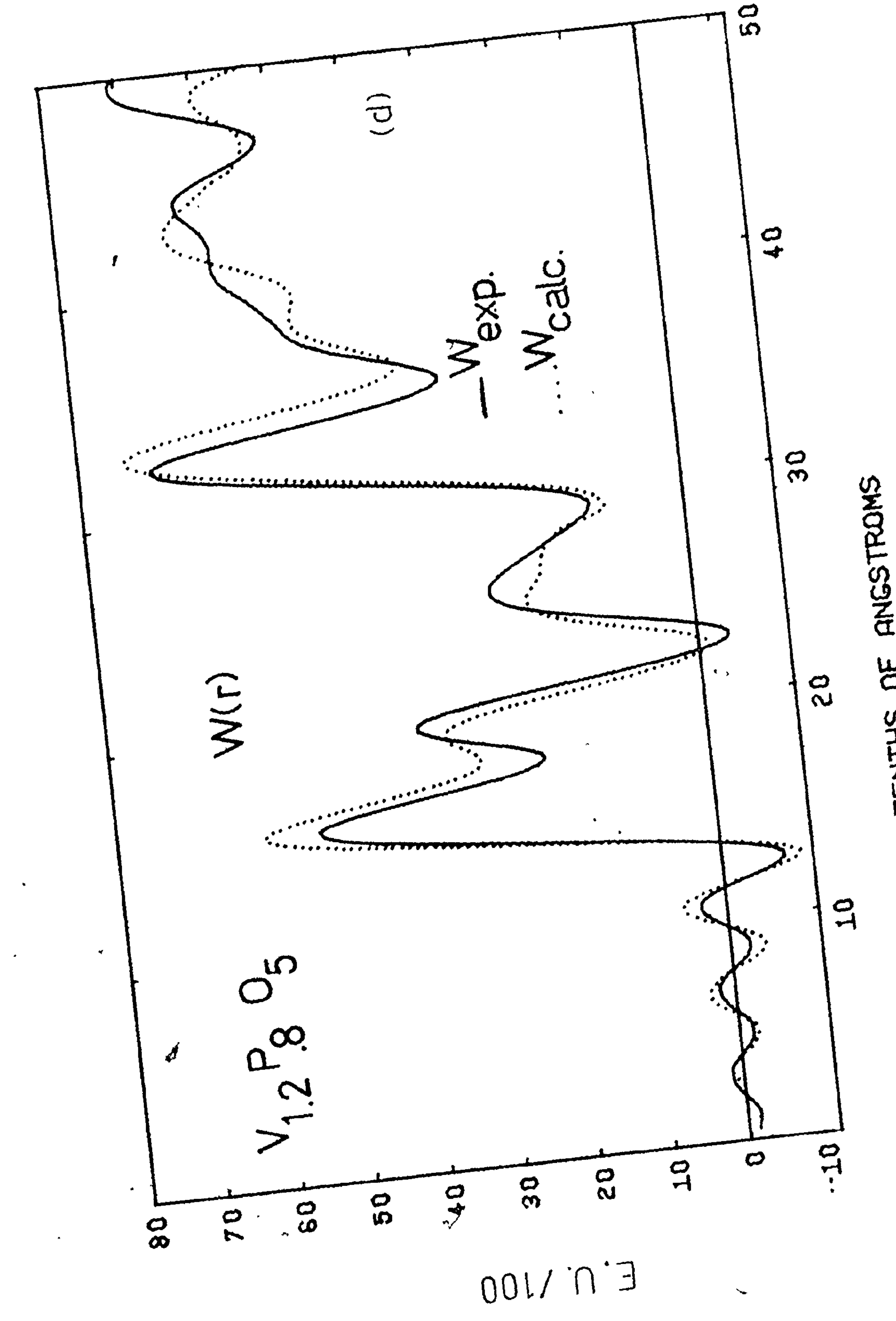

$V_{1.2}P_{.8}O_5$
W(r)
(d)
— $W_{exp.}$
····· $W_{calc.}$
80
70
60
50
40
30
20
10
0
-10
E.U./100
10
20
30
40
50
R IN TENTHS OF ANGSTROMS

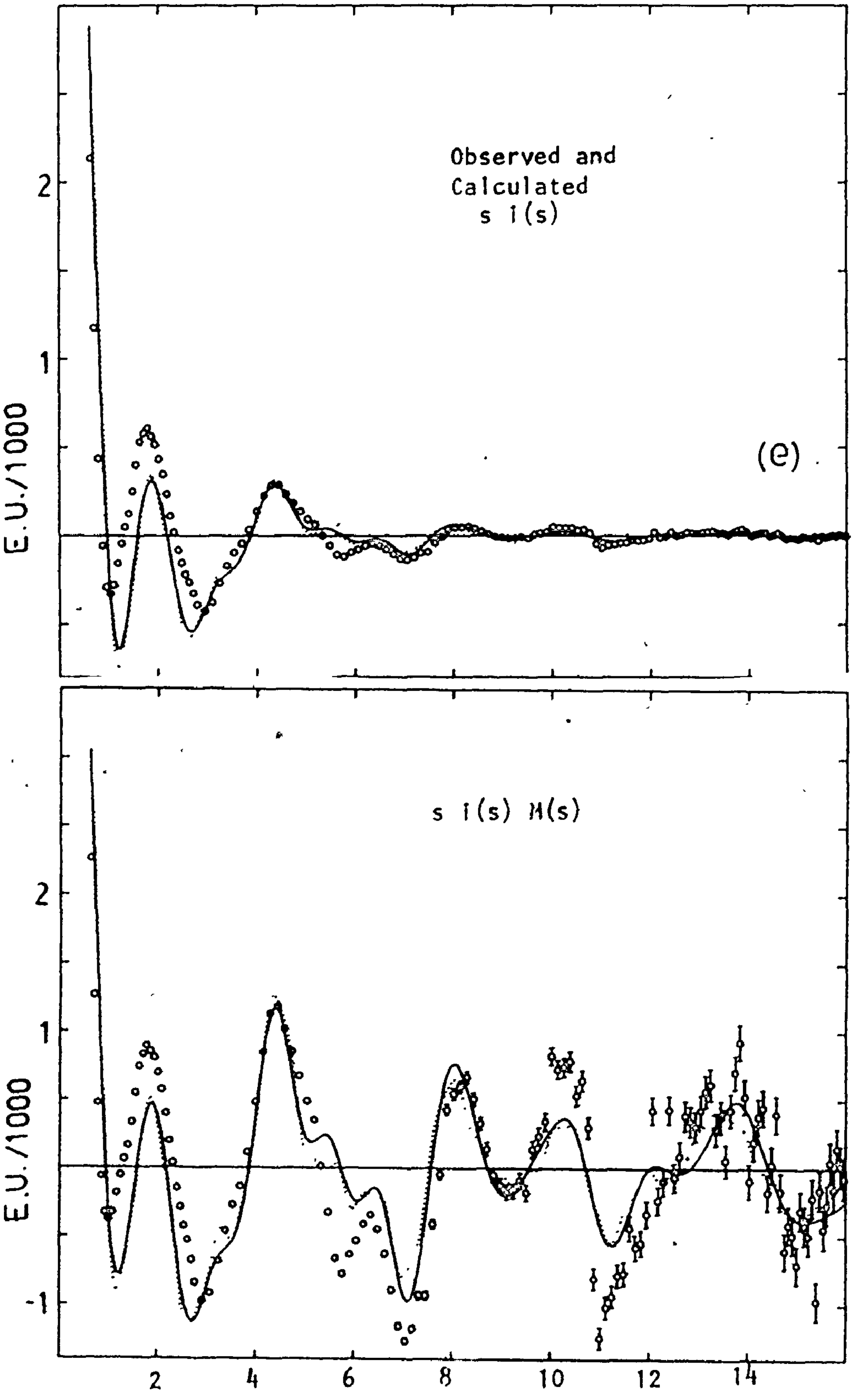
Observed and
Calculated
s I(s)
(e)
E.U./1000
2
1
s I(s) M(s)
E.U./1000
2
1
-1
2
4
6
8
10
12
14

Figure 6.7

Functions for $V_{1.33}P_{.67}O_5$ glass

(a) Measured intensity $I(s)$ in electronic units.

(b) The radial distribution function $r \cdot (D(r) + D_o(r))$ and $r\,D(r)$.

(c) The correlation function $g(r) = (D(r) + D_o(r))/D_o(r)$.

(d) The calculated and experimental $W(r)$ which is $\frac{\Pi}{2}\,(D(r) + D_o(r))$ in electronic units.

(e) The calculated and experimental $s\,i(s)$ curves and $s\,i(s)\,M(s)$ where $M(s) = \langle f(o)\rangle^2/\langle f(s)\rangle^2$, The dotted function is the unperturbed model function with average (V,P) scattering factors.

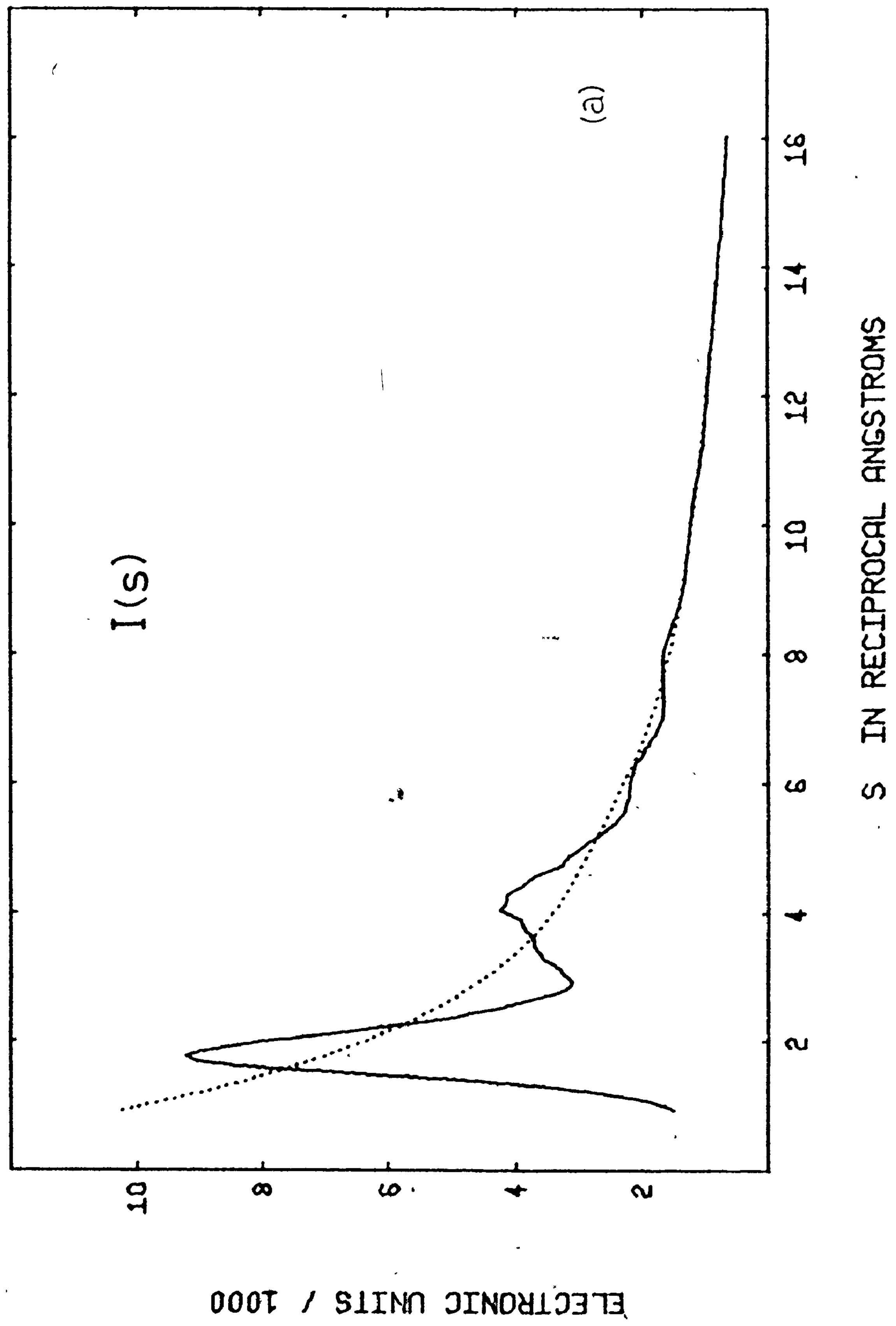
I(s)
(a)
S IN RECIPROCAL ANGSTROMS
2
4
6
8
10
12
14
16
ELECTRONIC UNITS / 1000
2
4
6
8
10

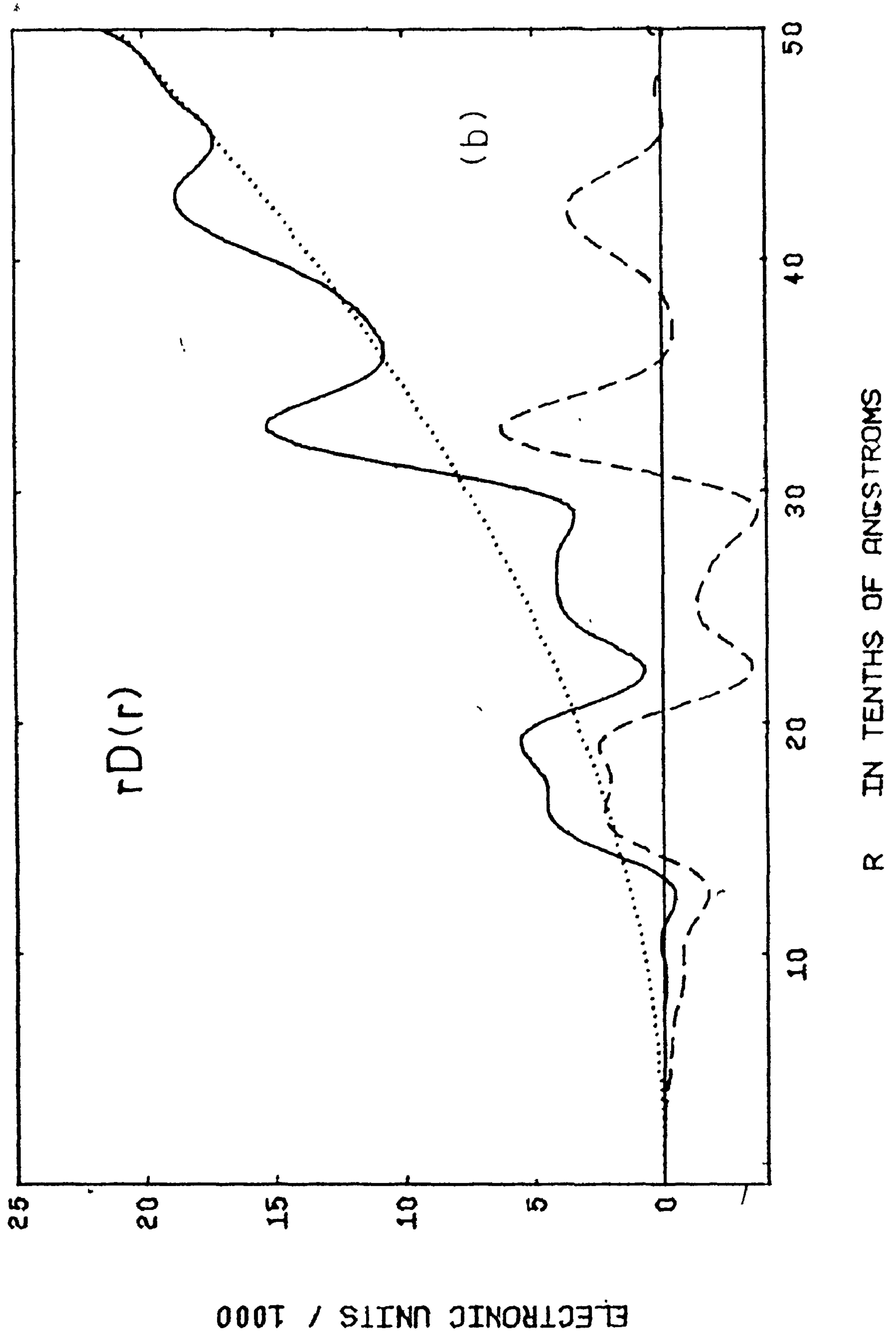
rD(r)
(b)
25
20
15
10
5
0
ELECTRONIC UNITS / 1000
10
20
30
40
50
R IN TENTHS OF ANGSTROMS

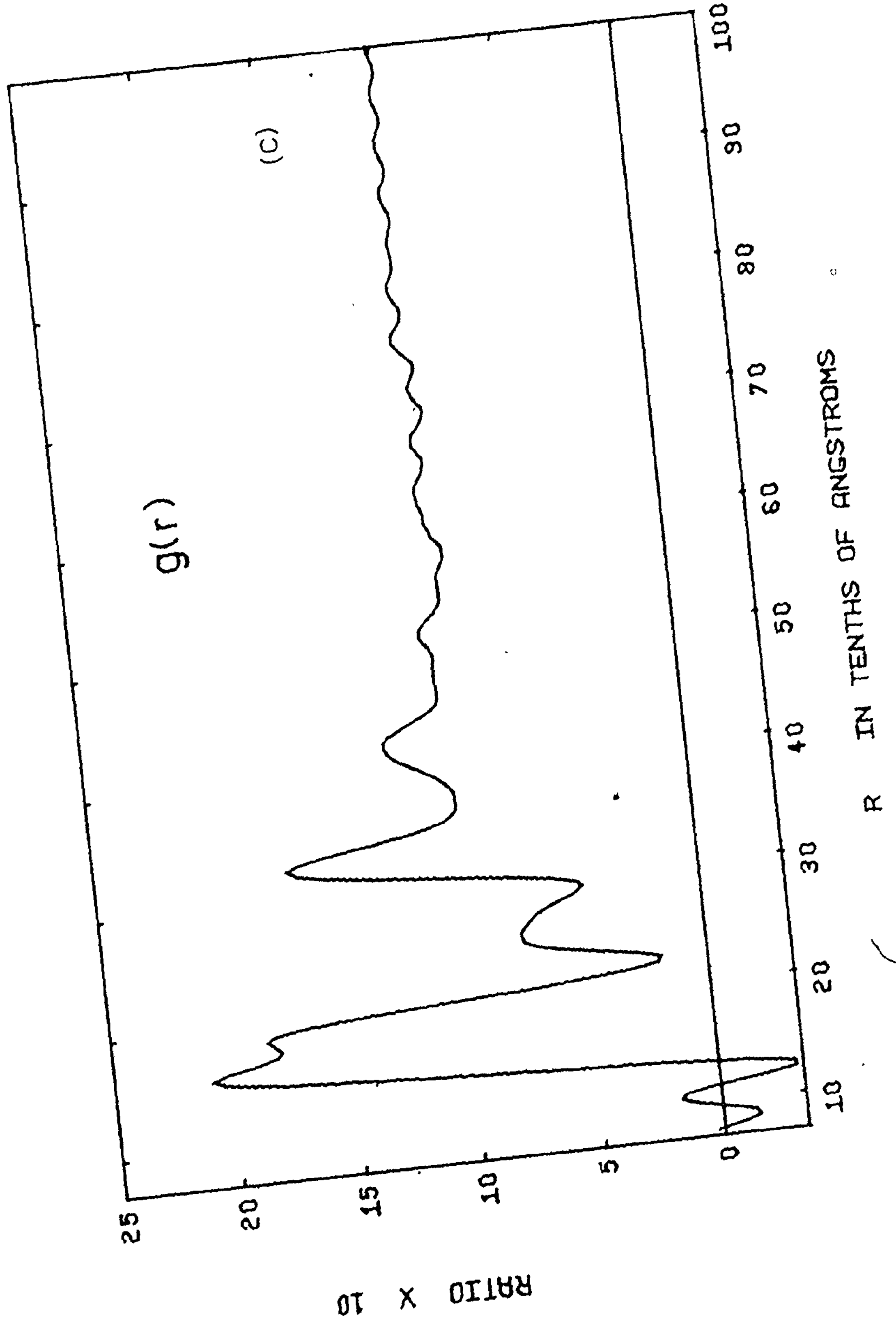
g(r)
(C)
RATIO X 10
0
5
10
15
20
25
R IN TENTHS OF ANGSTROMS
10
20
30
40
50
60
70
80
90
100

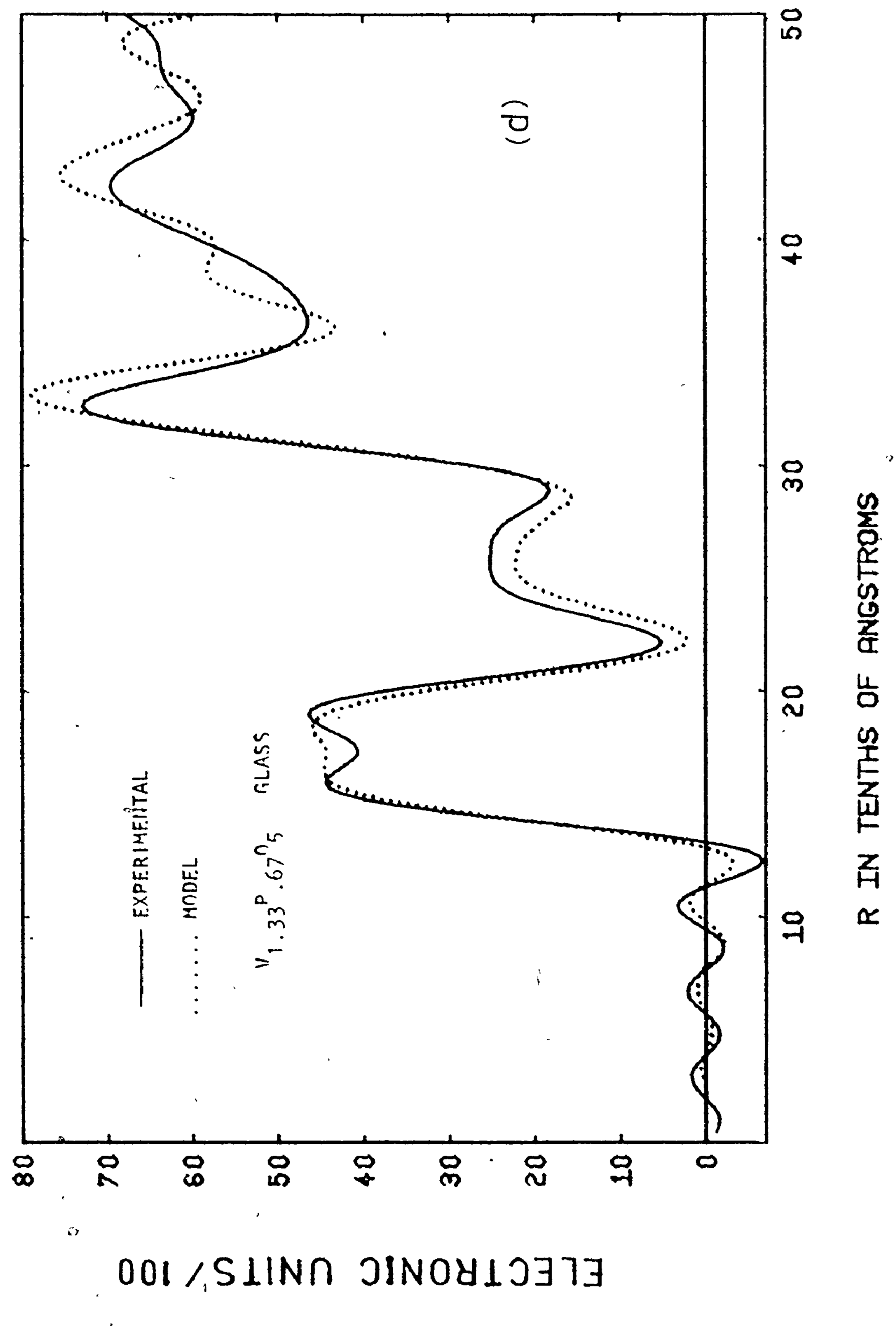
(d)
EXPERIMENTAL
MODEL
V1.33P.67O5 GLASS
R IN TENTHS OF ANGSTROMS
ELECTRONIC UNITS/100
0
10
20
30
40
50
60
70
80
10
20
30
40
50

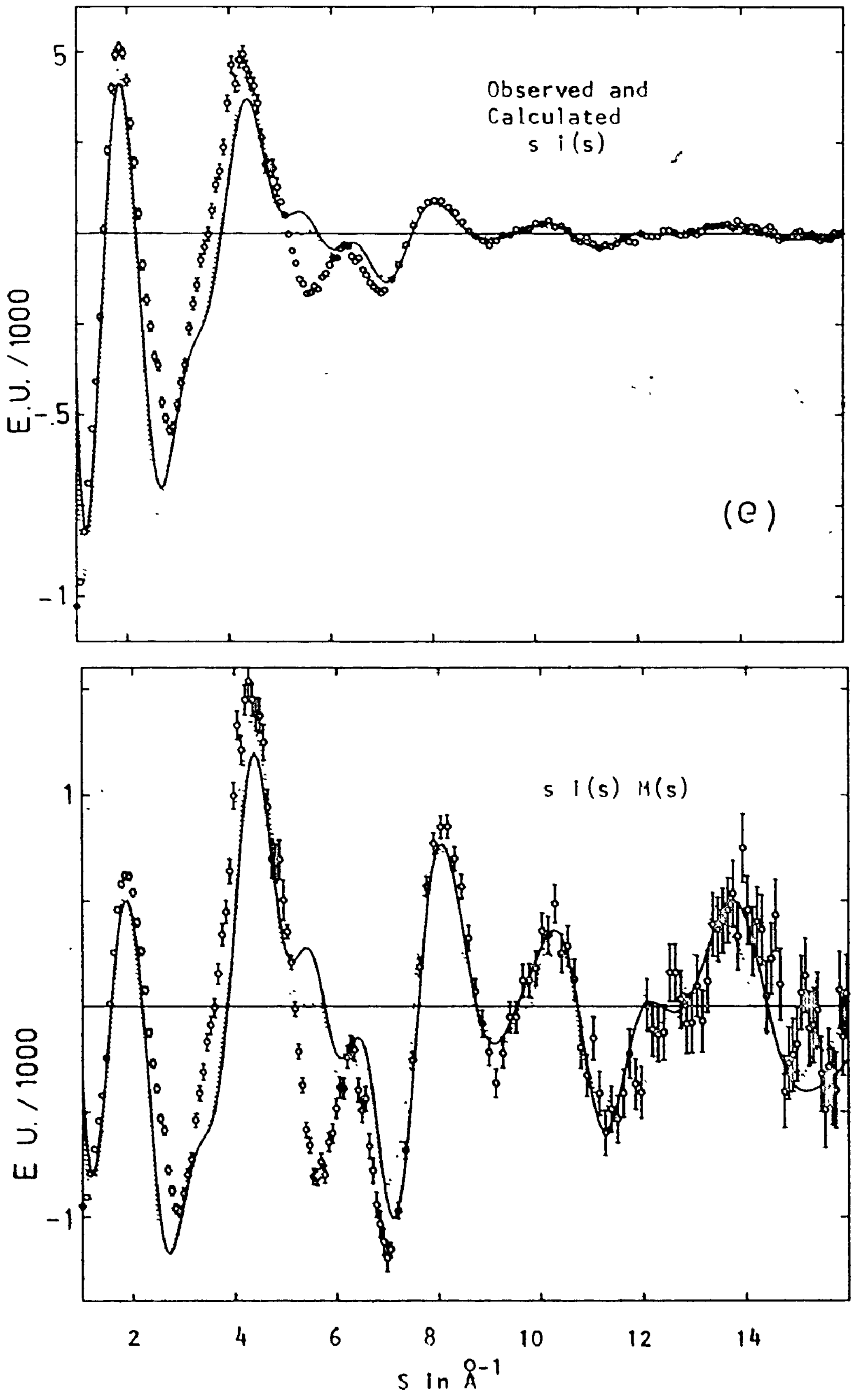
5
-.5
-1
E.U./1000
Observed and
Calculated
s i(s)
(e)
1
-1
E.U./1000
s I(s) M(s)
2
4
6
8
10
12
14
s in Å^{-1}

Figure 6.8

Functions for $V_{1.6}P_{.4}O_5$ Glass.

(a) The measured intensities $I(s)$ in electronic units.

(b) The radial distribution function $r\ (D(r) + D_o(r))$ and $r\ D(r)$.

(c) The correlation function $g(r) = (D(r) + D_o(r))/D_o(r)$.

(d) The calculated and experimental $W(r)$ which is $\frac{\Pi}{2}\ (D(r) + D_o(r))$.

(e) The calculated and experimental $si(s)$ and $s(i)\ M(s)$ curves. The dotted curve is the bare model function calculated with average (V,P) scattering factors. The function $M(s) =$ $M(s) = \langle f(o)\rangle^2/\langle f(s)\rangle^2$.

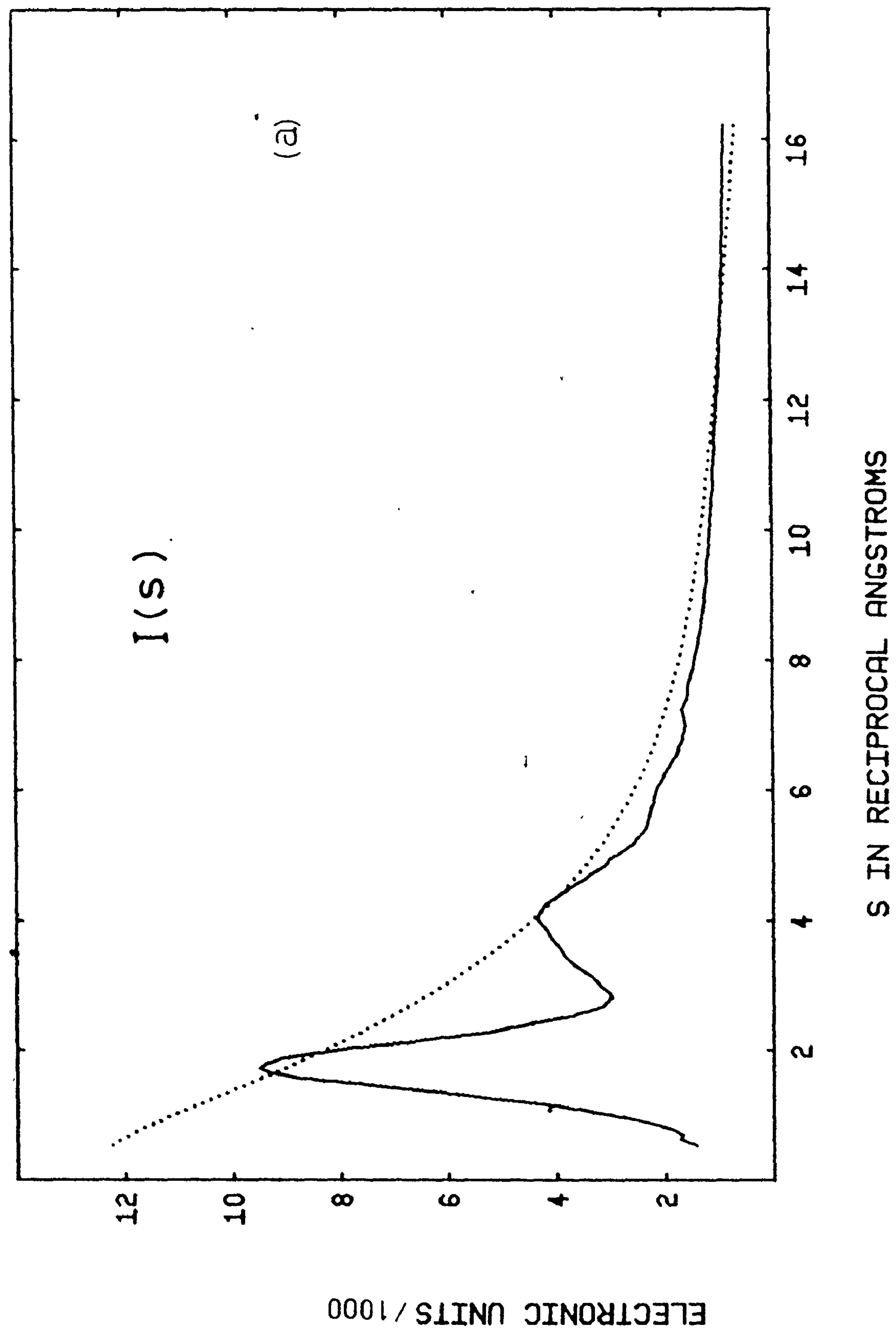

I(S)
(a)
2
4
6
8
10
12
14
16
S IN RECIPROCAL ANGSTROMS
2
4
6
8
10
12
ELECTRONIC UNITS/1000

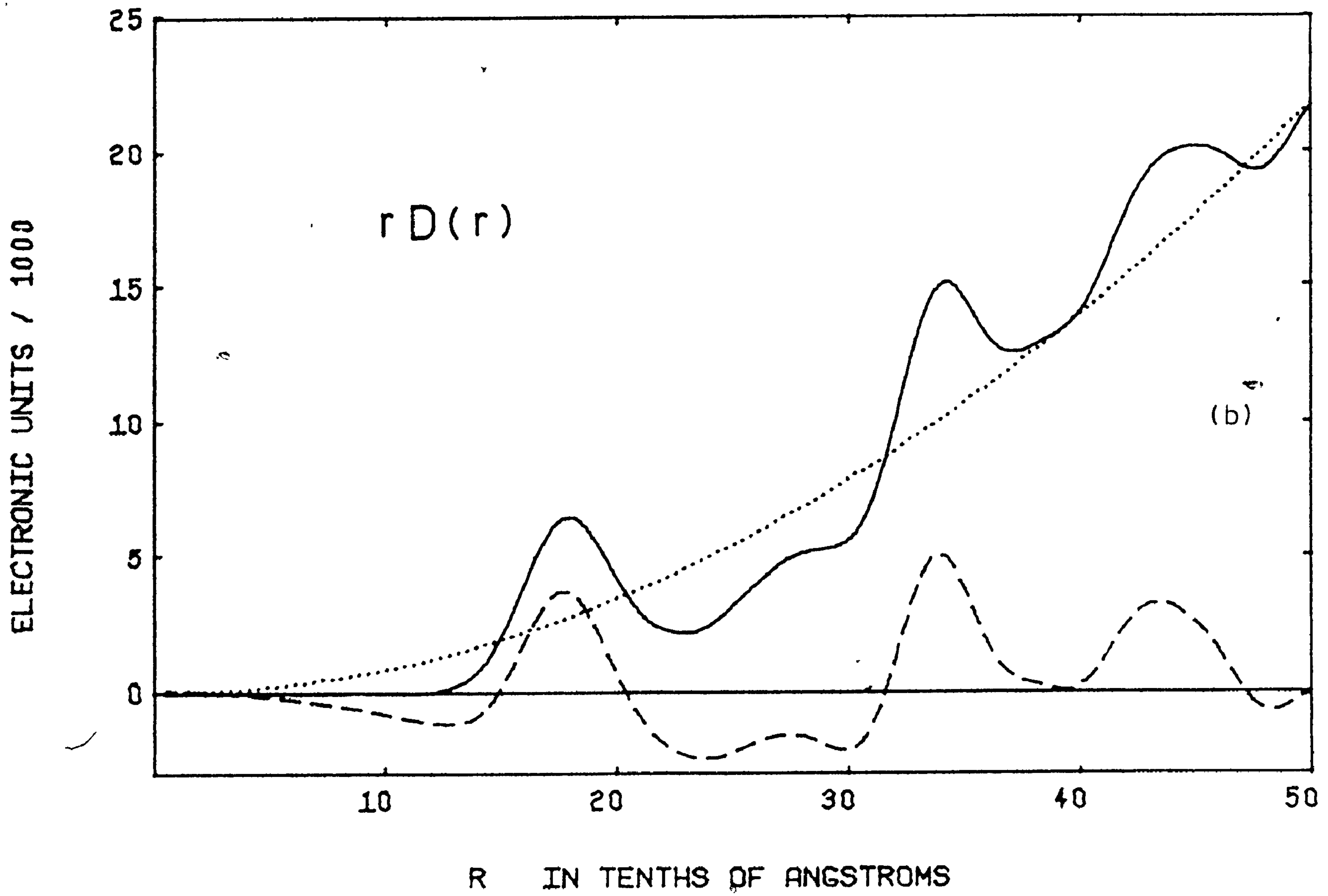
rD(r)
(b)
ELECTRONIC UNITS / 1000
0
5
10
15
20
25
10
20
30
40
50
R IN TENTHS OF ANGSTROMS

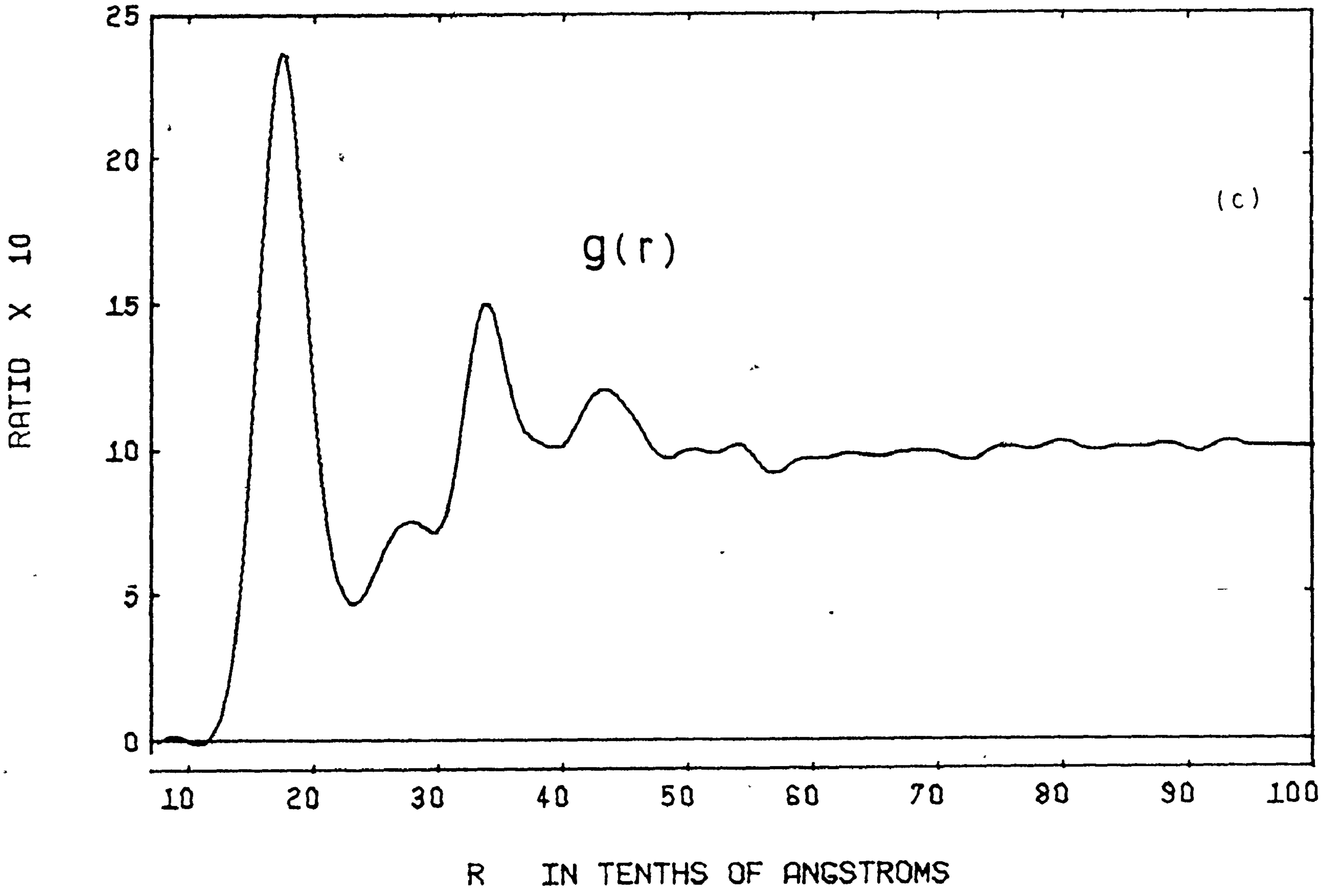
25
20
15
10
5
0
RATIO X 10
g(r)
(c)
10
20
30
40
50
60
70
80
90
100
R IN TENTHS OF ANGSTROMS

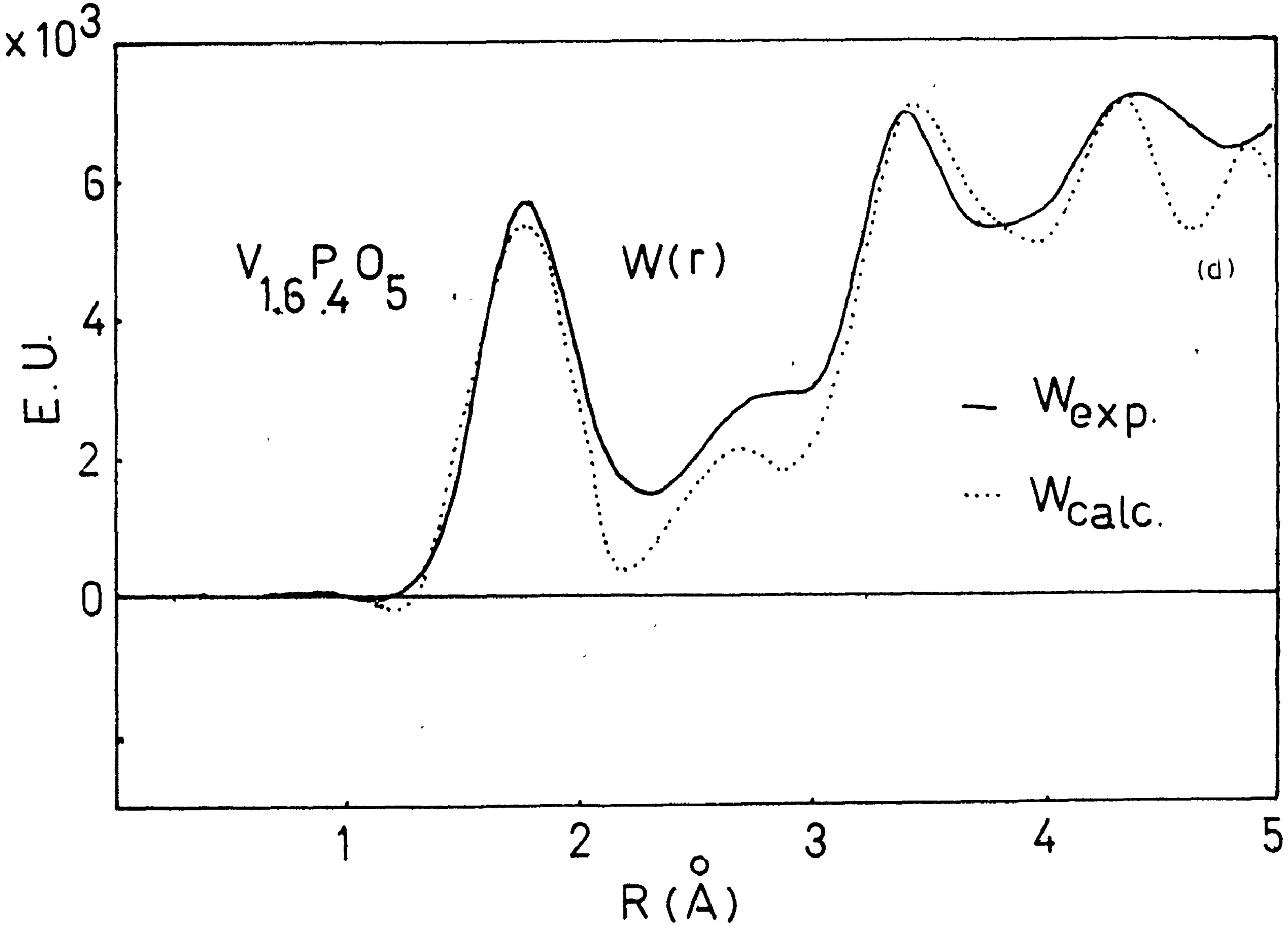
x 10^3
E.U.
6
4
2
0
1
2
3
4
5
R (Å)
V1.6 P.4 O5
W(r)
(d)
— Wexp.
··· Wcalc.

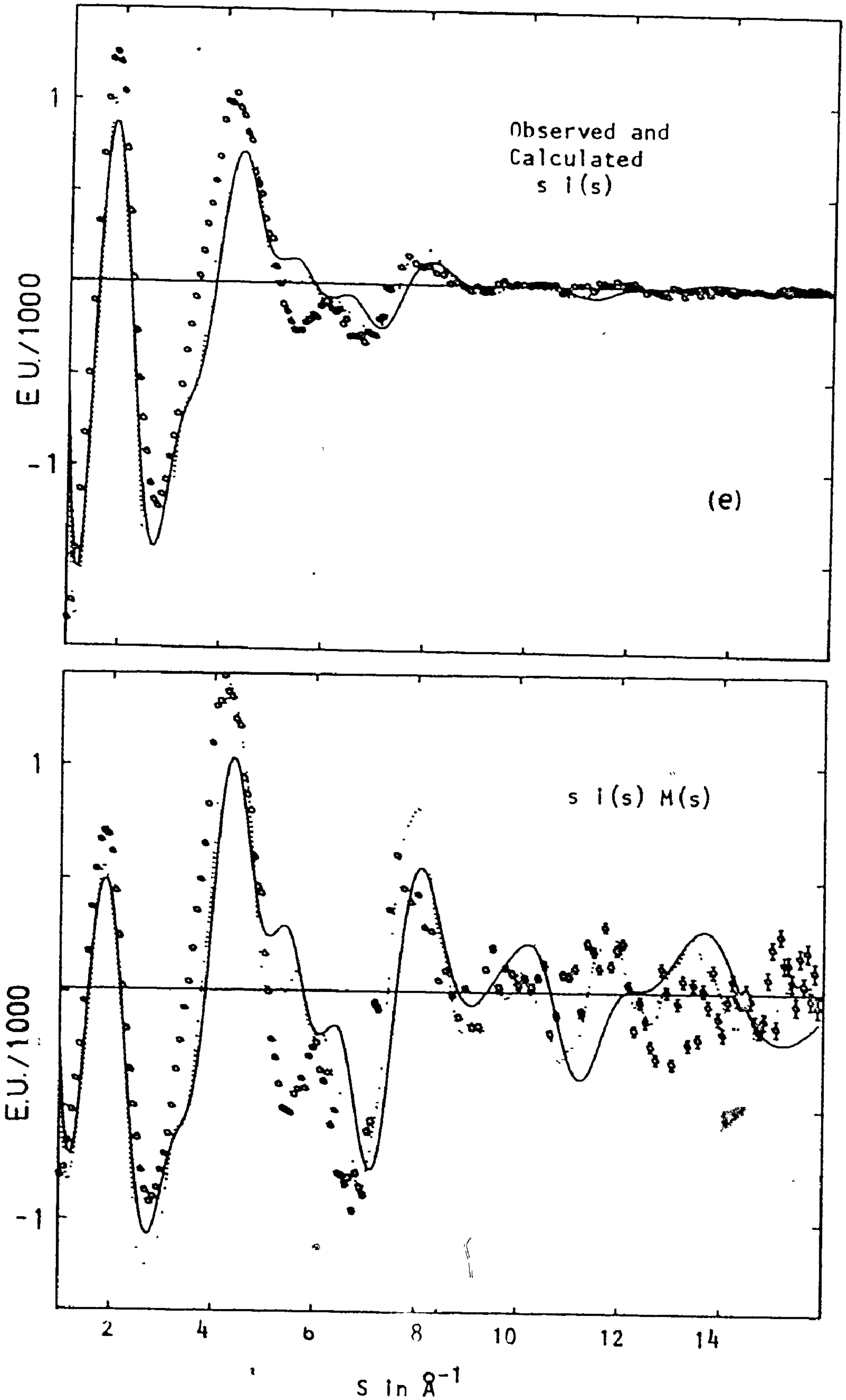
Observed and
Calculated
s i(s)
(e)
s i(s) M(s)
E.U./1000
1
-1
2
4
6
8
10
12
14
s in Å^{-1}

Figure 6.9

Functions for $V_{.8}P_{1.2}O_5$ Glass

(a) Observed intensity I(s)

(b) The radial distribution function $r(D(r) + D_o(r))$ and $r\,D(r)$.

(c) The correlation function $g(r) = (D(r) + D_o(r)/D_o(r)$.

(d) The calculated and experimental W(r) which is $\frac{\Pi}{2}(D(r) + D_o(r))$.

(e) The calculated and experimental si(s) and si(s)M(s) curves where $M(s) = \langle f(o)\rangle^2/\langle f(s)\rangle^2$.

This composition is unusual in two ways. The sample was too thin to remove from the mold and the mold lip limited the scattering data to an $S > 3\ \text{Å}^{-1}$. Secondly, the substitution aspect of the model cannot extrapolate to the phosphorous rich side. The model function plotted here is for an x = 0 glass with 95% reduction. This allows those portions which have changed relative to the VPO_5 glass to stand out. Enough of the region $3\text{Å} < r < 5\ \text{Å}$ is the same as the VPO_5 glass (if V-O peaks are weakened) to suggest that the basic structure may be intact except for V vacancies. A PO_4 with one terminal bond along the Z direction could satisfy three of the formerly V-O bridging oxygens. The resulting P-P peak would strengthen the pair function immediately below 3 Å.

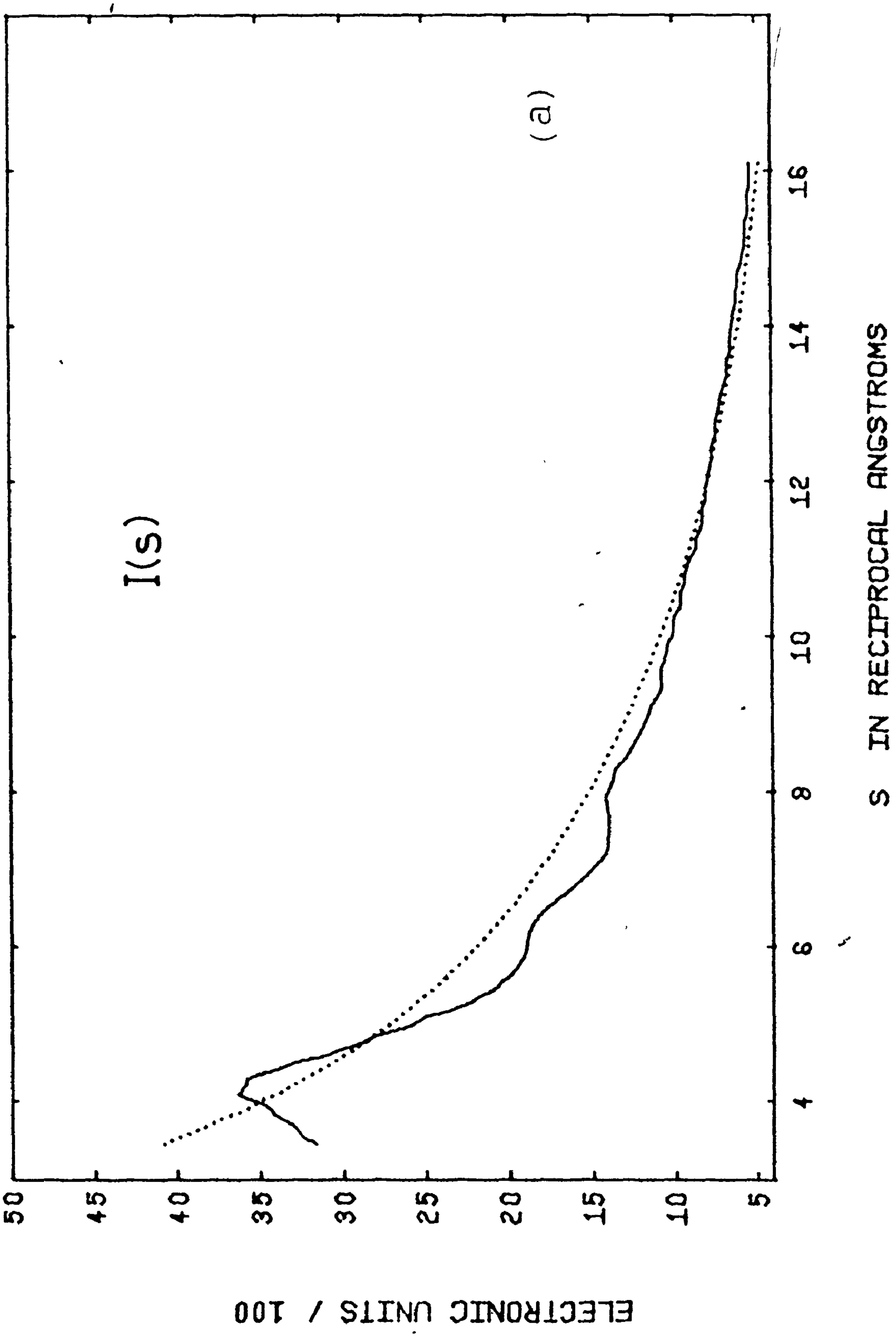
I(s)
(a)
50
45
40
35
30
25
20
15
10
5
ELECTRONIC UNITS / 100
4
6
8
10
12
14
16
S IN RECIPROCAL ANGSTROMS

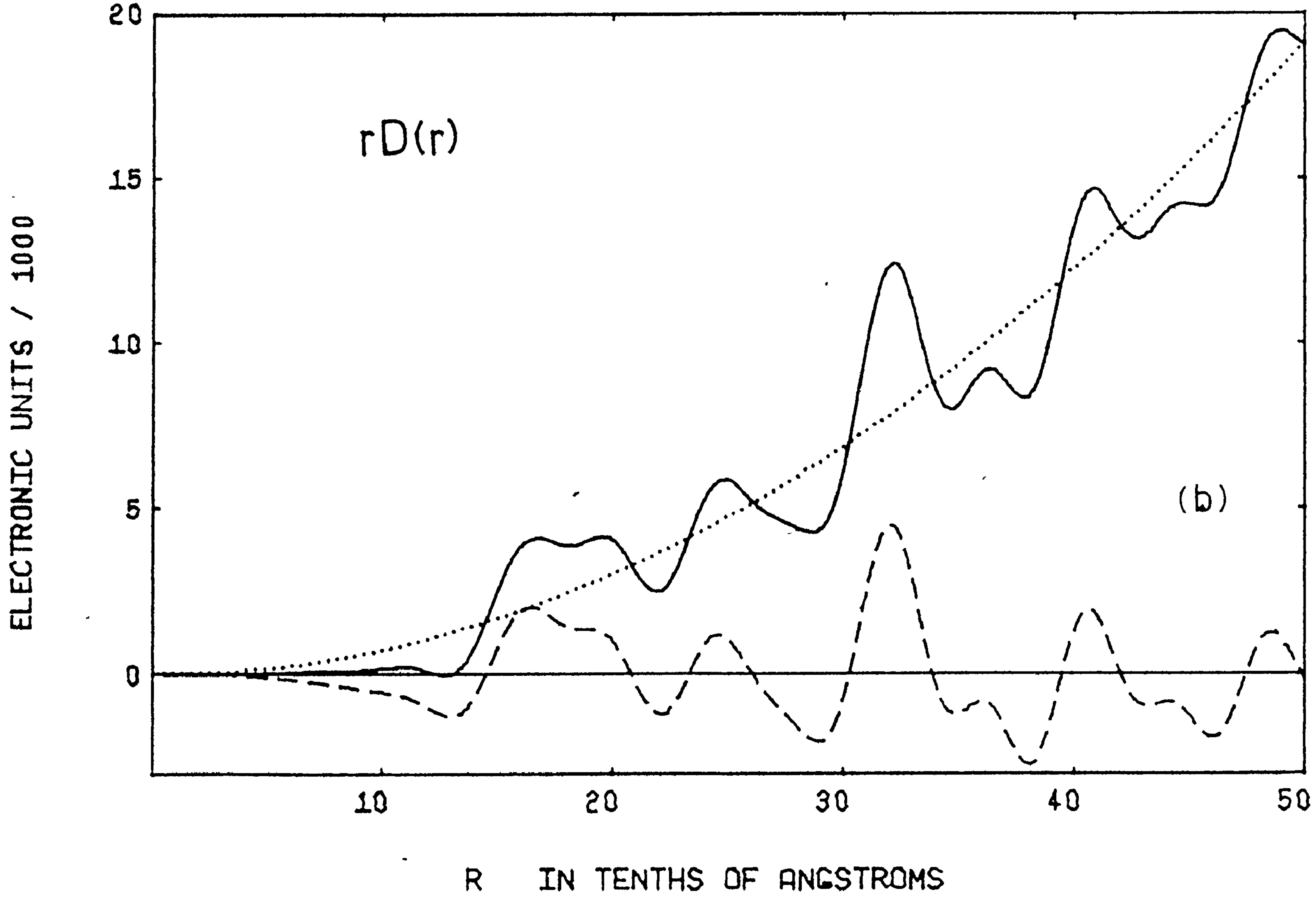
rD(r)
(b)
ELECTRONIC UNITS / 1000
20
15
10
5
0
10
20
30
40
50
R IN TENTHS OF ANGSTROMS

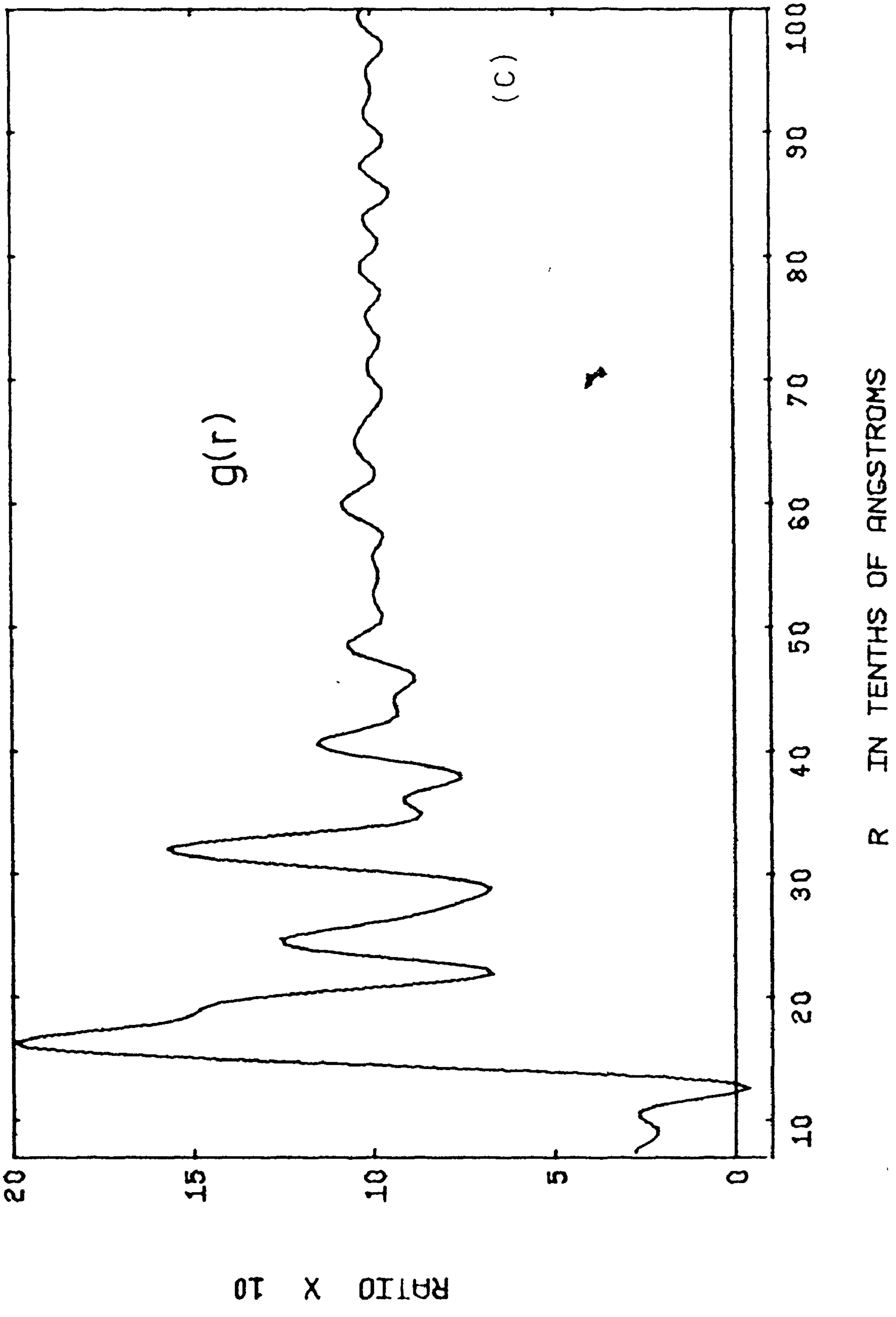
g(r)
(c)
20
15
10
5
0
RATIO X 10
10
20
30
40
50
60
70
80
90
100
R IN TENTHS OF ANGSTROMS

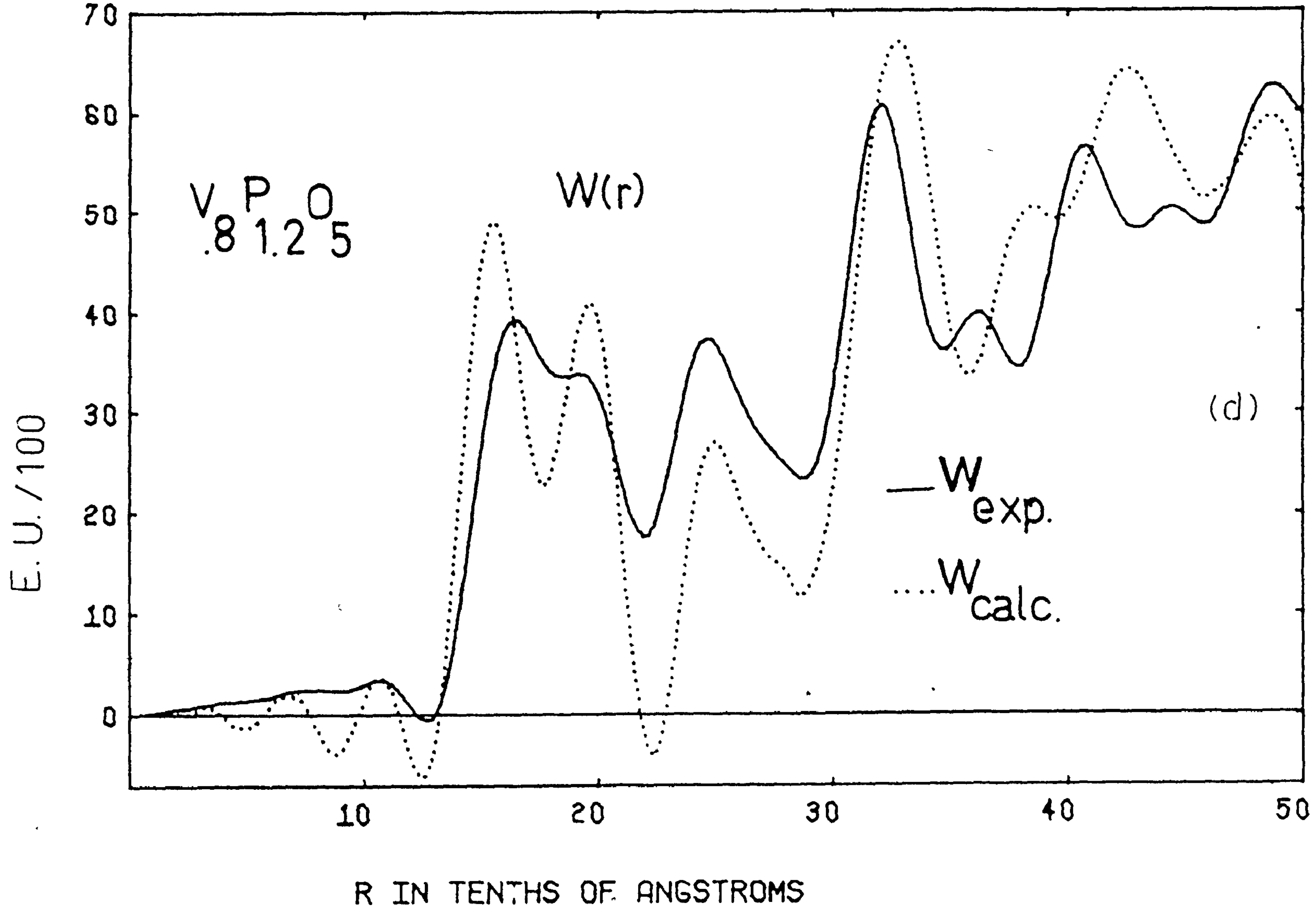
$V_{.8}P_{1.2}O_5$
W(r)
(d)
—$W_{exp.}$
....$W_{calc.}$
E. U. /100
70
60
50
40
30
20
10
0
10
20
30
40
50
R IN TENTHS OF ANGSTROMS

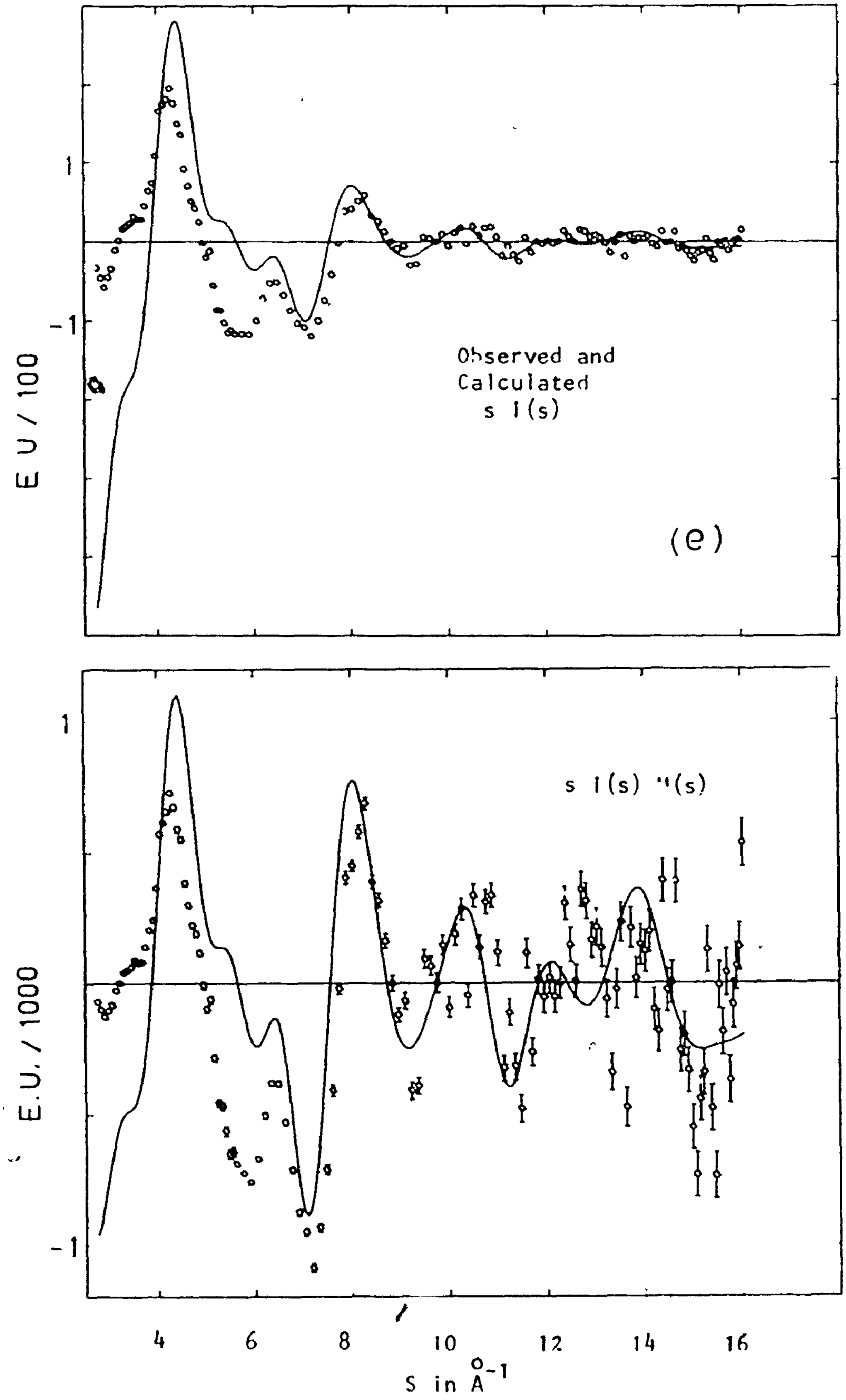
1
-1
E U / 100
Observed and
Calculated
s I(s)
(e)
1
-1
E.U. / 1000
s I(s) ''(s)
4
6
8
10
12
14
16
S in Å⁻¹

CHAPTER 7

IMPLICATIONS OF THE MODEL

The properties of vanadium phosphate glasses have been the object of many investigations. As a semiconductor with a temperature dependent activation energy for electronic conduction, the glass has attracted the interest of both experimentalists and theorists who have applied their efforts to the explanation of the conduction process and the degree to which it is influenced by the disorder inherent in the glassy state. The conductivity has been measured as a function of temperature for various compositions and degrees of vanadium reduction. The Seebeck coefficient, which comes from the voltage induced across a sample experiencing a thermal gradient, has been measured for various temperatures and as a function of vanadium degree of reduction (Linsley,*et al* 1970). Spectroscopic investigations into the structure of the glass have involved infrared absorption (IR), electron paramagnetic resonance (EPR), and nuclear magnetic resonance (NMR). Densities have been noted in several papers, and in some cases electron microscopy was used to test for phase separation or devitrification (crystallisation).

It is the object of the present section to discuss the implications of the various features of the structural model on the physical properties mentioned above.

The following notation will be used to denote the composition $V_{1+x}\ P_{1-x}\ O_{5-\frac{c'}{2}}$ where x is the proportion of PO_4 tetrahedra replaced by VO_4 tetrahedra and c is the ratio V^{4+}/V^{total}. In the formula, notation of c will usually be suppressed but is implied. The term "vanadate content" refers to x (or the vanadum to phosphorous concentration ratio). The term "percent reduction" means 100 c and $c' = c(1+x)$.

In a pair of papers Janakarama-Rao (1965-1966) studied a number of properties of the P_2O_5 - V_2O_5 - GeO_2 system. In the infrared spectrum of his glasses he noticed a prominent line at 1005 cm^{-1} in the vanadium rich glasses which became enveloped by a broad band as phosphorous was added. He correlated this line with one he observed in the spectrum of V_2O_5 at 1015 cm^{-1} and concluded from this that the vanadium environment in the glasses resembled that in crystalline V_2O_5. The line which he identified as the vanadium-oxygen stretch, has been shown by Gilson <u>et al</u>., (1973) in a single-crystal Raman scattering and infrared reflection experiment to be one of several distinct vanadium-oxygen stretches. The octahedral environment of vanadium in V_2O_5 (Bachmann, <u>et al</u>., 1961) is quite distorted with three different equatorial bond lengths as well as the axial long and short (vanadyl) bonds. The vibration to which Gilson <u>et al</u>. attribute the line seen by Janakirama-Rao is primarily the short terminal vanadium-oxygen bond (vanadyl bond). The similarity between the glasses and the V_2O_5 crystalline structure noted by Janakirama-Rao should not be generalised to imply that the vanadyl VO_5 or VO_6 units are linked in any way similar to that of V_2O_5. What could be deduced from the appearance of the line is that it is not caused by non-condensed VO_4 groups or by metavanadate chains (two bridging and two terminal oxygens per vanadium). Both alpha and beta VPO_5 have vanadyl VO_6 units although neither of the vanadium phosphates has the edge sharing configuration found in V_2O_5.

Landsberger and Bray (1970) reported a nuclear magnetic resonance experiment on several compositions of vanadium phosphate glass. They fitted their line profile to one generated on a computer by a procedure which calculated the line arising from an anisotropic chemical shift tensor and quadrupole coupling tensor for a fixed orientation of the magnetic field and tensors and averaged over all directions in space. They separated the broadening of the line due to the chemical shift from that due to the quadrupole shift by comparing data at two resonance frequencies. Axial symmetry about the vanadyl bond was assumed, and consequently the tensors were reported as a value parallel to the bond direction and one perpendicular. They found that as the phosphate content of the glass was increased, the chemical shift component in the direction parallel to the vanadyl bond decreased, but that the shift perpendicular to the vanadyl bond remained constant. They interpret the decrease in the chemical shift parallel to the vanadyl bond as evidence that the vanadyl bond has been made more ionic, and consequently weakened, by an attack by the phosphate. Interpreting Janakirama-Rao's (1966) infrared spectra to imply that the glasses were structually based on V_2O_5 - like sheets, they concluded that the axial nature of the change in the chemical shift implied that the phosphate attacked the vanadyl oxygen and replaced it with a PO_4 group. Changing the terminal vanadyl oxygen to a P-O-V bridging oxygen preserved the axis of symmetry and weakened the vanadyl bond. The decrease in the parallel component of the chemical shift was found to be linear in the proportion of vanadium which had been reduced to the four plus oxidation state. Because the V^{4+} content increases with phosphate content, it was concluded that the oxygen loss which gives rise to the vanadium reduction was due to the vanadyl oxygen replaced by the phosphate. Within the context of the model proposed in the present study, the loss of oxygen is connected with the formation of V_2O_9 units which are axially symmetric, and which replace a terminal vanadium oxygen bond with a bridging V-O-V bond. The axial symmetry of the whole V_2O_9 group arises more naturally from the structure than would be the case of the structure proposed by Landsberger and Bray. The V_2O_9 group has just those attributes of their model which they used to explain their data, namely, an increased ionic character to the axial V-O bond and axial symmetry for both VO_6 and V_2O_9 groups.

The model of Landsberger and Bray (1970) has only two types of vanadium environment; those bridged to phosphates, and those with vanadyl bonds. To incorporate the disorder assumed inherent in the glassy state, they allowed the elements of their parameter tensors to take on values about an average or "most probable" value and distributed according to a probability distribution parametrized by a width Δ. They found it necessary to employ a skewed distribution, and one could ask whether such a skewed curve might contain an unresolved bimodal distribution. The following page shows a schematic of their distribution.

Were the major cause of disorder about a vanadium site the distribution of phosphates, it should be assumed that the environment would be most disordered at high phosphate content. Indeed, it had been proposed by Janakirama-Rao (1965,1966) that the decrease in electrical conductivity at higher phosphate content was due to the progressive breakup of V_2O_5 sheets to accommodate more phosphate. It is found, however, that the width parameters Δ for the distribution of both the parallel and perpendicular components of the chemical shift tensor increase quite significantly with increased vanadium content. If there had been a minority component of the glass which increased with vanadium content, and if the tensor components of the minority feature were near or internal to the distribution of values generated by the majority component, then its observation could perhaps be

FIGURE 7.1

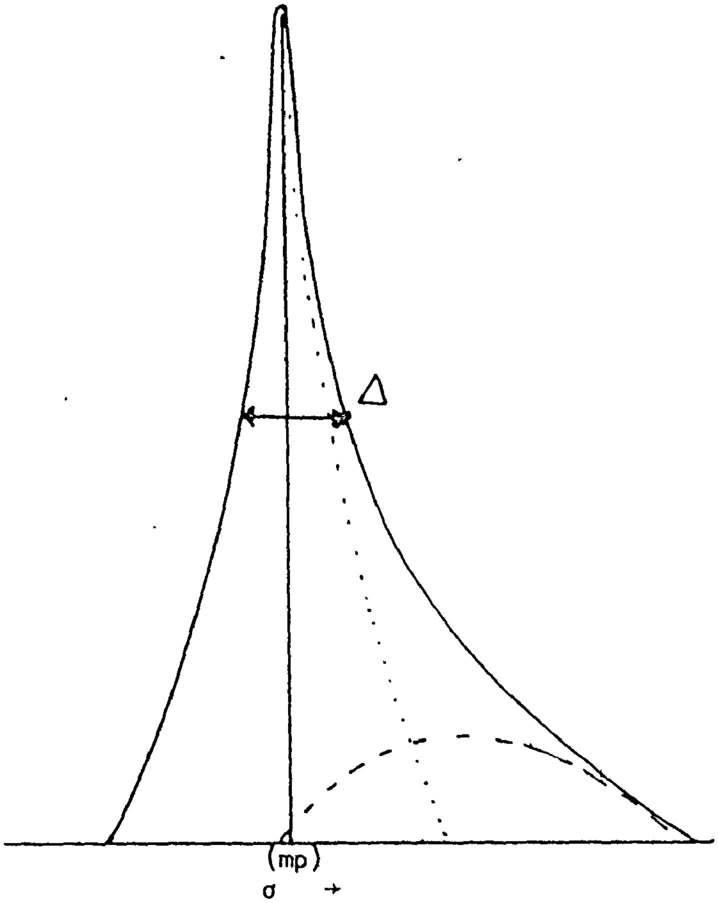

This is a schematic of the skewed probability distribution used by Landsberger and Bray (1970). The solid line is their curve centred about the "most probable" value (mp) and characterised by a width Δ. The dotted curves show how the apportionment between the members of an unresolved pair of peaks could be scaled by the width Δ.

obscured by the skewed distribution that was used. A candidate for that minority feature is the tetrahedral vanadium that has been proposed to explain the X-ray data in the present study.

Although Landsberger and Bray have two types of sites(VO_6 and $VO_4 - O - PO_3$) they find that they do not observe separate spectra for each type of site. They assume that their sites are close enough in the values of their chemical shifts that the averaging procedure superimposes the two signals to form a compound line the peak (most probable value - "mp") of which will be shifted to the weighted mean of the components. They plotted the following expression, in which σ_{11} and σ_1 are the respective chemical shift for the "parallel" and "perpendicular" directions, and where γ is the number fraction of P-O-V type environments.

$$(\sigma_{11}^{mp} - \sigma_{1}^{mp}) = \alpha + \gamma\,(\sigma_{POV}^{11} - \sigma_{V_2O_5}^{11})$$

The intercept α, is the parallel minus perpendicular components for pure V_2O_5 and it is assumed that σ_{POV}^{1} is the same as that in V_2O_5. The number fraction γ was taken as half the V^{4+} fraction on the assumption of one POV unit being formed for every oxygen lost. The slope of their linear plot yielded $\sigma_{POV}^{11} - \sigma_{POV}^{1}$ which they found to be 34×10^{-4} which is twice the maximum measured $\sigma_{mp}^{11} - \sigma_{mp}^{1}$ and almost four times the equivalent number for V_2O_5. If one assumes that the minority peak is due to V_2O_9 units instead of $O_4V\text{-}O\text{-}PO_3$ structures, both vanadiums of the V_2O_9 unit will contribute a resonance and hence γ will be twice as great and the slope will yield a chemical shift difference of 17×10^{-4} instead of 34×10^{-4}. The lower anisotropy (by half) predicted by the use of a V_2O_9 group brings the parameters of the two components (V_2O_9 and VO_6) closer in value and makes the hypothesis of two superimposed averaged peaks perhaps more reasonable.

7.1 The Density

The density of the samples used for the X-ray experiments was measured in one of two ways depending on how large a specimen could be dislodged from its holder without cracking. For two compositions, intact slabs of ten or more grams were looped with a wire and weighed in air and water to the nearest milligram. The depth of submersion was reproducible so that correction for the buoyancy of the wire could be made. The others were measured by a floatation technique (International Tables of X-ray Crystallography III , 1962) in which clips of the sample were matched in density by a benzene bromoform mixture and the density of the liquid mixture subsequently measured in a pycnometer.

As can be seen on the following page, the density measurements in this experiment are compatible with those of Greaves (1973), Janakarama-Rao (1965), and Caley and

Figure 7.2 Density of vanadium phosphate glass

Key:

●	This study
G	Greaves (1973)
C	Caley and Murthy (1970)
S(0)	Sayre and Mansingh (1972)
J-R	Janikirama - Rao (1966)
L(0)	Lynch *et al*. (1971) prepared under oxygen
L(A)	prepared under argon
— — —	Calculated assuming:

0 - 0 repulsion distance at slip is 2.82 Å

a axis expansion with x is 1%

c axis expansion with x is .15 Å

c axis contraction with V^{4+} is .15 Å

V^{4+} concentration varies as in Figure 7.7

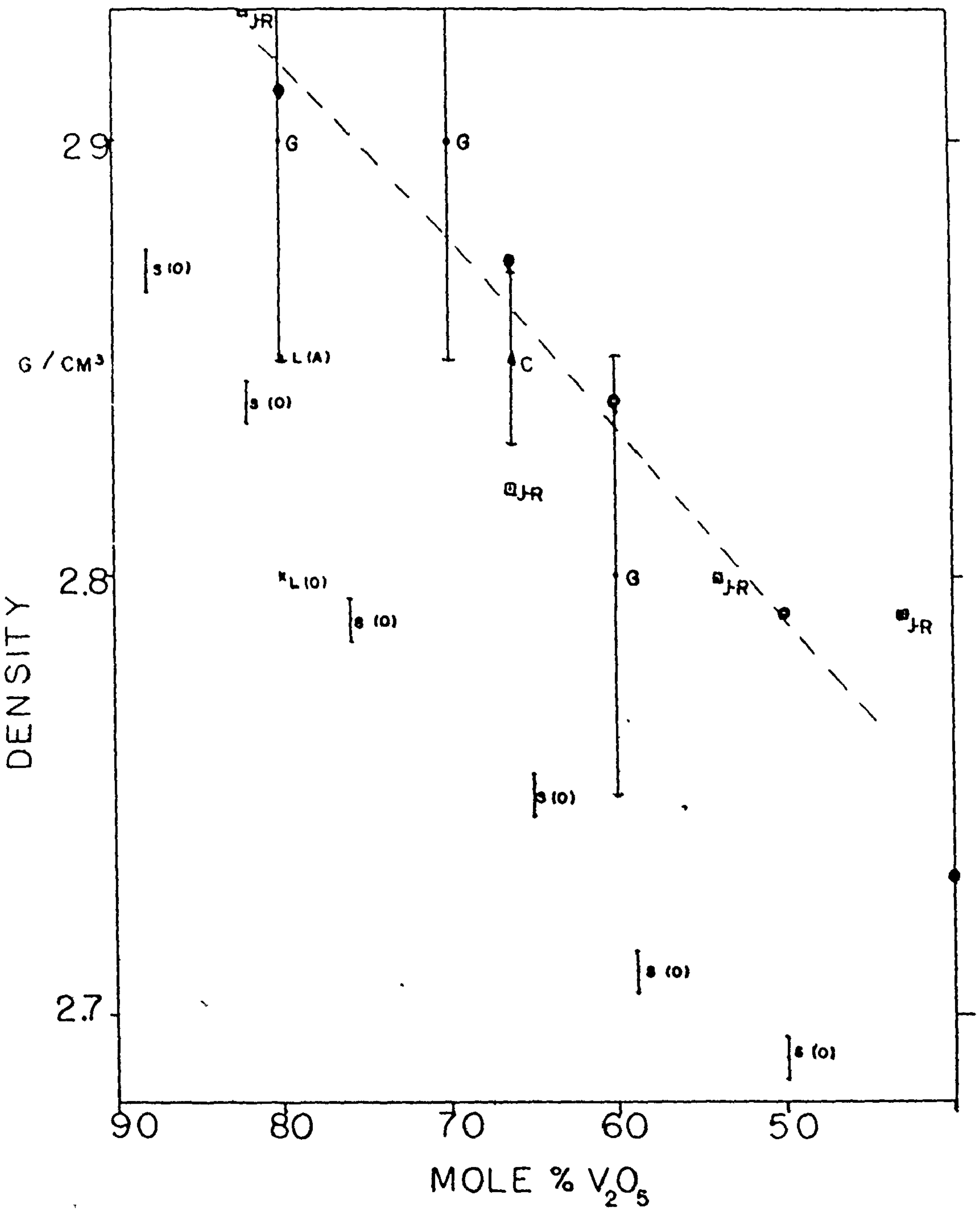

DENSITY
G / CM³
2.9
2.8
2.7
90
80
70
60
50
MOLE % V_2O_5
J-R
G
G
S (O)
L (A)
C
S (O)
J-R
L (O)
S (O)
G
J-R
J-R
S (O)
S (O)
S (O)

Murthy (1970). Those samples prepared in oxygen atmosphere by Sayre and Mansingh (1972) and in oxygen and in argon Lynch et al., (1971) are systematically lower by about four percent. Comparing the glass with fifty percent vanadate with the α-VPO_5 crystal indicates a seventeen percent decrease in density from the crystalline state. Only a slight change in density occurs as the vanadium content is increased. The variation with vanadium substitution is nearly linear with a rise of less than five percent. Simple mass change on substitution should give a twelve percent increase in density from the fifty percent vanadate to the one hundred percent vanadate, were it not for expansion.

The most prevalent feature of the density curve is the uniform drop of seventeen to twenty percent from the crystalline value and then the very mild increase across a wide compositional range. The double layer of α-VPO_5 sequence with the intervening slip dislocation as described in Chapter 6 gives just such a constant density decrement. The two sheets that compose the double layer could be pinched together by V_2O_9 groups to give the observed two percent increase in density with reduction, although Sayre and Mansingh's (1972) fifty and sixty percent vanadate glasses decrease from a reported forty percent reduction to eighteen percent reduction with no major change in the density. It would appear that much more data is needed to sort out the separate influences of V^{4+} and tetrahedral vanadium substitution. A moderate increase in volume on going from VPO_5 to $VOVO_4$ is indicated by the slope of the graph. The increased size of the VO_4 unit over the PO_4 unit should shift the V-P peak in the pair distribution function significantly and increase the volume of the "apparent" cell significantly if uniform expansion were to take place. The shift in the V-P peak is much more restrained, indicating that a rotation of the tetrahedral group about an axis normal to the layer to accommmodate much of the increased bond length may be taking place. The tetrahedra could rotate as much as about twenty degrees before oxygen-oxygen repulsion would intervene. A projection down the c-axis in the α-VPO_5 crystal structure shows a VO_6 octahedron and its n-glide generated mate. This pair of octahedra and the tetrahedra which join them, form a parallelogram (Fig. 5.3) with the innermost four oxygens of the group. Rotation of the tetrahedra increases the major diagonal of the parallelogram and decreases the minor diagonal. It is the oxygen-oxygen vector described by the minor diagonal of the parallelogram which would limit the rotation.

7.2 Homogeneity - The Literature

Two forms of heterogeneity have been discussed in the literature with respect to vanadium phosphate glasses. The first of these is devitrification. In some glasses nucleation and growth of crystals occurs when the specimens are heated or allowed to sit for an extended period of time. Although

Hamblen <u>et al</u>, (1963) have reported that they were able to induce devitrification in various ternary glasses which included vanadium phosphates by heat treatment, the question relevant to the present study is whether devitrification is to be expected in as-cast or moderately annealed samples. In the course of the present study, devitrification was observed in only a few samples. These specimens had been discarded because their thermal history was unknown due to a malfunction of the furnace control during their preparation. Over a period of several months to three years some of these discards lost their black glossy sheen and took on a dark green colouration on their surface which progressed with time into the bulk. Powder X-ray diffraction yielded crystalline and amorphous patterns. Samples for which a thermal history is known, have been stored as chunks or slabs for three or more years with no indication of degradation. It is a common practice among those workers experimenting on the transport properties to test their samples for devitrification by X-ray techniques. For example, Landsberger and Bray (1970), Sayre and Mansingh (1972), and Anderson and Luehrs (1968) used X-rays to screen samples for devitrification. Hench (1970) experimented with glasses in the systems V_2O_5 - P_2O_5 and V_2O_5 - KPO_3 to test the effect of quenching temperature and annealing on the electrical properties. He found slight differences in the electrical properties of glasses quenched from various temperatures above 700°C, but that glasses quenched from 550°C were quite different from the others. This was attributed to about 1% of the bulk having crystallized. Hamblen et al. (1963) had also noted marked changes in conductivity upon devitrification. It appears that devitrification is readily detectable when it is present and that for those compositions interior to the glass-forming regime and quenched from temperatures well above the melting temperature it is not common.

While devitrification does not appear at this time to be a centre of controversy, the other form of heterogeneity is. If two melts are immisible below a given temperature but form a solution above that temperature, and if the solution is quenched from above that temperature fast enough that the two components can only separate on the molecular scale before freezing into place, an intimate mixture of two glasses results. In systems in which this behaviour has been studied (see for example, Zarzycki and Naudin (1967)) the size of the domains could often be monitored by small-angle X-ray scattering as they grew upon annealing. Hench (1970) quotes the results of small-angle X-ray scattering experiments on .33 KPO_3 - .67 V_2O_5 glass, but does not give experimental details. He noted concommittant changes in the electrical behaviour and in the small-angle X-ray scattering when the samples were annealed at 288°C. Shaake and Hench (1970) discuss this further and propose a theory of the conduction process which is predicatedupon phase separation.

Two points are worthy of keeping in mind when considering Hench's results; having established that the change in conductivity upon annealing is a characteristic of glass-glass phase separation in the ternary glass (containing potassium) he does not find significant change in the electrical properties of the binary glass upon annealing, and secondly Illarionov et al. (1961) have published phase diagrams for the potassium oxide-phosphate-vanadate system which contain four crystalline phases one of which matches Hench's glass in vanadate to phosphate ratio. Hench (1970) concluded that the presence of sodium oxide, potassium oxide, or barium oxide in vanadium phosphate glass strongly changes tendencies of the glass for phase separation and crystallization. Mansingh et al., (1975) measured the AC conductivity of some glasses in the binary vanadate-phosphate system before and after annealing and found no change in the conductivity after annealing at 300°C. Aside from those of Greaves (1973), whose results they attribute to his use of vanadium electrodes, they could find no published data indicating an annealing induced change in conductivity. They interpret their results as evidence against phase separation in the binary glass system. The demonstrated sensitivity of phase separation to the presence of alkali oxides as a third component, and the absence of the characteristic behaviour in the binary glasses indicates that the presence of heterogeneity in the ternary glasses is a separate question from whether heterogeneity is present in the binary glasses. This is not to imply that the ternary glasses are structurally drastically different from the binary glasses, for that is, again, a separate question, and the very minor degree of change in the conductivity of the binary glasses as several percent of the third component is added (Caley and Murthy, 1970, and Baynton et al., 1957) suggests a high degree of similarity.

The strongest evidence for phase separation in the binary vanadate phosphate glass system comes from electron microscopy. Anderson and Luers (1968) examined glasses quenched from 900°C both as chips and as thin films blown from the melt under an electron microscope. The chips were problematic because of a tendency to melt in the electron beam when mounted on a cold stage at liquid nitrogen temperature. The equivalence of the thin films to the bulk glass is open to question, although Austin and Sayre (1974) were able to blow films in which the electrical properties matched those of the bulk glass. In the films, Anderson and Luers (1968) found no phase separation in glasses of eighty percent vanadate or less, but found evidence of phase separation in an 87.5% vanadate glass with the size of the heterogeneous regions being about 20 Å. Several other workers, such as Mackenzie (1964), Austin and Sayre (1974), Sayre and Mansingh (1971), and Sayre *et al.* (1971), have used electron microscopy to screen their glasses for heterogeneity and have not reported evidence of phase separation. Friebele, Wilson, and Kinser (1972) reported electron microscopic evidence of phase separation which begins between sixty and sixty five percent vanadate and increases with vanadate content to major proportion at ninety percent vanadate. The size of the heterogeneities on their photographs is an order of magnitude or more greater than those seen by Anderson and Luers (1968). In a later paper, Kinser and Wilson (1973) indicated phase separation on the phosphate rich side of a minimum in heterogeneity near 70% vanadate. They further suggest that the heterogeneity minimum coincides with the conductivity maximum when considered on a triangular phase diagram of V_2O_5 - V_2O_4 - P_2O_5. It is not clear that the latter conclusion is justified by the half dozen compositions investigated in that paper, but further evidence is promised in a "to be published" paper. An alternative explanation for the conductivity maximum in terms of the polaron-polaron repulsion hypothesis of Sayre and Mansingh (1972) and using the structural parameters of the model proposed herein will be given below. With regard to the electron micrographs a couple of points might be noted: the 800°C to 900°C quenching temperature used by Anderson and Luers (1968), Caley and Murthy (1970), Baynton et al. (1957), Sayre and Mansingh (1972), Hench (1970), and the present study is 200°C lower than that used by Friebele et al. (1972) and Kinser and Wilson (1973), and secondly, that the problems of local heating by the electron beam severe enough to melt samples of glass that had been mounted on a cold stage at liquid nitrogen temperature in the experiment of Anderson and Luers (1968) could also be effecting the samples in Kinser's work. Friebele et al., (1972) had noted an increase in phase separation in their samples upon annealing at 300°C. Measures to avoid local heating of that magnitude are not reported. Also no explanation has been offered as to why the stoichiometry for maximum homogeneity in one paper (Friebele et al. (1972))corresponds to a maximum inhomogeneity in the other (Kinser and Wilson 1973).

The other evidence for phase separation put forth by Friebele et al. (1972) is not as strong as the electron micrographs. They note a minimum in their EPR linewidth near 80% vanadium which they relate to the combined broadening of the line due to phase separation, dominant at high vanadate concentration, and inhomogeneity in the magnetic ion's local environment, dominant at lower vanadium content. Without their hypothesis of a V_2O_5 based glass structure, their argument does not explain the data. The VPO_5 based model proposed herein predicts the opposite trend in broadening due to variation of the local environment. If, as they claim, forcible reduction of the vanadium by the addition of sucrose enhances phase separation, or as Kinser and Wilson (1973) propose phase separation is enhanced for stiochiometries away from the conductivity maximum, a prime candidate for phase separation would be the forcibly reduced 80% vanadate specimen of Friebele et al. which had a smaller EPR linewidth than an unreduced 90% vanadate glass. Whatever the explanation of their EPR linewidth may be, its connection with phase separation is not obvious. Their other argument for phase separation involves the observation of EPR hyperfine structure lines. Lynch et al. (1971) were able to observe hyperfine lines in an 80% vanadate glass prepared under an oxygen atmosphere ($V^{4+}/V_{total} = c = .05$) but not in the glass prepared under argon ($c = .11$) Dipole-dipole broadening at higher V^{4+} concentration was given as the reason for the absence of hyperfine lines in the spectrum of the more reduced glass. Landsberger and Bray (1970) were unable to observe hyperfine lines in a 90% vanadate glass with $c = .06$. Lynch et al (1971) explain the discrepancy by noting weaknesses in Landsberger and Bray's procedure for analysing for V^{4+} content. Friebele et al (1972) take the results to imply that Landsberger and Bray's 90% vanadate glass was more phase separated with a higher effective V^{4+} concentration in a vanadium rich phase. As will be discussed below, the VPO_5 model for the glass with excess vanadium substituting for phosphorus on the tetrahedral sites, with the extra hypothesis that the itinerant electron does not come to rest on a tetrahedral vanadium, implies that the more relevant measure of V^{4+} concentration is the number of reduced vanadium atoms per octahedral site. Transforming to that parameter, Landsberger and Bray's glass is one and one third to one and one half times as reduced as that of Lynch *et al*. More data will be required before it can be ascertained whether this degree of enhancement of the effective V^{4+} concentration is adequate to smear out the hyperfine structure, but the apparent conflict between the two sets of spectra is significantly lessened.

The discussion of phase separation in the paper of Friebele *et al*. (1972) was incidental to the investigation of magnetic ordering in the glass. They measured the integrated intensity of the EPR signal as a function of temperature and found approximately a 15% variation which they attributed to the loss of signal from magnetically coupled V^{4+} sites. Lynch *et al*. (1971) had measured the EPR absorption curve directly, along with that of the standard, and integrated. Friebele *et al*. (1972) and Landsberger and Bray (1970) approximated the integral strength from the derivative curve as being proportional to the product of the peak to peak height and the square of the linewidth. Landsberger and Bray (1970) had pointed out that the proportionality constant is lineshape dependent, and consequently a change of lineshape rather than line intensity may have been responsible for some of the temperature variation observed by Friebele *et al*. (1970). However in a later paper Kinser and Wilson (1973) report that the linewidth had been temperature invariant. Lynch *et al*. (1971) had also measured the line strength as a function of temperature and found it invariant. The discrepancy lies in the size of the error bars, which are more than an order of magnitude smaller on the data of Friebele et al. than on that of Lynch et al. (1971) or of Landsberger and Bray (1970). The peak heights and widths would have to have been measured to four significant figures to give such precision.

Friebele et al found that the temperature variation of the EPR signal strength was slightly different for those samples considered to be phase separated, and the variation led them to suggest that the minority phase was V_2O_4-like but vitreous.

The X-ray model proposed herein has several implications for the question of heterogeneity in the glass. If the average electron density of the two phases were adequately different and if the domains were on the order of 20 Å as observed by Anderson and Luers (1968), then significant small angle scattering should have been observed. The VPO_5 structure and the V_2O_5 structure are both layered, and the layers are bonded to each other in both cases by the long V-O bond trans to a vanadyl bond. In spite of these similarities, it would be difficult to fit tetrahedra into a V_2O_5 based structure. Some examples have been found in the niobium phosphates(Roth et al.,1965; Levin and Roth,1970) in which small amounts of phosphate have been ordered at the corners of blocks of edge sharing NbO_6 octahedra. The high degree of ordering of the phosphates in these niobium phosphates makes this kind of structure a less desirable glass model. In as much as $VOVO_4$, the totally substituted $VOPO_4$, has not been observed, a maximum may exist in the degree of substitution beyond which the excess vanadate would form layers of V_2O_5 form. A maximum in vanadium concentration beyond which partial crystallisation takes place has been noted by several authors including Caley and Murthy (1970), Denton _et al_. (1954) and Grechanik _et al_ (1960). No X-ray data were taken on a sample with more than 80% vanadate content and the substituted $VOPO_4$ model appears to extrapolate well to that point, and no phase separation was seen by Anderson and Luers (1968) through that composition. Whether the model extrapolates right up to the limit of vitrification near 95% vanadate content remains open to speculation. A phase diagram published by Nador (1960) indicated a eutectic near 86% vanadate content, and Anderson and Luers (1968) interpreted this composition as the boundary beyond which vitreous phase separation begins. The composition at which they observed separation was 87.5% vanadate. The structural features discussed above would suggest that should phase separation take place in the 90% vanadate region the phases would be $V_{1+x} P_{1-x} O_5$ and V_2O_5 with x near .8. If these are indeed the phases which separate, it is not obvious why separation should occur near x = 0 or x = .2, as seen by Kinser and Wilson (1973), but not seen by Friebele, Kinser, and Wilson (1972).

7.3 Magnetism

Friebele et al. (1972) suggest that vanadium phosphate glass has antiferromagnetic coupling between some pairs of V^{4+} ions. They locate the transition temperature from their EPR line strength measurements and find that it agrees within error with the Currie temperature derived from the temperature dependence of the magnetic susceptibility. They take the agreement of the two temperatures to rule out superexchange. The magnetism is discussed as a property of the unseparated glass and is not predicated on a phase separation hypothesis. As was noted above, Lynch et al.(1971) observed no change in EPR line strength with temperature, but Friebele et al. (1972) with very much smaller error bars found significant variation. The results of Friebele et al. were very reproducible from sample to sample, also. If it is assumed, after them, that the coupling exists and that the temperature dependence rules out $V^{4+} - V^{5+}$ interactions, then the X-ray model may be searched for acceptable site pairs.

The closest $V^{4+} - V^{4+}$ separation would come from an octahedral and tetrahedral pair. Examples of tetrahedral V^{4+} are not abundant in nature. There are advantages in the interpretation of the conductivity to the hypothesis that the itinerant electrons do not lodge for long on tetrahedral vanadium sites. An effective g value - - - - - - - - - - - -

of approximately 1.960 has been observed in the EPR of the vanadium phosphate glasses throughout the composition range studied by Friebele et al. (1972), Bogomolova et al. (1968), Landsberger and Bray (1970), and in crystalline α-VPO_5 H.N. Ng (1973). If the EPR signal were due to V^{4+} on both tetrahedral and octahedral sites, either separate signals or an average signal with a centre which shifted with vanadium content should be expected. Alternatively, the EPR signal of tetrahedral V^{4+} could be so broadened (Siegel, 1964) even at liquid nitrogen temperature so as not to be observable. Were this the case, the V^{4+} on tetrahedral sites would be invisible to the EPR but still be counted in a chemical analysis, and, consequently, the EPR line strength should no longer correllate well with the chemically determined V^{4+} content, and the disagreement should be most severe at higher total vanadate concentrations. Friebele et al.(1972) have suggested that the magnetic coupling could cause the EPR to underestimate the V^{4+} concentration at high V^{4+} concentration, however they plot their EPR concentration results with those of Landsberger and Bray (1970) and the chemically determined concentrations of Mackenzie, with reasonable agreement between the three. The hypothesis that the tetrahedral sites should not be counted among the possible V^{4+} sites is consistent with the EPR results.

If the tetrahedral vanadium sites are excluded from consideration, the next closest vanadium neighbour set is in the V_2O_9 group, with a vanadium separation of approximately 3.9 Å. The oxygen between the two vanadium atoms could play a role in the exchange, however Friebele et al. (1972) suggest superexchange is not involved. The 4.4 Å vanadium separation, parallel to the vanadyl bond, between octahedra in adjacent sheets also has an intervening oxygen. Another candidate, although even more distant, is a 4.67 Å separation between a vanadyl site and two vanadiums in the sheet above whose vanadyl bonds are pointing down. No oxygen blocks the line of sight between these vanadium sites. All of these separations are much larger than the three Angstrom or less distances in edge or face sharing vanadium oxides. The site pair suggested by Friebele et al.(1972), using a V_2O_5 model for the glass would be separated by approximately 3.08 Å .

Stronger evidence for the existence of magnetic ordering would be desirable, such as magnetic neutron scattering above and below the reported Neel temperature of 203°K. Landsberger and Bray (1970) measured the magnetic susceptibility from 77°K to 300°K and found it to fit a Curie-Weiss law $\chi = C/(T - \theta)$ where χ is the magnetic susceptibility, T is the temperature, and C and θ are fitted constants. Their values for θ, the Curie temperature for two glasses were $13 \pm 5^{\circ}$K and $5 \pm 5^{\circ}$K. This is not consistent with the $\theta = -200^{\circ}$K observed by Friebele et al.(1972), but implies either paramagnetism or a magnetic ordering at very low temperatures. The long distances between vanadium sites implied by the X-ray model would be more consistent with a weaker exchange interaction, and a lower ordering temperature. Lynch and Sayre (1973a) suggest that magnetic ordering should occur at no more than a few degrees Kelvin and could be either ferromagnetic or antiferromagnetic. Along this line it may be helpful to note the observed magnetic ordering behaviour in related structures. VSO_5 has both an alpha and beta phase which are isostructural with the alpha and beta phases of VPO_5 respectively, (Longo and Kierkegaard 1965; Longo and Arnott, 1970). While the distances and spatial arrangement of the vanadium atoms correspond between the phosphate and matching sulphate structure, only a minority of the vanadium ions in the phosphate are in the magnetic V^{+4} state while all the vanadium ions in the sulphate are V^{4+}. One would expect magnetic ordering in the phosphate to be no easier than in the sulphate. Magnetic susceptibility data on both sulphate phases has been published by Longo and Arnott (1970). Above $100^{O}K$ the magnetic susceptibility of both phases follows a Curie -Weiss law with a Curie temperature of $-12^{O}K$, indicating ferrimagnetic ordering. The susceptibility of the alpha phase maintains this behaviour down to about $10^{O}K$ at which point a new line commences which indicates a Currie temperature of about $4.2^{O}K$. The susceptibility of the beta phase begins its deviation from the Curie -Weiss law at about $100^{O}K$ and its behaviour below that point is interpreted as indicating a Neel temperature of $25^{O}K$.

With such low ordering temperatures for the vanadium sulphates and particularly the alpha phase, it would be reasonable to expect the ordering in α-VPO_5 to be confined to temperatures lower than 4^oK. On the basis of the glass model proposed here, this would imply that magnetic ordering in the glass should be confined to low temperatures.

7.4 Electrical Properties

7.4.1 General

The conductivity of vanadium phosphate glasses has been discussed in a book (Mott and Davis 1971), in review articles (Mackenzie, 1964b, Austin and Mott, 1969, Adler,1971, Austin and Garbett, 1971), and in several research articles. Various theories are reviewed in Austin and Sayre,(1974) and extensive experimental data on binary V_2O_5 - P_2O_5 glasses is given in Sayre and Mansingh, 1972, and Linsley et al.(1972). Data from these last two papers will be drawn upon heavily in this discussion.

The conduction is usually regarded as a small-polaron hopping process. Oxygen evolving from the melt leaves some of the original V^{5+} ions reduced to V^{4+}, and as long as the V^{4+} ions are in the minority the conduction is electronic. In specimens reduced to majority V^{4+} concentration the Seebeck coefficient (Linsley et al., 1970, Greaves, 1973) shows hole type conduction. The transfer of charge can be seen (Mackenzie, 1964b) as a change from a V^{4+} - 0 - V^{5+} configuration to one of

$V^{5+} - O - V^{4+}$. The electron transfer from vanadium to vanadium is subject to two types of localisation, Landau localisation (1933) and Anderson localisation (1958). An extra electron in an ionic material can cause its immediate environment to distort enough in some cases to trap the electron (Landau localisation).

The conductive process of small polcron transport in a crystal is often described as band conduction at low temperature (T less than ½ Debye temperature($\approx\theta_D$)) and hopping conduction at higher temperature ($T>\frac{1}{2}\theta_D$). The slowly moving electron is seen to trap itself at higher temperatures in a potential well generated by its own induced polarisation of its environment (Landau, 1933). Whether the electron traps itself depends upon the "stiffness" of the host lattice and the electron's bandwidth. If Landau trapping is in effect, the electron is seen to hop from site to site with the assistance of one or more optical phonons. At low temperature the density of accessible optical phonons is small and the electron is seen as tunnelling between sites. If the host is not a well ordered crystal the energy of possible electron sites may differ from site to site by an energy of approximately W_D. If this modulation in site energy is large enough relative to the low temperature conduction band width, the band conduction is destroyed and the electron once again localised, this time by Anderson (1959) localisation. In disordered materials (Emin 1973) the theory usually involves hopping by way of accoustic phonon assistance at low temperatures.

There are two common ways of parametrizing the polaron energy or well depth W_p. This is the energy gained by the polaron by digging a well. Holstein (1959) has expressed W_p in terms of the phonon spectrum as $W_p = \frac{1}{2N} \sum_q |\gamma_q|^2 \hbar \omega_q$ where $\hbar \omega_q$ is the energy of a phonon of wave number q, N is the number of centres per unit volume, γ_q is the electron-phonon coupling constant for a phonon of wave number q. It is immediately seen that the stiffness of the host lattice will influence W_p through $\hbar\omega_q$ and stoichiometry will influence W_p through $(2N)^{-1}$.

The other parametrization commonly used is that of a polaron radius (Austin and Mott, 1969) in which W_p is equal to $\frac{1}{2} \frac{e^2}{\epsilon_p r_p}$ where r_p is a distance called the polaron radius, ϵ_p is an effective polaron dielectric constant given by $\epsilon_p^{-1} = \epsilon_\infty^{-1} - \epsilon_0^{-1}$ where ϵ_∞ is the optical (high frequency) dielectric constant and ϵ_0 is the static dielectric constant. The constant e is the charge of the electron. The difference of the dielectric constants comes from the net change in energy from the electron-lattice configuration before relaxation and after relaxation. Austin and Mott (1969) and Adler (1971) argue that r_p should be "somewhat less" than the metal-oxygen distance.

Bogolomov et al. (1968) have made an approximate integral over a Brillouin zone of the Holstein formula $\omega_q = \frac{1}{2N} \Sigma_q |\gamma_q|^2 \hbar w$ and parametrized the results in terms of the other form with $r_p = \frac{1}{2}(\frac{\pi}{6})^{1/3}\bar{a}$ where $\bar{a}$ is the average interionic separation(in this case V-V separation).

One approach to the theory of the small polaron in a disordered environment has been to simply multiply the hopping probability, R_{ij}, for a given pair of sites i and j, by a factor (Emin, 1973) $e^{+\Delta/2kT}$ where the energy of site j is incremented (decremented) relative to site i by an amount $\frac{1}{2}\Delta$, and kT is the thermal energy. The phonon description of the vibrational spectrum is carried over from the theory in the crystal. This could be problematic in as much as phonons are nonlocal in character, however the model used by Emin (1973), called the Molecular Crystal Model, assumes that the most important optical phonons in the process correspond to "molecular" vibrational modes of the host ion and its immediate coordination sphere. Specializing to the case of vanadium phosphate glass, this would correspond to the stretching and bending modes of the VO_6 distorted octahedron. Phenomenologically, the conductivity, as a function of inverse temperature, has three regions of interest. The high temperature region, and lowest temperature region are each characterised by a different activation energy, and the intermediate region contains a smooth interpolation between the activation energies at the two extremes. The interpolation is based on the availability of appropriate phonons at a given temperature to participate in the process. Multiphonon processes are assumed to dominate at higher temperatures, giving way to single optical phonon processes and then to acoustic phonons as the temperature is progressively lowered.

If the hopping frequency is small compared with an optical phonon frequency, the small polaron is said to be in the non-adiabatic regime. For this case, Austin and Garbett (1973), have summarised the parameters for the conductivity, with a slight change in notation, in the following way. At temperatures greater than one quarter of the Debye temperature, the hopping probability P, can be expressed as:

$$P = g(x,c)\nu e^{-(W_H\phi(T) + \frac{1}{2}W_D)/kT}$$

where the pre-multiplier g has been made a function of the stoichiometry of the glass and the density of charge carriers (c), and W_D is the averaged disorder energy (compare with Δ above), W_H is the hopping energy of the polaron ($\frac{1}{2}W_p$) and $\phi(T)$ is an interpolation function of temperature given by

$$\phi(T) = \tanh(\tfrac{1}{4}\hbar\omega_0\beta)/(\tfrac{1}{4}\hbar\omega_0\beta)$$

where β is 1/kT and $\hbar$ is Planck's constant divided by two pi, and ω_0 is a characteristic optical phonon frequency. The premultiplier ν, is an attempt to hop frequency and is assumed to be inversely proportional to the square root of the hopping energy W_H and kT and to have an exponential drop-off with hopping distance $e^{-\alpha R}$ where α is a tunnelling factor and R is the intersite distance.

At lower temperatures the conductivity activation energy approaches W_D. If the electron bypasses the nearest neighbours and tunnels to further sites to find a better energy match between sites, Mott (1968) has argued that the logarithm of the conductivity should be linear in $T^{-\frac{1}{4}}$ rather than T^{-1}.

7.4.2 Summary of Experimental Information

Electron paramagnetic data of Lynch et al (1971) and thermopower measurements (Brown, 1966; Linsley et al, 1971; Kennedy and Mackenzie, 1967) are consistent with a temperature independent carrier concentration above 150°K. The mobility is a function of temperature and the dielectric loss function (Mansingh et al, 1971) at lower temperature has a peak at a frequency f_0 which is itself a function of temperature. This peak in the dielectric loss function (A.C. conductivity) is shown to be thermally activated with nearly the same activation energy as the D.C. conductivity (Mansingh et al., 1971; Sayre and Mansingh, 1972) and is identified with the same process. Their result could be expressed as:

$$\sigma_{D.C.} = \sigma_0(R)\ g(c,x)\ f_0(T,\ x,c)$$

where R is the intersite separation, T is the temperature and x and c are defined by

$$V_{1+x}\,P_{1-x}\,O_{5-\frac{c'}{2}}$$

where $c' = c.(1+x)$.
The function f_0 is the hopping frequency, and σ_0 and g are premultipliers.

The temperature independent Seebeck coefficient (thermoelectric power) is taken to imply (Mott, 1968) that W_D is on the order of or less than kT for the temperature range over which it is constant. The equation used to describe the Seebeck coefficient as a function of $c(V^{4+}/V^{total})$ implies that the Seebeck coefficient should change sign at $c = \frac{1}{2}$. This function, the Heikes-Ure formula (1961), describes the measurements of Allersma and Mackenzie (1967) but fails to fit the more extensive data of Linsley et al (1970). Linsley et al (1970) formed samples with x constant and c variant, and the Seebeck coefficients for samples with a constant x fall on a separate curve which did not in general extrapolate to zero at $c = \frac{1}{2}$.

Linsley et al (1970) also found that for a given x, the conductivity was a maximum for a value of c between .1 and .2. The D.C. conductivity and A.C. conductivity both peaked at the same c and the activation energy dipped to a shallow minimum (variation by about .02 eV) near the same point to give an asymmetrical maximum to the conductivity. Sayre amd Mansingh (1972) were able to fit the data of Linsley et al. (1970) with a conductivity of the form $\sigma = \sigma_0 g(x,c) e^{-W(c)(kT)}$ only by varying both the exponential W(x,c) and the pre-exponential g(x,c).

The A.C. conductivity $\sigma(W)$ has the functional form (Mansingh et al., 1975) $\sigma(\omega) = A(x,c)\,\omega^{s(T)}$. The multiplier A is a function of x and c but the exponent s appears to be a function of temperature. The exponent s varies between .8 and .95. This behaviour was also found by other workers including Schmid(1968) who interpreted the result in terms of electrons moving easily down troughs, or paths along which the V site to site hopping energy is more easily accessible with a given energy kT. When an electron reaches the end of a trough it must hop to the next trough. The saturation that takes place as the electrons in a given trough queue up to hop to the next trough gives rise to the observed ω dependence. Jonsher (1973) considers the problem in terms of time rather than ω and concludes in general that the observed behaviour is a function of a path or sequence of events.

If the energy required to hop to a new trough is readily accessible at a given temperature the two troughs could be visualised as one longer trough. Austin and Sayre [illegible] an [illegible] in which they measured the conductivity at quite high fields but below the point of dielectric break down. They interpreted their results in terms of a "hard-hop" at the end of a chain of easier hops. The length of the chain was found to be weakly x dependent and also temperature dependent. The separation of "hard-hops", or effective chain length is found to be approximately 16 - 20 Å. They suspected a structural source for the hard-hop.

7.4.3 Dielectric Constant

The high frequency dielectric constant (Sayre and Mansingh (1972) is found to increase with x. The static dielectric constant ε_o was found to increase strongly with temperature (Sayre et al, 1971). However, using another method of extracting ε_o from the peak of the dielectric loss function, Mansingh et al (1972) and Sayre and Mansingh (1972) found ε_o to decrease with temperature in accordance with a functional form given by Austin and Mott (1969),

$$\varepsilon_o = \varepsilon_\infty + \frac{\phi(x,c,R)}{kT} e^{-W_D/kT}$$

where ϕ is a constant with respect to temperature but changing with composition, and W_D is the disorder energy. Sayre and Mansingh (1972) plotted ε_o versus the reciprocal of temperature and did not find as much deviation from linearity as would be dictated by a W_D of about .1eV. The W_D indicated by the analysis of the low temperature conductivity was of that order of magnitude.

As can be seen on the following page, W_H, the hopping energy is a reasonably linear function of x, the tetrahedral vanadium content. Mott (1968) and Austin and Mott (1969) have analysed the data of Nestor and Kingery (1963) by looking at the product of ε_∞ and W_H on the assumption that ε_p is near ε_∞ and if $W_H = \frac{W'}{\varepsilon_p r_p}$ then $\varepsilon_p . W_H$ should be a constant. This assumes that r_p is independent of x. For a series of four compositions the product of ε_∞ and W_H is 1.2, 1.2, 1.3, and 1.4.

The product of ε_p and W_H from the data of Sayre and Mansingh (1972) gives the following sequence: 1.7, 1.8, 1.8, 1.6, 1.6, 1.7 and they have extracted approximate r_p values from their data which range from 2.0 Å to 2.3 Å with an average near 2.1 Å. They used the formula of Bogomolov et al. (1967) to calculate an r_p but their interatomic distance was calculated from a random distribution of ions and decreases with greater vanadate content. Under the assumption that tetrahedral vanadium should be excluded from the counting, the relevant interatomic distances are 4.43 Å (one), 4.66 Å (four) and 4.94 Å (four) which give an average of 4.70 Å. The influence of V_2O_9 unit formation on the average distance between vanadium sites is on the order of one percent or less. With this average site separation the formula of Bogomolov

Figure 7.3

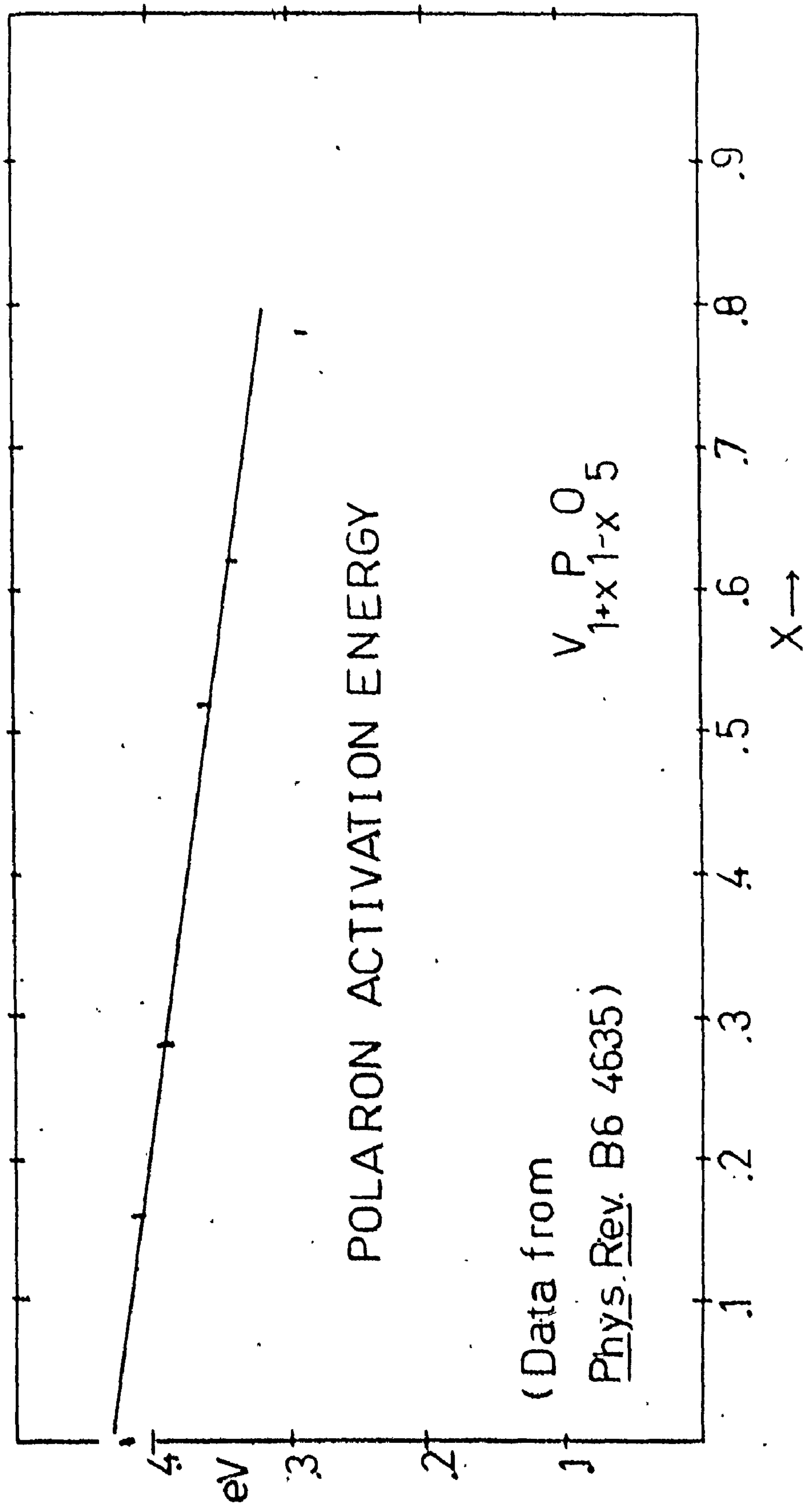
POLARON ACTIVATION ENERGY
$V_{1+x}P_{1-x}O_5$
(Data from
Phys. Rev. B6 4635)
X→
.1
.2
.3
.4
.5
.6
.7
.8
.9
eV
1
2
3
4

et al (1967) may be used to estimate the polaron radius r_p (= .403 $\bar{r}$). The value found is 1.92 Å. March and Jones (1974) have indicated that the polaron radius should be on the order of the interionic spacing or a bit less. Adler (1971) used the same rule to estimate r_p. The value estimated above from the formula of Bogomolov et al (1967) is slightly shorter (2 - 3 percent) than the equatorial V^{4+} - O bond length used in the X-ray model.

Mackenzie (1964a) has measured the conductivity of some V_2O_5 - P_2O_5 glasses at pressures of up to 50 thousand atmospheres (50 kbar). He found the activation energy to be a slight function of pressure (a change from .36 e.V at one atmosphere to .33 e.V at ten to thirty kbar). The conductivity increases nearly linearly with pressure over the first 15 kbar and the magnitude of the change appears commensurate with the change in activation energy.

The pressure coefficient of conductivity was found to be quite insensitive to V^{4+} content and the ratio V^{4+}/V^{total}. He ascribes most of the compressibility, which he quotes at 2-3%/10 kbar, to the contraction of the separation between structural units rather than compression of the individual octahedra and tetrahedra. The increased conductivity is ascribed to shorter average V - V separations.

The value of the polaron radius r_o should change with pressure to lower values and hence raise W_H. The observed slight decrease in W_H with pressure may be due to a change in ε_p. The mechanism mentioned by Goodenough (1970) and

Adler (1971) in which alterations to the ionic cage about a site changes the ability of the site to adjust fully to the pressure of a charge carrier, may be active in the decrease of W_H with pressure. Dielectric relaxation measurements as a function of pressure which would allow the extraction of ε_p, the polaron effective dielectric constant, would be useful in sorting out the influences on W_H. It is also worth noting that Mackenzie (1964a) found no difference in density or conductivity between samples before pressure treatment and after return to atmospheric pressure. No change in the form of devitrification was seen in electron micrographs either.

7.4.4. The Conductivity Paths

The hypothesis is made that the tetrahedral vanadium sites do not act as a ground state site for a hopping electron.

As noted on an earlier section the E.P.R. spectrum does not change when the composition is varied from 50% V_2O_5 - 50% P_2O_5, with no expected tetrahedral vanadium, to 80% V_2O_5 - 20% P_2O_5, in which a significant amount of tetrahedral vanadium appears on the X-ray results. Either the tetrahedral V^{4+} signal is so broad as to be undetected or is identical to the octahedral V^{4+} spectrum, or is absent. The correspondence between V^{4+} concentration measured by E.P.R. line strength and that measured chemically (Landsberger and Bray, 1970); Lynch et al, 1971) argues against a significant proportion of invisible V^{4+} tetrahedra. Accidental coincidence of the E.P.R. signal from such different crystal-field environments is not likely, however it appears to be the only obvious alternative to the hypothesis that the electron giving rise to the E.P.R. signal avoids the tetrahedral vanadium.

The vanadium tetrahedron is already significantly larger than the the phosphate tetrahedron it replaces and a further expansion to accommodate the larger ionic radius of V^{4+} might be difficult. The adiabatic transit of an electron through a VO_4^- site from one octahedral site to another would not require the VO_4 group to expand because the electron would not be there a long period compared to a vibration period. Goodenough (1970) has proposed for the conductivity path in β-vanadium bronzes a set of home sites and a set of sites through which conduction is short-circuited but at which the electron does not reside. The other alternative for the VO_4 group in the glasses is to act as an open circuit and be in that sense equivalent to a PO_4.

The easiest hopping distances between octahedra are the 4.43 Å V-V separation between two collinear vanadyl vanadiums and the 4.66 Å separation, between a vanadyl pointing upward and vanadyl from the layer above but pointing downward. If a V_2O_9 group is formed, the 4.43 Å separation is reduced to about 3.9 Å. The n-glide operation generates, from each vanadium, four vanadium neighbours in the same sheet and 4.94 Å away.

With the exception of the neighbours at 4.94 Å, which all vanadium atoms have, half the octahedral sites are internal and half external to a double layer. The external sites have two types of coordination with the neighbouring layer. In one of these coordinations there are two 4.6 Å hops to the next double layer, but in the other coordination there are none. Half the external octahedral sites have only one near vanadium neighbour.

The isolated surface site is a candidate for the "hard-hop" of Austin and Sayre (1974). For transport along the glass equivalent of the c axis in α-VPO_5 (the z direction) half the paths will encounter an easy bridge across the slip-fault (about a 4.6 Å hop) and half will encounter a hard-hop. On the average an electron could move in the z-direction through two double-layers before encountering a hard-hop. The distance equivalent to this path is twice the thickness of a double layer plus the gap between. This brings the dimension into the range observed by Austin and Sayre (1974). It should be noted that paths which detour slightly in the x-y plane can avoid such a hard-hop. This side-stepping must be done before the electron reaches the isolated octahedral site associated with the hard-hop. If the electron reaches the hard-hop position it must back track one layer before queuing up for the easier path across the slip-fault. At high frequencies, the conductivity due to this feature would be expected to show evidence of queuing and would show evidence of finite conduction paths with barriers at the end. At very high fields (Jonsher, 1974) the effective temperature of the charge carriers is increased and barriers that would be relatively insurmountable at the nominal temperature of the electrons can be crossed by the hot electrons. Also, at high field, the energy expended by an electron to back-track, against the field, from a hard-hop to detour to an easier crossing point, may make the path across the hard hop a more energetically favourable choice if the hot electron has the wherewithall for the jump. It is suggested here that this structural feature, the isolated octahedral vanadium site on the outside of a double-layer, could be considered as a candidate for the source of the hard-hop observed in the high-field conductivity experiment of Austin and Sayre (1974).

7.4.5 The Thermopower

The Seebeck coefficient, which is a measure of the thermoelectric power of the material, is of interest for two reasons. It has been measured at higher temperatures on several samples of vanadium phosphate glass (Allersma and Mackenzie, 1969; Kennedy and Mackenzie; 1967; Brown, 1966) and found to be temperature independent. At lower temperatures in low 150°K, Brown (1966) observed a rise in the Seebeck coefficient as the temperature lowered. The other feature of the Seebeck coefficient is the dependence on V^{4+}/Vtotal. Allersma and Mackenzie (1967) found a reasonably good fit to their data with a formula of (Heikes and Ure 1961).

$$S = \frac{k}{e}\left(\ln \frac{c}{1-c} + \alpha'\right)$$

where S is the Seebeck coefficient, k the Boltzman constant, e the electronic charge, c is V^{4+}/V^{total}, and α' is a constant. The value of α' has been discussed by several authors including Mott (1968), Klinger (1968), Schotte (1966), and Adler (1971), with a general consensus that α' is negligibly small.

This equation was derived under the assumption that $W_D = 0$ or $kT > W_H$, and the temperature independence of the Seebeck coefficient appears to lie in conflict with the assumed size of W_D (about .1 eV) as measured on the low temperature D.C. conductivity (Sayre and Mansingh, 1972).

Mott has [illegible] the [illegible] of con [illegible] in whi

W_D > kT but that the mobility due to electrons near the Fermi energy is small and predicts a rise in the thermopower at lower temperature as observed by Brown (1966) if kT > W_D. This would still imply a very small W_D because the Seebeck coefficient in Brown's data does not rise until the temperature is below 150°K.

Whether kT is large or small with respect to W_D (Mott, 1968) the Seebeck coefficient should change sign at $c = \frac{1}{2}$ unless the density of states is very lopsided. The Seebeck coefficients measured by Linsley *et al* (1970) fall on a family of curves, one curve for each total vanadium to phosphate ratio, and the curves do not in general extrapolate to cross the axis at $c = \frac{1}{2}$. The Seebeck coefficients measured by Kitiagovodski *et al*. (1960) are in agreement with those of Linsley *et al* (1970).

The hypothesis proposed in this study, that tetrahedral vanadium should not be counted as a potential ground-state site for V^{4+}, implies that $c' = V^{4+}/V^{\text{octahedral}} = c.(1 + x)$ where $c = V^{4+}/V^{\text{total}}$ and x is defined by $V_{1+x}\,P_{1-x}\,O_5$ is the concentration of V^{4+} relevant to the conduction process. On the following page, the data of Linsley *et al*, (1970), is re-plotted as a function of c' instead of c. It can be seen that, aside from the x = 0 composition which is anamolous, the curves from the various compositions have coalesced, with some scatter, into a common curve which crosses the axis at [illegible] $= \frac{1}{2}$. No [illegible] fo [illegible] be

Figure 7.4

SEEBECK COEFFICIENTS FOR $V_{1+x}P_{1-x}O_5$ GLASSES

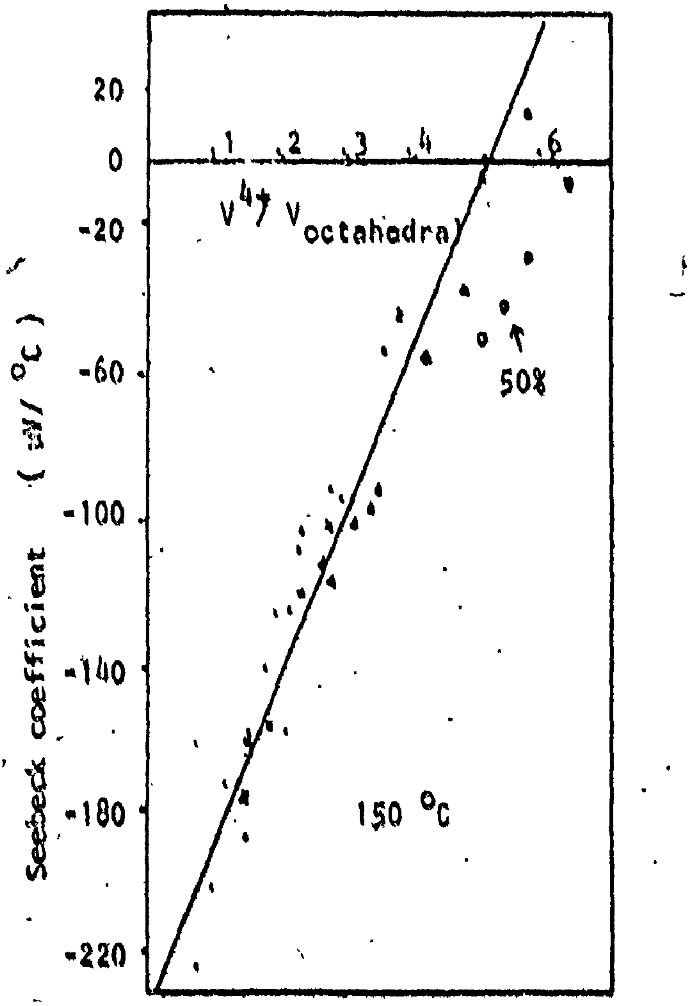

$V_{1+x}P_{1-x}O_5$ Glasses with x = 0, .2, .4, .6, .8

Data from Linsley et al. (1970)

The original graph from which this was taken was plotted as a function of V^{4+}/V_{total} and and contained a family of curves, one for each composition. Plotting vs. $V^{4+}/V_{octahedral}$ yields a composite curve with an intercept at .5. The x = 0 composition is anamalous.

kT has another alternative which will be of interest later. Austin and Mott (1969) have discussed the case in which the disorder is biomodal. If there are two types of site, A and B, which are separated in energy by a discrete value U, they argue that the conductivity will vary in proportion to $e^{-(W_H + U + \frac{1}{2}W_D)/kT}$ where W_H is the polaron hopping energy and U and W_D are as defined here. At low temperature the measured activation energy will give $U + \frac{1}{2}W_D$ as an effective W_D. If $U > kT$ and $W_D < kT$ this corresponds to charge carriers hopping from A site to A site by way of a B site. If $kT > W_D$, Austin and Mott (1969) expect the Seebeck coefficient to be given by Heikes formula where c refers to charge carriers per site and is independent of temperature. A schematic of the biomodal case is given on the following page.

7.4.6 The Disorder Energy, W_D

The process of thermally activated hopping against the Landau localization dies out at lower temperatures and in a crystal is replaced by the formation of a very narrow band which cannot form in a glass (Klinger, 1965). Conductivity at low temperatures is with the aid of acoustic phonons and has the form:

$$\sigma = g\, e^{-2\alpha R}\; e^{-W_D/kT}$$

where g is a function of concentrations and distances, α is

Figure 7.5

Schematic of Disordered Energy Distributions

(Austin and Mott, 1969)

Random Distribution of Width W_D

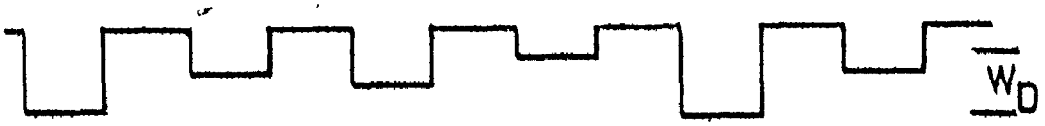

Bimodal Distribution

Energy of type A and type B sites separated by $U \pm W_D$

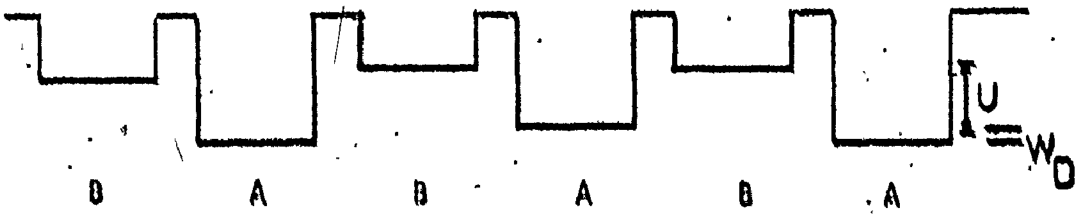

a tunnelling factor with dimensions Å^{-1}, R is the site separation and kT is the thermal energy (Mott, 1968). The disorder energy W_D could come from several sources and its source and size are questions of interest.

Two forms of disorder are prominant candidates for the cause of the observed W_D. The random distribution of Coulomb fields due to the electrons hopping about in the glass can give rise to a W_D proportional to $\frac{e^2}{\varepsilon_0 R}$ in the notation used above. This disorder energy due to a random distribution of Coulomb centres enters into the theory of impurity conduction of Miller and Abrahams (1960) and has been related to the theory of conductivity in vanadium phosphate glass by Schnakenberg (1968), Mott (1968) and to experiment by Sayre et al (1971). Sayre et al (1971) found that the Miller and Abrahams formula for W_D estimated a W_D larger than that observed. In later papers (Mansingh et al. (1972), Sayre and Mansingh (1972)) they used a different procedure for extracting the static dielectric constant from their dielectric loss data and found internal consistency between the two new analysis procedures and also consistency (Sayre and Mansingh, 1972) with the functional form predicted by Austin and Mott (1969). If the latter values of the dielectric constant are used and the site separation distance from the present study is substituted for their estimate, the predicted W_D is about .08eV at room temperature and roughly half that at liquid nitrogen temperature (based on ε_0 extrapolated from the graph of Sayre and Mansingh (1972)). Sayre et al (1972) emphasize that both W_H, the hopping energy and W_D receive a temperature variation from the dielectric constant. On this point it could be noted that W_H is much less sensitive to temperature from this source, because ϵ_p, which scales W_H is largely determined by ϵ_∞ which is assumed to be temperature invariant. If ϵ_0 doubles, W_D is halved, and W_H changes by about 15 percent. Only that part of the observed W_D which is due to Coulomb interactions should scale with the dielectric constant. Austin and Mott (1969) note in the data of Schmid (1968) that the activation energy for conductivity becomes very small at the lowest temperatures. They suggest as a possible explanation that the energy W_D is being decreased at lower temperatures by an increasingly large dielectric constant or alternatively that the electron prefers to hop further to find a site with lower W_D and consequently the observed W_D represents a selected sample rather than the full distribution of site energies in the glass. Mott and Davis (1973) also discuss the implication of an electron hopping a great distance to find an energetically more favourable site.

Distortions in the structure assumed to be characteristic of the vitreous state are the most obvious source of a disorder energy W_D. Converted to temperature, the observed distortion energy is considerably higher than the melting or quenching temperature of the glass. That would seem to imply that more distortion was frozen into the glass than was present in the parent melt. If the environment of a polaron site is distorted it could affect the ability of the polaron's environment to adjust and thereby change the depth of the well that the polaron can dig for itself. Adler (1971) has suggested that polarons which share an oxygen cannot dig wells as deep for themselves because they would be pushing on the oxygen from both sides. Goodenough (1970), discussing polaronic conductivity in beta vanadium bronzes, $M_xV_2O_5 - \beta$, in which M_x is a few percent of Cu, Li, Na, or As, suggests that the mechanism by which the M ions influence the polaron activation energy is by modestly changing the position of an oxygen adjacent to a polaron site. One way in which the glass disorder could influence the hopping energy would be by altering the ability of a $V^{5+}O_6$ unit to expand to a $V^{4+}O_6$ unit. It has been suggested on the X-ray model that the mechanism by which the glass structure adjusts to a replacement by PO_4 units by VO_4 units is by a distortion in which the VO_4 units and PO_4 units rotate a small angle nearly rigidly about V, and P positions increasing the V - O - P bond angles and causing some O - O compression but leaving P - O and V - O bond lengths nearly invariant. The operative variable through which the presence of VO_4 units may modulate the ability of a $V^{5+}O_6$ unit to expand to a $V^{4+}O_6$ unit may be more likely the available volume through a change in bond stretch constants. The illustration below is a view down the "c-axis" of a glass unit. On the crystal the O-O distance

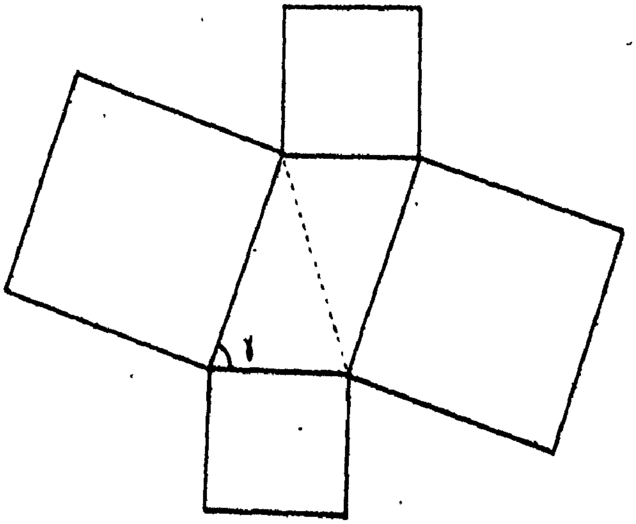

Figure 7.6

The Easiest Distortion

denoted by the dashed line has collapsed to about 3.08 Å at which mild O - O repulsion may have set in. A distortion which merely alters the angle marked γ compresses no bonds, bends few, and most directly involves only O - O repulsions. Either the tetrahedral component or the octahedral component may be expanded this way to accommodate VO_4 units or $V^{4+}O_6$ units but the O - O repulsion may be stronger when both adjustments are called for. The replacement of a PO_4 by a VO_4 increases the component of the O - O separation marked by the dashed line decreasing the strongest O - O repulsion. If the influence of the competition for volume on the ability of a VO_6 unit to expand to a $V^{4+}O_6$ unit were significant it should manifest itself as a decrease in the high temperature polaron hopping energy W_H for higher vanadium content glasses. It has already been shown that the observed decrease in W_H at increased x can be accounted for by an increase in the dielectric constant ϵ_p. This suggests that the glasses with a high concentrationof VO_4 units are not significantly less hospitable to polarons than glasses with few VO_4 units. Effects on the order of .01 eV to .03 eV may be hidden in the scatter and are difficult to rule out. A small degree of inhospitability may be enough to alter the equilibrium constants for the formation of V_2O_9 units in the melt for a given temperature and O_2 partial pressure. The data of Mackenzie (1969), Landsberger and Bray (1970), and Sayre et al (1973) for the V^{4+} concentration achieved by equilibrium in air are reasonably consistent between the three experiments and all indicate that glasses with higher vanadate content equilibrate at lower V^{4+} concentrations. This remains true even when the V^{4+} concentration is expressed as $V^{4+}/V^{\text{octahedral}}$. Austin and Garbett (1973) have applied the theory of Hillias (1968) to estimate how much fluctuation in jump distance is necessary to reproduce the observed W_D. The theory of Hillias (1968) assumed the hopping energy $W_H = W_H^0 (R_0) + a\Delta R$ where R_0 is the average hopping distance and a is a constant to be estimated and ΔR is the variation in hopping distance. They estimate that a ΔR of approximately .1 R_0 is necessary to give a W_D of .06eV. When just the 4.43 Å and 4.66 Å hopping distances from the X-ray model are considered only a two percent $\Delta R/R_0$ results and this is not much more than doubled when the contributions of 4.94 Å hops and V_2O_9 units are included. It is

Figure 7.7

The $V^4/V^{octahedral}$ concentration versus X. The horizontal axis is given in x and in mole percent V_2O_5. The larger squares come from the interpolated curve of the compound data set in Landsberger (1970) and correspond to equilibration in air. The lower (dashed) line with the smaller squares corresponds to data from Sayre and Mansingh (1972) which corresponds to equilibration of the melt under oxygen.

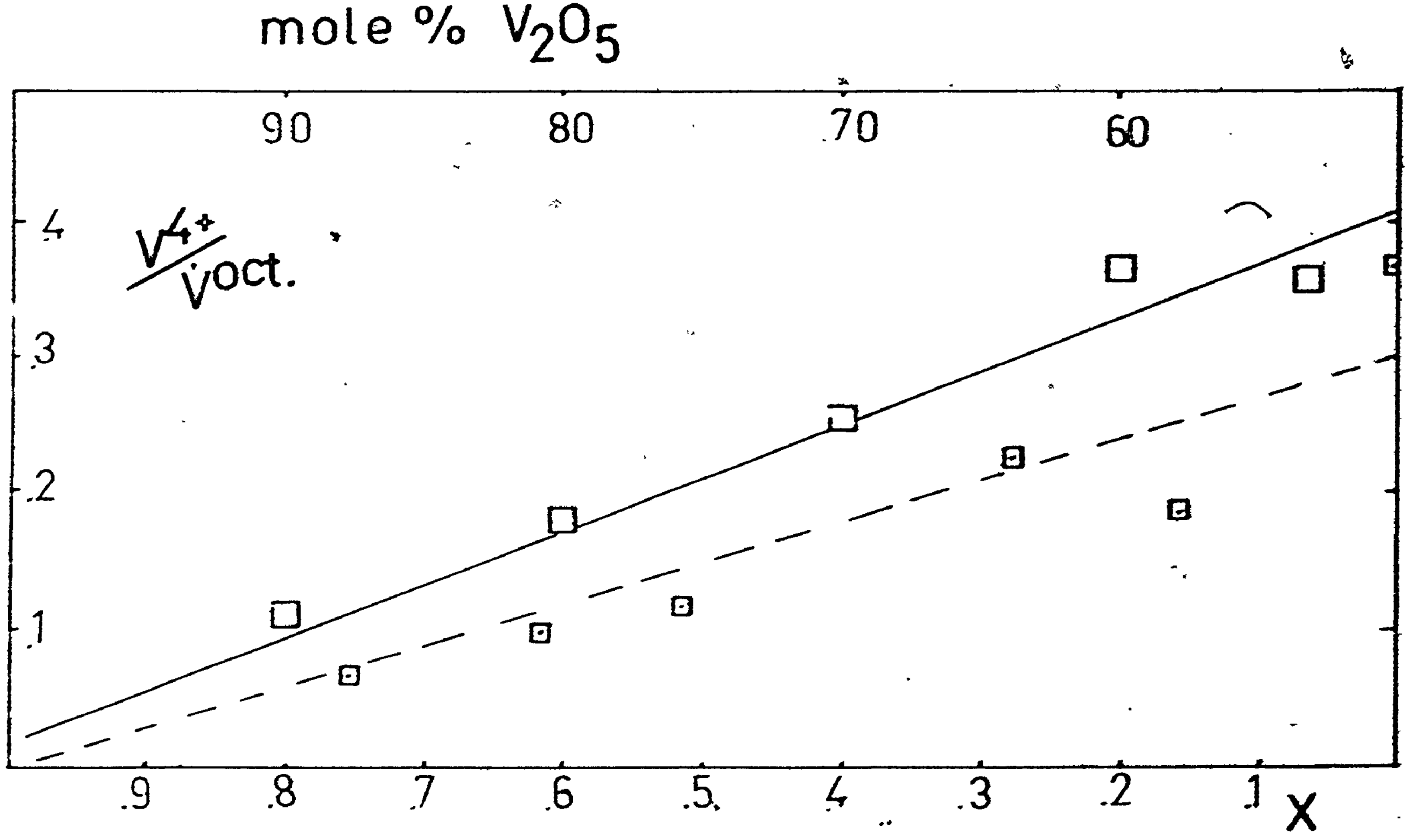
mole % V_2O_5
90
80
70
60
$V^{4+}/V_{oct.}$
.4
.3
.2
.1
.9
.8
.7
.6
.5
.4
.3
.2
.1
X

more likely that the distribution of hopping distances only contributes .01 eV to .03 eV to W_D based on these estimates. It can be suggested from this discussion that W_D may likely be due to a combination of effects from the structural disorder induced modulations on W_H, a possible contribution from the distribution of hopping distances, and an effect due to the Coulomb fields of the charge carriers. The last of these may be the dominant contribution.

7.4.7 The Conductivity Maximum

Perhaps the most puzzling phenomenon in the vanadium phosphate glasses is the conductivity maximum. A function $g(c,x)$ has been used up to this point as a pre-exponential function in the conductivity. If the conduction is by way of hopping, as assumed, the probability of a hop will be the product of the probability of having an electron at one site (c) and the probability of having an empty site near by to receive the electron $(1 - c)$. The function $g(c,x)$ should be $c'(1 - c')$ where the prime was placed on c to indicate that the x dependence has been accounted for by setting $c' = V^{4+}/V^{\text{octahedral}}$. This function implies that the maximum conductivity should occur when $c' = \frac{1}{2}$. Kitaigorodski *et al* (1960), and Munakata (1960) observed conductivity maxima for c values between .1 and .2. Linsley *et al* (1970) studied the conductivity maximum in detail and found that both the A.C. and D.C. conductivity peak near the

Figure 7. 8

$V_{1+x}P_{1-x}O_5$

THE CONCENTRATION OF V^{4+} RELATIVE TO TOTAL VANADIUM EXHIBITING THE MAXIMUM CONDUCTIVITY PLOTTED VERSUS PHOSPHORUS CONCENTRATION

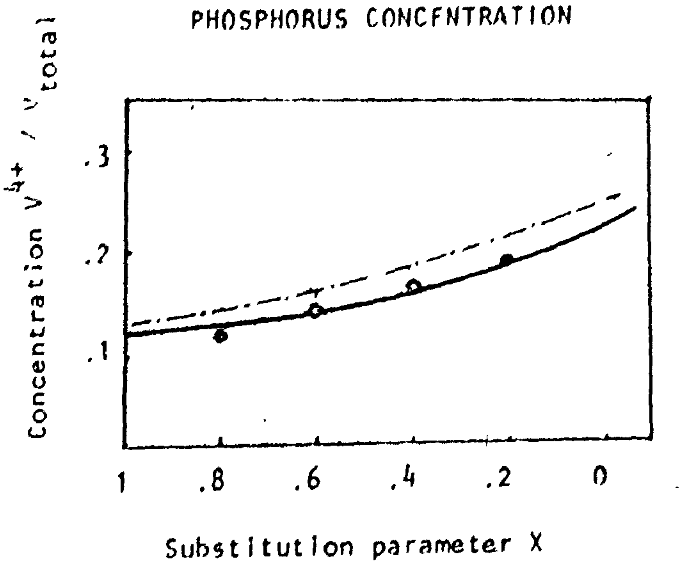

Data from Linsley *et al.* (1970)

Curve is $C(x) = 1/((1 + x)(2 + n))$

where $n = 2.5$ ————

$n = 2$ — — · — —

same c value for a given x and that W_H reaches a shallow minimum (about .02 eV.) near this same c and that the c for the conductivity maximum shifted with x. Several arguments have been suggested to explain the phenomenon but the most quantitatively successful to date appears to be that of Sayre and Mansingh (1972). Sayre and Mansingh (1972) assume polaron-polaron repulsion either in the form of Coulomb repulsion or through mutual pushing on a common neighbour. The polaron-polaron repulsion is assumed to be strong enough to disqualify a landing site for the polaron if that site has another polaron as a near neighbour. If each site has n neighbours this gives rise to a $g(c,x) = c(1 - c)^{n+1}$ and a conductivity maximum at $c = \frac{1}{2+n}$. To explain the x dependence it was necessary to assume that n increases with vanadate content. The dip in the activation energy is not explained by this argument but it was found necessary to include both the g(c,x) variation and the activation energy variation for them to reproduce the line shape of the observed conductivity maximum. If it is assumed that the outer sites have enough of an energy advantage that the charge carriers spend most of their time there and only use the inner sites for occasional transit, the inner sites will not likely have extra interactions with other occupied inner sites. Under this rather limiting hypotheses the number of outer sites in excess of two co-ordinating to an inner site is three (two at 2.44 Å and one at 4.43 Å). An outer site has only two additional outer sites or neighbours. This gives 2.5 as the average number of neighbours about a potential carrier site which may contribute a third constant contribution to the site. Sayre and Mansingh (1972) considered how the conductivity should change if polaron-polaron interactions due to any cause (Coulomb or sharing oxygens) were to disqualify a potential carrier site if one of its n neighbours were already occupied. The $c = V^{4+}/V^{total}$ dependence of the conductivity, included thus far as a proxponential function $g(c)$ will be changed from $(1 - c)$ to $(1 - c)^{n+1}$. The term $c(1 - c)$ is the product of the probability of having a filled site to contribute an electron and an empty site to accept one, The term $c(1 - c)^{n+1}$ restricts the accepting site and n of its neighbours to be empty. The value c_m which maximises the above expression is $c_m = 1/(2+n)$ If n is chosen as the 2.5 value noted above, the positions of c_m measured by Linsley et al (1970) are reproduced by the expression of Sayre and Mansingh (1972), Sayre and Mansingh (1972) had argued that n increases as the vanadium concentration x increased. This increase in n from 3.5 to 7 as they require is not needed in the present analysis because c should be changed to $c' = V^{4+}/V^{octahedral}$. In terms of c' the position of the maximum is found to be a constant.

The real advantage of the electronic configuration in which half the outer sites are occupied is that it provides a very low degree of fluctuation in m_i, the number of coulomb fields originating from within five Angstroms of site 1. The six and seven Angstrom interactions provide a reasonably uniform background with some modulation. If one increases the average occupancy of the number of V^{4+} octahedral sites beyond ½ the number of $m_i = 3$ sites will increase and this must mean square fluctuations in m will increase, thereby raising the disorder energy W_D. If fewer than ½ of the octahedral sites are occupied a number of $m_i = 2$ sites will be charged to $m_i = 1$ sites, which should also increase to fluctuation in m_i and raise W_D.

A shallow minimum (about .02 eV) in the total activation energy has been observed by Linsley et al (1970) to occur near or at the position of the optimal conductivity, c_m. If the fluctuation in the Coulomb environment of a site (the mechanism of Miller and Abrahams (1962)) increases W_D, the disorder energy, on both sides of $c' = V^{4+}/V^{\text{octahedral}} = ½$, the total activation energy should allow a shallow minimum at slightly higher V^{4+}/V^{total} than the c_m given above by the equation of Sayre and Mansingh (1972). It was found necessary by Sayre and Mansingh (1972) to use both the pre-exponential maximum and the exponential minimum to reproduce the shape of the conductivity maximum found by Linsley et al (1970), however the stronger contribution comes from the exponential term. This discussion is admittedly highly speculative. It has not been demonstrated that W_D is a minimum at $c' = ½$ but configurations on both sides have been calculated to have a higher variance in m_1. Measurement of W_D from low temperature conductivity as a function of c' would help resolve the problem. Estimates of the size of the Coulomb contribution based upon the dielectric constants of Sayre and Mansingh (1972) indicate that more than enough energy is available from this source to give the observed minimum in the activation energy. If the exponential minimum is at $c' = \frac{1}{2}$ it is not necessary to restrict n, the number of excluded neighbours in the equation of Sayre and Mansingh (1972) to 2.5. As the population of the inner sites increases n will increase and the minimum of the premultiplier shift to lower values of c'. Because the exponential term is dominant the c_m predicted will move little. Whatever the source of activation energy minimum is, the locus of values predicted by $c'_m \approx \frac{1}{2}$ correlates with the observed c_m. This simplified the problem somewhat by removing the dependence of c_m upon the total vanadium concentration.

The hypothesised picture in which some sites are momentarily discriminated against as receivers of a charge carrier because of their neighbours occupancy, or merely the heightened W_D, may give rise to a conductivity behaviour predicted by Mott (1968). In this theory the charge carrier prefers to hop to a more distant site at low temperatures if it can experience a lower W_D by doing so. The log of the conductivity is predicted in this case to be proportional to $T^{-\frac{1}{4}}$ where T is the temperature. Greaves (1973) has measured the D.C. conductivity as a function of temperature for three compositions of $V_{1+x}P_{1+x}O_5$ glass and found it to conform with Mott's $T^{-\frac{1}{4}}$ prediction.

7.5 Summary

The conductivity of the glass appears to be well characterized by the polaron model in which the activation energy is given by a sum of a polaron hopping energy W_H and a disorder energy W_D. The variation in W_H with vanadium concentration appears to be largely accounted for by the change in ε_p. As the structure is changed by the inclusion of more vanadium, W_H should be subject to the following influences.

(1) To the extent that ε_p is a function of V content ε_p will change W_H.

(2) W_H is expected to be a function of site separation of the form $W_H = \frac{1}{2}\frac{e^2}{\varepsilon_p}\left(\frac{1}{r_p} - \frac{1}{r}\right)$. (Mott, 1968)

(3) By altering the vibrational spectrum the new stoichiometry should acquire a new polaron radius r_p.

(4) The ability of the ion cage about a V^{4+} site to relax fully and achieve the maximum self trapping should be modulated by the local disorder.

That the effect of these features on W_H appears to be limited largely to their influence on ϵ_p would be consistent with the structural model proposed herein because the inter-vanadium (octahedral) distances are largely independent of x. Within the context of the X-ray model, it would also appear to imply that the substitution of VO_4 for PO_4 ions is done with minimal alteration of the octahedral site, structurally or vibrationally. The distances in the X-ray model, through the approximate formula of Bogomalov et al (1967), yield a value for polaron radius r_p close to the experimentally extracted value of Sayre and Mansingh (1972). A scenario such as that proposed by Janakirama-Rao (1965, 1966) and expanded upon by Landsberger and Bray (1970) in which V_2O_5 like sheets are progressively decomposed into smaller components by phosphates which supplant the vanadyl oxygen, would be harder to reconcile with the very slight and continuous change in density of the glass over a wide compositional range, also the apparent consistency of the polaron-radius, r_p, with a change in x right through the point at which phosphate ions are as numerous as vanadate ions.

With regard to the disorder energy W_D, it is suggested that W_D is a combination of energies due to site separation (Hillias, 1968; Austin and Garbett, 1973) local distortions and strains, and a Miller and Abrhams (1960) type of disorder due to a Coulomb fields from a random distribution of charge carriers. In the last case, a site may be considered to receive a discrete number of Coulomb interactions from its nearer neighbouring sites. This could provide the bimodal site energy distribution discussed by Austin and Mott (1969) in which the apparent W_D' is a sum of a discrete energy separation U and a real energy modulation W_D. This latter feature removes the conflict between a large (compared kT) W_D in the conductivity and a temperature independent Seebeck coefficient. The coincidental variation of the observed W_D (Sayre and Mansingh, 1972) with the static dielectric constant makes it tempting to suspect a significant portion of W_D to be due to Coulomb interactions.

Suggestions have been made on the basis of the X-ray model for sources of the conductivity maximum. The variation of both the Seebeck coefficient and the conductivity maximum with total vanadium concentration is shown to be explicable in terms of the substitution of PO_4 tetrahedron with VO_4 tetrahedra as in the X-ray model.

Distances in the X-ray radial distribution function which could be attributable to V_2O_4 or V_2O_5 like separated glass phases have not been seen and the X-ray results may be explained without hypothesis of a separated phase. It has been argued that it is not necessary to invoke phase separation to explain the conductivity maximum and that the failure of many workers to observe phase separation and the inconsistencies between the conditions under which it has been seen suggest that its presence is extraordinary rather than to be expected in ordinary samples. Annealing of the specimens by the heat of the electron-beam in the electron microscope may be a contributory factor.

It is argued that the nuclear magnetic resonance of Landsberger and Bray (1970) is at least as consistent with the hypothesis of the V_2O_9 unit in the X-ray model as it is with the model proposed by Landsberger and Bray (1970).

Evidence of the relative weakness of the attraction between layers and relative strength of ordering within a layer are to be found in the crystal structure of α-VPO_5. It has been seen in the α-VPO_5 crystal structure that the bonding between layers is essentially limited to a 2.8 Å long, very soft, V - O bond. A repulsive O - O interaction between oxygens on a PO_4 group and those on PO_4 groups immediately above and below (c-axis translated) maintains an orientational correlation between groups in adjacent layers. This interaction is so weak that crystals of α-VPO_5 have been observed to exhibit the growth of a statistical diagonal mirror plane which nearly reaches completion at slightly above room temperature. Some specimens of α-VPO_5 have been given which are still ordered at room temperature but a reasonable X-ray structural (positive definite temperature factors of reasonable magnitude and about the same R-factors as in the other specimens) refinement could only be achieved if about eight percent of the phosphates were replaced by tetrahedral vanadates. When identical parameter sets with the vanadium two percent off stoichiometry were refined on data from a crystal which disordered and one which did not at room temperature, the disordering crystal refined back to stoichiometry but the ordered crystal refined to four percent off stoichiometry. This latter behaviour is interpreted as evidence that the α-VPO_5 structure is capable of going off stoichiometry by replacement of PO_4 units by VO_4.

7.6 Conclusions

The model of VPO_5 glass upon which much of the analysis of conductivity and spectroscopic data in the past has been predicated is seen to be inconsistent with the X-ray diffraction data. A review of the findings of many of these studies has shown that an internally consistent explanation has been found in terms of the hypotheses. The basic hypothesis of this model is a striking similarity between the crystal local environment of α-VPO_5 and the local environment in the glass. The further hypotheses can be labeled; the double layer configuration, replacement, and the V_2O_9 unit. The crystal structure is seen to be made up of layers of VO_6 and PO_4 units corner sharing and generated from a single VO_4-PO_4 pair by repeated n-glide operations.

The double layer hypothesis assumed that on the average each layer has one layer above or below aligned with it and one layer related by a slip fault. This feature is invoked in counting interatomic vectors within and between layers in the X-ray model. It is also invoked to explain a drop of about 19% in the density of the glass relative to the crystal and gives a source of the "hard-hop" seen by Austin and Sayre (1973) in their high field conductivity data. A preferred ordering of the polarons in the double layer is consistent with the minimum in the hopping energy.

The second hypothesis of the X-ray glass model, the replacement of PO_4 by VO_4 as x increases in $V_{1+x}P_{1-x}O_5$, gives rise to a normalization factor (1 + x) which changes the relevant parameter from V^{4+}/V^{total} to $V^{4+}/V^{octahedral}$. The x dependance in the position of the conductivity maximum and the Seebeck coefficient data of Linsley et al (1970), can be described by this factor. For a given O_2 partial pressure and temperature range, the value $V^{4+}/V^{octahedral}$ at equilibrium appears to be proportional to 1 - x. If, as was assumed in the X-ray model and density analyses, the VO_4 units push apart the members of a double layer and V_2O_9 units pull them together, a mechanism by which the energetics of formation of a V_2O_9 unit may be influenced by the number of VO_4 units nearby, has been found. The apparent conflict between the observation of hyperfine lines in the EPR spectrum of x = .6, V^{4+}/V^{total} = .05 glass by Lynch et al (1971) and none in the EPR spectrum of x = .8, V^{4+}/V^{total} = .06 glass by Bogolyomov et al (1968) is much less of a conflict when comparison is made of $V^{4+}/V^{octahedra}$.

If the difference between glasses of varying x is limited to replacement of PO_4 by VO_4 with a small amount of orientational adjustment, the observed (Sayre and Mansingh, 1972) constant value of the polaron radius over a wide range of x as well as the very slight continuous change in density over the same x range makes much more sense than if major structural rearrangement were taking place.

Unlike the double layer configuration and VO_4 replacement hypotheses, the V_2O_9 hypothesis is not deeply rooted in the X-ray model. The observed loss of oxygen commensurate with the reduction of vanadium from V^{4+} to V^{5+} has very minor manifestation in the radial distribution function. The V_2O_9 unit was hypothesised as a configuration which could account for the lost oxygen with a minimal perturbation on the radial distribution function. Its manifestation in the radial distribution function gives a minor improvement in agreement with experiment. A more common value of a vanadium bridging oxygen bond length could be achieved if the layers of the double layer configuration were pulled together locally by .2 to .3 Å. In conjunction with the separation between members of the double layer caused by the larger VO_4 substituting for the smaller PO_4 this gives a better numerical prediction of the change in density of the glass with x. The V_2O_9 group has the same virtues as the structure proposed by Landsberger and Bray (1970) to explain their NMR results but gives an extrapolated value of the chemical shift which is more consistent with the unresolved composite peak hypothesis upon which their analysis is predicated.

Rawson (1957) found the V_2O_5-PbO system to be a good example of his theory that a deep eutectic is correlated with a glass forming region. It has been found that the supposed position of that eutectic (50% V_2O_5) corresponds to a crystalline phase PbV_2O_6 which melts congruently at about 100°C higher than the eutectic. The position of the eutectic may be a few percent toward V_2O_5 from PbV_2O_6. The crystal structure of PbV_2O_6 is found to be based on chains of VO_6 units. Each chain could be visualized as a staggered stack of dominoes with two edges showing VO_6 units per dominoe. The chains are related by an n-glide with each other but are only bound to each other through the lead atoms. Beta lead vanadium bronze (Galy et al, 1970) has the same staggered stack of dominoes but the stacks are connected to each other through a bridging oxygen on the corner of an outer dominoe. A further complex which could be visualised as a dominoe sitting on its long edge links one chain of octahedra to another. The glass forming region is between beta-vanadium bronze and PbV_2O_6 in composition and it is tempting to speculate upon a glass structure with PbV_2O_6 - like chains randomly cross-linked with features from the bronze. Lead is such a strong X-ray scatterer it is likely that a combined X-ray and neutron diffractive experiment would be necessary to ascertain the structure.

BIBLIOGRAPHY

D. Adler. CRC Critical Reviews in Solid State Sciences, 317 (1971).

T. Allersma, R. Hakim, T.N. Kennedy, and J.D. Mackenzie, J. Chem. Phys. 46, 154 (1967).

T. Allersma and J.D. Mackenzie. J. Chem. Phys. 47, 1406 (1967)

M. Amadori. Atti. r. ist. Veneto, 76, 419 (1916).

J.L. Amoros and M. Amoros. "Molecular Crystals: Their Transforms and Diffuse Scattering",, John Wiley and Sons, New York, 1968.

G.W. Anderson and W.D. Compton. J. Chem. Phys. 52, 6166 (1970).

G.W. Anderson and F.U. Luehrs, Jr.. J. Appl. Phys. 39, 1634 (1968).

P.W. Anderson. Phys. Rev. 109, 1492 (1958).

J. Angenault and A. Rimsky. C.R. Acad. Sci. Paris Ser. C, 267, 227 (1968).

A.J. Apling in "Electronic and Structural Properties of Amorphous Semiconductors", Ed. P.G. Le Comber and J. Mort, Academic Press, New York, 1973.

I.G. Austin and E.S. Garbett in "Electronic and Structural Properties of Amorphous Semiconductors", Ed. P.G. Le Comber and J. Mort, Academic Press, New York, 1973.

I.G. Austin and M. Sayre. J. Phys. C: Solid State Phys. 7, 905 (1974).

I.G. Austin and N.F. Mott. Advan. Phys. 18, 41 (1969).

S.N. Bagchi. Advan. Phys. 19, 119, (1970).

S.N. Bagchi. Acta Cryst. A28 560, (1972).

C.J. Ballhausen, B.F. Djurinskij, and K.J. Watson. J. Am. Chem. Soc. 90, 3305 (1968).

P.L. Baynton, H. Rawson, and J.E. Stanworth. J. Electrochem. Soc. 104, 239 (1957).

P.J. Becker and P. Coppens. Acta Cryst. A 31, 417, (1975).

S.G. Bishop and N.J. Shevchik. Solid State Comm., 15, 629 (1974).

P.J. Black and J.A. Cundall. Acta Cryst. 19, 807, (1965).

V.N. Bogomolov, E.K. Kudinov, and Yu. A. Firsov. Soviet Physics-Solid State, 9, 2502(1968).

W. Bol. J. Sci. Instrum., 44, 736, (1967).

E. Bordes and P. Courtine. C.R. Acad. Sc. Paris, 1270, 1375 (1972).

E. Bordes, P. Courtine, and G. Pannetier. Ann. Chim, 105, (1973).

J.C. Bouloux and J. Galy. Bull. Soc. Chim. Fr. 739 (1969).

J.C. Bouloux, G. Perez and J. Galy. Bull. Soc. Fr. Miner. Crist. 95, 130, (1972).

I.D. Brown and R.D. Shannon. Acta Cryst. A. 29, 266 (1973).

J.J. Brown and F.A. Hummel. Trans. Br. Ceram. Soc. 64, 419 (1965).

R.M. Brown, Ph.D. Thesis, University of Illinois (1966).

M.J. Buerger, "Crystal-structure Analysis", John Wiley and Sons, Inc., New York. (1960).

R.H. Caley and M.K. Murthy. J. Am. Ceramic Soc. 53, 254 (1970).

C. Calvo and D. Manolescu. Acta Cryst. B29, 1743 (1973).

G.S. Cargill. III. J. Appl. Phys. 41, 12 (1970).

G.S. Cargill. III. J. Appl. Cryst. 4, 277, (1971).

A.H. Compton and S.K. Allison. "X-rays in Theory and Experiment", D. Van Nostrand Company, Toronto, (1951).

J.R.D. Copley and S.W. Lovesey. Rept. Prog. Phys. 38, 461, (1975).

P. Coppens and W.C. Hamilton. Acta Cryst. A 26, 71 (1970).

D.T. Cromer, Acta Cryst, 18, 17, (1965).

D.T. Cromer. J. Chem. Phys. 50, 4857 (1969).

D.T. Cromer and D. Liberman. J. Chem. Phys. 53, 1891, (1970).

D.T. Cromer and J.B. Mann. J. Chem. Phys. 47, 1892 (1967).

D.T. Cromer and J.T. Waber, Acta Cryst., 18, 104, (1965).

D.W.J. Cruickshank, D.E. Pilliny, A. Bujosa, F.M. Lowell, and M. Truter, "Computing Methods in the Phase Problem", Pergamon Press, Oxford, 1961.

D. Crump, Ph.D, Thesis, McMaster University, 1970.

P. D'Antonio, C. George, A.H. Lowrey, and J. Karle. J. Chem. Phys. 55, 1071 (1971).

J. Darriet and J. Galy. Cryst. Struct. Comm. 2, 237 (1973)

J. Darriet, R. von der Muhll, and J. Galy. Bull. Soc. fr. Mineral. Cristallogy., 92, 17 (1969).

E.P. Denton, H. Rawson, and J.E. Stanworth. Nature, 173, 1030 (1954).

M.G. Duffy, D.S. Boudreaux and D.E. Polk. J. Non-Crystalline Solids, 15, 435 (1974).

C.W. Dwiggins and D.A. Park. Acta Cryst. (1971). A 27, 264.

P.A. Egelstaff, Advances in Physics, 16, 147, (1967).

H.A. Eick and L. Kihlborg. Acta Chem. Scand. 20, 722 (1966).

P. Eisenberger and P.M. Platzman. Phys. Rev. A., 2, 415 (1970).

D. Emin in "Electronic and Structural Properties of Amorphous Semiconductors", Ed. P.G. Le Comber and J. Mort, Academic Press, New York, 1973.

S. Ergun, J. Bayer, and W. Van Buren. J. Appl. Phys. 38, 3540 (1967).

O.E. Esval, Ph.D. Thesis, University of North Carolina, 1962.

L.N.G. Filon, Proc. Roy. Soc. Edinburgh, (A) 49, 38 (1928).

E.J. Friebele, L.K. Wilson, and D.L. Kinser, J. Amer. Ceram. Soc. 55, 164 (1972).

H. Fritzsche, "Annual Review of Materials Science", (ed. R.A. Huggins). Annual Reviews Inc., Palo Alto, Cal., 2, 697 (1972).

H. Fritzsche in "Electronic and Structural Properties of Amorphous Semiconductors". Ed. P.G. Le Comber and J. Mort, Academic Press, New York, 1973.

K. Furukawa. Rept. Prog. Phys., 25, 396 (1960).

J. Galy, J. Darriet, A. Casalot, and J.B. Goodenough. (1970). J. Solid State Chemistry 1, 339, (1970).

T.R. Gilson, O.F. Bizri, and N. Cheetham. J.C.S. Dalton, 291 (1973).

J.B. Goodenough. J. Solid State Chem. 1, 349 (1970).

J.B. Goodenough. Mat. Res. Bull. 5. 621 (1970).

R. Gopal, Ph.D. Thesis, McMaster University, 1972.

R. Gopal and C. Calvo. Acta Cryst. B 30, 2491 (1974).

L.A. Grechanik, N.V. Petrovykh, and V.G. Karpechenko. Soviet Phys.-Solid State 2, 1908 (1961).

H.U. Gruber and H. Krebs. Z. Anorg. Allgem. Chem. 369, 184 (1969).

A. Guinier, "X-ray Diffraction", W.H. Freeman and Company, San Francisco, 1963.

F. Hajdu. Acta Cryst. A. 28, 250 (1972).

N.C. Halder, R.J. Metzger, and C.N.J. Wagner. J. Chem. Phys. 45, 1259 (1966).

D.P. Hamblen, R.A. Weidel, and G.E. Blair. J. Amer. Ceram. Soc. 46, 499 (1963).

R.R. Heikes and R.W. Ure, "Thermoelectricity" (Interscience, New York, 1961).

L.L. Hench. J. Non-Crystalline Solids 2, 250 (1970).

T. Holstein, Ann. Phys. (N.Y.) 8 343, (1959)

R. Hosemann and S.N. Bagchi, "Direct Analysis of Diffraction by Matter", North-Holland Publishing Company, Amsterdam, 1962.

V.V. Illarionov, A.I. Soklakov, and E.V. Kil'disheva. Russ. J. Inorg. Chem. 6, 696 (1961).

International Tables for X-ray Crystallography. Vol. iii. Kynoch Press, Birmingham. 1963.

R.W. James. "The Optical Principles of the Diffraction of X-rays", Bell., London (1962)

B.V. Janakirama-Rao. J. Amer. Ceram. Soc., 48, 311 (1965).

B.V. Janakirama-Rao. J. Amer. Ceram. Soc. 49, 605 (1966).

W. Jones and N. March. "Theoretical Solid State Physics", Vol. 1, John Wiley and Sons, Inc., New York, 1973.

A.K. Jonsher. J. Non-Crystalline Solid. 8, 293 (1972).

A.K. Jonscher in "Electronic and Structural Properties of Amorphous Semiconductors", Ed. P.G. Le Comber and J. Mort, Academic Press, New York, 1973.

B.D. Jordan and C. Calvo, Can. J. Chem., 51, 2621, 1973.

B.D. Jordan and C. Calvo. Can. J. Chem., 52, 2701 (1974).

K.H. Jost. Acta Cryst. 17, 1539 (1964).

R. Kaplow, T.A. Rowe, and B.L. Averbach. Phys. Rev. 168, 1068 (1968).

R. Kaplow, S.L. Strong and B.L. Averbach. Phys. Rev. 138, A1336 (1965).

J. Karle and J.H. Konnert, Trans. Amer. Cryst. Assoc. 10, 29 (1974).

T.N. Kennedy, R. Hakim, and J.D. Mackenzie. Mat. Res. Bull. 2, 193 (1967).

T.N. Kennedy and J.D. Mackenzie, Physics and Chemistry of Glasses, 8, (1967), 169.

P.Kierkegaard, J.M. Longo, Acta Chem. Scand. 19, 1906 (1965).

P. Kierkegaard and J.M. Longo, Acta. Chemica Scandinavica, 24, 427, (1970).

P. Kierkegaard and M. Westerlund. Acta Chem. Scand. 18, 2217, (1964).

H.R. Killias. Physics Letters 20, 5 (1966).

D.L. Kinser and L.K. Wilson. Second Cairo Solid State Conference, Recent Advances in Science and Technology of Materials, The American University in Cairo and Ein Shams University, April 1973.

I.I. Kitaigorodskii, V.K. Frolov and Kuo-Cheng. Steklo i Keramika, 17, 5 (1960).

I.I. Kitaigorodskii, and V.G. Karpechenko. Glass Ceram. (USSR), 15, 294 (1960).

M.I. Klinger, Phys. Status Solidi 12, 765, (1965).

H.P. Klug and L.E. Alexander, 1974, "X-ray Diffraction Procedures", John Wiley and Sons, Toronto.

J.H. Konnert and J. Karle. Science, 179, 177 (1973).

J.H. Konnert and J. Karle. Acta Cryst., A29, 702, (1973)..

Z. Kopal. "Numerical Analysis", Chapman and Hall Ltd., London, (1955).

H. Krebs and H.U. Gruber. Z. Naturforschg. 22a, 96 (1966).

M.A. Krivoglaz, "Theory of X-ray and Thermal-Neutron Scattering by Real Crystals", Plenum Press, New York.(1969).

R. de L. Kronig. J. Optical Soc. America and Rev. Sci. Inst., 12, 547, (1926).

J. Krogh Moe. Acta Cryst. 9, 951, (1956).

G. Ladwig. Z. Anorg. Allg. Chem. 338, 266 (1965).

G. Ladwig. Z. Anorg. Allg. Chem. 364, 225 (1969).

L.D. Landau. Phys. Z. Sowjetunion, 3, 664, 1933.

F. Landsberger, Doctorate Thesis, Brown, 1970.

F.R. Landsberger and P.J. Bray, J. Chem. Phys., 53, 2757, 1970.

A.C. Larson. Acta Cryst. 23, 664, (1967).

R.M. Lawrence, J.R. Relford, and S.C. Habegger. Rev. Sci. Instrum. 43, 40 (1972).

A.J. Leadbetter and A.J. Apling. J. Non-Crystalline Solids, 15, 250, (1974).

A.J. Leadbetter and A.C. Wright. J. Non-Crystalline Solids 7, 23, (1972).

A.J. Leadbetter and S.C. Wright. J. Non-Crystalline Solids 7, 37, (1972).

A.J. Leadbetter and A.C. Wright. J. Non-Crystalline Solids, 7, 141, (1972).

A.J. Leadbetter and A.C. Wright. J. Non-Crystalline Solids 7, 156, (1972).

E.M. Levin and R.S. Roth. J. Solid State Chem. 2, 250, (1970).

H.A. Levy, M.D. Danford and A.H. Narten, "Data Collection and Evaluation with an X-ray Diffractometer Designed for the Study of Liquid Structure". ORNL-3960 (1966).

G.S. Linsley, A.E. Owen and F.M. Hayatee. J. Non-Crystalline Solids. 4, 208 (1970).

D.J. Lloyd and J. Galy. Cryst. Struct. Comm. 2, 209 (1973).

J.M. Longo and R.J. Arnott. J. Solid State Chem. 1, 394 (1970).

J.M. Longo, J.W. Pierce and J.A. Kafalas. Mater. Res. 6, 1157 (1971).

E.A. Lorch. J. Phys. C 2 229, (1969).

G.F. Lynch, M. Sayre, S.L. Segel, and G. Rosenblatt. J. Appl. Phys. 7, 2587 (1971).

G.F. Lynch and M. Sayre. J. Phys. C. Solid State Phys. 6, 3661 (1973).

J.D. Mackenzie, in "Modern Aspects of the Vitreous State", Vol. 3, Ed. J.D. Mackenzie, Butterworths, Washington (1964).

J.D. Mackenzie, in "Physics of Non-Crystalline Solids" edited by J.A. Prins (North-Holland Publishing Company, Amsterdam, 1965).

A. Mansingh, J.M. Reyes, and M. Sayer. J. Non-Crystalline Solids 7, 12 (1972).

A. Mansingh, J.K. Vaid, and R.P. Tandon. J. Phys. C: Solid State Phys. 8, 1023 (1975).

H. Margenau & G.M. Murphy. The Mathematics of Physics and Chemistry. 2nd Ed. D. Van Nostrand & Co., Princeton, 1956.

W. Marshall and S.W. Lovesey. "Theory of Thermal Neutron Scattering", Oxford University Press, London, 1971.

H.D. Megaw. "Crystal Structures: A Working Approach", W.B. Saunders Company, Toronto, 1973.

M.E. Milberg. J. Appl. Phys. 29, 64 (1958).

A. Miller and E. Abrahams. Phys. Rev. 120, 745 (1960).

N.F. Mott. J. Non-Crystalline Solids 1, 1 (1968).

N.F. Mott in "Electronic and Structural Properties of Amorphous Semiconductors", Ed. P.G. Le Comber and J. Mort, Academic

Press, New York, (1973).

N.F. Mott and E.A. Davis. "Electronic Processes in Non-crystalline Materials", Clarendon Press, Oxford, (1971).

R.L. Mozzi and B.E. Warren. J. Appl. Cryst., 2, 164 (1969).

R,L. Mozzi and B.E. Warren. J. Appl. Cryst. 3, 251 (1970).

M. Munakata, Solid State Electronics 1, 159 (1960).

M.F. Mydlar, N.J. Kreidl, J.K. Hendren and G.T. Clayton. Physics and Chemistry of Glasses, 11, 196 (1970).

B. Nador. Steklo Keram., 17, 18 (1960).

V.M. Nagiev. Soviet Physics-Solid State 7, 2204 (1966).

A.H. Narten, J. Chem. Phys. 56, 1185 (1972).

A.H. Narten. Trans. Amer. Cryst. Assoc. 10, 19 (1974).

H.H. Nester and W.D. Kingery, 7th Int. Congress on Glass, Brussels, June 1965.

H.N. Ng. Private Communication (1973).

H.N. Ng and C. Calvo. Can. J. Chem. 50, 3619 (1972)

N. Norman. Acta Cryst. 10, 370 (1957)

J.H. Perlstein, J. Solid State Chem. 3, 217 (1971).

C.J. Pings and J. Waser. J. Chem. Phys., 48, 3016 (1968)

P.M. Platzman. "Light Scattering in Solids" ed. M. Balkanski (Flammarion, Paris, 1971).

P.M. Platzman and N. Tzoar. Phys. Rev. 136, A11 (1964)

A. Rahman, J. Chem. Phys. 42, 3540 (1965).

H. Rawson. "Inorganic Glass-Forming Systems", Academic Press, New York, (1967)

M.D. Rechtin and B.L. Averbach. J. Non-Crystalline Solids 12, 391 (1973).

A.L. Renninger, M.D. Rechtin, and B.L. Averbach. J. Non-Crystalline Solids 16, 1 (1974).

R.S. Roth, A.D. Wadsley, and S. Andersson. Acta Cryst. 18, 643 (1965).

H. Ruppersberg and H. Reiter. Acta Cryst. A 28, 233 (1972).

W. Ruland. Brit. J. Appl. Phys., 15, 1301 (1964).

M. Sayre and G.F. Lynch. J. Phys. C. Solid State Phys. 6. 3675 (1973).

M. Sayre and A. Mansingh. Phys. Rev. B 6, 4629 (1972)

M. Sayre, A. Mansingh, J.M. Reyes, and G.F. Lynch in "Conduction in Low-mobility Materials", Ed. N. Klein, D.S. Tannhauser, and M. Pollak, Taylor and Francis Ltd., London, 1971.

M. Sayre, A. Mansingh, J.M. Reyes, and G. Rosenblatt. J. Appl. Phys. 42, 2587 (1971).

H.F. Schaake and L.L. Hench. J. Non-Crystalline Solids 2, 292 (1970).

A.P. Schmid. J. Appl. Phys., 39, 3140 (1968)

A.P. Schmid. J. Appl. Phys., 40, 4128 (1969)

J. Schnakenberg, Z. Physik, 185, 23 (1965).

J. Schnakenberg, Physica Status Solidi 28, 623 (1968).

K.D. Schotte. Z. Physik 196, 393 (1966)

R.D. Shannon and C. Calvo. Can. J. Chem. 51, 70 (1973).

R.D. Shannon and G.T. Prewitt. Acta Cryst. B. 25, 925 (1969).

N.J. Shevchik and W. Paul. J. Non-Crystalline Solids, 16, 55 (1974)

T. Shimohira, S. Iwai, and H. Tagai. J. Ceram. Assoc. Jap. 75, 352 (1967).

I. Siegel. Phys. Rev. 134A, 193 (1964)

G. Sperlich. Z. Physik 250, 335 (1972).

G.H. Stout and L.H. Jensen, "X-ray Structure Determination", The Macmillan Company, New York, 1968.

S.L. Strong and R. Kaplow. Rev. Sci. Instrum. 37, 1495 (1966).

N.J. Shevchik. Acta Cryst. A 29, 37 (1973).

F. Theobald and J. Galy. Acta Cryst. B 29, 2732 (1973).

F.R. Thornley and R.J. Nelmes. Acta Cryst. A 30, 748 (1974).

L. Van Hove. Phys. Rev. 95, 249 (1954).

C.N.J. Wagner in "Liquid Metals, Chemistry and Physics", Ed. S.Z. Berr, Marcel Dekker, Inc., New York, 1972.

C.N.J. Wagner H. Ocken, and M.L. Joshi. Z. Naturforschg. 20a, 325 (1965).

K. Waltersson, B. Forslund, K.A. Wilhelmi, S. Andersson, and J. Galy. Acta Cryst. B. 30, 2644 (1974).

B.E. Warren. "X-ray Diffraction", 1969, Addison-Wesley Publishing Company, Don Mills, Ontario.

B.E. Warren and G. Marvel. Rev. Sci. Instrum 36, 196 (1965).

B.E. Warren, H. Krutter & O Morningstar. J. of Am. Ceram. Soc. Vol. 19, p.202 (1936).

B.E. Warren and R.L. Mozzi. Acta Cryst. 21, 459 (1966)

B.E. Warren and R.L. Mozzi. J. Appl. Cryst. 3, 59, (1970).

J. Waser and V. Schomaker. Rev. Mod. Phys. 25, 671 (1953).

R.J. Weiss 1966, "X-ray Determination of Electron Distributions", North Holland Publishing Company, Amsterdam.

K.A. Wilhelmi and K. Waltersson. Private Communication. (1971)

R.A. Young. Z. Krist. 118, 233 (1963).

W.H. Zachariasen. Acta Cryst. 16, 1139, (1963)

W.H. Zachariasen. Acta Cryst. 23, 558 (1967).

J. Zarzycki and F. Naudin. C.R. Acad. Sc. Paris 265, 1456, (1967).